

Asymmetrical supply of induction machines : remedial operating strategies in case of converter faults

Citation for published version (APA):

Bosga, S. G. (1997). *Asymmetrical supply of induction machines : remedial operating strategies in case of converter faults*. [Phd Thesis 1 (Research TU/e / Graduation TU/e), Electrical Engineering]. Technische Universiteit Eindhoven. <https://doi.org/10.6100/IR492480>

DOI:

[10.6100/IR492480](https://doi.org/10.6100/IR492480)

Document status and date:

Published: 01/01/1997

Document Version:

Publisher's PDF, also known as Version of Record (includes final page, issue and volume numbers)

Please check the document version of this publication:

- A submitted manuscript is the version of the article upon submission and before peer-review. There can be important differences between the submitted version and the official published version of record. People interested in the research are advised to contact the author for the final version of the publication, or visit the DOI to the publisher's website.
- The final author version and the galley proof are versions of the publication after peer review.
- The final published version features the final layout of the paper including the volume, issue and page numbers.

[Link to publication](#)

General rights

Copyright and moral rights for the publications made accessible in the public portal are retained by the authors and/or other copyright owners and it is a condition of accessing publications that users recognise and abide by the legal requirements associated with these rights.

- Users may download and print one copy of any publication from the public portal for the purpose of private study or research.
- You may not further distribute the material or use it for any profit-making activity or commercial gain
- You may freely distribute the URL identifying the publication in the public portal.

If the publication is distributed under the terms of Article 25fa of the Dutch Copyright Act, indicated by the "Taverne" license above, please follow below link for the End User Agreement:

www.tue.nl/taverne

Take down policy

If you believe that this document breaches copyright please contact us at:

openaccess@tue.nl

providing details and we will investigate your claim.

Asymmetrical Supply of Induction Machines

Remedial Operating Strategies in case of Converter Faults

```
LDF @FfluxP_r_obs,R6
vecrot R6,R7,@cosphi_r_s_obs,@sinphi_r_s_obs,R4,R5
tu_2_3d R4,R5,@fluxP_rsab_obs,@fluxP_rsbc_obs,@fluxP_rsca_obs
;
;Flux controller
LDF @flux_r_des, R6
SUBP @flux_r_obs, R6 ; R6 = flux error
LDF @flux_r_des, R7
MPYF @_l_obs, R7
LDF R7, R8
MPYF -2, R7 ; neg. limit: -2*flux_r_des/l
MPYF 2, R8 ; pos. limit: 2*flux_r_des/l
piregel R6, 23, 0.27, R7, R8, Spii_s_b_des
CMPF R7, R0 ; limit also the P-part
LDFLT R7, R0
CMPF R8, R0
LDPGT R8, R0
STF R0, @i_s_b_des
```

```
... @i_s_s2,@cosphi_r_s_obs
;me1...
```

```
LDI @flux_r_obs,R6
MPYF @flux_r_obs,R6
STF R6,@flux_r_obs
```

```
... @i_s_s2,@cosphi_r_s_obs
```

```
... @i_s_s2,@cosphi_r_s_obs
```

```
... @flux_r_obs,@fluxP_rsab_obs,@fluxP_rsbc_obs,@fluxP_rsca_obs
```

```
... @flux_r_obs,@i_s_w,@lact,@theta,@mel,@sthor
```

```
... for display only
```

```
@flux_r_obs,@cosphi_r_s_obs,@sinphi_r_s_obs,@flux_r_sl,@flux_r_s2
```

```
i_s_b, R4
```

```
sig, R4
```

```
flux_r, R4
```

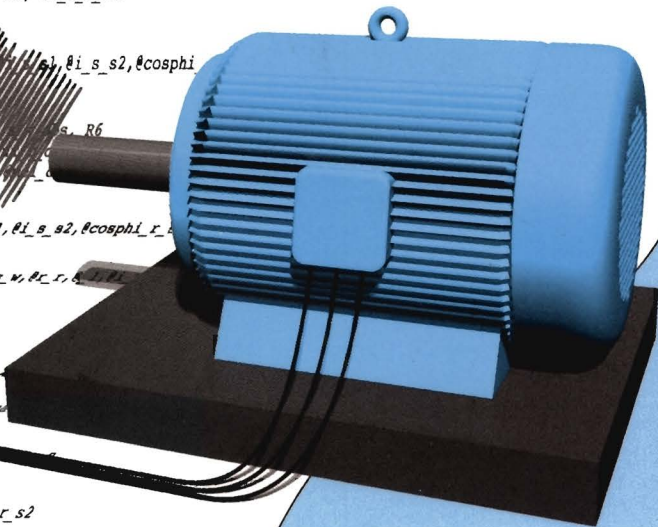
```
w, R5
```

```
R5
```

```
@cosphi_r_s_obs,@sinphi_r_s_obs,@flux_r_sl,@flux_r_s2
```

```
rents
```

```
@i_s_s2,x,@i_sa,@i_sb,@i_sc
```



Sjoerd G. Bosga

Asymmetrical Supply of Induction Machines

Remedial Operating Strategies in case of Converter Faults

Asymmetrical Supply of Induction Machines

Remedial Operating Strategies in case of Converter Faults

PROEFSCHRIFT

ter verkrijging van de graad van doctor aan de
Technische Universiteit Eindhoven, op gezag van
de Rector Magnificus, prof.dr. M. Rem, voor een
commissie aangewezen door het College van
Dekanen in het openbaar te verdedigen
op vrijdag 23 mei 1997 om 16.00 uur

door

Sjoerd G. Bosga

geboren te 's-Hertogenbosch

Dit proefschrift is goedgekeurd door de promotoren:

prof.dr.ir. A.J.A. Vandenput

en

Prof.Dr.-Ing. R.W. De Doncker

CIP-DATA LIBRARY TECHNISCHE UNIVERSITEIT EINDHOVEN

Bosga, Sjoerd G.

Asymmetrical supply of induction machines : remedial operating strategies in case of convertor faults / by Sjoerd G. Bosga. - Eindhoven : Technische Universiteit Eindhoven, 1997.

Proefschrift. - ISBN 90-386-0310-X

NUGI 832

Trefw.: elektrische aandrijvingen ; regelen / asynchrone machines ; regeling / betrouwbaarheid ; elektromechanica / statische omzetters.

Subject headings: torque control / induction motor drives / power convertors / electric machine control / variable speed drives.

Copyright © 1997 by Sjoerd G. Bosga

All rights reserved. No part of this thesis may be reproduced, stored in a retrieval system or transmitted in any form, by any means, electronic, mechanical, photocopying, recording or otherwise, without the prior written permission of the author.

The author makes no warranty, that the methods, calculations and data in this book are free from error. The application of the methods and results is at the user's risk and the author disclaims all liability for damages, whether direct, incidental or consequential, arising from such application or from other use of this book.

Abstract

Asymmetrical Supply of Induction Machines Remedial Operating Strategies in case of Converter Faults

The three-phase induction motor is a very robust and reliable machine that finds industrial application within a wide range of electrical drives. The increased use of power electronics to supply the induction machine, extends this range more and more into the field of – sometimes highly dynamical – adjustable speed drives. At the same time however, the addition of power electronics does not necessarily guarantee that the reliability of the complete drive equals or exceeds that of an induction machine connected to the grid directly, without power converter.

In practice, the failure of a single switching device or gate driver in the power converter is often followed by the shutdown of the complete drive. However, under certain conditions such a shutdown is not needed. If these unnecessary shutdowns were avoided, this would result in an increased reliability of the drive. It is therefore necessary to know what kind of operation of the drive is possible while a fault is present in the power converter.

In this thesis, a classification of such faults is presented, based on their effect on the drive. Current faults are those faults that are related to an open circuit in the converter, and voltage faults are related to short circuits. An important issue is also whether or not the star point of the stator windings of the machine is connected in a way that allows a homopolar current to flow. If so, more redundancy is present in the circuit and operation during a fault, the so-called remedial operation, can be realized much more easily.

In case a complete stator phase becomes disconnected, appropriate control of the homopolar current can guarantee remedial operation with a constant torque, which is however limited due to an increased current demand for the remaining two phases. To study this kind of operation, the standard machine model had to be extended with a homopolar impedance. Using this extended model, homopolar-current control has been implemented on a voltage-fed induction machine. Experiments showed successful remedial operation, but also demonstrated that a homopolar current causes saturation in the main-flux path.

Without star-point connection, the loss of a complete stator phase is a very serious fault, during which remedial operation will in most cases not be possible. Fast control of the current in the remaining phases can reduce the harmonic content of the inevitable torque ripple, or can be used to remove low-frequency components from this ripple. It is however not possible to reduce the amplitude of the ripple to less than 100% of the average torque, and substantial improvement of the torque requires a high peak current in the remaining phases. Remedial operation is therefore only possible if the mechanical system of the drive can withstand an important torque ripple and if the power converter can supply high peak currents.

An open circuit of a single switching device is a fault for which remedial operation can be realized with more success. Investigated was the case of a single-device open circuit in a six-switch voltage-source inverter. This fault opens one stator phase of the machine during a limited part of each period of the stator current. If the induction machine is used as a generator, the remaining devices can be used to obtain constant-torque remedial operation. This was realized using a new rotor-flux oriented control method, whose main idea consists of maintaining a constant torque while allowing – when necessary – a variation of the magnetizing current component. During motor operation, the open circuit of one phase lasts much longer. Unfortunately, it is for that case not possible to maintain a constant torque, nor can the amplitude of the torque variation be reduced below a theoretical 100% of the average torque. However, the new control reduces the width of the inevitable torque dip considerably. This reduction requires an increased current in most of the remaining devices. Also in this case the feasibility of remedial operation depends on the mechanical system and on the overcurrent capability of the converter.

Voltage faults – short circuits of a complete phase or of a single device – do in practice not allow any remedial operation of the induction machine. In the presence of a star-point connection, constant-torque remedial operation is theoretically possible even if a machine phase is constantly short-circuited. However, this would require extremely high currents, which no power converter is likely to be able to supply. For the case of a voltage-source inverter, operation during a short circuit of a single device also results in extremely high currents. It is theoretically impossible to control the remaining healthy devices yielding remedial operation without extreme torque dips and overcurrents.

To allow some kind of remedial operation, short circuits should therefore be avoided as much as possible. If they do occur, they should be transformed into an open circuit as soon as possible. Connecting the star point of the stator windings increases the possibilities for remedial operation considerably. Finally, faults should be limited to a single device whenever possible, leaving a maximum number of other devices intact.

Remedial operation requires an increase in the complexity of the control system. In this thesis, control systems as well as real-time simulations were implemented on a powerful digital-signal-processor system. Whereas further development of such systems will allow their application in industrial drives, it was shown that also using less sophisticated control hardware, remedial operating strategies can be implemented.

Acknowledgments

Preparing a Ph.D. thesis seems traditionally a very individualistic task. However, it is important to realize that this is only partly true. Discussing as well as working together with others on different related projects are an integral part of the work. Also the support and assistance from many people, whether related directly or indirectly to my project, was something that I could not do without and which helped me through the most difficult part.

First of all I therefore thank my parents for their support during all these years of studying. I realize that while spending a lot of time on my studies and time-consuming hobbies, I have often spent only little time with them. This I will surely regret when in future I will live at greater distance.

I especially thank my supervisor, Prof. Vandenput, for the discussions on the project as well as for the detailed comments on each chapter of this thesis. I also thank the members of the promotion committee for the suggestions and fruitful discussions. In particular I thank prof. De Doncker for the linguistic and other suggestions, as well as for the fact that he agreed to be my second supervisor. Always willing to improve the contents of my thesis, I am also very obliged to Prof. Kamerbeek, Prof. Schot and Dr. Bas Gravendeel for their detailed and sometimes fundamental comments, as well as to Dr. Jorge Duarte for his suggestions leading to some final improvements.

A special word of thanks is for Jos van der Burgt, with whom I was pleased to share an office during three years. It was very pleasant to discuss complicated and fundamental matters with him, so that together we could gain some insight. The fact that he started and finished his Ph.D. project one year before I did, meant that for some practical problems I could rely on his experience, and that I was warned about the quantity of time that the preparation of a thesis requires.

When developing the digital simulation and control system, as well as in the early practical experiments I learned very much from Dr. Blaschke. Many of the ideas which he implemented in analog electronics turned out to be invaluable also in a digital control system. For the development of the DSP system I owe many thanks to ing. Hans Verhagen and ing. Wim Thirion. For the practical work in the laboratory I am very obliged to Marijn Uyt de Willigen, who was always there to assist or find the required tools.

For the discussions on electrical machines, computers and other things I thank my colleague ir. Rob Kerkenaar. Often I believed that I would never succeed to convince him of the qualities of Apple Macintosh computers, but now I can invite anyone to ask him why he doesn't regret his decision. I sincerely regret his departure from the Electromechanics and Power Electronics group.

I also wish to thank all other colleagues from the Electromechanics and Power Electronics group, not only for their professional support but also for making a pleasant atmosphere. This also includes all Dutch and foreign students. Their presence was a positive contribution to the scientific, technical and social environment of the department. Moreover, I learned very much from the intelligent questions from different students – Dutch students as well as “IAESTE” trainees.

Last but not at least I thank all my friends from The Netherlands and abroad for their interest and their ability to share their time with me. Whereas I realize that especially during the last months I have not succeeded to free enough time to spend with them, I highly value making time for social contacts and greatly admire those who besides from doing a good job *always* are there for their friends. Thanks to all of you!

A handwritten signature in black ink that reads "Sjoerd Bosga". The script is cursive and fluid, with the first letter 'S' being particularly large and stylized.

Sjoerd Bosga

Table of Contents

1 Introduction	1
1.1 Asymmetrical supply of induction machines	1
1.2 Remedial operating strategies.....	3
1.3 Outline.....	4
2 Modeling the Induction Machine	7
2.1 Introduction	7
2.2 Assumptions	7
2.3 Creation of the air-gap flux.....	9
2.3.1 Relation between the currents and the magnetic flux density.....	9
2.3.2 Calculation of the self- and mutual inductances of the stator windings	11
2.3.3 Example-calculation of the magnetic flux density.....	12
2.3.4 Another method for calculating the self- and main inductances	17
2.4 Stator flux, air-gap flux and rotor flux	20
2.5 The electromagnetical torque and the mechanical equations	22
2.6 Transition to an equivalent orthogonal model	24
2.7 The voltage equations and simplification of the model using only one leakage inductance.....	29
2.8 Transition to the per-unit (pu) system.....	33
2.9 Summary of the equations of the induction machine.....	35
3 Field-Oriented Control of an Induction Machine	37
3.1 Introduction.....	37
3.2 Scalar control of an induction machine.....	38
3.3 Vector control of an induction machine.....	39
3.4 Field-oriented control of a current-fed induction machine.....	42
3.5 Field-oriented control of a voltage-fed induction machine.....	44
3.6 Methods to determine the flux vector.....	46
4 Modeling the Homopolar Impedance	49
4.1 Introduction.....	49
4.2 Calculation of the homopolar inductance	49
4.3 Extension to the orthogonal model	53
5 Classification of Asymmetrical Operation Modes	59
5.1 Introduction.....	59
5.2 The necessity for symmetrical operation	59
5.3 Current faults in case the star point is connected	62

5.3.1	A single-phase current fault	63
5.3.2	A two-phase current fault.....	66
5.4	Current faults in case the star point is not connected.....	67
5.5	Voltage faults	69
5.5.1	Voltage faults in two or more phases	69
5.5.2	A single-phase voltage fault in case the star point is connected	70
5.5.3	A single-phase voltage fault in case the star point is not connected.....	72
5.6	Overview of the different fault categories	73
5.7	Conditional faults	75
6	Asymmetrical Operation	
	of a Current-Fed Induction Machine	77
6.1	Introduction.....	77
6.2	Correcting a single-phase current fault using the homopolar current.....	78
6.3	Optimization of the remaining current in case two phase currents are zero	81
6.4	Addition of harmonic current components in order to minimize the torque ripple.....	81
6.4.1	Relation between harmonic current components and the torque	81
6.4.2	Numerical minimization of the torque ripple	85
6.5	Addition of harmonic current components to remove low-frequency torque ripple	90
6.5.1	Simplification of the torque equation for high speeds.....	90
6.5.2	Minimization of the rms value of the torque ripple	91
6.5.3	Removal of low-frequency torque-ripple components	93
6.6	A field-oriented approach to the torque-ripple problem	95
6.7	A comparison of the different fault-correction methods	100
7	Asymmetrical Operation of a Voltage-Fed	
	Induction Machine with the Star Point Connected	103
7.1	Introduction.....	103
7.2	Extension of the Voltage-Vector Calculator for operation with a homopolar current.....	103
7.3	Asymmetrical operation of the healthy drive.....	106
7.3.1	Simulation of the asymmetrically-fed drive.....	106
7.3.2	Experimental results with the asymmetrically-fed drive.....	112
7.4	Why asymmetrical operation causes a high saturation level	116
7.5	Asymmetrical operation in case of a single-phase current fault	120
7.5.1	Simulations of a single-phase open circuit without fault correction.....	120
7.5.2	Experiments of a single-phase open circuit without fault correction.....	126
7.5.3	Simulations of a single-phase open circuit using fault correction.....	129
7.5.4	Experiments of a single-phase open circuit using fault correction.....	130

7.6	Operation of the drive in other fault situations	132
7.6.1	Simulations of a two-phase open circuit without fault correction	132
7.6.2	Experiments of a two-phase open circuit without fault correction	138
7.6.3	Simulations of a single-phase short circuit	140
7.7	Conclusions.....	144
8	Asymmetrical Operation of a Voltage-Inverter-Fed Induction Machine	147
8.1	Introduction	147
8.2	Overview of the switching states of an inverter.....	148
8.3	Modeling the machine and the inverter for normal and fault situations.....	153
8.3.1	The model used for simulation of the machine and the inverter.....	153
8.3.2	The choice of a reference coordinate system for inverter control.....	159
8.3.3	Relation between the inverter state and the machine currents	162
8.3.4	The limit between normal and fault operation.....	167
8.4	Control methods for the voltage-source inverter	169
8.4.1	Three-phase hysteresis control.....	170
8.4.2	Optimized control for operation during faults.....	172
8.4.3	Implementation of the control on a multi-DSP system.....	177
8.5	Asymmetrical operation in case of a single-device fault.....	180
8.5.1	Simulation of the three-phase hysteresis control during an IGBT fault	180
8.5.2	Experiments with the three-phase hysteresis control during an IGBT fault.....	183
8.5.3	Simulation of the optimized control during an IGBT fault.....	185
8.5.4	Experiments with the optimized control during an IGBT fault.....	189
8.5.5	Limitations and problems related to the optimized control.....	193
8.5.6	Simulation of the optimized control during a single-device short circuit	194
8.6	Comparison with operation with one phase current equal to zero	195
8.7	Conclusions.....	198
9	Conclusions and Recommendations	201
9.1	Asymmetrical supply of induction machines	201
9.1.1	Current faults	202
9.1.2	Voltage faults	203
9.2	Remedial operating strategies.....	204
9.2.1	Current faults	204
9.2.2	Voltage faults	206
9.3	Recommendations.....	207
	References	209

A Real-Time Simulation of AC Drive Systems	215
A.1 Introduction	215
A.2 Requirements for a real-time digital drive simulator	216
A.3 Hardware description of the multi-DSP system.....	218
A.4 Simulation of an ac drive	219
A.4.1 Integration method and calculation order.....	219
A.4.2 From block diagram to simulation software	220
A.4.3 Additional DSP software	223
A.5 Conclusions.....	223
B Symbols and Notations	225
B.1 Notation.....	225
B.2 Symbols	226
B.3 Reference frames and vector components	226
B.4 Circuits, windings and coils.....	227
B.5 Harmonic components and other special notations	229
B.6 Examples	230
B.7 Elements used in block diagrams.....	231
C Description and Parameters of the Experimental Setup	233
C.1 Per-unit reference values.....	233
C.2 The cycloconverter-fed induction-motor drive	233
C.3 The voltage-source inverter-fed induction-motor drive	234
Samenvatting	235
Resumo	237
Curriculum Vitae	239

Chapter 1

Introduction

1.1 Asymmetrical supply of induction machines

Under normal operating conditions, standard three-phase induction machines are supplied in a symmetrical way. In other words, apart from a phase difference each winding is in steady state supplied with an identical voltage or current. Due to the symmetry in the electromagnetic construction of the machine itself, this is the most suitable way to supply the machine.

Symmetrical supply is however not the only suitable supply in all cases. Evidently, if a machine is constructed asymmetrically, the supply must be adapted to this situation. A recent paper on the behavior of asymmetrical machines is [Alwa-95], but also in the past many authors have examined this subject, often using the Space-Phasor theory introduced in [Štěp-67]. In an originally symmetrical machine, asymmetries can occur due to faults, causing asymmetrical supply. Short circuits in the stator windings and broken rotor bars are well-known examples of this. A large number of investigations targeted reliable detection of these faults.

Asymmetrical machines as well as faults inside the machine are however not very common. On the contrary, the induction machine by itself is a very robust and reliable machine. As reported in [Hann-93] and [Thor-95], industrial users consider the induction machine to be one of the most reliable components of a complete drive system. The supply of the machine on the other hand is much less reliable. For example, faults can occur in the utility grid, resulting in unbalanced voltages at the input of the power converter or the machine (see [Smol-92]). Serious faults at the grid side of a converter can have a considerable effect on the behavior of the machine, as shown for example in [Akpi-96]. The effect will of course depend on the fault, the type of converter, and last but not least the inverter/machine control system.

The surveys discussed in [Hann-93] and [Thor-95] indicate that an important category of failures of variable frequency drives is due to faults in the power converter. Some of these faults, such as a faulty cooling fan, will affect the complete converter. Others however, such as faulty devices or faulty control circuits, may initially affect only a single phase of the converter. Whereas [Thor-95] reports that most converter failures are related to the control circuits (53%) and a smaller percentage to the power part (38%), [Hann-93] reports that most problems are related to component failure (60%), 48% to failure in logic boards, 48% to a blown fuse, and 41% to tripping out.

The effects of a power device fault or a fault in the auxiliary circuits can sometimes be identical. For example, [Swam-93] reports a faulty optocoupler causing a power device to remain switched on. The result is the same as if a GTO had failed: a short circuit between one phase of the machine and the dc-link capacitor. Also, the effect of a blown fuse can be compared with the failure of an IGBT module: an open circuit of one or more phases.

If, in the presence of such a fault, there is still a possibility to supply the machine, i.e., not all converter phases are completely disabled, this supply will often be asymmetrical. An important question is therefore how the machine will react to different kinds of asymmetrical supply. For example, what will happen to the torque delivered by the machine in case one of the machine phases is opened? What will happen in case of a short circuit?

To find an answer to these questions, a model of the machine is required that can be used in case of asymmetrical supply. Also the control system, which has considerable influence on the behavior of the drive in case of a fault, must be taken into consideration. As it is virtually impossible to examine every possible fault in every possible converter, a classification of faults has to be introduced. For the most interesting fault categories, calculations, simulations and wherever possible also experiments can then be used to study the impact of the fault on the drive. In literature, except for [Elch-91] and [Gent-92], investigations on the behavior of electrical machines during converter faults have mainly been focused on types of machines other than the induction machine.

Asymmetrical supply related to unbalances, caused for example by small differences between the switching devices, will not be considered. The reason for this is that correction for unbalance requires a completely different strategy than correction for faults. For example, if the current in one device is lower than the current in other devices due to unbalance, correction would be targeted at increasing this current to remove the asymmetry. If a device current is zero due to a fault, increasing this current is no option. Instead, correction should target compensation of the loss using the other devices, maintaining the asymmetry.

This thesis will be limited to operation under asymmetrical supply of a standard, three-phase induction machine. Other types of machines, and also multi-phase induction machines (machines having more than three stator phases) will not be considered. For multi-phase machines (see [Jahn-80]), a fault that affects a single phase has a less serious impact on the behavior of the drive than is the case for the standard three-phase machine.

Also the actual detection of faults that cause asymmetrical supply, will not be considered in this thesis. If required, a fast and accurate diagnosis of a converter fault can relatively easily be obtained. In [Crai-93] it was shown that it is relatively easy to implement a detection mechanism to identify the exact device that has failed. Also the protection mechanisms built into standard converters can be used for converter-fault diagnosis.

1.2 Remedial operating strategies

The possibility to supply the machine asymmetrically might result in an increase of reliability of standard converter-fed three-phase induction-machine drives. If a converter fault is present, the machine might temporarily be supplied asymmetrically, until a suitable moment to repair the drive has arrived or until another system can take over.

In this thesis it will be examined what possibilities for such remedial operation are available without substantially extending or modifying the standard converter circuit. Evidently the number of possibilities would be much larger if such modifications were considered also. One possibility is for example to add a connection to the star-point of the machine, connecting it for example to a fourth inverter branch or to the midpoint of the dc-link capacitor. In [Elch-94] it was shown that then remedial operation while one machine phase is open-circuited is very well possible. In [Fu-93] a method was introduced to disconnect a converter phase in which a short circuit is present, and to use the star-point connection to allow remedial operation. In [Liu-91] and [Liu-93] this remedial operation was investigated further. Although simulations in these papers indicated an excellent behavior during the fault, measurements showed considerable variations of the torque.

For a standard inverter circuit, remedial operation in case one machine phase becomes open circuited is only possible if the mechanical system of the drive can withstand considerable stresses. It will be investigated how these stresses can be limited. Experimental results of one method to reduce stresses were shown in [Kast-94] and [Kast-95].

In practice, not every failure causes open- or short-circuiting of a complete phase. An interesting situation occurs if a fault is limited to a single device in a power converter. In this case the asymmetry is less serious, and it will be investigated whether and under which conditions remedial operation can be realized. Initially this case will be examined using field-oriented control, introduced in [Blas-71], because this method gives a clear insight in the behavior of the torque and the flux in the machine during the fault. For an improved behavior during faults, a new control method will be developed.

In literature some investigations were found related to remedial operation of other types of machines. A three-phase brushless dc drive was investigated in [Spée-90], showing an interesting possibility for remedial operation in case of an open-transistor fault. Fault operation of switched reluctance motors was investigated in [Arka-94]. That a specially designed machine can have a much better behavior during faults than a standard machine, was shown for a permanent-magnet machine in [Jack-96] and [Mecr-96]. Also multi-phase induction machines can effectively be used if remedial operation is required even in case of the loss of a complete phase, as shown for example in [Fu-93b] and [Zhao-96].

1.3 Outline

The objective of this thesis is to determine under which circumstances asymmetrical supply can be used to obtain increased reliability of standard converter-fed three-phase induction machine drives. It will be investigated which is the best operating strategy for the drive while a fault in the power converter is present, and what kind of stresses this remedial operation imposes on the drive.

In Chapter 2, a model of the induction machine will be derived that is valid for any kind of symmetrical and asymmetrical supply, under the assumption that the air-gap induction is a sinusoidal function of the position along the air gap. It will be shown that this assumption may not be valid if a homopolar current is present in the machine, a case that will be treated separately. The equations derived in this chapter will be identical to those used for example by Blaschke and Vandenput in [Blas-96], except for the modeling of the leakage inductance. The main purpose of this chapter is to examine the validity of the commonly used machine model for asymmetrical supply, and to introduce the physical background and modeling methods required to extend the model for the case a homopolar current is present.

Several more or less standard control methods of the induction machine will be presented in Chapter 3, for a current-fed as well as for a voltage-fed machine. The rotor-flux oriented machine models introduced in this chapter will be used throughout the rest of the thesis, to be extended only for the case a homopolar current is present.

The concept of a homopolar impedance will be introduced in Chapter 4. With this homopolar impedance it will be possible to model the effect of a homopolar current in the machine, which causes a third harmonic in the air-gap induction. Such a current will be present during remedial operation in case the star-point of the machine is connected. It will be shown how a standard machine model can be extended to include effects related to the homopolar impedance.

Chapter 5 will start with a more precise definition of symmetrical and asymmetrical supply, and will demonstrate that symmetrical sinusoidal supply is the preferred choice for no-fault steady-state operation. Then, a classification of asymmetrical operation modes will be presented. Operation modes will be distinguished by their ability to provide constant torque and by the kind of fault. Two kinds of faults will be investigated: voltage faults (short circuits) and current faults (open circuits).

An important parameter in the design of remedial operation modes for a machine is whether the machine is current- or voltage-fed. Of these two possibilities, Chapter 6 will present the case of an induction machine fed by an ideal current source. For different faults, the possibilities for remedial operation will be discussed. The larger part of this

chapter will be dedicated to operation in case only a single current is available to supply the machine.

The voltage-fed induction machine is modeled as a current-fed machine extended with the stator-voltage equations. In Chapter 7 it will first be shown how a homopolar current can be introduced in this machine, and how this affects the behavior of the machine. Experiments will be presented using a cycloconverter, i.e., a voltage-source converter in which a star point is naturally available for connection with the machine's star point. Experiments will show the behavior of the drive in different fault conditions, without and with correction using the homopolar current. Due to the limited bandwidth of the cycloconverter, it will not be possible to optimize the torque during fault situations in the way presented in Chapter 6 for the case of an ideal current-source converter.

A voltage converter with a much larger bandwidth will be presented in Chapter 8. For the current-controlled voltage-source inverter used in this chapter, a remedial operating strategy will be developed, allowing continued operation in case of a single-device fault. This remedial operation will be compared with a standard inverter control, to demonstrate what improvements to fault operation are theoretically possible. It will be shown that one of the control strategies designed in Chapter 6 for the machine fed by an ideal current source converter, can also be used for the current-controlled voltage-source inverter. However, whereas in Chapter 6 the loss of a complete phase is considered, this chapter will focus on the loss of a single device. It will be shown that this is a much more favorable situation.

Chapter 9 will present the conclusions of this thesis, as well as recommendations and some subjects remaining for future investigations.

An important part of the practical work related to this thesis consisted of the development of a real-time digital simulation and control system. Appendix A will present the multi-DSP (Digital Signal Processor) system and the software developed for this system in general and for this thesis in particular. This DSP system was an invaluable aid for the investigations on the different fault-operation modes, and was an absolute requirement to implement the control of the voltage-source inverter presented in Chapter 8.

A considerable amount of different symbols will be used in the equations and block diagrams throughout this thesis. Instead of providing a list, Appendix B will present the rules according to which the symbols are put together, as much as possible in a systematical way. This appendix also includes a list of the basic building blocks used in the different block diagrams.

Finally Appendix C will list the parameters of the converters and the machines used for the practical experiments.

Chapter 2

Modeling the Induction Machine

2.1 Introduction

In this chapter a model of the induction machine will be derived. Starting with a three-phase induction machine, an orthogonal two-phase model will be introduced. This model will however only be valid under the assumption that the magnetic induction in the air gap is a sinusoidal function of the position along the air gap.

The equations derived here, correspond to those commonly used in literature. The derivation in this chapter is however required to allow an extension of the model to obtain a more general validity. This is done in Chapter 4, where – using the same methods as will be used in this chapter – the model will be completed with the equations describing the effect of a homopolar current.

Before starting the actual derivation, a number of assumptions will be introduced. These are required to obtain a practically workable model, but will inevitably introduce a number of simplifications. A clear overview of all assumptions is required to explain differences between theoretical, simulated and experimental results.

2.2 Assumptions

Before deducing a model of the induction machine that will be used throughout this thesis, a number of assumptions has to be made. This is necessary to reduce the complexity of the machine model to a level where the equations are simple enough to be studied analytically and by simulations. The model parameters can then be obtained from relatively simple measurements or calculations based on the machine-design parameters. Due to these simplifications, differences between the real machine and the simulations will exist. A clear overview of all assumptions used to derive the model will help to understand the differences between simulated and experimental results. A list of assumptions is given below:

- * This thesis will consider only three-phase induction (asynchronous) machines. These machines have three windings on the stator. The rotor can either also have three windings or have a squirrel cage. The rotor circuit is always short-circuited. Wherever the choice of rotor type makes a difference, this will be indicated. For other types of machines and for machines with a different number of phases, the behavior and control during faults will generally be different. For example, in a multi-phase machine, a

machine with more than three phases, even after a complete loss of one phase, a constant torque can theoretically still be obtained. Some of the theory developed will however also be valid for other types of machines.

- * The three stator windings are identical and positioned symmetrically along the stator bore. In case of a wound rotor, the same is *mutatis mutandis* true for the rotor windings.
- * The stator and rotor are concentric and the air gap which separates them has constant width. Saliency will not be considered. Variation of the air-gap width due to the slots will roughly be compensated for by using an equivalent constant air-gap width, which is somewhat larger than the minimal distance between the stator and rotor iron. Dependency of leakage inductances on the rotor position, caused by the slots, is neglected.
- * End effects will not be considered. All calculations are performed on a two-dimensional model, thus also skewing effects are neglected.
- * An ideal magnetic circuit is assumed. This means that the relative magnetic permeability is constant and very large. As a consequence, no hysteresis losses will occur. Due to lamination no currents in axial direction can exist in the iron, while currents in other directions (Eddy currents) can be neglected.
- * All conductors have a negligible cross-section. The skin effect will therefore not be taken into account.
- * The air-gap width is very small compared to the length and the diameter of the stator bore. Therefore, only the radial component of the air-gap induction will be considered, which will be approximated by a constant function of the radial position.
- * The width of stator and rotor slot openings is negligible. The calculated magnetic induction in the air gap will therefore change stepwise as a function of the angular position. In some calculations the induction will however be approximated by a sum of sinusoidal functions.
- * Displacement currents are neglected.
- * Machine parameters that are not necessarily constant as a function of time are assumed to vary only so slowly that they can safely be treated as constants.
- * After Chapter 2, all calculations are performed based on a per unit system (pu), as explained in Section 2.8.
- * The machine is fed by a power converter that can act either as a voltage or as a current source. The applied voltages or currents are not necessarily sinusoidal or of constant frequency or amplitude.

* Only two-pole machines will be considered, except in some sections related to the calculation of inductances, where this will be stated explicitly. This is not a fundamental limitation of the theory described in this thesis, but merely facilitates understanding.

2.3 Creation of the air-gap flux

The objective of the electrical machine is the conversion from electrical into mechanical energy or vice versa. To produce torque, a non-zero radial component of the air-gap magnetic induction must be present. Typically this magnetic induction varies sinusoidally with the angular position along the air gap. In this section the relation between the currents in the stator windings (the stator currents) and the air-gap magnetic induction will be derived, and also the self- and mutual inductances of the stator windings. For these derivations the rotor currents are assumed to be zero. Finally, the derivation of the inductances will be compared with a more traditional method, found in literature.

2.3.1 Relation between the currents and the magnetic flux density

Figure 2.1 shows the magnetic flux density (the magnetic induction) in the air gap of a two-pole machine in the ideal case. Under most operating conditions the induction will vary sinusoidally as a function of both the angular position θ^s and the time t , resulting in a traveling induction wave. Equation 2.1 describes the radial component of the induction in the ideal case, where ω is an angular frequency and b denotes the maximum induction.

$$b_{\perp} = b \cdot \cos(\theta^s - \omega t) \quad (2.1)$$

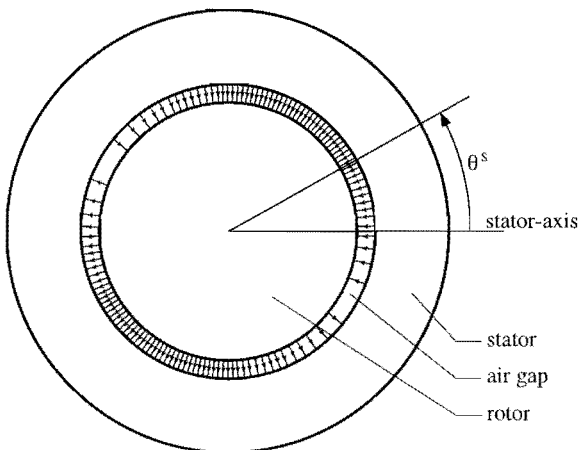


Figure 2.1. The magnetic induction in the air gap in the ideal case.

To obtain this ideal flux distribution in the air gap, it would be necessary to have a magnetomotive force that varies sinusoidally as a function of θ^s . This MMF can be created only by a sinusoidal current sheet along the air gap. However, in a real machine the current distribution is not sinusoidal. The current is present only in the conductors, which are located in the slots of the stator and the rotor iron.

To obtain b_1 for a given winding configuration, it will first be calculated for the case where a current i_{sa} is flowing in one coil having n_{sa1} turns, at a position ζ_{sa1}^s in the stator, as shown in figure 2.2. For simplicity, the slots have been drawn as if they were completely closed.

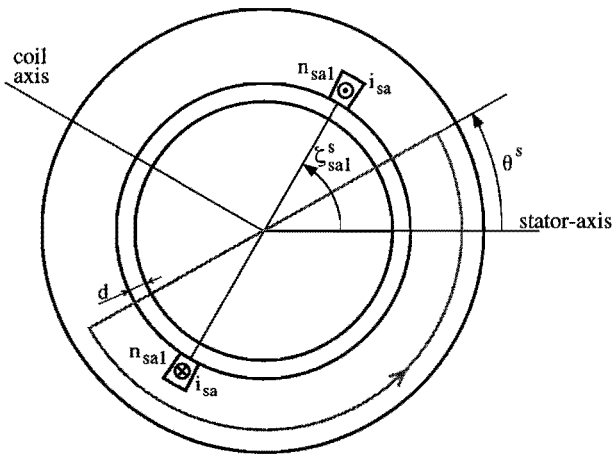


Figure 2.2. Calculation of the magnetic induction in case a single diameter coil is placed in the stator.

Only the case where opposite to each coil side there is another coil side with the same number of conductors will be considered. Furthermore, the current in the two coil sides is flowing in opposite directions. (However, the two coil sides should not necessarily belong to the same coil. As illustrated in the example of section 2.3.3, in practice this is usually not the case.) This premise guarantees a symmetrical yoke flux with respect to the coil axis (indicated in figure 2.2), yielding an optimal utilization of the stator iron.

It follows from figure 2.2 that the magnetomotive force acting in the path indicated at position θ^s can be calculated using $\oint h \cdot dl = i_{\text{enclosed}}$, by integrating in the indicated direction. The current coming out of the paper (indicated by \odot) should be taken positive, the current going into the paper (\otimes) negative. Due to the very high permeability of the stator and rotor iron, as assumed in section 2.2, the magnetic field strength h will be zero in the iron. The integral $\oint h \cdot dl$ can therefore be calculated easily, resulting in equation 2.2, keeping in mind the assumption that h is independent of the radial position in the air gap. Here $h_1(\theta^s)$ is the radial magnetic field strength in the air gap, which is taken positive in the direction toward the center of the rotor.

$$\begin{aligned} \left(\zeta_{\text{sal}}^s < \theta^s < \zeta_{\text{sal}}^s + \pi \right) \quad h_{\perp}(\theta^s) \cdot d - h_{\perp}(\theta^s + \pi) \cdot d &= n_{\text{sal}} \cdot i_{\text{sa}} \\ \left(\zeta_{\text{sal}}^s + \pi < \theta^s < \zeta_{\text{sal}}^s + 2\pi \right) \quad h_{\perp}(\theta^s) \cdot d - h_{\perp}(\theta^s + \pi) \cdot d &= -n_{\text{sal}} \cdot i_{\text{sa}} \end{aligned} \quad (2.2)$$

Because of symmetry it is evident that $h_{\perp}(\theta^s) = -h_{\perp}(\theta^s + \pi)$. Substituting this result into equation 2.2, equation 2.3 is obtained.

$$\begin{aligned} \left(\zeta_{\text{sal}}^s < \theta^s < \zeta_{\text{sal}}^s + \pi \right) \quad h_{\perp}(\theta^s) \cdot 2d &= n_{\text{sal}} \cdot i_{\text{sa}} \\ \left(\zeta_{\text{sal}}^s + \pi < \theta^s < \zeta_{\text{sal}}^s + 2\pi \right) \quad h_{\perp}(\theta^s) \cdot 2d &= -n_{\text{sal}} \cdot i_{\text{sa}} \end{aligned} \quad (2.3)$$

In the air gap, a linear relation exists between $b_{\perp}(\theta^s)$ and $h_{\perp}(\theta^s)$, namely $b_{\perp}(\theta^s) = \mu_0 \cdot h_{\perp}(\theta^s)$. The resulting $b_{\perp}(\theta^s)$ is shown in figure 2.3.

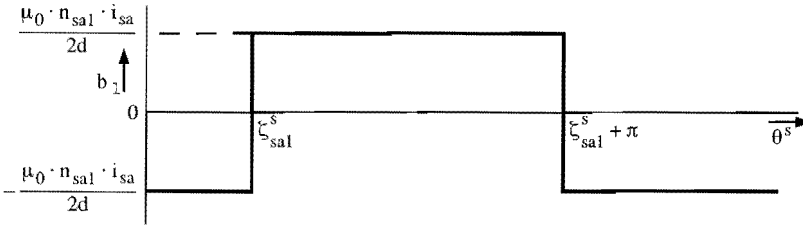


Figure 2.3. The air-gap induction for the case where a current flows in a single diameter coil.

In general, each of the three stator windings a, b and c consists of several groups. Each group consists of a number of coils connected in series. To simplify the analysis, only the case where all groups in one winding are connected in series is considered. This means that each coil in stator winding q will carry the same current i_{sq} . Under the assumption that no saturation occurs, the magnetic induction in the air gap can be calculated as a summation over the contributions from the k_{sq} coils of each of the windings. This is described by equation 2.4, where $b_{\perp qk}(\theta^s)$ is the induction caused by a current i_{sq} flowing in coil k of stator phase q.

$$b_{\perp}(\theta^s) = \sum_{q=a,b,c} \sum_{k=1}^{k_{\text{sq}}} b_{\perp qk}(\theta^s) \quad (2.4)$$

2.3.2 Calculation of the self- and mutual inductances of the stator windings

The magnetic flux linking a coil can be calculated by integrating the magnetic flux density b over an arbitrary open surface bounded by this coil and by multiplying the result by the number of turns in the coil. Equation 2.5 is obtained when choosing the integration

surface to be in the middle of the air gap and assuming that the coil is located in the air gap. Leakage flux, which is flux linking a coil which does not cross the air gap, is in this way neglected. In equation 2.5 ψ_{sqk} is the flux linking coil k , r is the radius of the rotor, ℓ is the effective axial length of the air gap, ζ_{sqk1}^s is the position of one coil side with respect to the stator and ζ_{sqk2}^s is the position of the other coil side, both belonging to coil k of stator phase q .

$$\psi_{sqk} = n_{sqk} \cdot \int_{\zeta_{sqk1}^s}^{\zeta_{sqk2}^s} b_1(\theta^s) d\theta^s \cdot r \cdot \ell \quad (2.5)$$

The total flux linking one winding, where all coils are assumed to be connected in series, is given by equation 2.6, where k_{sq} denotes the number of coils in stator winding q .

$$\psi_{sq} = \sum_{k=1}^{k_{sq}} \psi_{sqk} \quad (2.6)$$

The relation between this total air-gap flux linkage and the current in the corresponding winding, in case the currents in all other windings are zero, defines the self-inductance $l_{sq,q}$ of the winding, as given in equation 2.7. The self-inductances of the other windings, which are assumed to be identical, have the same value.

$$\psi_{sq} = l_{sq,q} \cdot i_{sq} \quad (2.7)$$

To find the mutual inductance $l_{sa,b}$ between the phase-a and phase-b stator windings, the currents in phase a and c are taken zero. The air-gap induction is then calculated as a function of the current in the coils of phase b. Using equations 2.5 and 2.6, the flux linking phase a can be determined. The mutual inductance can then be found using equation 2.8. The mutual inductances between the other stator phase windings can be calculated in the same way. Due to the symmetry of the machine all mutual inductances will be equal.

$$\psi_{sa} = l_{sa,b} \cdot i_{sb} \quad (2.8)$$

2.3.3 Example-calculation of the magnetic flux density

As an example, the winding configuration shown in figure 2.4 will be considered. This is a possible configuration for a two-pole three-phase machine, where 24 slots are filled with two layers of coil sides. The windings are so-called fractional pitch windings – the coils, of which one side is in the upper, the other in the lower layer, are shorter than the pole pitch

(180° for a two-pole machine). The number of turns of each coil is n_{sk} and the three phase currents are i_{sa} , i_{sb} and i_{sc} respectively. Again the slots are drawn as if they were closed.

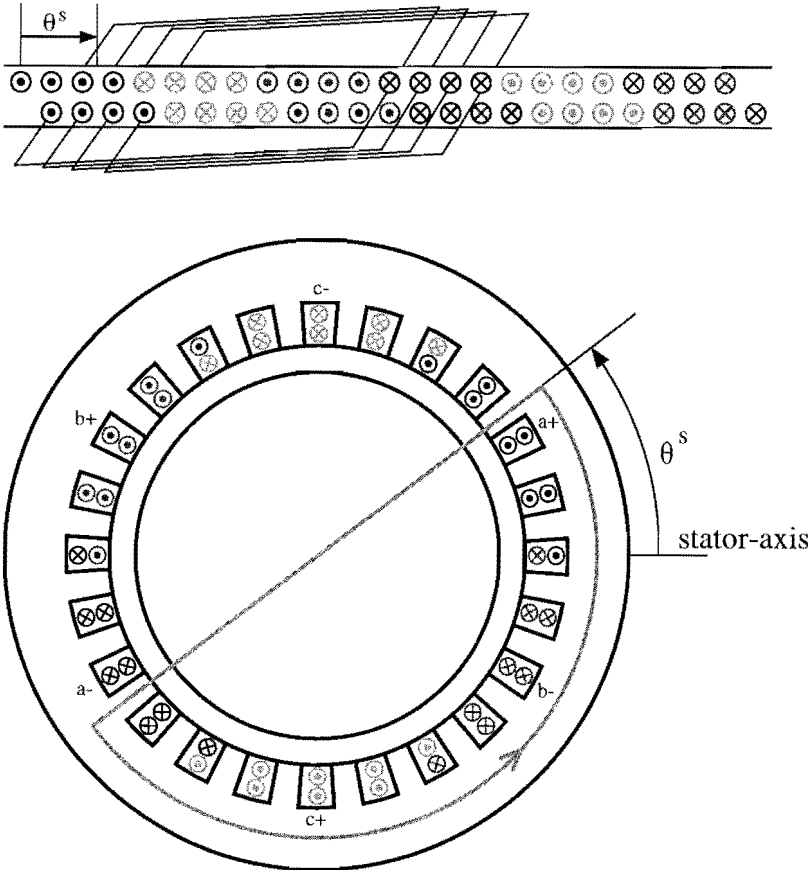


Figure 2.4. An example winding configuration with 24 slots and two layers.

Figure 2.5 illustrates the calculation of the air-gap induction in case $i_{sa} = i_s$, $i_{sb} = i_{sc} = 0$. The first two rows indicate how the coils are placed in the slots. For example, 'a+' indicates that in the concerning slot a coil side belonging to phase a is placed, in which the current i_{sa} will flow in positive direction with respect to the contour along which $\oint \mathbf{h} \cdot d\mathbf{l}$ is calculated.

The next two rows indicate the current in the coil sides, while the last row indicates the total current in each slot. The values have to be multiplied by $n_{sk} \cdot i_s$ to obtain the actual current. The graph shows the magnetomotive force (abbreviated MMF) $\oint \mathbf{h} \cdot d\mathbf{l}$ as a function of θ^s , calculated along the contour indicated in figure 2.4. Again, the scale factor $n_{sk} \cdot i_s$ should be applied.

Coil sides in slots:

a+ a+ a+ a+ c- c- c- b+ b+ b+ b+ a- a- a- a- c+ c+ c+ c+ b- b- b- b-
 b- a+ a+ a+ a+ c- c- c- c- b+ b+ b+ b+ a- a- a- a- c+ c+ c+ c+ b- b- b-

Currents (to be multiplied with $n_{sk} \cdot i_s$):

1	1	1	1	0	0	0	0	0	0	0	-1	-1	-1	-1	0	0	0	0	0	0	0	0	0
0	1	1	1	1	0	0	0	0	0	0	0	-1	-1	-1	-1	0	0	0	0	0	0	0	0
1	2	2	2	1	0	0	0	0	0	0	-1	-2	-2	-2	-1	0	0	0	0	0	0	0	0

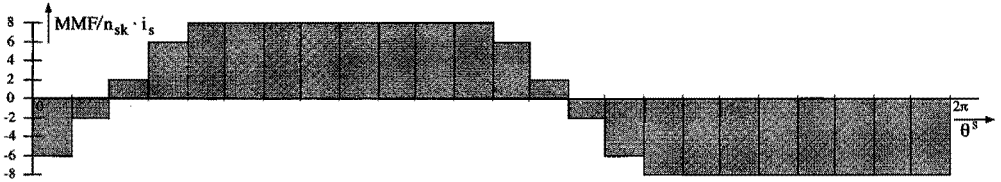


Figure 2.5. Calculation of the MMF for the example winding configuration.

As can be seen from equation 2.3, the magnetic field strength $h_1(\theta^s)$ can be found by dividing the MMF by $2d$. That this equation is valid although the coil sides are less than 180° apart can be understood considering that the same current distribution could be obtained using diameter coils. To obtain $b_1(\theta^s)$, a further multiplication by μ_0 is needed, resulting in equation 2.9.

$$b_1(\theta^s) = \mu_0 \cdot h_1(\theta^s) = \mu_0/2d \cdot \text{MMF}(\theta^s) \tag{2.9}$$

The induction $b_1(\theta^s)$ has thus the same waveform as the MMF. As can be seen from figure 2.6, if only one phase is used to generate the magnetic induction, the resulting waveform contains several space harmonics, including a third harmonic. A much better waveform is obtained when all three windings are symmetrically supplied with a current. This is shown in figures 2.7 and 2.8, which are explained later in this section.

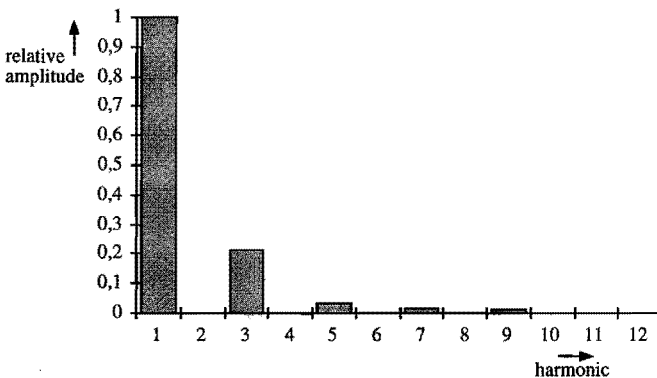


Figure 2.6. The frequency spectrum of $b_1(\theta^s)$ in the example winding configuration.

The main reason to supply more than one winding with current is of course the generation of a rotating magnetic flux distribution, which has been described by equation 2.1 for the ideal case. In the example given here only the most common case will be

studied, where the three phase currents are sinusoidal and have a phase difference of 120° . Equation 2.10 describes the currents for this case.

$$\begin{aligned} i_{sa} &= i_s \cdot \cos(\omega t) \\ i_{sb} &= i_s \cdot \cos(\omega t - 2\pi/3) \\ i_{sc} &= i_s \cdot \cos(\omega t - 4\pi/3) \end{aligned} \tag{2.10}$$

Figure 2.7 shows the currents in each slot and the MMF at $t=0$ ($i_{sa}=i_s$, $i_{sb}=i_{sc}=-1/2 i_s$), for the same winding configuration as in the previous example. Again, the numerical values have to be multiplied by $n_{sk} \cdot i_s$. A comparison of the resulting spectrum of the magnetic induction waveform along the air gap with the previous case, shows that now a much better waveform is obtained. In this case, no third harmonic is present, as can be seen in figure 2.8. In general, if a symmetrical three-phase machine is fed in such a way that the sum of the currents is zero, no third harmonic will be present in the air-gap magnetic induction. The same is true for any space harmonic which is a multiple of three.

Coil sides in slots:

a+ a+ a+ a+ c- c- c- c- b+ b+ b+ b+ a- a- a- a- c+ c+ c+ c+ b- b- b- b-
 b- a+ a+ a+ a+ c- c- c- c- b+ b+ b+ b+ a- a- a- a- c+ c+ c+ c+ b- b- b- b-

Currents (to be multiplied with $n_{sk} \cdot i_s$):

1	1	1	1	0,5	0,5	0,5	0,5	-0,5	-0,5	-0,5	-0,5	-1	-1	-1	-1	-0,5	-0,5	-0,5	-0,5	0,5	0,5	0,5	0,5	
0,5	1	1	1	1	0,5	0,5	0,5	0,5	-0,5	-0,5	-0,5	-0,5	-1	-1	-1	-1	-0,5	-0,5	-0,5	-0,5	0,5	0,5	0,5	0,5
1,5	2	2	2	1,5	1	1	1	0	-1	-1	-1	-1,5	-2	-2	-2	-1,5	-1	-1	-1	0	1	1	1	

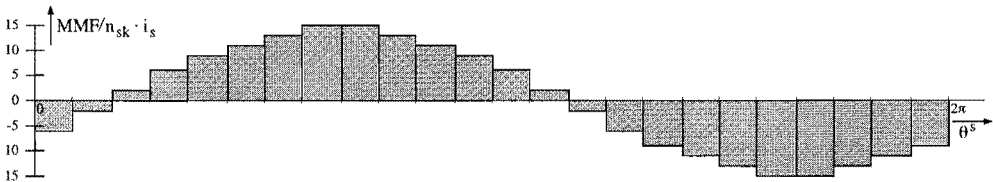


Figure 2.7. Calculation of the MMF for the example winding configuration when a symmetrical three-phase current system is supplied, at $t=0$.

To calculate the flux ψ_{sa} linking phase a, the integration given in equation 2.5 has to be performed for each coil belonging to the phase-a winding, substituting therefore a for q. After this, the flux can be calculated using the summation from equation 2.6. For the first example, where all currents except i_{sa} are zero, the following result is obtained (with $i_{sa}=i_s$):

$$\psi_{sa} = 24 \frac{2}{3} \cdot \frac{\mu_0 \pi r \ell (n_{sk})^2 i_s}{d} \tag{2.11}$$

Using equation 2.7 the self-inductance $l_{sa,a}$ of phase a can be calculated. The result is given in equation 2.12.

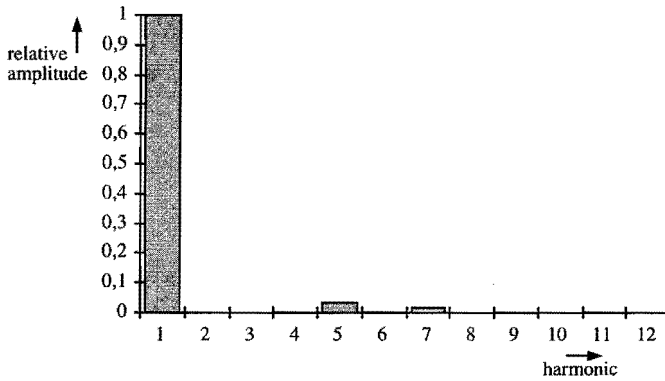


Figure 2.8 The frequency spectrum of $b_1(\theta^s)$ in the example winding configuration when a symmetrical three-phase current system is supplied, at $t=0$.

$$l_{sa,a} = 242/3 \cdot \frac{\mu_0 \pi r \ell (n_{sk})^2}{d} \quad (2.12)$$

If the same equations are applied to the second example, the calculated flux is not only the flux created by the current i_{sa} in the phase-a winding but also by the currents i_{sb} and i_{sc} in the other two windings, due to the mutual coupling between the stator windings, as shown in equation 2.13.

$$\psi_{sa} = l_{sa,a} \cdot i_{sa} + l_{sa,b} \cdot i_{sb} + l_{sa,c} \cdot i_{sc} \quad (2.13)$$

This equation can be simplified using the fact that the mutual coupling between phase a and c will be the same as between phase a and b. In case of a supply for which the sum of the three phase currents equals zero, a further simplification is possible. The result is shown in equation 2.14.

$$\psi_{sa} = l_{sa,a} \cdot i_{sa} + l_{sa,b} \cdot (i_{sb} + i_{sc}) = l_{sa,a} \cdot i_{sa} + l_{sa,b} \cdot (-i_{sa}) \quad (2.14)$$

By combining the two inductances $l_{sa,a}$ and $l_{sa,b}$ into one single inductance this equation is transformed into equation 2.15.

$$\psi_{sa} = (l_{sa,a} - l_{sa,b}) \cdot i_{sa} = l_{sq} \cdot i_{sa} \quad (2.15)$$

The inductance l_{sq} introduced by this equation is the so-called main inductance. It can be calculated using the equations 2.5, 2.6 and 2.7, with the data from figure 2.7. The result is given in equations 2.16 and 2.17. As can be seen from equation 2.17, the main inductance is approximately 1.5 times larger than the self-inductance $l_{sa,a}$ calculated in equation 2.12. As will be shown in the next section, this factor will be exactly 1.5 in case sinusoidally distributed windings are considered.

$$\psi_{sa} = 35\frac{1}{3} \cdot \frac{\mu_0 \pi r \ell (n_{sk})^2 i_s}{d} \quad (2.16)$$

$$l_{sq} = 35\frac{1}{3} \cdot \frac{\mu_0 \pi r \ell (n_{sk})^2}{d} \quad (2.17)$$

2.3.4 Another method for calculating the self- and main inductances

Most textbooks on electrical-machine design use a method for calculating the self- and main inductances which is different from the one described in the previous section. For comparison in this section the method described in [Jord-75] will shortly be discussed. Due to the somewhat different approach, the symbols used in this section are not completely in agreement with the list of symbols in Appendix B.

In a first approximation Jordan considers an m -phase $2p$ -pole machine where each stator winding consists of p diameter coils of n_{sq}/p turns each. This means that if there is current in only one phase the air-gap induction will be a $2p$ -pole square wave.

In the subsequent equations it is however assumed that there is a sinusoidal magnetic induction $b_1 = b \cdot \cos(p\theta^s - \omega t)$ in the air gap of this machine (cf. equation 2.1). Equation 2.18 is obtained by integrating this induction over the surface of each coil and summing over all coils in a phase (cf. equations 2.5 and 2.6). In this equation ψ_s is the peak value of the flux linking a phase.

$$\psi_s = n_{sq} \cdot \frac{2}{\pi} b \frac{r\pi}{p} \ell = 2 n_{sq} b \frac{r\ell}{p} \quad (2.18)$$

Jordan actually calculates the rms value of the induced voltage for this case, but this is not necessary here. The peak value b of the sinusoidal magnetic induction is calculated from the square-wave magnetic field strength $h(\theta^s)$ caused by a single phase current by multiplying its amplitude with $4/\pi \mu_0$. The magnetic field strength itself is calculated according to equation 2.2. In an m -phase machine supplied by a symmetrical set of currents, the first harmonic of the induction is higher than for the case a single phase is fed. To account for this effect, a further multiplication of b by $m/2$ is required. The resulting b is given in equation 2.19.

$$b = \frac{m}{2} \cdot \mu_0 \frac{4}{\pi} \cdot \frac{1}{2d} \cdot \frac{n_{sq}}{p} i_s = \mu_0 \frac{mn_{sq}}{\pi dp} i_s \quad (2.19)$$

Substituting this equation into 2.18 and dividing the flux by the current, a value for the main inductance is found, given in equation 2.20.

$$l_{sq} = \mu_0 \frac{2\pi r \ell}{\pi d p^2} (n_{sq})^2 \quad (2.20)$$

The inductance calculated here is smaller than if the actual air-gap induction had been used, because all harmonics were neglected. Especially in this simplified case where the actual induction is a square wave, the difference is considerable. Jordan calls this difference the *Oberwellenstreuungsfeld*, a leakage flux due to higher harmonics in the air-gap induction, because it appears as a supplementary, not calculated flux in the equations. Other leakage fluxes, such as those caused by end effects or by slot effects, appear in a similar way. It is accounted for by using a higher value of the total stator leakage inductance.

In a machine with distributed windings, where the coils of each phase are in different slots and in different layers, the waveform of the induction will be closer to a sine wave, and the calculation method used by Jordan will be a better approximation. However, both the relations between the current and b and between b and ψ_s will be different from those in equations 2.18 and 2.19. Jordan proves that this difference can be accounted for by replacing the number of turns n_{sq} in a winding by an effective number of turns, $\xi_1 n_{sq}$, in both equations, and thus also in equation 2.20.

To calculate the value of this so-called winding factor ξ_1 , Jordan bases his calculations on the Fourier development of the current distribution along the air gap caused by the current in a single conductor. Because a current can only be present in a closed circuit, the return current is in this way of reasoning supposed to flow outside of the machine, and only in a later stage of his calculations the return current is placed to where it belongs, i.e. in another stator slot.

The current distribution, the current per unit of length along the stator surface, obtained for the case of a single conductor is given in equation 2.21.

$$a_{sk}(\theta^s) = \frac{i_s}{2\pi r} \sum_{v=-\infty}^{\infty} e^{-jv\theta^s} \quad (2.21)$$

From a given total current distribution $a_s(\theta^s)$ along the air gap, the air-gap induction can be calculated by integrating equation 2.22, using $\int_{-\pi}^{\pi} h_1(\theta^s) r d\theta^s = 0$ and $b_1(\theta^s) = \mu_0 \cdot h_1(\theta^s)$.

$$-h_1(\theta^s) \cdot d + \left(h_1(\theta^s) + \frac{dh_1(\theta^s)}{d\theta^s} \cdot d\theta^s \right) \cdot d = a_s(\theta^s) r d\theta^s \quad (2.22)$$

The total current distribution $a_s(\theta^s)$ and therefore also $b_1(\theta^s)$ is written as a double summation over all harmonic components and all coil sides. For the simple case where the coil sides for one pole of a phase are equally distributed over adjacent slots, the summation over the coil sides yields the so called distribution factor ξ_{zv} (in German called the

Zonenfaktor), given in equation 2.23. In this equation n denotes the number of slots per pole per phase, and v is a number indicating the harmonic under consideration.

$$\xi_{zv} = \frac{\sin\left(\frac{v\pi}{2pm}\right)}{n \sin\left(\frac{v\pi}{2pm} \cdot \frac{1}{n}\right)} \quad (2.23)$$

If the winding consists of two layers, and the distribution of the coil sides in one layer is shifted over Δ slots with respect to the other layer, a second factor is introduced, the so called pitch factor. Do *not* refer to [IEEE-93] for a definition of this factor. In German the pitch factor ξ_{sv} is called *Sehnungsfaktor*. It is given in equation 2.24, where S is the total number of slots, equal to $2pm$.

$$\xi_{sv} = \cos\left(v \frac{\pi}{S} \Delta\right) \quad (2.24)$$

The total winding factor for the fundamental, ξ_1 , is found by multiplying these two factors, and substituting $v = 1$ in equation 2.25.

$$\xi_v = \xi_{zv} \cdot \xi_{sv} \quad (2.25)$$

To compare the results obtained using this method with those from the previous section, the main inductance will be calculated for the example winding configuration presented there. Hence the following values will be substituted in the above equations (see figures 2.5 and 2.7): $S = 24$, $p = 1$, $m = 3$, $\Delta = 1$, $n = 4$, and $n_{sq} = 8n_{sk}$ (the number of turns per winding is eight times the number of turns per coil). For the winding factor and the main inductance equations 2.26 and 2.27 are obtained.

$$\xi_1 = \frac{\sin\left(\frac{\pi}{2pm}\right)}{n \sin\left(\frac{\pi}{2pm} \cdot \frac{1}{n}\right)} \cdot \cos\left(\frac{\pi}{S} \Delta\right) = \frac{\sin\left(\frac{\pi}{2 \cdot 1 \cdot 3}\right)}{4 \sin\left(\frac{\pi}{2 \cdot 1 \cdot 3} \cdot \frac{1}{4}\right)} \cdot \cos\left(\frac{\pi}{24} \cdot 1\right) = 0.9495 \quad (2.26)$$

$$L_{sq} = \mu_0 \frac{2m r \ell}{\pi d p^2} \xi_1^2 (n_{sq})^2 = \frac{2m \xi_1^2 8^2}{\pi^2 p^2} \frac{\mu_0 \pi r \ell (n_{sk})^2}{d} = 35.08 \frac{\mu_0 \pi r \ell (n_{sk})^2}{d} \quad (2.27)$$

If this result is compared with equation 2.17 of the previous section, it is clear that the two methods yield very similar results. As expected, Jordan's method yields a smaller value for L_{sq} , due to the neglected harmonics in the air-gap induction. For this case, the difference is 0.7%. If the number of slots is increased to 36 this difference is even smaller, 0.3%. However, in cases where the air-gap induction is very different from a sine wave, the difference between both methods becomes larger. If, due to a fault, an air-gap induction is obtained which is no longer sinusoidal, it will therefore be better to use the first method, or at least compare the results of the two methods again.

2.4 Stator flux, air-gap flux and rotor flux

In the previous section it was assumed that all magnetic flux linking one turn of a stator winding crosses the air gap. Moreover, the magnetic induction in air had only a radial component, and slot effects were not considered. However, in a real machine leakage fluxes will be present. The flux linking a winding will therefore be somewhat larger than was calculated in the previous section, which has a considerable influence on the behavior of the machine. In this section it will be shown how these leakage fluxes can be taken into account in the equations of the machine. Also the terminology related to the different leakage and winding fluxes will be introduced.

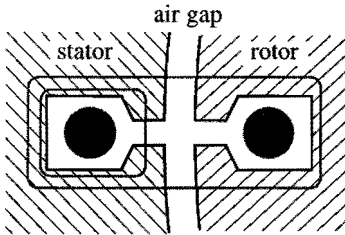


Figure 2.9. Part of a cross section of a machine, showing different flux paths

Figure 2.9 shows a part of a cross section of a machine, where a coil side belonging to a stator winding is placed in a slot on the stator side, and a coil side belonging to a rotor winding is placed in a rotor slot. For simplicity, this rotor slot is assumed to be exactly opposite to the stator slot. In reality, this position will change as the rotor turns, causing a change in the leakage fluxes. The effect of a leakage inductance depending on the rotor position will not be considered here. The figure shows some flux lines for the case a current is present in the stator winding, but not in the rotor.

To calculate the flux linking a stator winding in this case, the magnetic induction in the air gap has to be calculated first. This can be done in the same way as in section 2.3, resulting in equation 2.4. However, because the stator coils are not located in the air gap, to calculate the flux linking a coil it is not enough to integrate only the induction in the air gap, as was done in equation 2.5. Now an additional integration has to be performed over the surface between the stator conductors and the air gap. The total surface that has to be considered now is shown in figure 2.10, where end effects are still being neglected. The supplementary surface which has to be considered is indicated in grey in this figure.

As can be seen from figure 2.9, the supplementary surface over which the induction has to be integrated is crossed by a leakage flux. This flux will be proportional to the stator coil current, and the proportionality factor is the so-called stator leakage inductance. For the flux ψ_{sqk} linking stator coil k (belonging to stator phase q) equation 2.28 is now obtained.

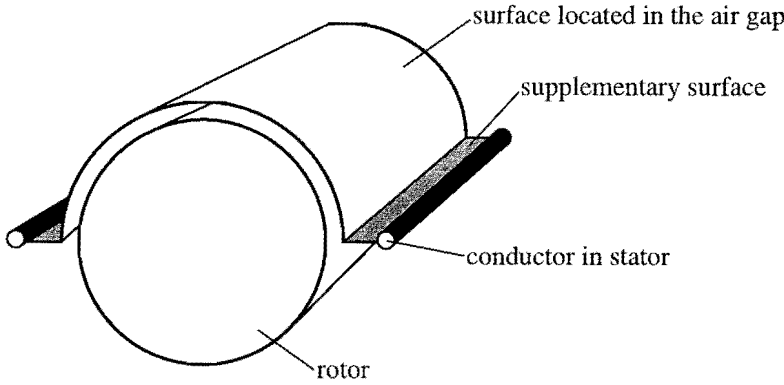


Figure 2.10. The surface of a stator coil.

$$\Psi_{sqk} = \Psi_{1sqk} + l_{\sigma sqk} \cdot i_{sq} \quad (2.28)$$

In this equation, Ψ_{1sqk} denotes the integral over the part of the surface which is located in the air gap, and which is calculated using equation 2.5. The leakage inductance for coil k of stator phase q is denoted by $l_{\sigma sqk}$. To obtain the total flux linkage of the phase- q winding a summation over all coils is needed (cf. equation 2.6), resulting in equation 2.29.

$$\Psi_{sq} = \Psi_{1sq} + l_{\sigma sq} \cdot i_{sq} \quad (2.29)$$

Here Ψ_{1sq} is the total flux linkage of the stator phase- q winding in case it were located in the air gap. The term $l_{\sigma sq} \cdot i_{sq}$ represents the leakage flux linking this winding caused by the current in this winding. Leakage flux caused by current in other stator windings is neglected, as was done in [Krau-86] and [Jord-75].

In case of a wound rotor, exactly the same reasoning is valid when calculating the flux Ψ_{rq} linking rotor-winding q , resulting in equation 2.30.

$$\Psi_{rq} = \Psi_{1rq} + l_{\sigma rq} \cdot i_{rq} \quad (2.30)$$

Note that Ψ_{1rq} is not necessarily equal to Ψ_{1sq} , even if the winding axes of the stator and rotor winding under consideration coincide. The reason for this is that the number of turns and the configuration of the coils in the rotor is not necessarily equal to those in the stator. However, a simplification is possible if the transition to the per-unit system is made (see section 2.8). In the per-unit (pu) system, stator and rotor quantities are both normalized to their rated values. Considering only sinusoidal winding distributions it is clear that for a given spatial distribution of the air-gap induction, Ψ_{1rq} will be equal to Ψ_{1sq} , provided that they refer to windings with identical winding axes and that both fluxes are expressed in per unit. This allows the usage of the term air-gap flux: the flux linking a winding placed in the air gap normalized to the rated flux linkage of that winding. For this air-gap flux the symbol Ψ_{1q} will be used.

After defining the air-gap flux, the stator and rotor flux can be defined as the flux linking a stator or rotor winding, which consists of the air-gap flux plus a term equal to the current in that winding times the leakage inductance for that winding. In case of a squirrel-cage rotor the same definitions and equations can be used assuming that an equivalent wound rotor can be defined, as shown for example in [Jord-75].

2.5 The electromagnetical torque and the mechanical equations

In this section the relation between the current distribution, the magnetic induction and the electromagnetical torque will be derived, and the equations describing the interaction with the mechanical subsystem will be presented.

One way to calculate the electromagnetical torque produced by the machine is to assume that the stator windings are located at the surface of the stator iron, and that a torque results from the interaction of the air-gap induction with the stator currents. The torque acting on the rotor is equal but opposite to the torque on the stator. It can therefore be found by multiplying the total tangential force acting on all stator conductors by minus the rotor radius, $-r$ (neglecting the air gap width, as $d \ll r$).

The force acting on a single conductor is equal to $\mathbf{f} = (\mathbf{i} \times \mathbf{b}) \cdot \ell$, where \mathbf{i} is a vector pointing in the direction of the current in space, \mathbf{b} represents the magnetic induction, ℓ is the length of the conductor, and \times denotes a vector product. Figure 2.11 shows the direction of these vectors at the stator surface. The induction is positive in the direction into the rotor, the current in the direction coming out of the paper. The resulting force would make the stator turn in clockwise (negative) direction, corresponding to a positive torque acting on the rotor.

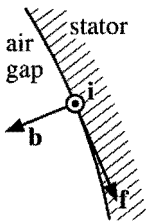


Figure 2.11. The force acting on a conductor in the stator.

Instead of summing the forces acting on all conductors to calculate the total torque, another approach will be used which gives more usable results. This approach does not use the current in the individual conductors, but rather a current sheet. This current sheet is described by the current-distribution function $a_s(\theta^s)$. Using Fourier analysis, any current distribution can be described by equation 2.31. The index n used in this equation

can be seen as the number of pole pairs for each of the Fourier components of the current distribution. The amplitude of each of the components is denoted by a_n and the phase angle by η_n .

$$a_s(\theta^s) = \sum_{n=1}^{\infty} a_n \cdot \cos(n\theta^s - \eta_n) \quad (2.31)$$

Also the air-gap magnetic induction can be written in the same form, shown in equation 2.32. Again n is used to indicate the number of pole pairs of the considered harmonic, while b_n is the amplitude and τ_n the phase angle.

$$b_{\perp}(\theta^s) = \sum_{n=1}^{\infty} b_n \cdot \cos(n\theta^s - \tau_n) \quad (2.32)$$

The electromagnetical torque can now be calculated using equation 2.33. A multiplication by r instead of $-r$ is used due to the sign convention explained by figure 2.11.

$$m_{el} = r \cdot \int_0^{2\pi} a_s(\theta^s) \cdot b_{\perp}(\theta^s) \cdot \ell \cdot r \, d\theta^s \quad (2.33)$$

Substituting equations 2.31 and 2.32 into this equation yields equation 2.34. This result can be simplified to equation 2.35, because the integration will yield zero if the number of pole pairs of the stator-current distribution is not equal to that of the air-gap induction.

$$\begin{aligned} m_{el} &= r^2 \ell \cdot \int_0^{2\pi} \sum_{n=1}^{\infty} \sum_{i=1}^{\infty} a_n \cdot b_i \cdot \cos(n\theta^s - \eta_n) \cos(i\theta^s - \tau_i) \, d\theta^s \\ &= r^2 \ell \cdot \sum_{n=1}^{\infty} \sum_{i=1}^{\infty} a_n \cdot b_i \cdot \int_0^{2\pi} \cos(n\theta^s - \eta_n) \cos(i\theta^s - \tau_i) \, d\theta^s \end{aligned} \quad (2.34)$$

$$m_{el} = \pi r^2 \ell \cdot \sum_{n=1}^{\infty} a_n \cdot b_n \cdot \cos(\tau_n - \eta_n) \quad (2.35)$$

From this equation it can be seen that the torque will be zero if the phase angle between the current distribution and the induction equals 90° . However, if the currents in the rotor are zero, the phase angle between the stator-current distribution and the resulting air-gap induction will have exactly this value. Thus, torque can only be produced if there is a rotor-current distribution (seen from the stator) with the same number of poles as the stator-current distribution. Together they result in an induction with a phase angle with respect to the stator-current distribution different from 90° .

Due to the symmetry of the winding distributions, the total current distribution and the resulting magnetic induction contain only odd harmonics. Furthermore, it should be noted that if the machine is supplied with a symmetrical set of currents as given by

equation 2.10, those harmonics that are a multiple of three are excluded (see figure 2.8). In most cases, the winding configuration is designed in such a way that the 5th, 7th and higher harmonics are small enough to be neglected, and equation 2.35 can thus be simplified to equation 2.36. In this equation a_s is the amplitude of the fundamental of the stator-current distribution, and b_1 the amplitude of the fundamental of the air-gap induction. The phase angle between these two fundamental waves is denoted by $\tau - \eta$.

$$m_{cl} = \pi r^2 \ell \cdot a_s \cdot b_1 \cdot \cos(\tau - \eta) \quad (2.36)$$

The electromagnetical torque m_{cl} minus the load torque m_{load} (which includes friction) will cause an acceleration of the machine and the load, as described by equation 2.37. The parameter Θ denotes the moment of inertia of the rotor plus the load, and $\dot{\rho}^s$ ($=d\rho^s/dt$) is used to indicate the rotor speed. The rotor position with respect to the fixed stator is written as ρ^s . Equation 2.38 gives the relation between the rotor position and the rotor speed.

$$m_{cl} - m_{load} = \Theta \frac{d\dot{\rho}^s}{dt} \quad (2.37)$$

$$\rho^s = \int \dot{\rho}^s dt \quad (2.38)$$

2.6 Transition to an equivalent orthogonal model

When modeling the behavior of the induction machine, a considerable simplification can be obtained by transforming the equations of the three-phase machine into equivalent equations of a semi-four-phase machine (see for example [Leon-85] or [Blas-96]). In this machine, which is often called a two-phase machine, the two phase windings have an angle of 90° , are therefore not mutually coupled and are usually fed with two sinusoidal currents having a phase difference of 90° . This is an important simplification compared to the three-phase machine, mainly because there the windings are mutually coupled. Furthermore, as the essential behavior of the machine is related to quantities that vary sinusoidally along the air-gap, two phase windings are sufficient to describe this behavior. Finally, in many situations the current in the third phase is determined by the current in the other two phases. Hence it is not necessary to perform calculations for all three phases independently. In this section the three-phase machine model used previously will therefore be replaced by an equivalent two-phase model. The relations between the three-phase and equivalent two-phase currents and fluxes will be derived, as well as a relation for the main inductance and the torque of the two-phase machine.

However, the transformation from a three-phase machine into an equivalent two-phase machine has a serious limitation. The behavior of the space harmonics of the air-gap

induction can not be transformed directly. For example, if the MMF caused by the current in a winding contains a third harmonic, in a three-phase machine fed with a symmetrical set of currents there will be no third harmonic in the resulting MMF (see figure 2.8). In a two-phase machine fed with a symmetrical set of currents this cancellation does not occur. Or if the MMF contains a 5th harmonic, in the three-phase machine the resulting MMF will contain a 5th harmonic wave traveling in the opposite direction as the fundamental, while in the two-phase machine it will have the same direction.

Thus the equivalency will be valid only if all space harmonics in the MMF can be neglected. This is not the case when the sum of the three phase currents is not zero, as for example in the calculation of the spectrum shown in figure 2.6. Applying the equivalent orthogonal model for this case would lead to erroneous conclusions. An extension of the model will therefore be introduced in section 4.3.

To obtain the relation between the three-phase currents and the equivalent two-phase currents, consider the current distribution along the air gap caused by each of the currents, given in equation 2.39. In this equation it has been assumed that each current distribution has only a fundamental component. The factor v_{s1} , which has not been calculated here, is a proportionality factor relating the amplitude of the current distribution to the actual winding current. The position of the phase-a winding has been chosen in such a way that its winding axis (cf. figure 2.2) coincides with the stator axis.

$$\begin{aligned} a_{sa}(\theta^s) &= i_{sa} \cdot v_{s1} \cdot \cos\left(\theta^s + \frac{\pi}{2}\right) \\ a_{sb}(\theta^s) &= i_{sb} \cdot v_{s1} \cdot \cos\left(\theta^s + \frac{\pi}{2} - \frac{2\pi}{3}\right) \\ a_{sc}(\theta^s) &= i_{sc} \cdot v_{s1} \cdot \cos\left(\theta^s + \frac{\pi}{2} - \frac{4\pi}{3}\right) \end{aligned} \quad (2.39)$$

For the two-phase machine it has been assumed that identical windings are used, i.e. windings with the same number and distribution of coils and the same number of turns as in the three-phase machine. The relation between a phase current and its current distribution along the air gap is then the same for both machines. The resulting relations are given in equation 2.40. The two phase currents are identified by the superscripts $s1$ and $s2$, because the stator winding axes coincide with the axes of an orthogonal coordinate system fixed to the stator. As described in Appendix B, superscripts identify the individual components of a vector and the coordinate system in which they are given, hence $i_s^s = \begin{bmatrix} i_s^{s1} & i_s^{s2} \end{bmatrix}^T$.

$$\begin{aligned} a_{s1}(\theta^s) &= i_s^{s1} \cdot v_{s1} \cdot \cos\left(\theta^s + \frac{\pi}{2}\right) \\ a_{s2}(\theta^s) &= i_s^{s2} \cdot v_{s1} \cdot \cos\left(\theta^s\right) \end{aligned} \quad (2.40)$$

To obtain equivalency, the current distributions caused by the individual currents should be added and the result must be equal for both cases. This yields the following relation between the two- and three-phase currents:

$$\begin{aligned} i_s^{s1} &= i_{sa} - \frac{1}{2} i_{sb} - \frac{1}{2} i_{sc} \\ i_s^{s2} &= \frac{\sqrt{3}}{2} i_{sb} - \frac{\sqrt{3}}{2} i_{sc} \end{aligned} \quad (2.41)$$

A short intermezzo on space phasors is added here for the interested reader. It is not essential for the rest of the theory.

Considering equations 2.39 and 2.40 again, the concept of space phasors, used by some authors and introduced by Štěpina in [Štěp-67], can be explained. As can be seen from these equations, the current distribution can be written in the following form (taking for example $a_s^{s1} = i_s^{s2} \cdot v_{s1}$ and $a_s^{s2} = -i_s^{s1} \cdot v_{s1}$):

$$a_s(\theta^s) = a_s^{s1} \cdot \cos(\theta^s) + a_s^{s2} \cdot \sin(\theta^s) \quad (2.42)$$

The current distribution $a_s(\theta^s)$ can thus be represented by a vector a_s^s , consisting of the components a_s^{s1} and a_s^{s2} . The length of this vector, a_s , is equal to the peak value of $a_s(\theta^s)$, and the angle of this vector indicates the position of this peak value. This corresponds to the definition of a space phasor: a vector which represents a quantity that can be written as a sinusoidal function of a position, and where the peak value of that quantity and its position are represented by the amplitude and the angle of that vector.

The current vector $i_s^s = \begin{bmatrix} i_s^{s1} & i_s^{s2} \end{bmatrix}^T$ is, in the way it was introduced here, not a space phasor. However, it is interesting to notice that there is a simple relation between the vectors a_s^s and i_s^s , given in equation 2.43.

$$a_s^s = \begin{bmatrix} a_s^{s1} \\ a_s^{s2} \end{bmatrix} = v_{s1} \cdot \begin{bmatrix} 0 & 1 \\ -1 & 0 \end{bmatrix} \cdot \begin{bmatrix} i_s^{s1} \\ i_s^{s2} \end{bmatrix} \quad (2.43)$$

Thus the current vector is related to a space phasor by a rotation over 90° and a multiplication by a constant. This fact might be used to justify calling i_s^s a space vector. The vector i_s^s is then the space vector representing the rotated and multiplied sinusoidal current distribution. Furthermore, the current vector i_s^s is proportional to the induction vector b_{1s}^s , which is the space phasor representing the air-gap induction. This fact leads to the common assumption that i_s^s is a space phasor representing the air-gap induction, although it has the dimension of a current. In the per-unit system, where all quantities are dimensionless, this assumption makes more sense. In this thesis i_s^s will merely be seen as a current vector, representing the currents in the windings of the equivalent two-phase machine.

A further relation which has to be established is that between the air-gap fluxes linking the windings in the equivalent two-phase machine, ψ_{1s}^{s1} and ψ_{1s}^{s2} , and the fluxes linking the windings of the three-phase machine, ψ_{1sa} , ψ_{1sb} and ψ_{1sc} . It is clear that while the current distributions and hence the air-gap inductions are equal, the fluxes ψ_{1s}^{s1} and ψ_{1sa} must be equal, because the winding in the $s1$ -axis was identical with the phase- a winding. For the flux in the other phase, ψ_{1s}^{s2} , some calculations are needed.

To calculate the air-gap flux linking a sinusoidally distributed winding, for each element of the winding the flux linkage has to be calculated, after which the total flux can be found

by integrating over all winding elements. For the fluxes linking the three phase windings this is done in equations 2.44, 2.45 and 2.46, in which a_{sq}/i_{sq} is the winding distribution. The current distributions $a_{sq}(\theta^s)$ are given in equation 2.39, and the sinusoidal air-gap induction is given by $b_{\perp}(\theta^s) = b_{\perp 1}^{s1} \cdot \cos(\theta^s) + b_{\perp 1}^{s2} \cdot \sin(\theta^s)$, in which the subscript '1' indicates the fundamental.

$$\psi_{1sa} = \int_{\theta^s=0}^{\pi} \frac{a_{sa}(\theta^s)}{i_{sa}} r \int_{\tau^s=\theta^s-\pi}^{\theta^s} -b_{\perp}(\tau^s) \ell r d\tau^s d\theta^s = \int_{\theta^s=0}^{\pi} v_{s1} \cdot \sin \theta^s r d\theta^s$$

$$\int_{\tau^s=\theta^s-\pi}^{\theta^s} \left(b_{\perp 1}^{s1} \cdot \cos(\tau^s) + b_{\perp 1}^{s2} \cdot \sin(\tau^s) \right) \ell r d\tau^s d\theta^s = \pi r^2 \ell v_{s1} b_{\perp 1}^{s1} \quad (2.44)$$

$$\psi_{1sb} = \int_{\theta^s=\frac{2\pi}{3}}^{\frac{5\pi}{3}} \frac{a_{sb}(\theta^s)}{i_{sb}} r \int_{\tau^s=\theta^s-\pi}^{\theta^s} -b_{\perp}(\tau^s) \ell r d\tau^s d\theta^s = \pi r^2 \ell v_{s1} \left(-\frac{1}{2} b_{\perp 1}^{s1} + \frac{1}{2} \sqrt{3} b_{\perp 1}^{s2} \right) \quad (2.45)$$

$$\psi_{1sc} = \int_{\theta^s=\frac{4\pi}{3}}^{\frac{7\pi}{3}} \frac{a_{sc}(\theta^s)}{i_{sc}} r \int_{\tau^s=\theta^s-\pi}^{\theta^s} -b_{\perp}(\tau^s) \ell r d\tau^s d\theta^s = \pi r^2 \ell v_{s1} \left(-\frac{1}{2} b_{\perp 1}^{s1} - \frac{1}{2} \sqrt{3} b_{\perp 1}^{s2} \right) \quad (2.46)$$

In the same way, now using 2.40, the flux linking the windings of the equivalent two-phase machine is calculated in equations 2.47 and 2.48.

$$\psi_{1s}^{s1} = \int_{\theta^s=0}^{\pi} \frac{a_{s1}(\theta^s)}{i_s^{s1}} r \int_{\tau^s=\theta^s-\pi}^{\theta^s} -b_{\perp}(\tau^s) \ell r d\tau^s d\theta^s = \pi r^2 \ell v_{s1} b_{\perp 1}^{s1} \quad (2.47)$$

$$\psi_{1s}^{s2} = \int_{\theta^s=\frac{\pi}{2}}^{\frac{3\pi}{2}} \frac{a_{s2}(\theta^s)}{i_s^{s2}} r \int_{\tau^s=\theta^s-\pi}^{\theta^s} -b_{\perp}(\tau^s) \ell r d\tau^s d\theta^s = \pi r^2 \ell v_{s1} b_{\perp 1}^{s2} \quad (2.48)$$

By comparing equations 2.47 and 2.48 with 2.44, 2.45 and 2.46 relation 2.49 is found between the fluxes in the two- and three-phase systems. Note however that the three fluxes ψ_{1sa} , ψ_{1sb} and ψ_{1sc} are not independent, so that also a different relation could have been given in which for example ψ_{1sc} had been eliminated.

$$\begin{aligned}\psi_{1s}^{s1} &= \psi_{1sa} \\ \psi_{1s}^{s2} &= +\frac{1}{\sqrt{3}}\psi_{1sb} - \frac{1}{\sqrt{3}}\psi_{1sc}\end{aligned}\quad (2.49)$$

An interesting consideration on whether the air-gap flux vector $\boldsymbol{\psi}_1^s = [\psi_{1s}^{s1} \ \psi_{1s}^{s2}]^T$ can be considered a space phasor is found in [Štěp-67]. The author shows that the flux which crosses a yoke section of the machine is a quantity that varies sinusoidally as a function of the position, and may thus be represented by a space phasor. The air-gap flux vector used in this thesis has an amplitude proportional to this phasor, but its angle differs by 90° . The flux vectors in this thesis are therefore no real space phasors, and will hence merely be referred to as vectors.

The stator main inductance l_s of the equivalent two-phase machine, describing the relation between the current in and the air-gap flux linking a stator winding in case of a symmetrical supply, is not the same as for the three-phase machine. Consider the case when $i_{sa} = 2/3 i_s$, $i_{sb} = -1/3 i_s$, $i_{sc} = -1/3 i_s$. The flux linking phase a, ψ_{1sa} , is then equal to $l_{sq} \cdot i_{sa} = l_{sq} \cdot 2/3 i_s$. Using equation 2.49 the flux ψ_{1s}^{s1} can be calculated, which is found to equal $l_{sq} \cdot 2/3 i_s$. According to equation 2.41 the current $i_s^{s1} = i_s$, and using the relation between the flux ψ_{1s}^{s1} and this current, $\psi_{1s}^{s1} = l_s \cdot i_s^{s1}$, the following relation is obtained:

$$l_s = \frac{2}{3} l_{sq} \quad (2.50)$$

Note that due to the neglectance of space harmonics of the air-gap induction, it is no longer relevant which of the two methods presented is used to calculate this inductance.

Finally the torque equation (2.36) will be rewritten in terms of the stator currents and the flux linkages. Starting from equation 2.33, using equation 2.40 and substituting a sinusoidal air-gap induction $b_{11}(\theta^s) = b_{11}^{s1} \cdot \cos(\theta^s) + b_{11}^{s2} \cdot \sin(\theta^s)$ the torque becomes:

$$\begin{aligned}m_{el} &= r^2 \ell v_{s1} \int_0^{2\pi} \left(-i_s^{s1} \sin \theta^s + i_s^{s2} \cos \theta^s \right) \left(b_{11}^{s1} \cos \theta^s + b_{11}^{s2} \sin \theta^s \right) d\theta^s \\ &= \pi r^2 \ell v_{s1} \left(i_s^{s2} b_{11}^{s1} - i_s^{s1} b_{11}^{s2} \right)\end{aligned}\quad (2.51)$$

Equation 2.51 should now be compared with the equations giving the relation between the flux linkages and the induction, 2.47 and 2.48. The result of the comparison is given in equation 2.52, in which $\mathbf{i}_s^s = [i_s^{s1} \ i_s^{s2}]^T$ and $\boldsymbol{\psi}_{1s}^s = [\psi_{1s}^{s1} \ \psi_{1s}^{s2}]^T$.

$$m_{el} = i_s^{s2} \cdot \psi_{1s}^{s1} - i_s^{s1} \cdot \psi_{1s}^{s2} = \begin{bmatrix} 0 & -1 \\ 1 & 0 \end{bmatrix} \cdot \boldsymbol{\psi}_{1s}^s \cdot \mathbf{i}_s^s \quad (2.52)$$

Together with equations 2.41, 2.49 and 2.50 this completes the transition to an equivalent orthogonal model, except for the voltage equations. These were also not yet

introduced for the three-phase machine. The voltage equations will be the subject of the next section.

2.7 The voltage equations and simplification of the model using only one leakage inductance

To complete the set of equations of the induction machine, in this section the voltage equations will be added, both for the general case of the three-phase machine, and for the equivalent two-phase machine. The machine model obtained in this way will then be written in a simplified form with the help of block diagrams.

For the voltage u_{sq} across a three-phase winding equation 2.53 is valid, where r_{sq} is the resistance of a stator phase. The different fluxes and the leakage inductance have been explained in section 2.4, equation 2.29.

$$u_{sq} = r_{sq} \cdot i_{sq} + \frac{d\psi_{sq}}{dt} = r_{sq} \cdot i_{sq} + l_{\sigma sq} \cdot \frac{di_{sq}}{dt} + \frac{d\psi_{1sq}}{dt} \quad (2.53)$$

For the equivalent two-phase machine the voltage equations can be written in an analog way, shown in equation 2.54. The voltages across the stator windings of the equivalent machine are written as u_s^{s1} and u_s^{s2} , while r_s and $l_{\sigma s}$ are the resistance and the leakage inductance of these windings.

$$\begin{aligned} u_s^{s1} &= r_s \cdot i_s^{s1} + \frac{d\psi_s^{s1}}{dt} = r_s \cdot i_s^{s1} + l_{\sigma s} \cdot \frac{di_s^{s1}}{dt} + \frac{d\psi_{1s}^{s1}}{dt} \\ u_s^{s2} &= r_s \cdot i_s^{s2} + \frac{d\psi_s^{s2}}{dt} = r_s \cdot i_s^{s2} + l_{\sigma s} \cdot \frac{di_s^{s2}}{dt} + \frac{d\psi_{1s}^{s2}}{dt} \end{aligned} \quad (2.54)$$

By substituting equations 2.41 and 2.49 into this equation, and comparing the result (equation 2.55) with equation 2.53 while $i_{sa} = i_{sb} = i_{sc} = 0$, the relation between the voltages in the two- and three-phase systems is obtained, given in equation 2.56. Hence for the voltages the same transformation is valid as for the fluxes (equation 2.49).

$$\begin{aligned} u_s^{s1} &= r_s \cdot \left(i_{sa} - \frac{1}{2} i_{sb} - \frac{1}{2} i_{sc} \right) + l_{\sigma s} \cdot \frac{d \left(i_{sa} - \frac{1}{2} i_{sb} - \frac{1}{2} i_{sc} \right)}{dt} + \frac{d\psi_{1sa}}{dt} \\ u_s^{s2} &= r_s \cdot \left(\frac{\sqrt{3}}{2} i_{sb} - \frac{\sqrt{3}}{2} i_{sc} \right) + l_{\sigma s} \cdot \frac{d \left(\frac{\sqrt{3}}{2} i_{sb} - \frac{\sqrt{3}}{2} i_{sc} \right)}{dt} + \frac{d \left(\frac{1}{\sqrt{3}} \psi_{1sb} - \frac{1}{\sqrt{3}} \psi_{1sc} \right)}{dt} \end{aligned} \quad (2.55)$$

$$\begin{aligned} u_s^{s1} &= u_{sa} \\ u_s^{s2} &= \frac{1}{\sqrt{3}} u_{sb} - \frac{1}{\sqrt{3}} u_{sc} \end{aligned} \quad (2.56)$$

Using equations 2.56, 2.55 and 2.53 and assuming that $i_{sa} + i_{sb} + i_{sc} = 0$, the following relation is obtained between the parameters of the equivalent two-phase and the three-phase machine (compare with equation 2.50 where the same relation has been found for the stator main inductance):

$$\begin{aligned} r_s &= \frac{2}{3} r_{sq} \\ l_{\sigma s} &= \frac{2}{3} l_{\sigma sq} \end{aligned} \quad (2.57)$$

To simplify the use of the voltage equations, they will from now on be written as vector equations, as in equation 2.58, which is the equivalent of equation 2.54.

$$\mathbf{u}_s^s = r_s \cdot \mathbf{i}_s^s + \frac{d\boldsymbol{\psi}_s^s}{dt} = r_s \cdot \mathbf{i}_s^s + l_{\sigma s} \cdot \frac{d\mathbf{i}_s^s}{dt} + \frac{d\boldsymbol{\psi}_{1s}^s}{dt} \quad (2.58)$$

The same derivation method can be used to obtain the equations for the two-phase model of a three-phase wound rotor. The rotor voltages however are equal to zero, due to the short-circuiting of the rotor. Hence equation 2.59 describes the relation between the rotor currents and the flux linking the rotor windings.

$$\mathbf{u}_r^r = r_r \cdot \mathbf{i}_r^r + \frac{d\boldsymbol{\psi}_r^r}{dt} = r_r \cdot \mathbf{i}_r^r + l_{\sigma r} \cdot \frac{d\mathbf{i}_r^r}{dt} + \frac{d\boldsymbol{\psi}_{1r}^r}{dt} = \mathbf{0} \quad (2.59)$$

In contrast with equation 2.58, which was given in the stator reference frame, this equation uses the rotor reference frame, because the coils linked by the flux are fixed to the rotor. The relation between the air-gap flux in the rotor and the stator reference frames is given in equation 2.60. The multiplication of the flux vector with the matrix $R(\rho^s)$ corresponds to a rotation over an angle ρ^s . The elements of the rotation matrix are shown in equation 2.61.

$$\boldsymbol{\psi}_{1r}^s = R(\rho^s) \cdot \boldsymbol{\psi}_{1r}^r \quad (2.60)$$

$$R(\rho^s) = \begin{bmatrix} \cos \rho^s & -\sin \rho^s \\ \sin \rho^s & \cos \rho^s \end{bmatrix} \quad (2.61)$$

Now that a current is present in the rotor, the air-gap flux is no longer proportional to the stator current only. Both the stator-current distribution and the rotor-current distribution contribute equally to the air-gap induction, and hence to the air-gap flux. Assuming that identical windings are used for the stator and the rotor, the air-gap flux linking the stator and rotor windings will be equal: $\boldsymbol{\psi}_{1r}^s = \boldsymbol{\psi}_{1s}^s = \boldsymbol{\psi}_1^s$. In that case also the stator and rotor main inductances are equal: $l_r = l_s = l$. The same is true for a machine in which stator and rotor windings are not identical, but where all quantities are expressed in an appropriate per-unit system. The relation between the currents and the air-gap flux is given in equation 2.62.

$$\Psi_{\perp}^s = 1 \cdot (\mathbf{i}_s^s + \mathbf{i}_r^s) \quad (2.62)$$

Using equations 2.58, 2.59, 2.60 and 2.62 a block diagram can be drawn, as shown in figure 2.12. This block diagram will be used to illustrate a simplification of these equations. For an overview of the different blocks see appendix B.

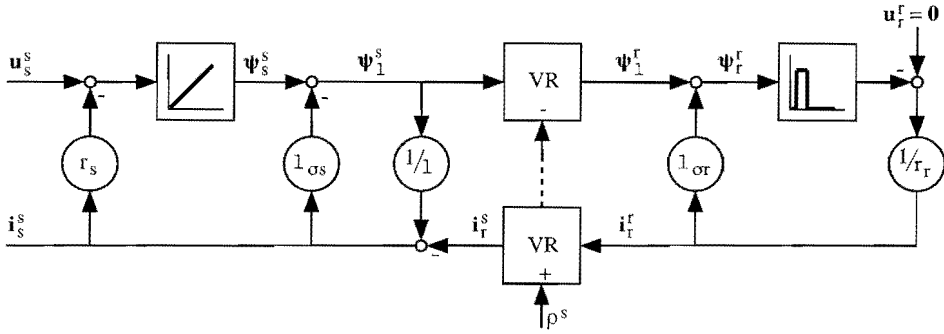


Figure 2.12. A block diagram of the machine.

In this block diagram it is possible to move the multiplication by $1_{\sigma r}$ of the rotor current to the left of the rotators. In this way, equation 2.63 is obtained. The stator current can now be expressed as a function of the rotor flux and the rotor current, shown in equation 2.64.

$$\Psi_r^s = \Psi_s^s - 1_{\sigma s} \mathbf{i}_s^s + 1_{\sigma r} \mathbf{i}_r^s \quad (2.63)$$

$$\mathbf{i}_s^s = \frac{\Psi_r^s}{1} - \frac{1_{\sigma r} + 1}{1} \mathbf{i}_r^s \quad (2.64)$$

From these two equations equation 2.65 can be deduced, which introduces a total leakage inductance 1_{σ} . The relation between 1_{σ} and the other inductances is given in equation 2.66. In a real machine, 1_{σ} is the only leakage inductance that can be measured from the “outside” of the machine – the stator and rotor leakage inductances can not measured independently. Therefore it is reasonable to use a model of the machine with only one leakage inductance. The corresponding block diagram, deduced from the previous diagram using equations 2.64 and 2.65, is shown in figure 2.13.

$$\Psi_r^s = \Psi_s^s - \left(1_{\sigma s} + \frac{1_{\sigma r}}{1 + 1_{\sigma r/1}} \right) \cdot \mathbf{i}_s^s + \frac{1_{\sigma r/1}}{1 + 1_{\sigma r/1}} \Psi_r^s = \Psi_s^s - 1_{\sigma} \mathbf{i}_s^s + \frac{1_{\sigma r/1}}{1 + 1_{\sigma r/1}} \Psi_r^s \quad (2.65)$$

$$1_{\sigma} = 1_{\sigma s} + \frac{1_{\sigma r}}{1 + 1_{\sigma r/1}} \quad (2.66)$$

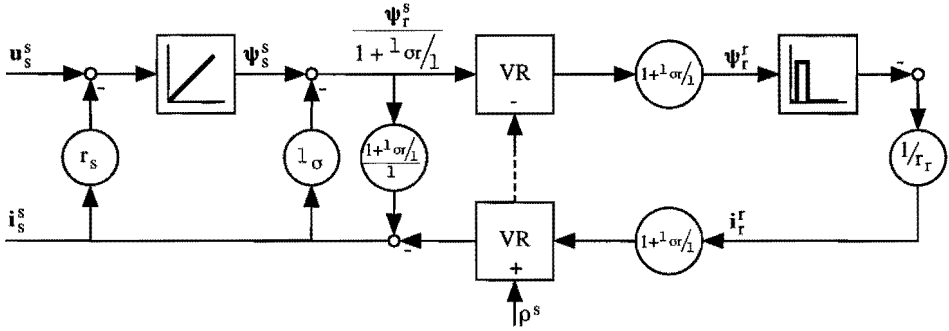


Figure 2.13. A block diagram of the machine, using only one leakage inductance.

A further simplification of the block diagram is possible by introducing some new quantities and parameters, as in equations 2.67 to 2.70. The resulting block diagram is shown in figure 2.14.

$$l' = \frac{l}{1 + l_{\sigma/l}} \tag{2.67}$$

$$r'_r = \frac{r_r}{(1 + l_{\sigma/l})^2} \tag{2.68}$$

$$\psi_r^{s'} = \frac{\psi_r^s}{1 + l_{\sigma/l}} \tag{2.69}$$

$$i_r^{s'} = i_r^s \cdot (1 + l_{\sigma/l}) \tag{2.70}$$

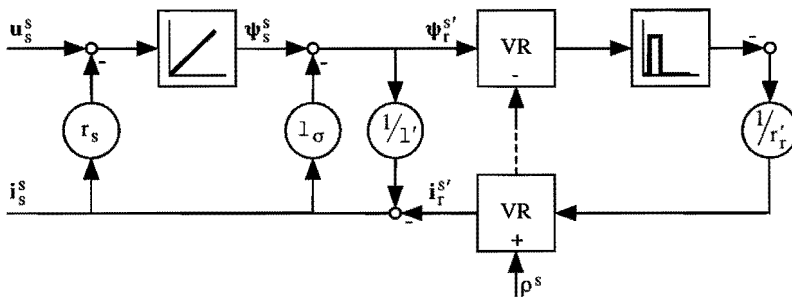


Figure 2.14. A block diagram of the machine, using the new parameters.

Finally, the torque equation 2.52 will be rewritten as a function of $\psi_r^{s'}$. This is necessary because the air-gap flux could only be calculated if $l_{\sigma s}$ and $l_{\sigma r}$ were known separately. Starting from equation 2.52, substituting $\psi_1^s = \psi_r^s - l_{\sigma r} \cdot i_r^s$ and using equations 2.64 and finally 2.69, equation 2.71 is obtained.

$$m_{el} = \frac{1}{1 + l_{\sigma r}/l} \left(\psi_r^{s1} \cdot i_s^{s2} - \psi_r^{s2} \cdot i_s^{s1} \right) = \psi_r^{s1'} \cdot i_s^{s2} - \psi_r^{s2'} \cdot i_s^{s1} \quad (2.71)$$

It is interesting to notice that if in the equation set deduced for a machine with $l_{\sigma r} = 0$ (see for example [Blas-96]) all occurrences of ψ_r , which in that case equals ψ_l , are replaced with ψ_r' , i_r with i_r' , $l_{\sigma s}$ with l_{σ} , l with l' and r_r with r_r' , the resulting set of equations is the same as was deduced here. This means that all control structures which are designed for the case $l_{\sigma r} = 0$ can be used without modification for the general case with $l_{\sigma r} \neq 0$, introducing only a scale factor as in equations 2.67 to 2.70.

2.8 Transition to the per-unit (pu) system

In the analysis and control of electrical machines often the so-called per-unit or pu system is used. In this system all quantities are treated as dimensionless numbers, which are obtained by dividing the real value by a reference value. These reference values are chosen in such a way that the numbers obtained are within a limited range of e.g. -1 to 1. For voltages, currents and speed usually the rated values are used as references. Not all references can be chosen independently, though. To obtain a so-called coherent-unity system, in which the equations written in dimensionless numbers are identical to those using the real quantities, references must be chosen in such a way that no extra scale factors are needed. For example, if references are chosen for voltage and current, the reference for resistance can be found by dividing the voltage reference by the current reference.

An important advantage of using the per-unit system is that theories, simulations and control systems can easily be fitted to one machine or another, even if the two machines have a completely different voltage, power or speed rating. Measured signals are transformed into the per-unit system before being input into the control system, and control outputs are transformed back into real values. The same control system can therefore be used for different machines, changing primarily its interface. The machine parameters required in most control systems must however also be adapted, especially if the power rating of one machine is very different from the other.

However, the use of the pu system has also important practical advantages – in many cases, there is an absolute necessity to use it. In the time when analog controllers and simulators were used, it was necessary to limit all voltages in the analog system to $\pm 10V$, due to the limitations of the analog electronics. This could be achieved by using the pu system, setting $1pu=10V$ or $1pu=5V$. Also in digital systems the same problem arose. There all quantities had to be expressed as integers, using a limited number of bits (eg. 8 or 16). To fully use this bit range, which is necessary to reduce the error caused by the

discretization, scaling of all quantities was needed, and here again the pu system showed its usefulness.

Modern computers and digital signal processors (DSPs) more and more often use floating point numbers in all calculations, which eliminates the need to limit numerical values to a certain range. However, as soon as these systems are interfaced with a real machine, or even in the case where an analog oscilloscope is used to view rapidly changing signals from a real-time digital simulation system, the limitations of analog electronics and integer numbers have to be faced once again. Voltage and current sensors, oscilloscopes, etc. all have a limited voltage range, and the converters used for the translation between analog and digital systems use integer values with a limited number of bits. This means that even if the computer could calculate with real numbers (which in any way are dimensionless) there are still many advantages to using the pu system.

Throughout this thesis all equations will use the pu system, for which the reference values are given below. First of all, four independent reference values have been chosen (equations 2.72 to 2.75). The factor $3/2$ in the current reference is related to the transformation from a three-phase to an equivalent two-phase system.

$$[\mathbf{u}]_{\text{ref}} = \sqrt{2} [\mathbf{u}_{\text{sa}}]_{\text{rated,rms}} \quad (2.72)$$

$$[\mathbf{i}]_{\text{ref}} = \frac{3}{2}\sqrt{2} [\mathbf{i}_{\text{sa}}]_{\text{rated,rms}} \quad (2.73)$$

$$[\omega]_{\text{ref}} = [\omega_{\text{s}}]_{\text{rated}} \quad (2.74)$$

$$[\theta]_{\text{ref}} = 1 \text{ rad} \quad (2.75)$$

In these equations $[\mathbf{x}]_{\text{rated,rms}}$ denotes a rated rms value; $[\omega_{\text{s}}]_{\text{rated}}$ is the rated angular frequency of the voltage or current at the stator side, and θ is an arbitrary angle. It is assumed that the number of pole pairs is equal to one, so the reference for the mechanical frequency will be equal to the reference for the electrical frequency. The references that can be derived from the above ones are given in equations 2.76 to 2.81. A detailed explanation of these derivations is found in [Blas-96].

$$[\mathbf{r}]_{\text{ref}} = \frac{[\mathbf{u}]_{\text{ref}}}{[\mathbf{i}]_{\text{ref}}} \quad (2.76)$$

$$[\mathbf{t}]_{\text{ref}} = \frac{[\theta]_{\text{ref}}}{[\omega]_{\text{ref}}} \quad (2.77)$$

$$[\psi]_{\text{ref}} = \frac{[\mathbf{u}]_{\text{ref}}}{[\omega]_{\text{ref}}} \quad (2.78)$$

$$[1]_{\text{ref}} = \frac{[u]_{\text{ref}}}{[\omega]_{\text{ref}}[i]_{\text{ref}}} \quad (2.79)$$

$$[m]_{\text{ref}} = \frac{[u]_{\text{ref}}[i]_{\text{ref}}}{[\omega]_{\text{ref}}} \quad (2.80)$$

$$[\Theta]_{\text{ref}} = \frac{[u]_{\text{ref}}[i]_{\text{ref}}}{[\omega]_{\text{ref}}^3} \quad (2.81)$$

Please note that also the time is calculated in pu. In case of a rated stator frequency of 50 Hz the reference for time will be $[t]_{\text{ref}} = 3.18 \text{ ms}$. The values of the other references can be found in Appendix C.

2.9 Summary of the equations of the induction machine

In this section the equations of the two-phase equivalent model of the induction machine as they were derived in the previous sections are summarized. Due to the introduction of the pu system, it is no longer necessary to distinguish between the air-gap flux linking stator or rotor windings, and the simplifications introduced in section 2.7 can be used without the restriction of identical stator and rotor windings.

The accents introduced in equations 2.67 to 2.70 will be omitted, and this convention will be maintained throughout the rest of this thesis.

The equations presented here are valid only for the equivalent two-phase machine, which was derived from the three-phase machine under the assumption that the air-gap induction and the current distribution along the air gap contain no space harmonics. Under this assumption the difference between the two methods to calculate the main inductance is no longer relevant.

If however the three-phase machine is no longer fed in such a way that the sum of the phase currents is zero, a third (space) harmonic may appear in the air-gap induction, in which case some additions to these equations have to be made. This will be shown in Chapter 4.

$$\mathbf{u}_s^s = r_s \cdot \mathbf{i}_s^s + \dot{\boldsymbol{\psi}}_s^s \quad (2.82)$$

$$\boldsymbol{\psi}_s^s = \int \dot{\boldsymbol{\psi}}_s^s dt \quad (2.83)$$

$$\boldsymbol{\psi}_r^s = \boldsymbol{\psi}_s^s - l_\sigma \cdot \mathbf{i}_s^s \quad (2.84)$$

$$\boldsymbol{\psi}_r^s = \mathbf{l} \cdot (\mathbf{i}_s^s + \mathbf{i}_r^s) \quad (2.85)$$

$$\mathbf{0} = r_r \cdot \mathbf{i}_r^r + \dot{\boldsymbol{\psi}}_r^r \quad (2.86)$$

$$\boldsymbol{\psi}_r^r = \int \dot{\boldsymbol{\psi}}_r^r dt \quad (2.87)$$

$$m_{el} = \left[\mathbf{R}\left(\frac{\pi}{2}\right) \cdot \boldsymbol{\psi}_r^s \right]^T \cdot \mathbf{i}_s^s \quad (2.88)$$

$$\dot{\rho}^s = \frac{1}{\Theta} \cdot \int (m_{el} - m_{load}) dt \quad (2.89)$$

$$\rho^s = \int \dot{\rho}^s dt \quad (2.90)$$

$$\mathbf{x}^s = \mathbf{R}(\rho^s) \cdot \mathbf{x}^r \quad (2.91)$$

Chapter 3

Field-Oriented Control of an Induction Machine

3.1 Introduction

In most applications of the three-phase induction machine – in the past, but even today – the machine is coupled directly with the utility grid. Ideally this means that the machine is fed from a sinusoidal symmetrical three-phase voltage source with constant voltage and frequency. Although this has been proved to be a simple and robust drive implementation in many applications, there are some serious drawbacks. This is especially true if variable speed is needed.

To operate an induction machine in a stable and optimal way with regard to losses and utilization of the machine, the frequency of the applied voltages or currents should be approximately equal to the rotor speed, and the peak value of the air-gap magnetic induction should be maintained at a constant level. The surface integral of this induction equals the flux linkage, to which the stator phase voltages are approximately proportional. This means that for a constant induction level, these voltages must be approximately proportional to the frequency of the flux-linkage variation, which in turn is approximately equal to the rotor speed. Hence to operate an induction machine at different speeds, it is necessary to vary both the applied voltage and the frequency. If both are constant, the machine can only operate satisfactorily in a very limited speed range, and special care has to be taken when starting the machine.

Many solutions to this problem have been developed in the past, including double-cage rotors, switchable stator windings to vary the number of poles or the stator voltage, rotor windings to which an external resistance can be added to change the slip frequency, soft starters which reduce the voltage, etc. Nowadays, the introduction in electrical drive systems of power electronics combined with advanced control techniques results in a much more flexible and optimal usage of the machine. In this chapter one of these control techniques, the so-called field-oriented control, will be introduced for both a current-fed and a voltage-fed induction machine. The field-oriented machine models as well as the related control systems presented in this chapter will serve throughout the rest of this thesis to investigate and improve the behavior of the drive during faults.

3.2 Scalar control of an induction machine

The most common type of control applied to induction machines is the so-called scalar control. Vector control, which will be discussed in section 3.3, is used in only a small percentage of all controlled three-phase induction drives. In scalar control, only the magnitude of quantities such as the voltage is controlled – the angles of the different vectors that describe the state of the machine (equations 2.82 to 2.91) are not controlled and are thus left as the outputs of an open loop system. This control method relies on the steady state behavior of the machine, and consequently is not optimized for dynamic behavior. As a result the transient response is usually far from ideal.

A common form of scalar control is shown in figure 3.1. Here the stator voltage and the stator frequency are varied proportionally, $u_s = c \cdot |\dot{\alpha}_s^s|$. The control circuitry of the converter uses these signals to generate firing pulses for the power switches in such a way that the fundamental waveform of the output voltage vector corresponds to the desired values for the amplitude and the frequency.

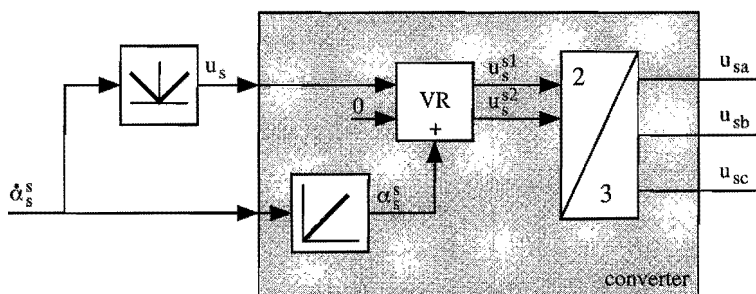


Figure 3.1. Block diagram of an ideal voltage converter with voltage/frequency control.

The converter used for this type of control is mostly a pulse-width modulated (PWM) voltage-source inverter (VSI). Its main circuit, consisting of six switching devices and six diodes, is shown in figure 3.2. Additional components such as snubbers, fuses, etc. are not shown in this figure. The power switches which are used are mostly GTOs (Gate Turn-Off thyristors), IGBTs (Insulated-Gate Bipolar Transistors), BJT's (Bipolar Junction Transistors) or MOSFETs (Metal-Oxide Semiconductor Field-Effect Transistors). The choice for either of them depends on the required power, current and voltage rating as well as on the desired switching frequency. For the highest power ratings (within the megawatt range) no alternative to the GTO is expected (see [Jae93] and [Wyk95]) to appear in the near future. The IGBT will however extend its range of application to ever higher power ratings, offering the advantage of reduced driving, snubbing and protection requirements. Whereas many new converter topologies such as resonant converters and multi-level VSIs are currently under investigation, their industrial application is still very limited. Both [Jae93] and [Wyk95] expect much more of an evolution in manufacturing and packaging (in the medium to high power range) than in the

introduction of new topologies or devices. In this thesis special attention will therefore only be given to the PWM VSI based on IGBTs, and to a less extent also to the PWM VSI based on GTOs.

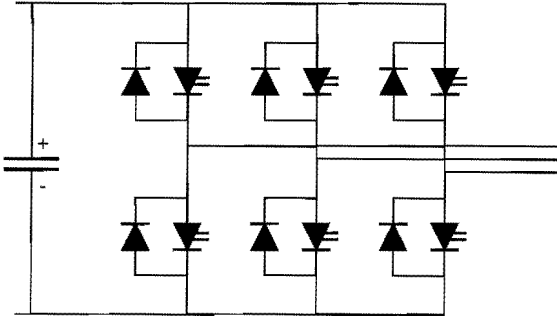


Figure 3.2. Simplified diagram of a voltage-source inverter with arbitrary turn-on-turn-off devices.

To obtain the desired fundamental output voltages, numerous PWM techniques are available, which differ with respect to the harmonic content of the output voltage, the switching frequency (fixed or variable), the harmonic content of the dc current, the dependence on the dc-voltage level, the complexity of the control circuit, etc.

Often the above-mentioned voltage/frequency control is extended with some extra components. Considering equation 3.1, deduced from 2.82 and 2.84, it is clear that if at a certain speed the current varies due to a changing load, the voltage has to be adapted in order to maintain the same (rotor) flux level. This is especially needed at low frequencies, where the voltage drop across the stator resistance becomes large in comparison with the other terms.

$$\mathbf{u}_s^s = r_s \cdot \mathbf{i}_s^s + \mathbf{l}_\sigma \cdot \dot{\mathbf{i}}_s^s + \dot{\boldsymbol{\psi}}_r^s \quad (3.1)$$

Several types of correction of the voltage are possible, based on current measurements (the stator currents or the dc-link current), on estimation of the slip frequency while measuring the rotor speed, or using a closed loop flux controller for which flux measurement or estimation is needed. Although these control methods can result in a very satisfactory steady-state behavior, they are not very well suited if the dynamic behavior of the system is important.

3.3 Vector control of an induction machine

If an electrical machine is to be used in servo applications, the speed and/or the position of the axis have to be controlled dynamically. For these applications a scalar-controlled induction machine is not an appropriate choice. From the torque equation of the

induction machine, equation 2.88, it can be seen that the torque is in fact a vector product of the stator current and the rotor-flux vector. It would be very practical if, instead, the torque were the result of a scalar multiplication of a flux and a current. The torque could then be controlled easily by varying the current while maintaining the flux at a constant level. There *is* another type of machine for which this is the case: the separately-excited dc machine. Consider the torque equation (3.2) of this machine.

$$m_{el} = c \cdot i_f \cdot i_a \quad (3.2)$$

In this equation i_f is the field current, resulting in a magnetic induction that is always perpendicular to the direction of the axis of the armature winding due to the mechanical commutator. The armature current i_a and the field current can be controlled completely independently. The resulting torque m_{el} is proportional to these currents (with a constant factor c , if saturation can be avoided and compensation windings are used), and thus an accurate, scalar control of these two currents is sufficient to obtain an accurate torque control (see eg. [Leon-85]). However, the mechanical commutator which yields this excellent behavior is also the cause of many relative disadvantages of the dc machine: it restricts the power and speed of the machine, requires periodical maintenance, increases the inertia and the axial length and prohibits the use of the dc machine in areas with an explosive atmosphere.

The torque equation of the induction machine (3.3) looks far more complicated at first sight. This is due to the fact that both the current and the magnetic induction (or the flux) have to be considered as rotating vectors instead of as scalars. In the dc machine a scalar approach was possible because the current and the induction had a fixed physical position with respect to the stator of the machine. Apart from this, the current and the rotor flux vector in an induction machine are normally not perpendicular to each other.

$$m_{el} = \psi_r^{s1} \cdot i_s^{s2} - \psi_r^{s2} \cdot i_s^{s1} \quad (3.3)$$

Equations similar to those of the dc machine can be obtained if the induction machine is considered in such a way that the air-gap induction is seen as a non-moving excitation field. Imagine, for example, an observer rotating at the same speed as the rotor-flux vector, at a position φ_r^s , equal to the direction of the rotor-flux vector with respect to the stator. The rotor-flux vector itself becomes then per definition a scalar, as in equation 3.4.

$$\psi_r^{\psi r} = \begin{bmatrix} \psi_r^{\psi r1} \\ \psi_r^{\psi r2} \end{bmatrix} = R(-\varphi_r^s) \cdot \begin{bmatrix} \psi_r^{s1} \\ \psi_r^{s2} \end{bmatrix} = \begin{bmatrix} \psi_r \\ 0 \end{bmatrix} \quad (3.4)$$

Also the stator current vector can now be considered in this reference frame, as indicated in equation 3.5. A graphical representation of the different vectors and angles is given in figure 3.3.

$$\mathbf{i}_s^{\psi r} = \begin{bmatrix} i_s^{\psi r1} \\ i_s^{\psi r2} \end{bmatrix} = \mathbf{R}(-\varphi_r^s) \cdot \begin{bmatrix} i_s^{s1} \\ i_s^{s2} \end{bmatrix} \quad (3.5)$$

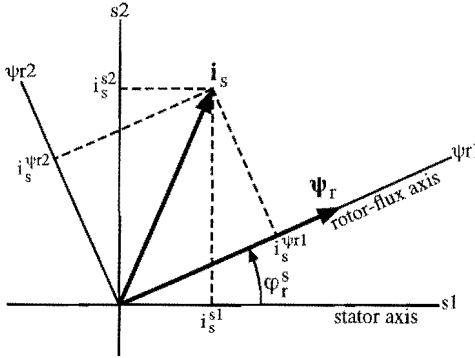


Figure 3.3. The stator-current vector in different reference frames.

Using equations 3.4 and 3.5 the torque from equation 2.88 can be written as a function of the flux and the current vector seen by this observer, as in 3.6.

$$m_{el} = \left[\mathbf{R}\left(\frac{\pi}{2}\right) \cdot \mathbf{R}(\varphi_r^s) \cdot \boldsymbol{\psi}_r^{\psi r} \right]^T \cdot \mathbf{R}(\varphi_r^s) \cdot \mathbf{i}_s^{\psi r} = \left[\mathbf{R}\left(\frac{\pi}{2}\right) \cdot \boldsymbol{\psi}_r^{\psi r} \right]^T \cdot \mathbf{i}_s^{\psi r} = \psi_r \cdot i_s^{\psi r2} \quad (3.6)$$

This means that for this observer the torque is simply the product of the rotor flux and the perpendicular component of the stator current. Thus, by transforming the stator current from a three-phase to a two-phase system, and then rotating it over minus the flux angle φ_r^s , the stator current is decomposed into two components, to one of which the torque is proportional. Of the other, the average is proportional to the amplitude of the flux vector, as will be shown later. A control system which uses this decomposition is called a field-oriented control system. The method was invented around 1970 by Blaschke ([Blas-71], [Blas-73]) and forms the basis for a whole new generation of machine control systems. An overview covering 20 years of field orientation is found in [Leon-91].

Apart from orientation on the rotor-flux vector it is also possible to use other rotating reference frames, oriented on the stator flux or the air-gap flux (for a comparison see eg. [Donc-95]), the desired stator flux (see [Velt-94]), or the rotor. An advantage of using the rotor-flux vector will be shown in the next section. The actual control of the torque and the flux using these different reference frames can be realized in many different ways. In traditional field-orientation, the power converter is seen as an ideal voltage or current source. More recent control methods couple the switching actions of the power converter directly to the variation of field-oriented quantities ([Taka-86], [Depe-85], [Tiit-95]). All these methods have in common that using a vectorial approach they can dynamically control the machine.

3.4 Field-oriented control of a current-fed induction machine

In this section the equations of the induction machine will be rewritten in the rotor-flux-oriented reference frame and an elementary control system will be designed for a current-fed machine – i.e. a machine of which the stator currents are directly imposed by the control circuit.

The equations in stator and rotor coordinates have been given in equations 2.82 to 2.91. By rotating both the flux and the currents to rotor-flux coordinates, equation 2.85 is transformed into equation 3.7.

$$\boldsymbol{\psi}_r^{\psi r} = 1 \cdot (\mathbf{i}_s^{\psi r} + \mathbf{i}_r^{\psi r}) \rightarrow \begin{cases} \psi_r = 1 \cdot (\mathbf{i}_s^{\psi r1} + \mathbf{i}_r^{\psi r1}) \\ 0 = 1 \cdot (\mathbf{i}_s^{\psi r2} + \mathbf{i}_r^{\psi r2}) \end{cases} \quad (3.7)$$

Equation 2.86 can be transformed using a rotation over φ_r^r , the angle between the rotor flux and the rotor, as in equation 3.8. The time derivative of the rotation matrix is calculated separately in equation 3.9, and then substituted in 3.8, resulting in 3.10.

$$\mathbf{0} = \frac{d}{dt} (\mathbf{R}(\varphi_r^r) \cdot \boldsymbol{\psi}_r^{\psi r}) + r_r \cdot \mathbf{R}(\varphi_r^r) \cdot \mathbf{i}_r^{\psi r} = \frac{d\mathbf{R}(\varphi_r^r)}{dt} \cdot \boldsymbol{\psi}_r^{\psi r} + \mathbf{R}(\varphi_r^r) \cdot (\dot{\boldsymbol{\psi}}_r^{\psi r} + r_r \cdot \mathbf{i}_r^{\psi r}) \quad (3.8)$$

$$\frac{d\mathbf{R}(\varphi_r^r)}{dt} = \frac{d}{dt} \begin{bmatrix} \cos \varphi_r^r & -\sin \varphi_r^r \\ \sin \varphi_r^r & \cos \varphi_r^r \end{bmatrix} = \dot{\varphi}_r^r \cdot \begin{bmatrix} \cos(\varphi_r^r + \frac{\pi}{2}) & -\sin(\varphi_r^r + \frac{\pi}{2}) \\ \sin(\varphi_r^r + \frac{\pi}{2}) & \cos(\varphi_r^r + \frac{\pi}{2}) \end{bmatrix} = \dot{\varphi}_r^r \cdot \mathbf{R}(\varphi_r^r) \cdot \mathbf{R}(\frac{\pi}{2}) \quad (3.9)$$

$$\mathbf{R}(\varphi_r^r) \cdot \mathbf{R}(\frac{\pi}{2}) \cdot \dot{\varphi}_r^r \cdot \boldsymbol{\psi}_r^{\psi r} + \mathbf{R}(\varphi_r^r) \cdot \dot{\boldsymbol{\psi}}_r^{\psi r} = -r_r \cdot \mathbf{R}(\varphi_r^r) \cdot \mathbf{i}_r^{\psi r} \quad (3.10)$$

By eliminating the rotation over φ_r^r from equation 3.10 and splitting the vector equation into its components, equation 3.11 is obtained.

$$\begin{aligned} \dot{\psi}_r &= -r_r \cdot \mathbf{i}_r^{\psi r1} \\ \dot{\varphi}_r^r \cdot \psi_r &= -r_r \cdot \mathbf{i}_r^{\psi r2} \end{aligned} \quad (3.11)$$

Equation 3.11 together with 3.7 describe the core part of the machine model which is shown in figure 3.4. Equations 3.6, 2.89 and 2.90 give the relation between the rotor flux, the torque-producing current component $\mathbf{i}_s^{\psi r2}$, the torque, the speed and the rotor position. Equation 2.41 describes how the three phase currents are transformed to the two-phase system, and 3.5 transforms this current vector to the flux coordinate system by means of a rotation. Finally, equation 3.12 gives the relation between some angles: the angle of the rotor flux with respect to the stator equals the angle of that flux with respect to the rotor plus the angle of the rotor with respect to the stator.

$$\varphi_r^s = \varphi_r^r + \rho^s \tag{3.12}$$

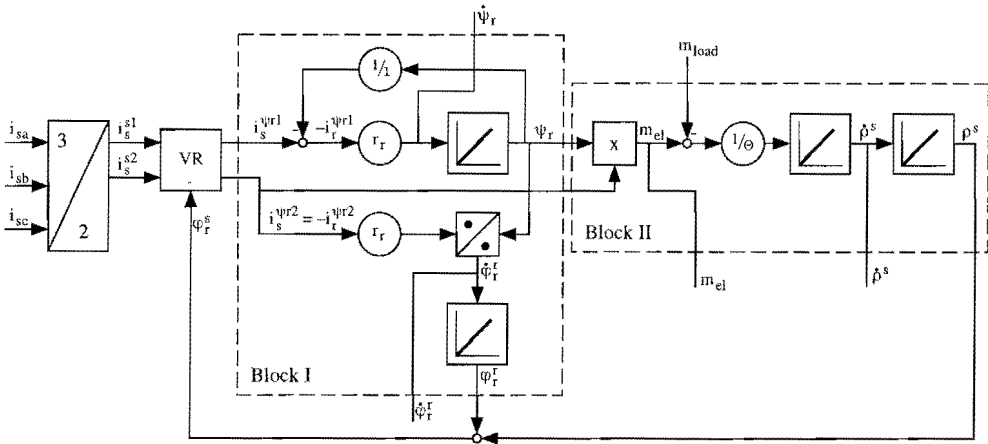


Figure 3.4. Block diagram in rotor-flux coordinates of a current-fed induction machine.

An interesting part of the block diagram shown in figure 3.4 is the relation between the magnetizing current component $i_s^{\psi r1}$ and the rotor flux ψ_r . The complex transfer function from the current to the flux, derived from equations 3.7 and 3.11, is given in equation 3.13, in which s denotes the Laplace operator. This function describes a low-pass filter with a cutoff frequency which for industrial machines is lower than 0.03 pu. This means that rapid oscillations of $i_s^{\psi r1}$, down to frequencies much lower than the rated speed, will be damped considerably. This kind of oscillations will therefore not have any noticeable effect on the amplitude of the rotor flux and, as a consequence, on the delivered torque as well.

$$\underline{\psi}_r = \frac{r_r}{s + r_r/l} \cdot i_s^{\psi r1} \tag{3.13}$$

The decomposition of the stator current into rotor-flux oriented components has thus the effect of splitting the current into $i_s^{\psi r2}$, a component of which every small variation will be noticed in the electromagnetical torque, and a second component, $i_s^{\psi r1}$, which is allowed to contain rapid oscillations. Only the average of $i_s^{\psi r1}$ is required to remain constant in order to maintain a constant flux level. This will turn out to be an important advantage of rotor-flux orientation (see section 8.3.2).

From the block diagram shown in figure 3.4, the essential part of the circuit needed to implement field-oriented control of a current-fed induction machine can easily be derived. Figure 3.5 shows how the desired field-oriented current components are rotated to the stator frame. These currents are then transformed to three current command values. These can be used in e.g. a hysteresis current controller to control the three phase currents of the machine.

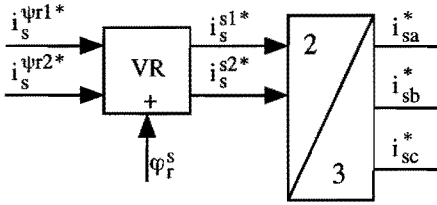


Figure 3.5. Basic circuit for field-oriented control of a current-fed induction machine.

The basic control circuit shown in figure 3.5 has three inputs: two currents and an angle. The desired field-oriented current components can easily be calculated from the desired rotor flux and the desired torque. Using equations 3.6 and 3.13, equations 3.14 and 3.15 are obtained. If the flux does not need to be varied dynamically, equation 3.15 can be simplified to 3.16. Unfortunately, these equations contain two machine parameters: the rotor resistance and the main inductance. Knowing these parameters at all times might represent a problem, especially as they are not necessarily constant. The notation $\hat{\psi}_r$ resp. \hat{i}_r is used to distinguish the parameters used in the control circuit from the real parameters of the machine.

$$i_s^{\psi r2*} = m_{el}^* / \psi_r^* \quad (3.14)$$

$$i_s^{\psi r1*} = \frac{\psi_r^*}{\hat{l}} + \frac{1}{\hat{i}_r} \cdot \frac{d\psi_r^*}{dt} \quad (3.15)$$

$$i_s^{\psi r1*} = \frac{\psi_r^*}{\hat{l}} \quad (3.16)$$

There is however an important problem with field orientation which is not yet fully solved for all operating conditions. As shown in figure 3.5, the position of the rotor flux with respect to the stator also has to be known. In section 3.6 some methods to obtain this information are presented.

3.5 Field-oriented control of a voltage-fed induction machine

To model or to control a voltage-fed induction machine, the stator-voltage equation, equation 3.1, must also be transformed to rotor-flux coordinates. This is done in equations 3.17 and 3.18, after which the voltage equation is split into its two components in equation 3.19.

$$R(\varphi_r^s) \cdot \mathbf{u}_s^{\psi r} = r_s \cdot R(\varphi_r^s) \cdot \mathbf{i}_s^{\psi r} + l_\sigma \cdot \frac{d}{dt} (R(\varphi_r^s) \cdot \mathbf{i}_s^{\psi r}) + \frac{d}{dt} (R(\varphi_r^s) \cdot \psi_r^{\psi r}) \quad (3.17)$$

$$\mathbf{u}_s^{\psi r} = r_s \cdot \mathbf{i}_s^{\psi r} + \mathbf{1}_\sigma \cdot \left(\dot{\hat{\phi}}_r^s \cdot R\left(\frac{\pi}{2}\right) \cdot \mathbf{i}_s^{\psi r} + \dot{\mathbf{i}}_s^{\psi r} \right) + \left(\hat{\phi}_r^s \cdot R\left(\frac{\pi}{2}\right) \cdot \boldsymbol{\psi}_r^{\psi r} + \dot{\boldsymbol{\psi}}_r^{\psi r} \right) \quad (3.18)$$

$$\begin{aligned} u_s^{\psi r1} &= r_s \cdot i_s^{\psi r1} - \mathbf{1}_\sigma \cdot \dot{\hat{\phi}}_r^s \cdot i_s^{\psi r2} + \mathbf{1}_\sigma \cdot \dot{i}_s^{\psi r1} + \dot{\psi}_r \\ u_s^{\psi r2} &= r_s \cdot i_s^{\psi r2} + \mathbf{1}_\sigma \cdot \dot{\hat{\phi}}_r^s \cdot i_s^{\psi r1} + \mathbf{1}_\sigma \cdot \dot{i}_s^{\psi r2} + \dot{\hat{\phi}}_r^s \cdot \psi_r \end{aligned} \quad (3.19)$$

Equation 3.19 can then be used to create the block diagram of the voltage-fed induction machine, shown in figure 3.6. The parts of the block diagram which are common for both the voltage-fed and the current-fed machines (block I and block II) are not shown in detail in this figure – they can be found in figure 3.4 instead.

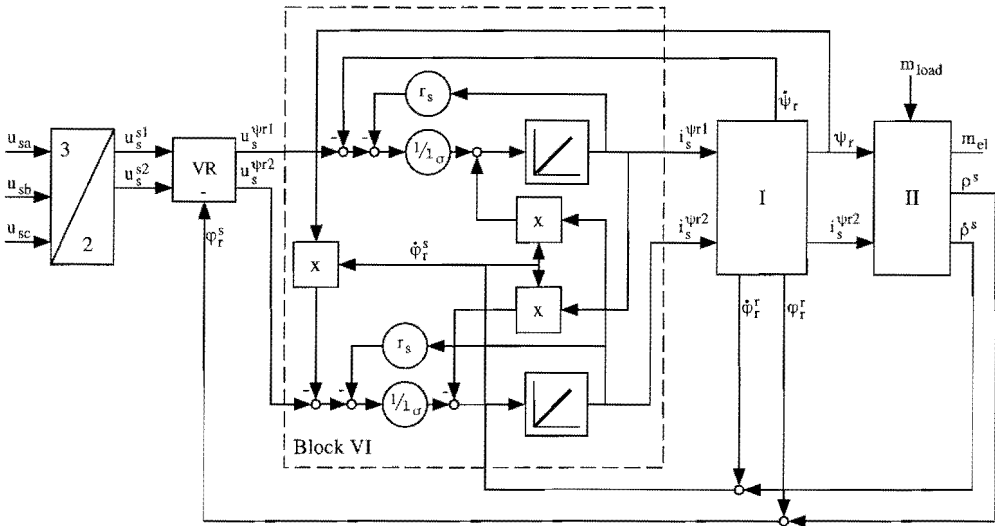


Figure 3.6. Block diagram in rotor-flux coordinates of a voltage-fed induction machine.

Equation 3.19 can also be used to calculate the desired voltages as a function of the desired currents, as a part of the field-oriented control scheme shown in figure 3.7. The abbreviation “VVC” used for this block stands for Voltage-Vector Calculator. The desired field-oriented currents can again be calculated by using equations 3.14 and 3.15 or 3.16.

In this control circuit not only the flux angle has to be known to obtain a correct field orientation, but also the flux amplitude and its derivative and the derivative of the flux angle. Apart from this, two more machine parameters must be known: the stator resistance r_s and the leakage inductance $\mathbf{1}_\sigma$. In figure 3.7 they are denoted by \hat{r}_s and $\hat{\mathbf{1}}_\sigma$ to indicate that these are estimated parameters which are not necessarily equal to the real machine parameters at any moment of time.

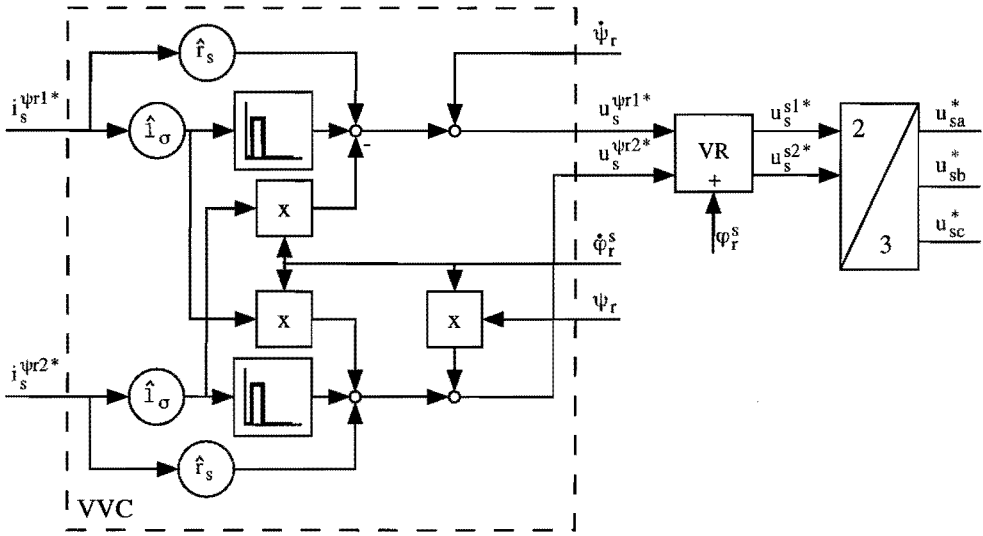


Figure 3.7. Basic circuit for field-oriented control of a voltage-fed induction machine.

3.6 Methods to determine the flux vector

The most essential part of any field-oriented control system is the circuit determining the flux vector, because the angle of this vector is needed to rotate the desired field-oriented quantities to the quantities which are imposed at the stator. The methods to determine this vector can be divided into two categories: the direct methods, which use measured electrical quantities to calculate the flux vector, and the indirect methods, which use apart from electrical quantities also a mechanical quantity, the rotor position. Both methods will now be discussed shortly.

The most elementary of the direct methods is based on the measurement of the air-gap induction by means of Hall sensors. Assuming a sinusoidal distribution of the induction, two sensors are sufficient to determine the air-gap induction and thus the air-gap flux vector. This method is never used in industry, because it would add vulnerable and unconventional components to the otherwise robust and standard induction machine. Apart from this, the signals from the Hall sensors are in practice highly distorted by the effects of rotor slots.

Another direct method uses the measured stator voltages and currents to determine the stator flux, taking into account that $\mathbf{u}_s^s = r_s \cdot \mathbf{i}_s^s + \dot{\boldsymbol{\psi}}_s^s$. If, apart from the stator resistance, also the leakage inductance l_σ is known, the rotor flux can be determined according to equation 3.1. While this model to calculate the flux relies on the measured voltages and currents it is referred to as the voltage model (see eg. [Leon-91]), or as the voltage/current (u/i) model. A block diagram of the u/i-model is shown in figure 3.8. The main difficulty

in this model is the stability at and near zero flux frequency, because in that case the induced voltages will be relatively small compared to estimation errors caused by drift of the integrators or by a u/i -model resistance \tilde{r}_s being unequal to the machine stator resistance r_s .

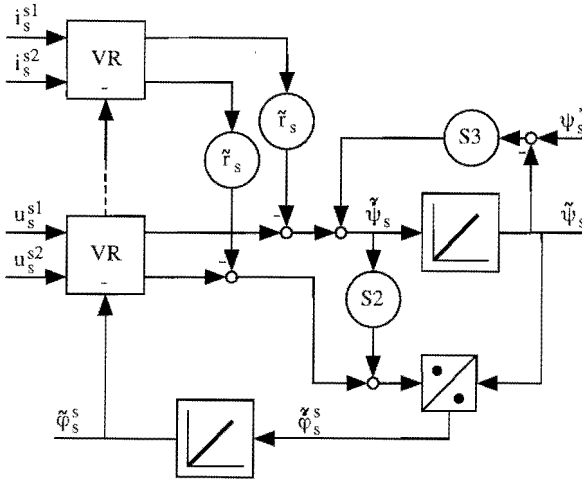


Figure 3.8. The u/i -model with the feedbacks proposed by van der Burgt.

Van der Burgt (see [Burg-95] or [Burg-96]) shows that the stability of the u/i -model at high frequencies is guaranteed using the feedback parameter S2, and that a considerable improvement in the low frequency range is obtained using feedback parameter S3. The feedback with S2 is based on the fact that in normal operation the derivative of the stator-flux amplitude will be zero, and that a deviation from this situation is caused by drift or parameter deviation, and should thus be minimized. Consequently, it is clear that the influence of S2 should be kept to a minimum if operation with a nonconstant stator-flux amplitude is required. Parameter S3 uses the fact that in normal operating conditions the stator flux $\tilde{\psi}_s$ in the machine model will be equal to the stator-flux desired value ψ_s^* and that a deviation from this can also be corrected by a feedback in the u/i -model.

A problem with parameter S3 might arise during operation with a fault in the power converter. If, due to such a fault, the real-machine stator flux ψ_s deviates from the desired value ψ_s^* , forcing the u/i -model flux $\tilde{\psi}_s$ by means of S3 to track the desired value will make the model flux deviate from the real flux. Therefore, the influence of S3 should be kept to a minimum, by taking S3 as small as possible. If another method to determine the flux at very low speeds is available, S3 can be omitted completely.

The indirect method of flux-vector determination does not have a problem at low speeds. This method uses the desired field-oriented stator-current components and the measured rotor speed or position to estimate the rotor-flux position. A block diagram of the corresponding circuit, the so-called current or current/rotor-speed (i/ρ^s) model, is shown

in figure 3.9 (compare with figure 3.4). This method relies on knowledge of the rotor resistance r_r and the main inductance l . Especially the need of the rotor resistance is problematic, because during operation this parameter will change due to heating of the rotor. An on-line adaptation scheme is therefore required. The main inductance will depend on the saturation of the machine, but this dependency could be measured beforehand.

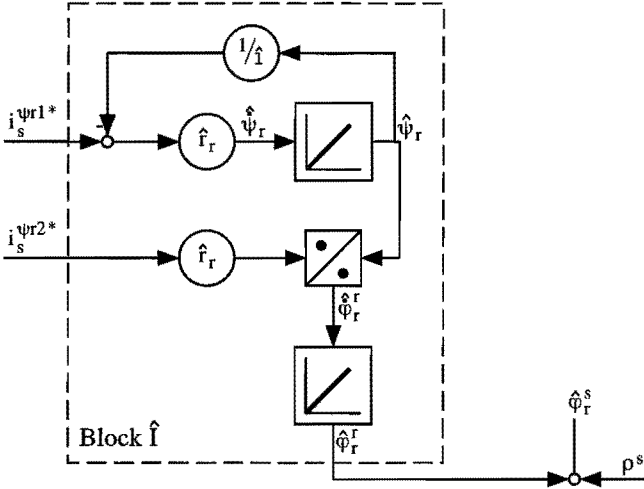


Figure 3.9. Flux-estimation model used for indirect field-oriented control.

Measuring the rotor position is undesirable in applications where an accurate position control is not required, and where a position sensor would thus normally not be needed. At this moment, new flux estimation methods are still under investigation, which will eventually eliminate the need for a position sensor in the full operation range of the induction machine, including the area of very low flux frequency (see eg. [Schr-93], [Blas-96b]).

For the experiments and simulations in this thesis, the u/i -model with the two feedback parameters S2 and S3 has been used. This method was chosen because operation at very low speeds was not an important issue, while at high speeds the u/i -model is much less sensitive to parameter detuning than the i/ρ^s -model.

Chapter 4

Modeling the Homopolar Impedance

4.1 Introduction

In the second half of Chapter 2 (starting from section 2.6) and in Chapter 3 it was assumed that only the fundamental component of the air-gap magnetic induction had to be considered. With this assumption the machine has been described by an equivalent two-phase model. However, in certain cases, which will be specified in this chapter, it is necessary to extend the model in such a way that at least the effect of a third space harmonic in the induction is accounted for. The importance of this harmonic can be understood from figure 2.6, showing a third harmonic with an amplitude of more than 20% of the fundamental.

The instrument used to model this effect will turn out to be a homopolar impedance, which defines a relation between the homopolar current and voltage components. Here the word “homopolar” refers to those components that are equally present in all phases. Traditionally, the homopolar impedance is related to axial fluxes in the machine. In this chapter it will be shown that a non-zero homopolar impedance is also present in case the winding distribution of a phase, which equals the current distribution divided by the winding current, contains a third harmonic, while no axial fluxes are present.

This chapter will present a calculation method for the homopolar impedance, and introduces an extension to the equations and machine model derived previously.

4.2 Calculation of the homopolar inductance

To study the effect of a third harmonic in the air-gap induction, consider the case where the stator-current distribution along the air gap contains a third harmonic. The third-harmonic current distributions caused by the three phase currents are given by equation 4.1 (cf. equation 2.39 for the fundamental components).

$$\begin{aligned} a_{sa3}(\theta^s) &= i_{sa} \cdot v_{s3} \cdot \cos\left(3\theta^s + \frac{\pi}{2}\right) \\ a_{sb3}(\theta^s) &= i_{sb} \cdot v_{s3} \cdot \cos\left(3\left(\theta^s - \frac{2\pi}{3}\right) + \frac{\pi}{2}\right) \\ a_{sc3}(\theta^s) &= i_{sc} \cdot v_{s3} \cdot \cos\left(3\left(\theta^s - \frac{4\pi}{3}\right) + \frac{\pi}{2}\right) \end{aligned} \quad (4.1)$$

The total third-harmonic component of the air-gap current distribution $a_s(\theta^s)$ can be found by adding these components. The result is given in equation 4.2. This equation shows that a third harmonic in the current distribution is present only if the sum of the phase currents is not equal to zero. This sum, which is equal to the current flowing in the star-point connection (see figure 4.1) is called the homopolar current, defined in equation 4.3. If the star point is not connected, no homopolar current can flow, and therefore also the air-gap current distribution $a_s(\theta^s)$ will not contain a third harmonic.

$$a_{s3}(\theta^s) = (i_{sa} + i_{sb} + i_{sc}) \cdot v_{s3} \cdot \cos\left(3\theta^s + \frac{\pi}{2}\right) \quad (4.2)$$

$$i_{s0} = i_{sa} + i_{sb} + i_{sc} \quad (4.3)$$

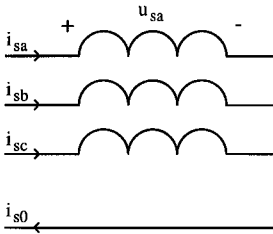


Figure 4.1. Representation of an induction machine showing the three phase currents and the homopolar current.

Equation 4.3 introduces a third current component, which is independent of i_s^{s1} and i_s^{s2} as introduced previously. The three independent phase currents i_{sa} , i_{sb} and i_{sc} are thus completely determined by two orthogonal and one homopolar component. In case the star point is not connected, the three phase currents are not independent. Then i_s^{s1} and i_s^{s2} alone determine all currents, and i_{s0} will be zero. Combining equations 2.41 and 4.3 results in equation 4.4.

$$\begin{aligned} i_s^{s1} &= i_{sa} - \frac{1}{2} i_{sb} - \frac{1}{2} i_{sc} \\ i_s^{s2} &= \frac{\sqrt{3}}{2} i_{sb} - \frac{\sqrt{3}}{2} i_{sc} \\ i_{s0} &= i_{sa} + i_{sb} + i_{sc} \end{aligned} \quad (4.4)$$

In matrix notation this equation can be written as in equation 4.5. As the three equations are independent, this relation can also be inverted. This inverse transformation is given in equation 4.6.

$$\begin{bmatrix} i_s^{s1} \\ i_s^{s2} \\ i_{s0} \end{bmatrix} = \begin{bmatrix} 1 & -\frac{1}{2} & -\frac{1}{2} \\ 0 & \frac{\sqrt{3}}{2} & -\frac{\sqrt{3}}{2} \\ 1 & 1 & 1 \end{bmatrix} \cdot \begin{bmatrix} i_{sa} \\ i_{sb} \\ i_{sc} \end{bmatrix} \quad (4.5)$$

$$\begin{bmatrix} i_{sa} \\ i_{sb} \\ i_{sc} \end{bmatrix} = \begin{bmatrix} \frac{2}{3} & 0 & \frac{1}{3} \\ -\frac{1}{3} & \frac{1}{\sqrt{3}} & \frac{1}{3} \\ -\frac{1}{3} & -\frac{1}{\sqrt{3}} & \frac{1}{3} \end{bmatrix} \cdot \begin{bmatrix} i_s^{s1} \\ i_s^{s2} \\ i_{s0} \end{bmatrix} \tag{4.6}$$

To determine the homopolar inductance, the three phase currents will now be chosen in such a way that the fundamental of the stator-current distribution $a_s(\theta^s)$ equals zero. This fundamental can be written as the sum of the two orthogonal components from equation 2.40, from which it can be seen that the two orthogonal current components i_s^{s1} and i_s^{s2} have to be zero for this case. This is described by equation 4.7, resulting in equation 4.8.

$$\begin{aligned} 0 &= i_{sa} - \frac{1}{2} i_{sb} - \frac{1}{2} i_{sc} \\ 0 &= \frac{\sqrt{3}}{2} i_{sb} - \frac{\sqrt{3}}{2} i_{sc} \end{aligned} \tag{4.7}$$

$$i_{sa} = i_{sb} = i_{sc} \quad (= i_{s0}/3) \tag{4.8}$$

Thus, the fundamental component of the stator-current distribution can be eliminated by making all phase currents equal.

The calculation of the flux linking a winding when the machine is fed by a homopolar current component only, assuming the rotor currents to be zero, is very much the same as the calculation performed in section 2.3.3. In that section the relation between the current and the flux was derived for the symmetrical set of currents from equation 2.10, in which no homopolar component was present. Figure 4.2 shows the currents in each slot and the MMF for the same example winding configuration, for the case when $i_{sa} = i_{sb} = i_{sc} = i_{s0}/3$.

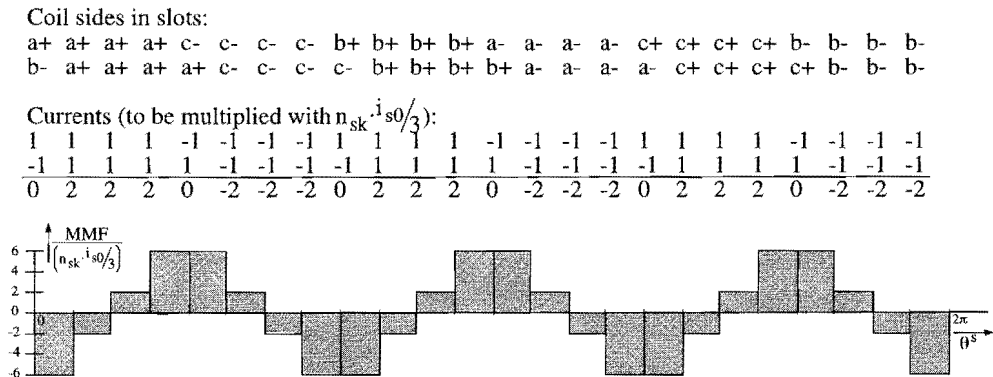


Figure 4.2. Calculation of the MMF for the example winding configuration when only a homopolar current is supplied.

When a harmonic analysis of the MMF from figure 4.2 is performed, only odd harmonics which are a multiple of three are found, as expected. Using equations 2.5 and 2.6, as in section 2.3.3, the flux linking a winding is obtained. The result is given in equation 4.9. It should be noted that again leakage fluxes are not considered.

$$\psi_{sa} = 3^{1/3} \cdot \frac{\mu_0 \pi r \ell (n_{sk})^2 \cdot i_{s0/3}}{d} \quad (4.9)$$

The inductance describing the relation between the flux linking a winding and the current in that winding in case the same current is present in all windings is the so-called homopolar stator inductance l_{sq0} , given in equation 4.10.

$$l_{sq0} = \frac{\psi_{sq}}{i_{s0/3}} = 3^{1/3} \cdot \frac{\mu_0 \pi r \ell (n_{sk})^2}{d} \quad (4.10)$$

Some further calculations have shown that the value of l_{sq0} strongly depends on the winding configuration. For example, shifting the outer layer with respect to the inner one results in a large variation of this parameter. This is a well known phenomenon – it also occurs for higher harmonics, and is used by machine designers to minimize the amplitude of the 5th and 7th harmonics in the current distribution.

Of course, also the method described in [Jord-75], used in section 2.3.4 for the case with the symmetrical supply, can be used to calculate the homopolar inductance. When all windings are supplied by the same current, the number of phases actually becomes one, so $m = 1$. The number of pole pairs however is increased from one to three: $p = 3$. Because the third harmonic of the air-gap induction is concerned, in equations 2.23 and 2.24 $\nu = 3$ has to be substituted. Finally, in equation 2.19, the factor $m/2$ must be replaced by 3, because when all windings carry the same current the resulting induction will be three times larger than when a single winding is supplied. Equation 4.11 gives the total winding factor for this case, and equation 4.12 the homopolar stator inductance.

$$\xi_3 = \frac{\sin\left(\frac{3\pi}{2pm}\right)}{n \sin\left(\frac{3\pi}{2pm} \cdot \frac{1}{n}\right)} \cdot \cos\left(\frac{3\pi}{S} \Delta\right) = \frac{\sin\left(\frac{3\pi}{2 \cdot 3 \cdot 1}\right)}{4 \sin\left(\frac{3\pi}{2 \cdot 3 \cdot 1} \cdot \frac{1}{4}\right)} \cdot \cos\left(\frac{3\pi}{24} \cdot 1\right) = 0.6036 \quad (4.11)$$

$$l_{sq0} = \mu_0 \frac{2 \cdot 6 r \ell}{\pi d p^2} \xi_3^2 (n_{sq})^2 = \frac{2 \cdot 6 \xi_3^2 8^2}{\pi^2 p^2} \cdot \frac{\mu_0 \pi r \ell (n_{sk})^2}{d} = 3.150 \frac{\mu_0 \pi r \ell (n_{sk})^2}{d} \quad (4.12)$$

Again the method used by Jordan gives a smaller result than the method which includes also higher harmonics of the air-gap induction, as noted previously concerning equation 2.27.

By comparing equation 4.12 with 2.27, substituting the correct values for p and n , the relation between the main inductance and the homopolar inductance can be found. The result, given in 4.13, is the same as was obtained by Jordan in [Jord-54].

$$L_{sq0} = \frac{2}{9} \cdot \left(\frac{\xi_3}{\xi_1} \right)^2 \cdot L_{sq} \quad (4.13)$$

4.3 Extension to the orthogonal model

An important question is whether the homopolar current and flux also contribute to the electromagnetical torque. As shown in section 2.5, torque is created only if the rotor currents cause a magnetic induction with the same number of poles as caused by the stator currents. In the case of a wound rotor, this is only possible if a homopolar current can flow in the rotor as well as in the stator. However, usually the rotor windings have a Y-connection in which the star point is not connected, so no homopolar currents can flow and thus no torque will result.

In a squirrel cage rotor on the contrary, currents will be induced by the induction caused by the homopolar stator current. A detailed calculation of the resulting torque can be found in [Lax-42]. Without repeating this detailed analysis, some remarks on this torque will be made. The induction caused by a sinusoidal homopolar current is a standing wave, which can be decomposed into two traveling waves rotating in opposite directions. The speed at which they travel equals one third of the speed of the traveling wave caused by a symmetrical set of currents with the same frequency. Because of this, no resulting torque will be present at standstill, an accelerating torque will result for speeds below approximately one third of the stator-current frequency, and a braking torque appears for higher speeds. Thus, in normal operating conditions, i.e. when the machine is running with a low slip frequency, the addition of a homopolar current with the same frequency as the non-homopolar stator currents will add a braking torque.

In this thesis only the case where a wound rotor in which no homopolar current can flow will be considered further. The presence of a homopolar stator current and flux will thus not have any influence on the torque. From equation 4.5, substituting identical values for the three phase currents, it can be seen that the currents i_s^{s1} and i_s^{s2} are not affected by a homopolar current. To obtain no resulting torque (using equation 2.88 to calculate the torque) also the fluxes in the two-phase machine model should not be affected. This is obtained by assuming that the windings of the equivalent two-phase machine do not generate a third space harmonic in the air-gap induction, and therefore no resulting flux related to such a third harmonic air-gap induction is linking them. This is shown in the equations given below.

Assuming that the induction can be written as in equation 4.14, the flux linking the two-phase windings can be calculated in the same way as in equations 2.47 and 2.48, and the result is given in 4.15 and 4.16.

$$b_{1l}(\theta^s) = b_{11}^{s1} \cdot \cos(\theta^s) + b_{11}^{s2} \cdot \sin(\theta^s) + b_{13}^{s1} \cdot \cos(3\theta^s) + b_{13}^{s2} \cdot \sin(3\theta^s) \quad (4.14)$$

$$\psi_{1s}^{s1} = \int_{\theta^s=0}^{\pi} \frac{a_{s1}(\theta^s)}{i_s^{s1}} r \int_{\tau^s=\theta^s-\pi}^{\theta^s} -b_{1l}(\tau^s) \ell r d\tau^s d\theta^s = \pi r^2 \ell v_{s1} b_{11}^{s1} \quad (4.15)$$

$$\psi_{1s}^{s2} = \int_{\theta^s=-\frac{\pi}{2}}^{\frac{3\pi}{2}} \frac{a_{s2}(\theta^s)}{i_s^{s2}} r \int_{\tau^s=\theta^s-\pi}^{\theta^s} -b_{1l}(\tau^s) \ell r d\tau^s d\theta^s = \pi r^2 \ell v_{s1} b_{11}^{s2} \quad (4.16)$$

The fluxes linking the three phase windings will however consist of a part caused by the fundamental of the air-gap induction, as calculated in equations 2.44, 2.45 and 2.46, and a part caused by the third harmonic. Assuming that the current distribution caused by a phase current is the summation of a fundamental (as in equation 2.39) and a third harmonic (equation 4.1), the flux linking each of the phases can be calculated as in equations 4.17, 4.18 and 4.19.

$$\begin{aligned} \psi_{1sa} &= \int_{\theta^s=0}^{\pi} \frac{a_{sa}(\theta^s)}{i_{sa}} r \int_{\tau^s=\theta^s-\pi}^{\theta^s} -b_{1l}(\tau^s) \ell r d\tau^s d\theta^s = \\ &= \int_{\theta^s=0}^{\pi} \left(v_{s1} \cdot \sin \theta^s + v_{s3} \cdot \sin(3\theta^s) \right) r \cdot \int_{\tau^s=\theta^s-\pi}^{\theta^s} b_{1l}(\tau^s) \ell r d\tau^s d\theta^s \quad (4.17) \\ &= \pi r^2 \ell v_{s1} b_{11}^{s1} + \frac{\pi}{3} r^2 \ell v_{s3} b_{13}^{s1} \end{aligned}$$

$$\psi_{1sb} = \pi r^2 \ell v_{s1} \left(-\frac{1}{2} b_{11}^{s1} + \frac{1}{2} \sqrt{3} b_{11}^{s2} \right) + \frac{\pi}{3} r^2 \ell v_{s3} b_{13}^{s1} \quad (4.18)$$

$$\psi_{1sc} = \pi r^2 \ell v_{s1} \left(-\frac{1}{2} b_{11}^{s1} - \frac{1}{2} \sqrt{3} b_{11}^{s2} \right) + \frac{\pi}{3} r^2 \ell v_{s3} b_{13}^{s1} \quad (4.19)$$

The part which is common for the air-gap fluxes linking the three phases, and which is related to the third harmonic of the induction, is the air-gap homopolar flux ψ_{1s0} , calculated with equation 4.20. The relation between this flux and the homopolar current is given in equation 4.21, derived from equations 4.10 and 4.20.

$$\psi_{1s0} = \frac{1}{3} (\psi_{1sa} + \psi_{1sb} + \psi_{1sc}) \quad (4.20)$$

$$\psi_{1s0} = l_{sq0} \cdot \frac{i_{s0}}{3} \quad (4.21)$$

From equations 4.15 to 4.19 the relation between the two- and three-phase fluxes can be derived. In contrast with the situation in equations 2.44 to 2.46, the three fluxes are now independent, so that the relation between the three-phase fluxes and the orthogonal fluxes is a unique relation. This relation is given in equation 4.22.

$$\begin{aligned} \psi_{1s}^{s1} &= \frac{2}{3} \psi_{1sa} - \frac{1}{3} \psi_{1sb} - \frac{1}{3} \psi_{1sc} \\ \psi_{1s}^{s2} &= \quad \quad + \frac{1}{\sqrt{3}} \psi_{1sb} - \frac{1}{\sqrt{3}} \psi_{1sc} \end{aligned} \quad (4.22)$$

Combining this equation with equation 4.20, and considering that the same relation is valid for the stator and rotor fluxes as for the air-gap fluxes, a transformation matrix for fluxes is found. This transformation is given in equation 4.23 for the stator fluxes, in the same way as for the currents in equation 4.5. Also in this case the matrix can be inverted, resulting in equation 4.24, which describes how the fluxes linking the individual phase windings can be found from the fluxes in the orthogonal model and the homopolar flux.

$$\begin{bmatrix} \psi_s^{s1} \\ \psi_s^{s2} \\ \psi_{s0} \end{bmatrix} = \begin{bmatrix} \frac{2}{3} & -\frac{1}{3} & -\frac{1}{3} \\ 0 & \frac{1}{\sqrt{3}} & -\frac{1}{\sqrt{3}} \\ \frac{1}{3} & \frac{1}{3} & \frac{1}{3} \end{bmatrix} \cdot \begin{bmatrix} \psi_{sa} \\ \psi_{sb} \\ \psi_{sc} \end{bmatrix} \quad (4.23)$$

$$\begin{bmatrix} \psi_{sa} \\ \psi_{sb} \\ \psi_{sc} \end{bmatrix} = \begin{bmatrix} 1 & 0 & 1 \\ -\frac{1}{2} & \frac{\sqrt{3}}{2} & 1 \\ -\frac{1}{2} & -\frac{\sqrt{3}}{2} & 1 \end{bmatrix} \cdot \begin{bmatrix} \psi_s^{s1} \\ \psi_s^{s2} \\ \psi_{s0} \end{bmatrix} \quad (4.24)$$

Finally, the relation between the homopolar air-gap flux and the homopolar stator flux still has to be specified. The homopolar stator flux is the flux linking a stator winding in case all phases are fed with a current of $i_{s0}/3$. The homopolar air-gap flux is then given by equation 4.21, and the stator flux can be found using equation 2.29, resulting in equation 4.25. The homopolar inductance l_0 , which includes stator leakage, is introduced here as specified in equation 4.26.

$$\psi_{s0} = \psi_{1s0} + l_{\sigma sq} \cdot \frac{i_{s0}}{3} = l_0 \cdot i_{s0} \quad (4.25)$$

$$l_0 = \frac{l_{sq0}}{3} + \frac{l_{\sigma sq}}{3} \quad (4.26)$$

As was the case in section 2.7, the relations between the voltages across the three stator phases and the voltages in the two-phase-plus-homopolar system are the same as those for the fluxes. These relations are given in equations 4.27 and 4.28.

$$\begin{bmatrix} u_s^{s1} \\ u_s^{s2} \\ u_{s0} \end{bmatrix} = \begin{bmatrix} \frac{2}{3} & -\frac{1}{3} & -\frac{1}{3} \\ 0 & \frac{1}{\sqrt{3}} & -\frac{1}{\sqrt{3}} \\ \frac{1}{3} & \frac{1}{3} & \frac{1}{3} \end{bmatrix} \cdot \begin{bmatrix} u_{sa} \\ u_{sb} \\ u_{sc} \end{bmatrix} \quad (4.27)$$

$$\begin{bmatrix} u_{sa} \\ u_{sb} \\ u_{sc} \end{bmatrix} = \begin{bmatrix} 1 & 0 & 1 \\ -\frac{1}{2} & \frac{\sqrt{3}}{2} & 1 \\ -\frac{1}{2} & -\frac{\sqrt{3}}{2} & 1 \end{bmatrix} \cdot \begin{bmatrix} u_s^{s1} \\ u_s^{s2} \\ u_{s0} \end{bmatrix} \quad (4.28)$$

This consideration has led to the introduction of the homopolar voltage u_{s0} , which is the voltage across each of the phases in case only a homopolar current is flowing in the machine. Using equations 4.27, 2.53, 4.23, 4.5 and 4.25, u_{s0} can be written as in equation 4.29.

$$u_{s0} = \frac{1}{3} r_{sq} \cdot i_{s0} + \frac{d\psi_{s0}}{dt} = \frac{1}{3} r_{sq} \cdot i_{s0} + l_0 \cdot \frac{di_{s0}}{dt} \quad (4.29)$$

By introducing the new parameter r_{s0} , defined in equation 4.30, this equation can be simplified to 4.31, which can now be added to the machine model shown in figure 3.6, resulting in figure 4.3.

$$r_{s0} = \frac{1}{3} r_{sq} \quad (4.30)$$

$$u_{s0} = r_{s0} \cdot i_{s0} + l_0 \cdot \frac{di_{s0}}{dt} \quad (4.31)$$

With this simple addition and the new three-to-two-phase transformations, the block diagram has become suited for modeling a machine in which a homopolar current is present. By defining the windings of the equivalent two-phase machine as windings that do not cause a third harmonic in the current distribution, all equations of the equivalent two-phase machine could remain unchanged. The third harmonic in the air-gap induction that will be present in case the machine is fed with a homopolar current has been modeled by adding one single equation, as if one more winding were added to the two-phase machine. A limitation of the newly derived model is that it is valid only for machines in which the rotor is constructed in such a way that the rotor-current distribution can not contain a third space harmonic.

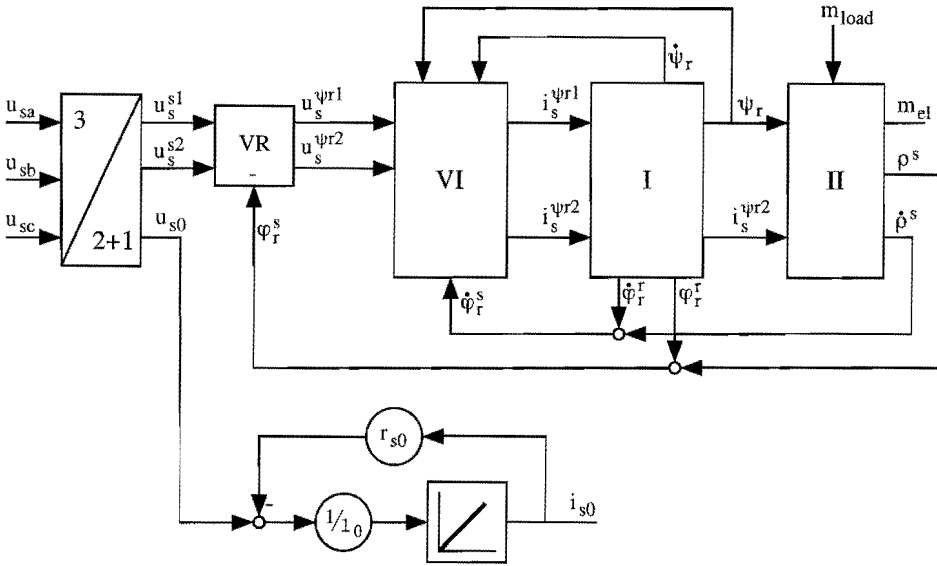


Figure 4.3. Block diagram of a voltage-fed induction machine including the homopolar current and voltage.

Chapter 5

Classification of Asymmetrical Operation Modes

5.1 Introduction

In Chapter 1 some faults resulting in asymmetrical operation of an induction machine were mentioned. In section 2 of this chapter a mathematical definition of symmetrical supply will be given, and it will be shown why symmetrical supply is desirable. Among the different kinds of asymmetries however, some affect the operation in a more serious way than others. Therefore, in this chapter a classification of asymmetries will be presented, along with some considerations on the theoretical possibilities of operating the machine while the asymmetry is present. A distinction is made between voltage- and current-fed machines, as they will require different fault-correcting strategies.

5.2 The necessity for symmetrical operation

Before the reasons for symmetrical operation can be discussed, it is necessary to define what “symmetrical operation” means. It will be defined for steady state operation of a machine with sinusoidally distributed windings, in which the torque m_{el} , the rotor flux ψ_r and the rotor speed $\dot{\rho}^s$ are constant. Note that a constant rotor flux is not necessary to obtain a constant torque, but variation of the rotor flux would introduce an unnecessary transfer of energy to and from the machine, and is therefore not considered. In that case the supply will be called symmetrical if the current flowing in one phase is equal to that in another phase, but with a phase delay in time that corresponds to the different positions of the windings in the machine.

For a three-phase machine in which the identical sinusoidal windings are placed in a symmetrical way – they are positioned at equal distances along the air gap – the currents required for symmetrical operation are given by equation 5.1, in which ξ_s^s is the stator-current frequency in per unit and t is the time, also in pu. This definition shows that the current in phase b lags behind the current in phase a, and the same is true for the current i_{sc} with respect to i_{sb} . In turn, i_{sa} lags behind i_{sc} . This however implies that the currents are periodical, because each winding can be said to be located at a distance of 2π radians from itself.

$$\begin{aligned}
 i_{sb}(t) &= i_{sa}\left(t - \frac{2\pi}{3} \cdot \frac{1}{\dot{\epsilon}_s^s}\right) \\
 i_{sc}(t) &= i_{sb}\left(t - \frac{2\pi}{3} \cdot \frac{1}{\dot{\epsilon}_s^s}\right) = i_{sa}\left(t - \frac{4\pi}{3} \cdot \frac{1}{\dot{\epsilon}_s^s}\right) \\
 i_{sa}(t) &= i_{sc}\left(t - \frac{2\pi}{3} \cdot \frac{1}{\dot{\epsilon}_s^s}\right) = i_{sa}\left(t - 2\pi \cdot \frac{1}{\dot{\epsilon}_s^s}\right)
 \end{aligned} \tag{5.1}$$

Symmetrical voltage supply can be defined in the same way, but it can be proved that in a symmetrical machine symmetrical currents yield symmetrical voltages and vice versa.

A special kind of symmetrical supply is the case when the three currents are sinusoidal with a frequency of $\dot{\epsilon}_s^s$. This is the kind of supply which is mostly used in electrical drives, except that due to the switching character of the power converter the currents are usually not exactly sinusoidal and symmetrical. If the frequency components related to the switching are however neglected, sinusoidal and symmetrical currents appear.

What are the reasons for using a symmetrical and sinusoidal supply? The reasons are closely related to the design of the machine. As the identical windings are placed in a completely symmetrically distributed way along the circumference of the air-gap, there is no apparent reason why for steady state operation one of them should be supplied in a different way than the others. If the windings are supplied in a symmetrical way, also the losses will be distributed symmetrically over the machine, which avoids that some parts of the machine get overheated while others are at a much lower temperature. The main reason however is that to obtain a constant torque and a constant flux level with a minimum of (copper) losses, symmetrical and sinusoidal supply is needed. This can be derived from the machine equations in the following way.

For a constant rotor flux ψ_r , according to the block diagram in figure 3.4, a constant magnetizing current $i_s^{\psi r1}$ is needed. With constant flux, a constant torque m_{el} is obtained only if the torque producing current $i_s^{\psi r2}$ is also constant. Together with the constant flux, this results in a constant slip frequency $\dot{\phi}_r^f$. As the rotor speed $\dot{\rho}^s$ was assumed constant, also $\dot{\phi}_r^s$, the frequency of the flux vector with respect to the stator, will be constant. The current vector in stator coordinates is given by equation 5.2, which can also be deduced from the block diagram using the definition of the vector rotator. With the above mentioned assumptions this vector can also be written as in equation 5.3, in which i_s , $\dot{\epsilon}_s^s$ ($= \dot{\phi}_r^s$) and ϵ_{s0}^s are constants.

$$\begin{aligned}
 i_s^{s1} &= i_s^{\psi r1} \cdot \cos \varphi_r^s - i_s^{\psi r2} \cdot \sin \varphi_r^s \\
 i_s^{s2} &= i_s^{\psi r1} \cdot \sin \varphi_r^s + i_s^{\psi r2} \cdot \cos \varphi_r^s
 \end{aligned} \tag{5.2}$$

$$\begin{aligned}
 i_s^{s1} &= i_s \cdot \cos \left(\dot{\epsilon}_s^s t + \epsilon_{s0}^s \right) \\
 i_s^{s2} &= i_s \cdot \sin \left(\dot{\epsilon}_s^s t + \epsilon_{s0}^s \right)
 \end{aligned} \tag{5.3}$$

The locus of the current vector $\mathbf{i}_s^s = [i_s^{s1} \ i_s^{s2}]^T$ is drawn in figure 5.1, which shows that to obtain constant flux and constant torque, the current vector must follow a circular path around the origin of the fixed stator frame, at a constant speed. In this figure the angle ϵ_s^s is equal to $\epsilon_{st}^s + \epsilon_{s0}^s$.

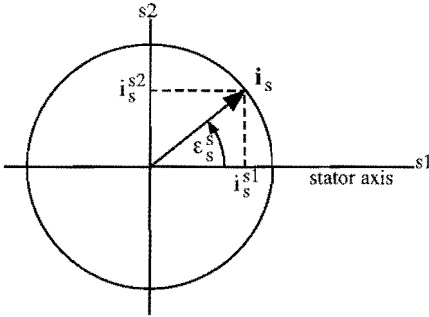


Figure 5.1. The locus of the current vector in steady-state operation with constant torque and constant rotor flux.

Now that a condition has been derived for the currents in the equivalent two-phase model, this condition has to be translated to the three-phase system. By transforming equation 5.3 to the three-phase system using equation 4.6, equation 5.4 is obtained. The homopolar current i_{s0} can be chosen freely as it does not affect the current vector \mathbf{i}_s^s nor the torque.

$$\begin{aligned} i_{sa} &= \frac{2}{3} i_s \cdot \cos(\epsilon_{st}^s + \epsilon_{s0}^s) + \frac{1}{3} i_{s0} \\ i_{sb} &= \frac{2}{3} i_s \cdot \cos(\epsilon_{st}^s + \epsilon_{s0}^s - \frac{2\pi}{3}) + \frac{1}{3} i_{s0} \\ i_{sc} &= \frac{2}{3} i_s \cdot \cos(\epsilon_{st}^s + \epsilon_{s0}^s - \frac{4\pi}{3}) + \frac{1}{3} i_{s0} \end{aligned} \quad (5.4)$$

The set of currents obtained in this way is neither necessarily symmetrical nor sinusoidal, due to the possible presence of a homopolar current i_{s0} . However, to minimize the copper losses in the machine the sum of the squares of the currents, $i_{sa}^2 + i_{sb}^2 + i_{sc}^2$, has to be minimized. From equation 5.4 it follows that then i_{s0} has to be taken zero, and the result is a symmetrical set of sinusoidal currents, given in equation 5.5.

$$\begin{aligned} i_{sa} &= \frac{2}{3} i_s \cdot \cos(\epsilon_{st}^s + \epsilon_{s0}^s) \\ i_{sb} &= \frac{2}{3} i_s \cdot \cos(\epsilon_{st}^s + \epsilon_{s0}^s - \frac{2\pi}{3}) \\ i_{sc} &= \frac{2}{3} i_s \cdot \cos(\epsilon_{st}^s + \epsilon_{s0}^s - \frac{4\pi}{3}) \end{aligned} \quad (5.5)$$

If for some reason it is not possible to supply the machine with this symmetrical sinusoidal set of currents, the requirement of minimizing the copper losses may be omitted. The homopolar current i_{s0} can then be used to obtain a set of currents which satisfies equation 5.4, still resulting in a constant torque and flux.

In fact, the presence of i_{s0} in equation 5.4 introduces an extra degree of freedom in the choice of the phase currents. It allows to choose an arbitrary current for one of the phases, and use the other two phases to obtain a resulting “circular” current vector. For example, i_{s0} can be taken equal to $-2 i_s \cdot \cos(\hat{\epsilon}_s^s t + \epsilon_{s0}^s)$ – the current in phase a then becomes zero.

The fact that a set of currents is not symmetrical and sinusoidal does therefore not necessarily mean that the machine is not operated with constant torque and flux – asymmetrical supply is thus not necessarily inconvenient for the behavior of the machine, and can be used successfully in those cases where a symmetrical supply can not be realized.

However, if the homopolar current can not be chosen freely, for example when the star point is not connected and therefore $i_{s0} = 0$, this extra degree of freedom is no longer present, and it is no longer possible to choose one of the phase currents freely. With $i_{s0} = 0$ the three phase currents have to be symmetrical and sinusoidal as in equation 5.5. Any deviation from this will cause the stator-current vector to deviate from its circular, constant-speed trajectory and the flux and/or the torque will no longer be constant. Whether or not the star point is connected is therefore an important parameter in the classification of asymmetries.

For the stator voltages the same reasoning can be made as for the currents. If the star point is connected to the voltage source, the homopolar voltage u_{s0} can be chosen freely, which results in an extra degree of freedom in the choice of the phase voltages. If the star point is not connected this degree of freedom is lost, and the voltages have to be symmetrical and sinusoidal to obtain a constant torque and flux.

5.3 Current faults in case the star point is connected

A fault which occurs in a power converter generally means that the current or voltage in one or more machine phases can no longer be controlled in the desired way. For example, an open circuit in one of the phases means that one of the phase currents will necessarily be zero, which corresponds to the loss of one degree of freedom. As was shown in the previous section, the homopolar current introduces one extra degree of freedom, which suggests that a certain category of faults can be compensated for by choosing an appropriate homopolar current. The seriousness of a fault thus depends on whether the homopolar current can be controlled freely.

A distinction has to be made between faults that affect in the first place a current, and those that have a direct effect on a voltage. An example of a current fault is the open

circuit, which imposes $i = 0$ for the circuit under consideration. In an analog way the short circuit is the typical example of a voltage fault: it imposes $u = 0$.

To study the effect of different faults, a number of fault categories will be defined, which differ with respect to the kind of fault (current or voltage), the number of phases involved and the connection of the star point. The machine model used to study each of these categories further depends on whether the machine is voltage- or current-fed.

The first category of faults that will be considered consists of the current faults for the case where the star point is connected. Current faults are defined as faults which impose certain conditions on the currents flowing into the machine. The most elementary current fault is the open circuit, which imposes a current zero in the faulty circuit, possibly due to a blown fuse, a loose contact, a faulty device driver, or a switching device that refuses to close when it is commanded to do so. It is a rather common fault – even more because in case of a short circuit fuses or circuit breakers usually transform the short circuit into an open circuit.

5.3.1 A single-phase current fault

Open circuits can occur in one phase, two phases or all three phases. The three-phase open circuit is not very interesting – all control over the machine is lost. The single phase open circuit is shown in figure 5.2. First the case of the current-fed machine will be considered, shown in figure 5.2a.

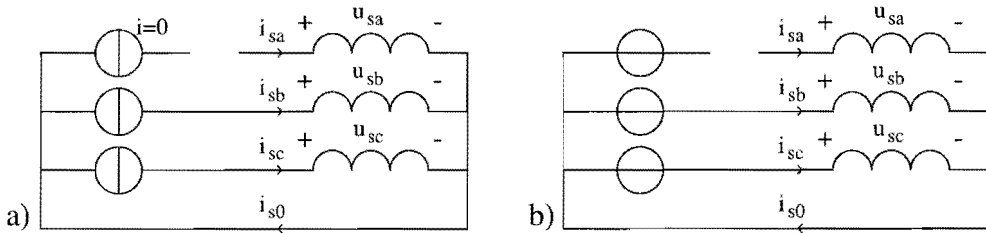


Figure 5.2. A single-phase open circuit in case the star point is connected, shown for a current-fed (a) and a voltage-fed (b) machine.

As can be seen from figure 5.2 the open circuit has the following effect on the phase currents (equation 5.6).

$$\begin{aligned} i_{sa} &= 0 \\ i_{sb}, i_{sc} &\text{ arbitrary, independent} \end{aligned} \quad (5.6)$$

If the current transformation from equation 4.5 is applied to these currents, equation 5.7 results. This equation shows that i_s^{s1} and i_s^{s2} can still be controlled independently by means of i_{sb} and i_{sc} , so that it is still possible to obtain a “circular” current vector. With

a proper control circuit it is therefore possible to correct this fault and continue to operate the machine with a constant torque and flux level.

$$\begin{aligned} i_s^{s1} &= -\frac{1}{2} i_{sb} - \frac{1}{2} i_{sc} \\ i_s^{s2} &= \frac{\sqrt{3}}{2} i_{sb} - \frac{\sqrt{3}}{2} i_{sc} \end{aligned} \quad (5.7)$$

A block diagram that can be used to model the machine in this case is shown in figure 5.3. The homopolar voltage is calculated from the homopolar current using equation 4.31, while the voltages u_s^{s1} and u_s^{s2} can be found using equation 3.19 or the block diagram from figure 3.7 with the real machine parameters. The three phase voltages can be found by adding the homopolar voltage in the transformation block at the right side of figure 3.7, according to the transformation described by equation 4.28.

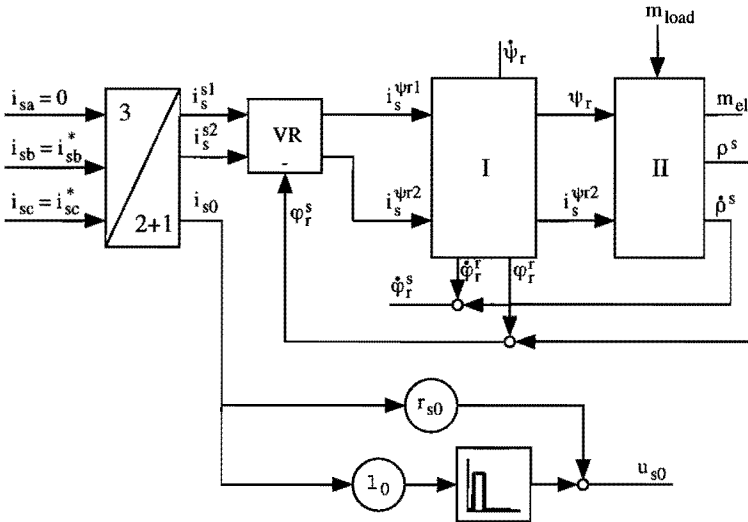


Figure 5.3. Block diagram of a current-fed induction machine with a single-phase current fault, if the star point is connected.

Modeling a voltage-fed machine with a single-phase current fault is slightly more complicated, because this is a case of mixed supply: two phases are voltage-fed, one phase is current-fed (the current is zero). It is therefore advantageous to model the three phases separately, instead of using vectors in field-oriented coordinates. Starting from equations 3.1 and 4.31 (repeated in 5.8), the voltage equation for each of the phases can be deduced, first for the general case.

$$\begin{aligned} \mathbf{u}_s^s &= r_s \cdot \mathbf{i}_s^s + l_\sigma \cdot \dot{\mathbf{i}}_s^s + \dot{\boldsymbol{\psi}}_r^s \\ u_{s0} &= r_{s0} \cdot i_{s0} + l_0 \cdot \frac{di_{s0}}{dt} \end{aligned} \quad (5.8)$$

The voltage across phase a is found using $u_{sa} = u_s^{s1} + u_{s0}$, from equation 4.28. From equation 4.6 it can further be deduced that $i_s^{s1} = 3/2 i_{sa} - 1/2 i_{s0}$. Using equation 5.8 this results in equation 5.9.

$$u_{sa} = \frac{3}{2} r_s \cdot i_{sa} + \frac{3}{2} l_\sigma \cdot \frac{di_{sa}}{dt} + \frac{d\psi_r^{s1}}{dt} + \left(r_{s0} - \frac{1}{2} r_s \right) \cdot i_{s0} + \left(l_0 - \frac{1}{2} l_\sigma \right) \cdot \frac{di_{s0}}{dt} \quad (5.9)$$

By using the fact that $r_{sq} = 3/2 r_s$ and $l_{\sigma q} = 3/2 l_\sigma$ in analogy with equation 2.57, and $r_{s0} = 1/3 r_{sq}$ from 4.30, this equation can be simplified, which results in equation 5.10.

$$u_{sa} = r_{sq} \cdot i_{sa} + l_{\sigma q} \cdot \frac{di_{sa}}{dt} + \frac{d\psi_r^{s1}}{dt} + \left(l_0 - \frac{1}{3} l_{\sigma q} \right) \cdot \frac{di_{s0}}{dt} \quad (5.10)$$

In the same way the voltage equations for the other two phases can be deduced – they are given in equation 5.11.

$$\begin{aligned} u_{sb} &= r_{sq} \cdot i_{sb} + l_{\sigma q} \cdot \frac{di_{sb}}{dt} + \frac{d}{dt} \left(-\frac{1}{2} \psi_r^{s1} + \frac{\sqrt{3}}{2} \psi_r^{s2} \right) + \left(l_0 - \frac{1}{3} l_{\sigma q} \right) \cdot \frac{di_{s0}}{dt} \\ u_{sc} &= r_{sq} \cdot i_{sc} + l_{\sigma q} \cdot \frac{di_{sc}}{dt} + \frac{d}{dt} \left(-\frac{1}{2} \psi_r^{s1} - \frac{\sqrt{3}}{2} \psi_r^{s2} \right) + \left(l_0 - \frac{1}{3} l_{\sigma q} \right) \cdot \frac{di_{s0}}{dt} \end{aligned} \quad (5.11)$$

For the rotor fluxes the transformation given in equation 5.12 is valid. This equation is identical to equation 4.24 except that, from the assumptions in Chapter 4, no homopolar rotor flux exists. The physical interpretation of ψ_{rsa} is the flux linking stator-phase winding q if this winding were located in the rotor. Using equation 5.12, the three phase-voltage equations can finally be simplified to equation 5.13. This same equation is *mutatis mutandis* also valid for the other two phases.

$$\begin{bmatrix} \psi_{rsa} \\ \psi_{rsb} \\ \psi_{rsc} \end{bmatrix} = \begin{bmatrix} 1 & 0 \\ -\frac{1}{2} & \frac{\sqrt{3}}{2} \\ -\frac{1}{2} & -\frac{\sqrt{3}}{2} \end{bmatrix} \cdot \begin{bmatrix} \psi_r^{s1} \\ \psi_r^{s2} \end{bmatrix} \quad (5.12)$$

$$u_{sa} = r_{sq} \cdot i_{sa} + l_{\sigma q} \cdot \frac{di_{sa}}{dt} + \frac{d\psi_{rsa}}{dt} + \left(l_0 - \frac{1}{3} l_{\sigma q} \right) \cdot \frac{di_{s0}}{dt} \quad (5.13)$$

To complete the machine model, finally the rotor flux derivatives $\dot{\psi}_r^{s1}$ and $\dot{\psi}_r^{s2}$ have to be written as a function of the rotor-flux related variables present in the field-oriented machine model. This is done in equation 5.14. The resulting block diagram is shown in figure 5.4.

$$\begin{bmatrix} \dot{\psi}_r^{s1} \\ \dot{\psi}_r^{s2} \end{bmatrix} = \frac{d}{dt} \left(\mathbf{R}(\varphi_r^s) \cdot \begin{bmatrix} \psi_r \\ 0 \end{bmatrix} \right) = \mathbf{R}(\varphi_r^s) \cdot \left(\begin{bmatrix} \dot{\psi}_r \\ 0 \end{bmatrix} + \dot{\varphi}_r^s \cdot \mathbf{R}\left(\frac{\pi}{2}\right) \cdot \begin{bmatrix} \psi_r \\ 0 \end{bmatrix} \right) = \mathbf{R}(\varphi_r^s) \cdot \begin{bmatrix} \dot{\psi}_r \\ \dot{\varphi}_r^s \cdot \psi_r \end{bmatrix} \quad (5.14)$$

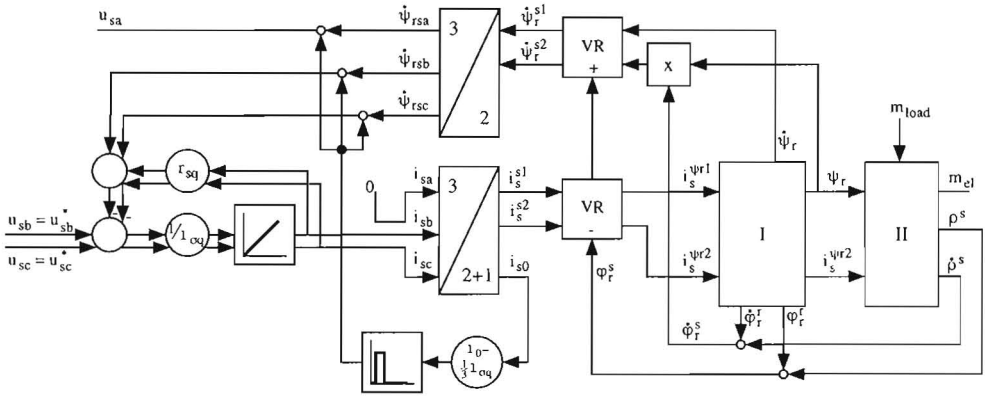


Figure 5.4. Block diagram of a voltage-fed induction machine with a single-phase current fault, if the star point is connected.

5.3.2 A two-phase current fault

In case two phases of a machine of which the star point is connected are opened, only one phase remains, as can be seen in figure 5.5. The phase currents are now given by equation 5.15.

$$\begin{aligned}
 i_{sa} &= 0 \\
 i_{sb} &= 0 \\
 i_{sc} &\text{ arbitrary}
 \end{aligned}
 \tag{5.15}$$

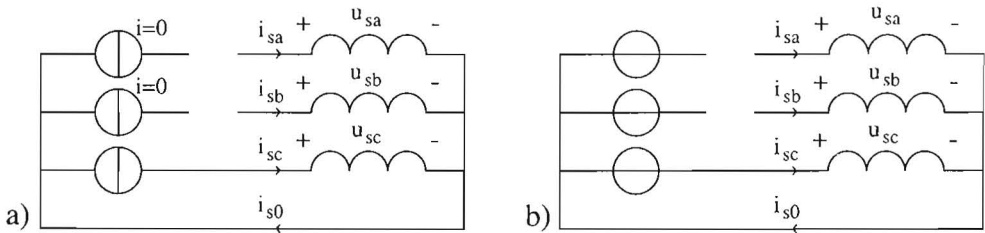


Figure 5.5. A two-phase open circuit in case the star point is connected, shown for a current-fed (a) and a voltage-fed (b) machine.

It is interesting to calculate the effect of this current fault on the stator-current vector in stator coordinates. Using transformation 4.5 equation 5.16 is obtained.

$$\begin{aligned}
 i_s^{s1} &= -\frac{1}{2} i_{sc} \\
 i_s^{s2} &= -\frac{\sqrt{3}}{2} i_{sc}
 \end{aligned}
 \tag{5.16}$$

From this, equation 5.17 can be derived, which makes it very clear that this fault is much more serious than the previous one. The stator current can now only move on a straight line in stator coordinates, instead of the circle which is required for constant torque and flux operation. It is therefore theoretically impossible to design a control system which allows continued operation with constant torque and flux for this case.

$$i_s^{s1} = \frac{1}{\sqrt{3}} \cdot i_s^{s2} \tag{5.17}$$

Modeling of the machine with this fault is very much the same as for the single-phase fault. For the current-fed machine, the model from figure 5.3 can be used, in which $i_{sb} = 0$ has to be substituted. The model for the voltage-fed machine can be derived from figure 5.4, in which $i_{sb} = 0$ replaces the calculation of i_{sb} from the input voltage u_{sb}^* . The phase-b voltage u_{sb} is now calculated in the same way as was u_{sa} in figure 5.4.

5.4 Current faults in case the star point is not connected

When the star point of a machine is not connected, the homopolar current i_{s0} is zero. This means that one degree of freedom is lost, and in contrast with the case of the machine with the star point connected, the single-phase current fault can no longer be compensated by choosing an appropriate homopolar current. If the machine is current-fed, one of the current sources has to be commanded with a value dependent on the other two sources, to avoid conflicts.

Already the loss of a single phase is in this case a very serious fault. If even two phase currents become zero, automatically the third will be zero too, which means that all control is lost. Figure 5.6 shows the machine and its supply in case a fault occurs which makes only one of the phase currents equal to zero. For the current-fed machine the current source for the third phase must be commanded to minus the value of the second source, to avoid a conflict between these sources. The resulting phase currents are given in equation 5.18.

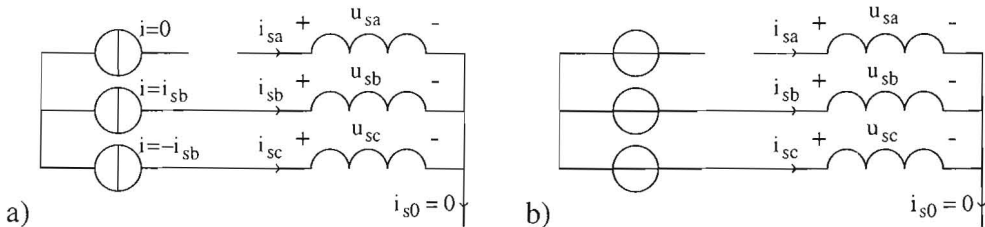


Figure 5.6. A single-phase open circuit in case the star point is not connected, shown for a current-fed (a) and a voltage-fed (b) machine.

$$\begin{aligned} i_{sa} &= 0 \\ i_{sb} &= -i_{sc}, \text{ arbitrary} \end{aligned} \tag{5.18}$$

This case is very similar to the two-phase fault when the star point is connected, described in section 5.3.2, because it also limits the movement of the stator-current vector to a straight line in stator coordinates, as is shown in equation 5.19. It is therefore also in this case not possible to obtain a constant torque and flux level.

$$\begin{aligned} i_s^{s1} &= 0 \\ i_s^{s2} &= \sqrt{3} i_{sb} \end{aligned} \tag{5.19}$$

Comparing equation 5.19 with 5.16 shows that the angle between the stator-current vector and the reference frame is however different for the two cases. Another difference is the relation between the length of the current vector and the phase current. For equation 5.16, $i_s = i_{sc}$, while for 5.19 $i_s = \sqrt{3} i_{sb}$. This difference is due to the fact that in the latter case two windings still carry a current, while in the first case only one winding is active.

To model the current-fed machine, the block diagram of figure 5.3 can again be used, after substitution of the appropriate values for the phase currents. As the homopolar current is zero, the homopolar part of the block diagram can be omitted.

From figure 5.6b it can be seen that for the voltage-fed machine the phase voltages u_{sb} and $-u_{sc}$ have to be put in series to calculate the remaining current $i_{sb} = -i_{sc}$. Using the equivalent of equation 5.13 for phase b and c equation 5.20 is found. The corresponding block diagram is shown in figure 5.7.

$$\begin{aligned} u_{sb} - u_{sc} &= r_{sq} \cdot (i_{sb} - i_{sc}) + l_{\sigma q} \cdot \frac{d(i_{sb} - i_{sc})}{dt} + \frac{d(\psi_{rsb} - \psi_{rsc})}{dt} \\ &= 2r_{sq} \cdot i_{sb} + 2l_{\sigma q} \cdot \frac{di_{sb}}{dt} + \frac{d(\psi_{rsb} - \psi_{rsc})}{dt} \end{aligned} \tag{5.20}$$

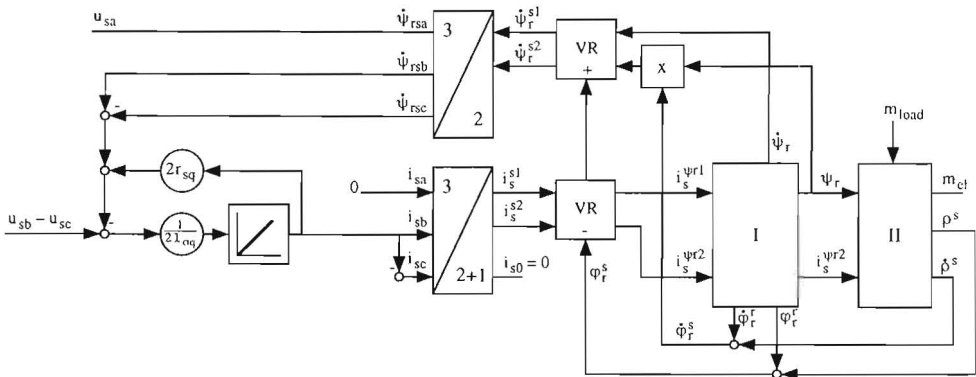


Figure 5.7. Block diagram of a voltage-fed machine with a single-phase current fault, if the star point is not connected.

From this figure and also from figure 5.6 and equation 5.20 it can be seen that in this case it is actually the voltage between two phases, the line voltage, that determines the behavior of the machine, not the voltage across a single phase.

In cases where the star point is not connected or not available for measurements, or when the star point does not exist because the windings are in a delta connection, it could therefore be useful to model the stator windings as if they were in a delta connection. The input voltages are then the line voltages, from which the currents in the delta-connected circuit are calculated. Using an appropriate transformation matrix, the corresponding stator-current vector can be calculated. This method was used in certain simulations, as will be explained in more detail in section 8.3.1.

5.5 Voltage faults

Voltage faults are those faults that impose specific conditions or limitations on the stator voltages of the machine. Examples of this category of faults are switching devices that refuse to open (such as faulty GTOs), short circuits in other devices such as diodes, and short circuits caused by some external reason. This kind of fault makes the voltage across a winding or between windings equal to zero, or, as in the case of a shorted switch of a voltage-source inverter, it restricts the applied voltage between two windings to either positive or negative values, which also means that a voltage will be zero during at least a part of a period.

5.5.1 Voltage faults in two or more phases

In case three windings get connected to each other due to a fault, the three stator voltages u_{sa} , u_{sb} and u_{sc} will become equal and – according to equation 4.27 – as a result the voltage vector $\mathbf{u}_s^s = [u_s^{s1} \ u_s^{s2}]^T$ will be zero. It goes without saying that this completely disables further operation of the machine.

Also with a short circuit between two phases operation is no longer possible, independent of whether or not the star point is connected and whether or not the star point of the machine or of the power supply is involved in the short circuit. This can be seen from the following equations. Assume that due to a short circuit u_{sa} equals u_{sb} . Using equation 5.13 and its equivalent for phase b, the following equation (5.21) is obtained, from which equation 5.22 is then deduced.

$$r_{sq} \cdot i_{sa} + l_{\sigma q} \cdot \frac{di_{sa}}{dt} + \frac{d\psi_{rsa}}{dt} = r_{sq} \cdot i_{sb} + l_{\sigma q} \cdot \frac{di_{sb}}{dt} + \frac{d\psi_{rsb}}{dt} \quad (5.21)$$

$$\left(r_{sq} + l_{\sigma q} \cdot \frac{d}{dt} \right) (i_{sa} - i_{sb}) + \frac{d}{dt} (\psi_{rsa} - \psi_{rsb}) = 0 \quad (5.22)$$

In case of a “circular” rotor-flux vector ψ_r^s , which is the case for normal operation, the fluxes ψ_{rsa} and ψ_{rsb} will always have a phase difference of $2\pi/3$, so the amplitude of $(\psi_{rsa} - \psi_{rsb})$ will be $\sqrt{3} \cdot \psi_r$. Assuming that the stator resistance at the considered speed can be neglected with respect to the leakage inductance, and assuming a rated flux level of 1, the amplitude of the current difference $(i_{sa} - i_{sb})$ will be equal to $\sqrt{3}/1_{\sigma q}$, which can be as large as 8 pu.

This means that in case of a short circuit between two phases the current in one or both of these phases will be unacceptably high, so that it is not possible to design a strategy for continued operation with this kind of fault.

5.5.2 A single-phase voltage fault in case the star point is connected

The remaining voltage faults are those in which a short circuit occurs in a single phase. Here a distinction has to be made between the circuit with and without a star-point connection. Figure 5.8 shows a short circuit which – due to the star-point connection – shortens at the same time one phase of the machine and one phase of the supply. The corresponding voltage equations are given in equation 5.23.

$$\begin{aligned} u_{sa} &= 0 \\ u_{sb}, u_{sc} &\text{ arbitrary, independent} \end{aligned} \quad (5.23)$$

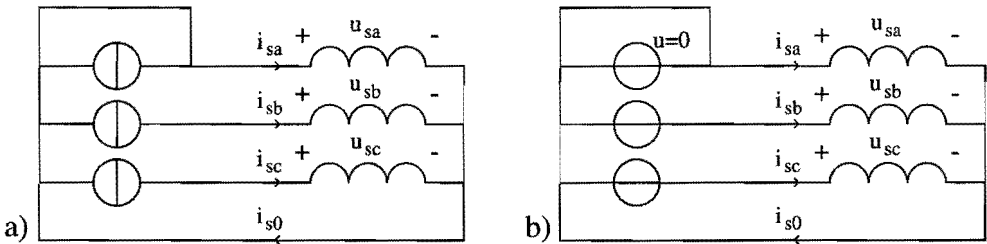


Figure 5.8. A single-phase short circuit in case the star point is connected, shown for a current-fed (a) and a voltage-fed (b) machine.

Modeling a machine with this fault is achieved using the block diagram in figure 4.3 for the case of a voltage-fed machine, be it that now one of the phase voltages is zero. For the current-fed machine the block diagram is given in figure 5.9. This figure is very similar to figure 5.4 derived in section 5.3.1, due to the fact that both figures represent a machine fed with a mixed supply of both currents and voltages.

Theoretically, this fault can be compensated by introducing an appropriate homopolar voltage or current, because two inputs remain independently controllable. In practice however, a problem arises. Consider equation 5.24, which is the voltage equation for the shortened phase, derived from equation 5.8 using $u_{sa} = u_s^1 + u_{s0}$, $\psi_{rsa} = \psi_r^1$ and $i_s^1 = 3/2 i_{sa} - 1/2 i_{s0}$.

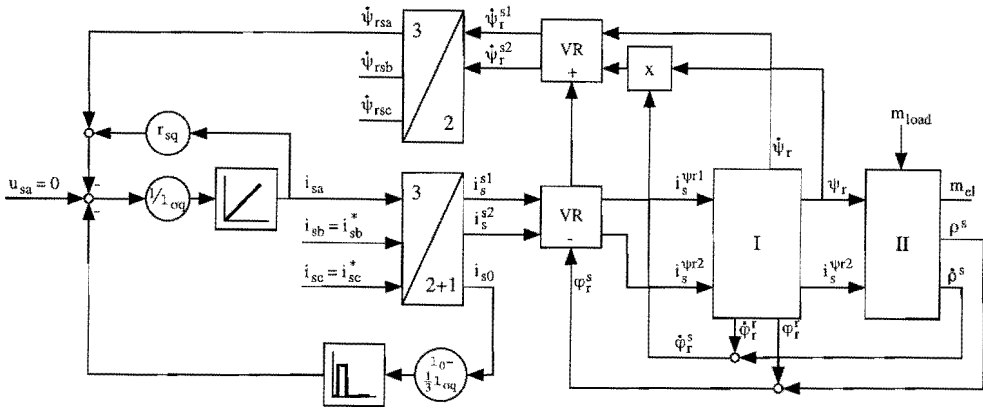


Figure 5.9. Block diagram of a current-fed machine with a single-phase voltage fault, if the star point is connected.

$$0 = u_{sa} = \left(r_s + l_\sigma \cdot \frac{d}{dt} \right) \left(\frac{3}{2} i_{sa} - \frac{1}{2} i_{s0} \right) + \frac{d\psi_{rsa}}{dt} + u_{s0} \quad (5.24)$$

If the fault would be compensated, the non-homopolar part of i_{sa} , which is the part of i_{sa} that contributes to the stator current vector, $i_{sa} - \frac{1}{3}i_{s0}$, should have the same value as in normal operating conditions, and the same holds for $d\psi_{rsa}/dt$. This leads to the following equation:

$$0 = u_{sa} = [u_{sa}]_{\text{normal}} + u_{s0} \quad (5.25)$$

Thus, to compensate the fault, the voltage u_{s0} , which normally would be zero, should be made equal to minus the value which u_{sa} would have had if no fault were present. This value required for u_{s0} is at high speed mainly determined by ψ_{rsa} (cf. equation 5.13), and the resulting i_{s0} mainly by l_0 (cf. equation 5.8). The value of l_0 depends strongly on the winding configuration and on the leakage inductance. When l_0 is for example equal to 0.2, the resulting i_{s0} at rated flux will have an amplitude of 5 pu. If the homopolar inductance is smaller, an even higher homopolar current will result. This means that due to the high currents which would be required, this fault can not be compensated, except if the machine is specially designed to have a high homopolar inductance.

A machine for which a special design seems to be suitable is the permanent magnet machine, as was suggested in [Jack-96]. In this type of machine the leakage inductance has a much higher value compared to the main inductance than is the case for the induction machine. If, at the same time, the coupling between phases is kept as low as possible, the current in the short-circuited phase will not reach an unacceptable level. A drive with such a special PM machine can thus be designed for continued operation in case of a single-phase short circuit.

5.5.3 A single-phase voltage fault in case the star point is not connected

If the star point is not connected there are two possibilities for a single-phase short circuit: a short circuit of one machine phase, and a short circuit of one supply phase. In case of a short circuit of a machine phase, the current in that winding will at high speeds be limited only by the leakage inductance $l_{\sigma q}$, resulting in an unacceptably high value. Continued operation is therefore not possible. The case of a short circuit of one of the supply phases is shown in figure 5.10.

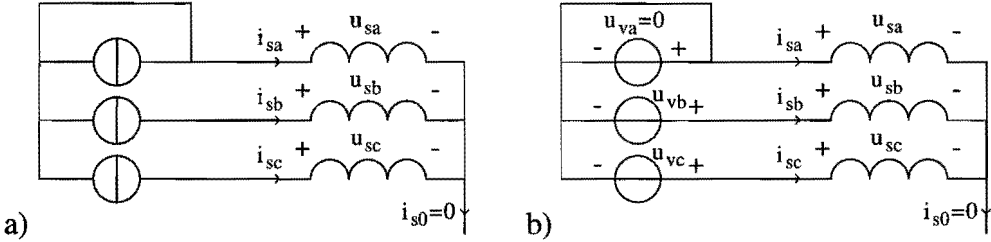


Figure 5.10. A single-phase short circuit in case the star point is not connected, shown for a current-fed (a) and a voltage-fed (b) machine.

In case the machine is current-fed as in figure 5.10a, short-circuiting of one of the supply sources does not represent any problem – one of the sources was redundant anyway. The same is true for the voltage-fed machine (figure 5.10b), except that while one of the sources has become zero, the other two sources should now alone supply the required sinusoidal voltages of sufficient amplitude. If, for example, these sources are only capable of delivering positive output voltages, correct operation is no longer possible.

The reason why, normally, operation with three such sources is possible lies in the fact that the homopolar source voltage is not relevant for the machine. This can be seen from the following equations, in which the supply voltages have the subscript “v”. From figure 5.10b, relation 5.26 between the stator voltages and the supply voltages is found.

$$u_{va} - u_{sa} = u_{vb} - u_{sb} = u_{vc} - u_{sc} \quad (5.26)$$

Using the voltage-transformation equations 4.27, equation 5.27 is obtained. This equation shows that the stator-voltage vector does not depend on a homopolar supply voltage. The homopolar stator voltage is a function of the homopolar current only, which is zero.

$$\begin{aligned} u_s^{s1} &= \frac{1}{3}(u_{sa} - u_{sb}) + \frac{1}{3}(u_{sa} - u_{sc}) = \frac{1}{3}(u_{va} - u_{vb}) + \frac{1}{3}(u_{va} - u_{vc}) = u_v^{s1} \\ u_s^{s2} &= \frac{1}{\sqrt{3}}(u_{sb} - u_{sc}) = \frac{1}{\sqrt{3}}(u_{vb} - u_{vc}) = u_v^{s2} \end{aligned} \quad (5.27)$$

In practice, this situation can occur in the inverter-fed machine, as shown in figure 3.2. The output voltages of the inverter can be defined as the voltages between the machine terminals and the negative side of the dc-link capacitor. These voltages can never become negative, and a short circuit in one of the phases does indeed represent a serious problem. This case will be discussed in detail in section 8.5.6.

5.6 Overview of the different fault categories

An overview of different faults is shown in figure 5.11. In this figure no distinction is made between voltage or current sources – an open circle is used as a general symbol for both. For the control scheme required to correct the fault as well as for the block diagram needed to model the machine with the fault there is of course a considerable difference. To determine whether or not a fault is theoretically correctable this distinction is however not required.

An important distinction that has to be made, is whether or not the star point is connected. In the code at the right side of each diagram a non-connected star point is indicated with the letter *n*. The number in this code denotes the number of lost degrees of freedom with respect to the situation when all three phases and the star point are connected. Operation with constant torque and constant flux requires at least two currents to be controllable independently. This means that the number of lost degrees of freedom should not exceed 1.

In case two degrees of freedom are lost, only one independent phase current remains, and although continued operation is possible, a constant torque and flux cannot be maintained. The loss of three degrees of freedom means a complete loss of control over the machine. Not all possible current faults causing this situation are indicated.

Voltage faults, which are indicated with *U* or *U'* in contrast to the current faults (*I*), often cause high phase currents, or would require high currents to compensate them. Therefore only some voltage faults are indicated in this overview. The difference between the faults indicated with *U* and those with *U'* is whether the fault occurs across a supply phase or a machine phase – if the star point is connected this evidently does not make any difference.

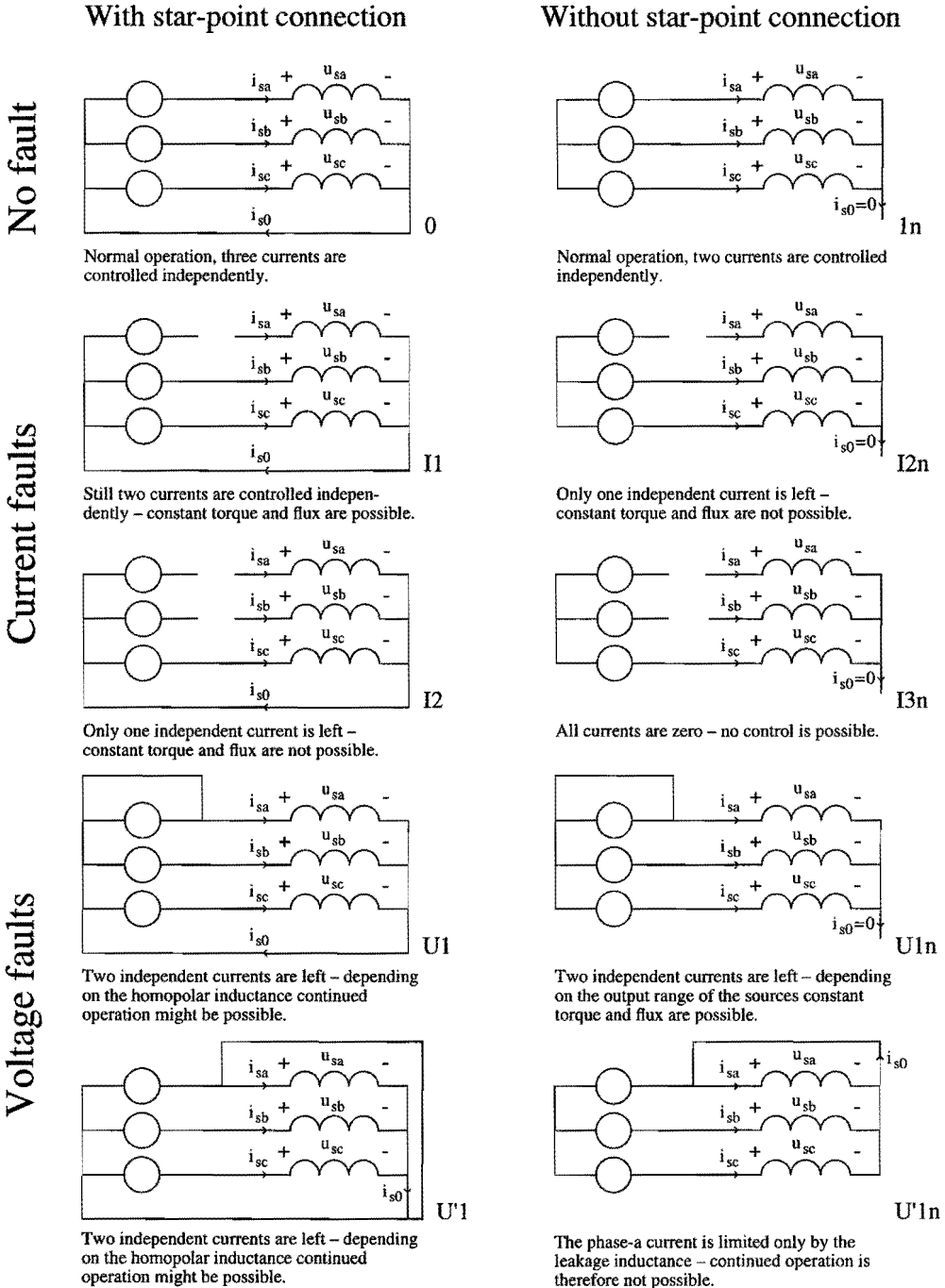


Figure 5.11. An overview of different faults and the possibilities for continued operation.

5.7 Conditional faults

Faults occurring in real converters are often more complicated than the faults mentioned in the previous sections. For example, if in some types of power converter the control signal of one of the switching devices is lost, the diode connected antiparallel to this device will cause the fault to depend on the sign of the corresponding phase current and of the voltage across this diode. In that case, different situations will occur during one period of the stator current. Operation of the drive will alternate between normal operation and operation with one of the phase currents equal to zero or with limitations in the applicable voltages. These voltage limitations can often be translated into a short circuit in one of the phases or between two phases.

The fault situations presented in the previous sections are therefore more than just theoretical cases that rarely occur in practice – they represent the different states that describe the system during a period of time, until certain conditions on the (signs of the) currents or voltages make the system change to another state. When studying a fault in a real converter, the transitions from one state to another are very important. Some converter faults cause no serious problems for the operation of the machine if the control can avoid the transition from a healthy to a faulty state. Whether this is possible will also depend on the operation mode of the machine. For the above mentioned example with the diode, the phase difference between the stator voltages and currents plays an important role, which is related to whether the machine is used as a motor or as a generator (braking mode). This will be discussed in more detail in section 8.5.

Chapter 6

Asymmetrical Operation of a Current-Fed Induction Machine

6.1 Introduction

In the previous chapter an overview was given of the different fault situations that can occur in an electrical drive system consisting of a power converter and an induction machine. Voltage faults – or short circuits – were shown to result in unacceptably high currents for most cases. Continued operation is therefore hardly ever possible and will not be studied in much detail. Current faults – open circuits that result in the loss of current control in one or two phases of the machine – do not result in unacceptably high currents or voltages in the remaining circuit, and therefore it is useful to study whether and how continued operation of the machine can be realized when they occur.

As was shown in the previous chapter, current faults are most easily modeled for a current-fed machine, because the fault and the supply then have the same nature. Therefore this chapter will examine the theoretical case of an induction machine fed by ideal current sources and of which the values of all parameters are exactly known. It is also assumed that under all conditions the rotor-flux vector (represented by its amplitude ψ_r and its angle φ_r^s with respect to the stator) is known, so that ideal field orientation can be achieved. In a real situation however, the current sources are not perfect (often current-controlled voltage sources are used), the values of the machine parameters can only be estimated, and the flux has to be estimated using one of the methods described in section 3.6. A practical case like this will be treated in Chapter 8.

The block diagram of the machine considered in this chapter is shown in figure 3.4, while the basic control system is found in figure 3.5, combined with equations 3.14 and 3.15. In case the star point is connected, the three phase currents can be controlled independently, and a homopolar current i_{s0} can flow. Saturation effects that might be caused by this current are not considered. The resulting homopolar voltage is not of any importance and does not need to be calculated. If the star point is not connected, the homopolar current is zero, and one of the phase currents will therefore depend on the other two.

The first fault under consideration is the case where one of the phase currents is zero while the star point is connected (fault I1 in figure 5.11). The corresponding diagrams are shown in figure 5.2 and 5.3. A correcting circuit will be derived for this case, allowing continued operation with constant torque and flux.

The second fault under consideration is the case where two phase currents are zero while the star point is connected (fault I2, figure 5.5). It will be shown that continued operation with constant torque can not be achieved, but by changing the waveform of the remaining current, the torque ripple can be influenced in such a way that – depending on the requirements of the mechanical system of the drive – continued operation might be possible. Starting the machine from standstill is however not possible.

Finally also the fault shown in figure 5.6, the case where one phase current is zero and the star point is not connected (fault I2n), has to be considered. In this situation the homopolar current i_{s0} will be zero. According to equation 4.4, relation 6.1 will now exist between the phase currents. This shows that one of the phase currents is dependent on the other two – in the no-fault situation there are only two independent currents.

$$i_{sa} + i_{sb} + i_{sc} = 0 \quad (6.1)$$

If, due to a fault, one of the phase currents becomes zero, only one independent current is left. Therefore this fault is very similar to the previous one. Furthermore, in both cases the resulting stator current vector \mathbf{i}_s^s is limited to moving on a straight line, shown by equations 5.17 (for figure 5.5) and 5.19 (figure 5.6). The difference between these cases is the angle of this current trajectory with respect to the fixed stator reference frame, and the number of windings in which still a current can flow. The case where the star point is not connected is in that sense more favorable, because the ratio of the length of the current vector with respect to the remaining independent current is higher (cf. the text below equation 5.19), so that a lower phase current is required to achieve the same torque. Because of the similarity between these two faults, only the I2 fault will be treated. The optimal current waveform for the I2n fault can be derived from this using the appropriate transformations, consisting of a phase shift and a change in amplitude.

6.2 Correcting a single-phase current fault using the homopolar current

In all fault-correcting strategies the ultimate goal is to achieve a constant electromagnetic torque of a desired amplitude, without causing further damage to the power converter or to the machine. If possible, the system should be able to reach the same torque level as before the fault; if this is not possible, due to the dimensioning of the system, at least in a limited power range a constant torque should be achieved. This allows to continue operation at reduced power, until it is convenient to switch off the system or to allow another system to take over. As will be derived below, in case of a single-phase current fault when the star point is connected, this goal can easily be achieved using the homopolar current.

According to the equations derived in section 5.2, a constant torque and flux level is achieved if and only if the phase currents can be written as in equation 5.4, repeated in 6.2, in which i_s , \dot{e}_s^s and e_{s0}^s are constants, while i_{s0} is an arbitrary homopolar current.

$$\begin{aligned} i_{sa} &= \frac{2}{3} i_s \cdot \cos \left(\dot{e}_s^s t + e_{s0}^s \right) + \frac{1}{3} i_{s0} \\ i_{sb} &= \frac{2}{3} i_s \cdot \cos \left(\dot{e}_s^s t + e_{s0}^s - \frac{2\pi}{3} \right) + \frac{1}{3} i_{s0} \\ i_{sc} &= \frac{2}{3} i_s \cdot \cos \left(\dot{e}_s^s t + e_{s0}^s - \frac{4\pi}{3} \right) + \frac{1}{3} i_{s0} \end{aligned} \quad (6.2)$$

To operate the machine with, for example, the current in the phase-a winding equal to zero, it is sufficient to set the homopolar current to the value given by equation 6.3.

$$i_{s0} = -2 \cdot i_s \cdot \cos \left(\dot{e}_s^s t + e_{s0}^s \right) \quad (6.3)$$

Considering relation 6.4 (derived from 4.6) between the desired currents for the three phases and the desired two-phase-plus-one currents, the relation between the desired homopolar current and the two-phase currents to obtain a zero phase-a current is easily found, as in equation 6.5. It is assumed that the converter will function in such a way that each of the three stator currents will be equal to its desired value. When, due to a fault, one of the phase currents is equal to zero, setting the desired current for that phase equal to zero will make this assumption valid also during this fault.

$$\begin{aligned} i_{sa}^* &= \frac{2}{3} i_s^{s1*} + \frac{1}{3} i_{s0}^* \\ i_{sb}^* &= -\frac{1}{3} i_s^{s1*} + \frac{1}{\sqrt{3}} i_s^{s2*} + \frac{1}{3} i_{s0}^* \\ i_{sc}^* &= -\frac{1}{3} i_s^{s1*} - \frac{1}{\sqrt{3}} i_s^{s2*} + \frac{1}{3} i_{s0}^* \end{aligned} \quad (6.4)$$

$$i_{s0}^* = -2 i_s^{s1*} \quad (6.5)$$

To make the current in one of the other two phases instead of phase a equal to zero, the desired value for the homopolar current can be derived in the same way, resulting for phase b in equation 6.6 and for phase c in 6.7.

$$i_{s0}^* = i_s^{s1*} - \sqrt{3} \cdot i_s^{s2*} \quad (6.6)$$

$$i_{s0}^* = i_s^{s1*} + \sqrt{3} \cdot i_s^{s2*} \quad (6.7)$$

Thus, in the most general form, the required i_{s0}^* can be written as a simple function of i_s^{s1*} and i_s^{s2*} , as given in equation 6.8. The two parameters k_i^{s1} and k_i^{s2} have to be chosen in function of which of the phase currents has to be zero, corresponding to equations 6.5 to 6.7. Hence, for i_{sa} equal to zero, $(k_i^{s1}, k_i^{s2}) = (-2, 0)$, for i_{sb} , $(k_i^{s1}, k_i^{s2}) = (1, -\sqrt{3})$ and for i_{sc} , $(k_i^{s1}, k_i^{s2}) = (1, \sqrt{3})$.

$$i_{s0}^* = k_i^{s1} \cdot i_s^{s1*} + k_i^{s2} \cdot i_s^{s2*} \tag{6.8}$$

The effect of different values for k_i^{s1} and k_i^{s2} on the desired three-phase currents is shown in figure 6.1. In this figure, the desired two-phase currents i_s^{s1*} and i_s^{s2*} are the same for every period. In spite of the asymmetrical behavior shown here, the currents i_s^{s1} and i_s^{s2} will be equal to their desired values, provided that the three converter output currents are equal to their desired values.

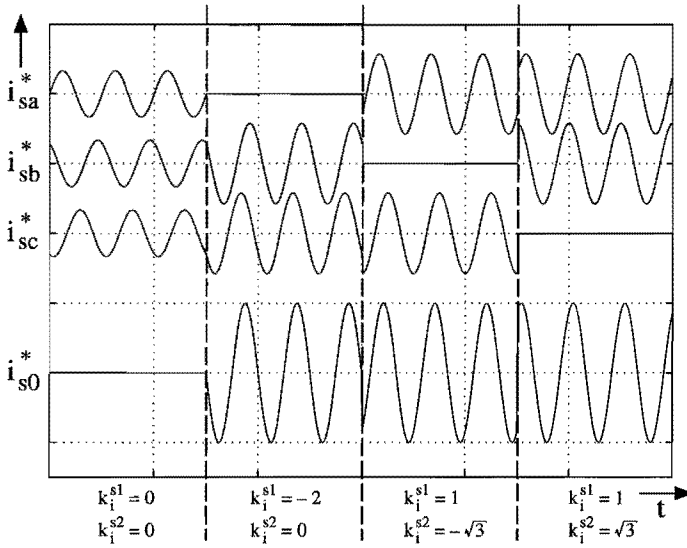


Figure 6.1. The three-phase reference currents for different values of k_i^{s1} and k_i^{s2} .

Finally, the control circuit in which the calculation of i_{s0}^* is implemented, is shown in figure 6.2. A comparison with figure 3.5 shows that only a simple addition to the basic control circuit is needed. A fault-detection mechanism which senses that the current in one of the phases has become zero unintentionally, can be used to set k_i^{s1} and k_i^{s2} to the values required to correct for this fault.

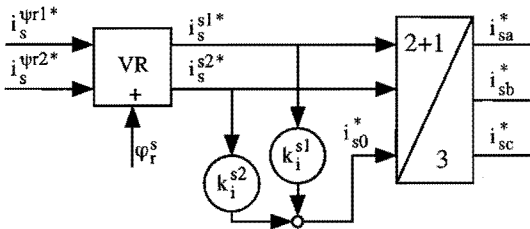


Figure 6.2. Circuit for field-oriented control of a current-fed induction machine allowing operation with one of the phase currents equal to zero.

6.3 Optimization of the remaining current in case two phase currents are zero

If, due to a fault, the current is zero in two of the three stator phase windings of a machine, equation 6.2 can no longer be satisfied. It is therefore no longer possible to obtain a constant torque and flux, except of course, in the special case where all currents are zero, which results in zero torque and corresponds to disconnecting the machine completely. An important question is therefore how, in steady-state operation, the torque can be kept as constant as possible, using the single remaining current.

Different approaches to this problem can be chosen. If the total harmonic distortion of the torque waveform is important, an algorithm can be derived that minimizes the distortion by adding harmonic components to the initially sinusoidal current. This is done in section 6.4. However, this method does not guarantee that the resulting torque waveform will not contain harmonics of a certain frequency. In section 6.5 it will be shown that it is possible to eliminate certain frequency components of the torque waveform by adding harmonics with a specific frequency, amplitude and angle with respect to the fundamental current. A third approach is based on the field-oriented current components. Assuming that the rotor flux is constant, the torque is determined by only one of the two current components, and the torque waveform can therefore be studied and optimized by considering this component only. This method is used in section 6.6, while section 6.7 compares the different approaches. The rotor speed has been assumed constant in sections 6.4 to 6.7.

6.4 Addition of harmonic current components to minimize the torque ripple

In this section, the torque ripple will be minimized for steady-state operation in case of single-phase supply. For this purpose in section 6.4.1 the torque will be expressed as a function of the harmonic components of the stator-current vector in a general case, assuming however that i_s^s is periodic. In section 6.4.2 this expression will be adapted to the case of single-phase supply. The result will then be used for numerical minimization of the torque ripple.

6.4.1 Relation between harmonic current components and the torque

To optimize the torque by using a single remaining phase current, first the relation between harmonic components of the stator-current vector in a general, no-fault case and the torque will be derived. To understand the decomposition of i_s^s used here, consider the equivalent complex vector I_s^s , defined in equation 6.9.

$$\mathbf{I}_s^s = i_s^{s1} + j \cdot i_s^{s2} \quad (6.9)$$

If the stator current is periodic, with an angular frequency $\dot{\epsilon}_s^s$ and without dc component, this complex vector can be written as in 6.10, which is a complex Fourier decomposition. This equation can be rewritten to obtain 6.11. In these equations c_n and c_{-n} are real numbers.

$$\mathbf{I}_s^s = \sum_{n=1}^{\infty} c_n \cdot e^{j(n\dot{\epsilon}_s^s t + \epsilon_{s0n}^s)} + c_{-n} \cdot e^{-j(n\dot{\epsilon}_s^s t + \epsilon_{s0(-n)}^s)} \quad (6.10)$$

$$\mathbf{I}_s^s = \sum_{n=1}^{\infty} \left\{ \begin{array}{l} c_n \cos(n\dot{\epsilon}_s^s t + \epsilon_{s0n}^s) + c_{-n} \cos(-n\dot{\epsilon}_s^s t - \epsilon_{s0(-n)}^s) + \\ j \cdot \left(c_n \sin(n\dot{\epsilon}_s^s t + \epsilon_{s0n}^s) + c_{-n} \sin(-n\dot{\epsilon}_s^s t - \epsilon_{s0(-n)}^s) \right) \end{array} \right\} \quad (6.11)$$

Using the fact that $i_s^{s1} = \text{Re}(\mathbf{I}_s^s)$ and $i_s^{s2} = \text{Im}(\mathbf{I}_s^s)$ equation 6.12 is derived.

$$\begin{bmatrix} i_s^{s1} \\ i_s^{s2} \end{bmatrix} = \sum_{n=1}^{\infty} \left\{ \begin{array}{l} \left[c_n \cos(n\dot{\epsilon}_s^s t + \epsilon_{s0n}^s) \right] + \left[c_{-n} \cos(-n\dot{\epsilon}_s^s t - \epsilon_{s0(-n)}^s) \right] \\ \left[c_n \sin(n\dot{\epsilon}_s^s t + \epsilon_{s0n}^s) \right] + \left[c_{-n} \sin(-n\dot{\epsilon}_s^s t - \epsilon_{s0(-n)}^s) \right] \end{array} \right\} \quad (6.12)$$

This equation shows that each frequency component of the stator-current vector can be seen as the sum of two vectors, which rotate at the same speed but in opposite directions, and which may have different (constant) lengths c_n and c_{-n} and different initial angles ϵ_{s0n}^s and $\epsilon_{s0(-n)}^s$.

In a more general way the stator current vector can also be written as a sum of components as in equation 6.13. The index i used in this equation does not correspond to the relative frequency of the harmonic, as was the case with the index n in the previous equations. For example, for the case no even harmonics are present, $\dot{\epsilon}_{s1}^s = \dot{\epsilon}_s^s$, $\dot{\epsilon}_{s2}^s = -\dot{\epsilon}_s^s$, $\dot{\epsilon}_{s3}^s = 3\dot{\epsilon}_s^s$, etc.

$$\begin{bmatrix} i_s^{s1} \\ i_s^{s2} \end{bmatrix} = \sum_{i=1}^{\infty} \begin{bmatrix} i_{si}^{s1} \\ i_{si}^{s2} \end{bmatrix} = \sum_{i=1}^{\infty} \begin{bmatrix} i_{si} \cos(\dot{\epsilon}_{si}^s t + \epsilon_{s0i}^s) \\ i_{si} \sin(\dot{\epsilon}_{si}^s t + \epsilon_{s0i}^s) \end{bmatrix} \quad (6.13)$$

Each of these stator-current-vector components corresponds to an (approximately sinusoidal) current distribution along the air gap, rotating at a speed of $\dot{\epsilon}_{si}^s$, which is a positive or negative multiple of $\dot{\epsilon}_s^s$. This current distribution causes a magnetic induction in the air gap, which in turn induces a current in the rotor. This rotor-current vector will rotate with the same speed with respect to the stator as the stator-current vector, and therefore causes also a magnetic induction in the air gap rotating at this same speed. The sum of the magnetic inductions caused by the stator- and rotor-current components determines a flux linking the stator windings. In summary, each of the stator-current components

causes a rotor-flux vector with a constant amplitude and speed, in the same way as previously the total current in case of symmetrical sinusoidal supply. Figure 6.3 shows the relation between a stator-current component and the resulting rotor-flux component (cf. figure 3.4).

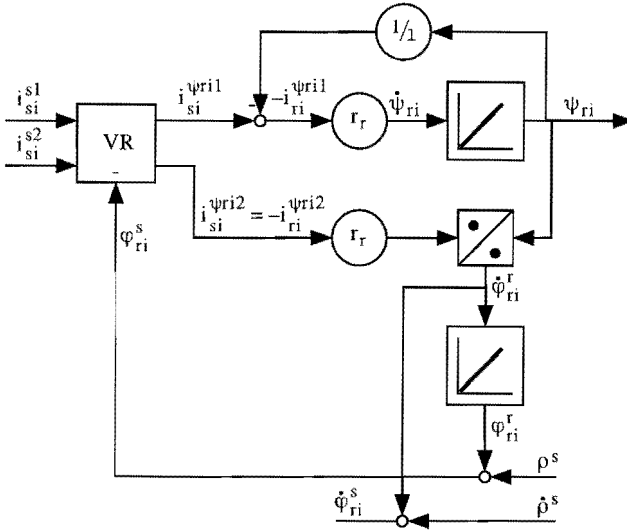


Figure 6.3. Block diagram showing the relation between a stator-current component and the resulting rotor-flux component.

The total rotor flux can now be found from a summation over all rotor-flux components, as given in equation 6.14.

$$\psi_r^s = \begin{bmatrix} \psi_r^{s1} \\ \psi_r^{s2} \end{bmatrix} = \sum_{i=1}^{\infty} \begin{bmatrix} \psi_{ri}^{s1} \\ \psi_{ri}^{s2} \end{bmatrix} = \sum_{i=1}^{\infty} \begin{bmatrix} \psi_{ri} \cos(\varphi_{ri}^s) \\ \psi_{ri} \sin(\varphi_{ri}^s) \end{bmatrix} \quad (6.14)$$

The torque produced by the machine is found from the total stator-current vector and the total rotor-flux vector using equation 2.88, which can be rewritten as in equation 6.15 using equation 6.14. Using again equation 6.14 equation 6.16 is obtained.

$$m_{el} = \begin{bmatrix} -\psi_r^{s2} \\ \psi_r^{s1} \end{bmatrix}^T \cdot \begin{bmatrix} i_s^{s1} \\ i_s^{s2} \end{bmatrix} = \sum_{i=1}^{\infty} (\psi_{ri}^{s1} \cdot i_s^{s2} - \psi_{ri}^{s2} \cdot i_s^{s1}) \quad (6.15)$$

$$m_{el} = \sum_{i=1}^{\infty} \left(\psi_{ri} \cdot \left(\cos(\varphi_{ri}^s) \cdot \sum_{j=1}^{\infty} i_{sj}^{s2} - \sin(\varphi_{ri}^s) \cdot \sum_{j=1}^{\infty} i_{sj}^{s1} \right) \right) \quad (6.16)$$

Using equation 6.17, which describes the relation between the stator-current components in stator coordinates and in the coordinates of the corresponding flux component, equation 6.18 is obtained.

$$\begin{bmatrix} i_{sj}^s \\ i_{sj}^s \\ i_{sj}^s \end{bmatrix} = \mathbf{R}(\varphi_{rj}^s) \cdot \begin{bmatrix} i_{sj}^{\psi rj1} \\ i_{sj}^{\psi rj2} \\ i_{sj}^{\psi rj2} \end{bmatrix} = \begin{bmatrix} \cos \varphi_{rj}^s & -\sin \varphi_{rj}^s \\ \sin \varphi_{rj}^s & \cos \varphi_{rj}^s \end{bmatrix} \cdot \begin{bmatrix} i_{sj}^{\psi rj1} \\ i_{sj}^{\psi rj1} \\ i_{sj}^{\psi rj2} \end{bmatrix} \quad (6.17)$$

$$m_{el} = \sum_{i=1}^{\infty} \left(\psi_{ri} \cdot \sum_{j=1}^{\infty} \left(i_{sj}^{\psi rj1} \sin(\varphi_{rj}^s - \varphi_{ri}^s) + i_{sj}^{\psi rj2} \cos(\varphi_{rj}^s - \varphi_{ri}^s) \right) \right) \quad (6.18)$$

A simplification of equation 6.18 is possible using equation 6.19, which relates the current components in one flux-component coordinate system with another. The result is given in equation 6.20. This equation shows that, as would be expected, the torque is found by multiplying each of the rotor-flux components with all stator-current components that are perpendicular to it. This equation is very similar to equation 3.6.

$$\begin{bmatrix} i_{sj}^{\psi ri1} \\ i_{sj}^{\psi ri2} \\ i_{sj}^{\psi ri2} \end{bmatrix} = \mathbf{R}(-\varphi_{ri}^s) \cdot \begin{bmatrix} i_{sj}^s \\ i_{sj}^s \\ i_{sj}^s \end{bmatrix} = \mathbf{R}(-\varphi_{ri}^s) \cdot \mathbf{R}(\varphi_{rj}^s) \cdot \begin{bmatrix} i_{sj}^{\psi rj1} \\ i_{sj}^{\psi rj2} \\ i_{sj}^{\psi rj2} \end{bmatrix} = \mathbf{R}(\varphi_{rj}^s - \varphi_{ri}^s) \cdot \begin{bmatrix} i_{sj}^{\psi rj1} \\ i_{sj}^{\psi rj2} \\ i_{sj}^{\psi rj2} \end{bmatrix} \quad (6.19)$$

$$m_{el} = \sum_{i=1}^{\infty} \left(\psi_{ri} \cdot \sum_{j=1}^{\infty} i_{sj}^{\psi ri2} \right) \quad (6.20)$$

If the (periodic) stator-current vector is decomposed in the way described by equation 6.13, in which i_{si} , ε_{si}^s and ε_{s0i}^s are constants, the length ψ_{ri} of the corresponding flux-vector component will be constant, as can be derived from the block diagram in figure 6.3. The relation between ψ_{ri} and $i_{si}^{\psi ri1}$ is for that case given in equation 6.21. Together with equation 6.20 this shows that if the arbitrary periodic stator-current vector i_s^s is decomposed in a suitable way, the resulting torque can easily be calculated.

$$\psi_{ri} = 1 \cdot i_{si}^{\psi ri1} \quad (6.21)$$

To calculate the torque according to equation 6.18, the angle φ_{ri}^s between the stator frame and each rotor-flux component is needed. It can be obtained by simulating the block diagram from figure 6.3, but it is also possible to derive an analytical relation. This will be shown below.

The angle φ_{ri}^s can be calculated from the current angles ε_{si}^s and $\varepsilon_{si}^{\psi ri}$, as shown in figure 6.4 and equation 6.22. From figure 6.4 also the relation between the current angle $\varepsilon_{si}^{\psi ri}$ and the flux-oriented current components, equation 6.23, is derived. Using the block diagram from figure 6.3 and assuming a steady-state situation, the second part of equation 6.23 is obtained.

$$\varphi_{ri}^s = \varepsilon_{si}^s - \varepsilon_{si}^{\psi ri} \quad (6.22)$$

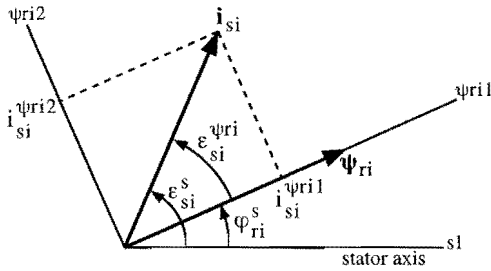


Figure 6.4. Relation between the current and flux angles.

$$\tan(\varepsilon_{si}^{\psi ri}) = \frac{i_{si}^{\psi ri 2}}{i_{si}^{\psi ri 1}} = \frac{\dot{\Phi}_{ri}^r \cdot \psi_{ri} \cdot 1/r_r}{\psi_{ri} \cdot 1/l} = \dot{\Phi}_{ri}^r \cdot \frac{1}{r_r} \quad (6.23)$$

From the block diagram also equation 6.24 is derived, in which the speed $\dot{\varepsilon}_{si}^s$ of the current vector with respect to the stator is equal to that of the flux, in steady state.

$$\dot{\Phi}_{ri}^r = \dot{\Phi}_{ri}^s - \dot{\rho}^s = \dot{\varepsilon}_{si}^s - \dot{\rho}^s \quad (6.24)$$

By combining equations 6.22 to 6.24 into equation 6.25 the angle φ_{ri}^s is found as a function of two machine parameters, the rotor speed, and the speed and angle of the current vector under consideration.

$$\varphi_{ri}^s = \varepsilon_{si}^s - \arctan\left(\left(\dot{\varepsilon}_{si}^s - \dot{\rho}^s\right) \cdot \frac{1}{r_r}\right) \quad (6.25)$$

6.4.2 Numerical minimization of the torque ripple

The case to be considered here is that in which only a current can flow in phase a, i.e. $i_{sb} = 0$ and $i_{sc} = 0$. As a result, the stator-current vector i_s^s can be written as in equation 6.26, according to the current-transformation equation 4.4.

$$i_s^s = \begin{bmatrix} i_s^{s1} \\ i_s^{s2} \\ i_s^s \end{bmatrix} = \begin{bmatrix} i_{sa} \\ 0 \end{bmatrix} \quad (6.26)$$

The current i_{sa} will be a periodic function, and can therefore be written as in equation 6.27. Using equation 6.26, the stator-current vector can now be written in the form of equation 6.12, as shown in 6.28. Here each harmonic component has been split into two components, with equal amplitude and initial angle, but rotating in opposite directions.

$$i_{sa} = \sum_{n=1}^{\infty} i_{sn} \cos(n\dot{\varepsilon}_s^s t + \varepsilon_{s0n}^s) \quad (6.27)$$

$$\begin{bmatrix} i_s^{s1} \\ i_s^{s2} \end{bmatrix} = \sum_{n=1}^{\infty} \left\{ \begin{bmatrix} \frac{i_{sn}}{2} \cdot \cos(n\hat{\epsilon}_s^s t + \epsilon_{s0n}^s) \\ \frac{i_{sn}}{2} \cdot \sin(n\hat{\epsilon}_s^s t + \epsilon_{s0n}^s) \end{bmatrix} + \begin{bmatrix} \frac{i_{sn}}{2} \cdot \cos(n\hat{\epsilon}_s^s t + \epsilon_{s0n}^s) \\ -\frac{i_{sn}}{2} \cdot \sin(n\hat{\epsilon}_s^s t + \epsilon_{s0n}^s) \end{bmatrix} \right\} \quad (6.28)$$

Using the equations derived previously, if the Fourier decomposition of i_{sa} is known, the torque waveform can be calculated. An example is shown in figure 6.5. In this example and in the case studied afterwards, the fundamental angular frequency of the current is set to $\hat{\epsilon}_s^s = 0.5$. The desired torque m_{el}^* is equal to 0.5 and the desired rotor flux $\psi_r^* = 1$. With $1 = 3$, using equations 3.14 and 3.16, the desired values for the field-oriented current components are found, from which the length i_s^* of the desired current vector can be calculated as in equation 6.29. Using the fact that $\hat{\phi}_r^s = \hat{\epsilon}_s^s$ and calculating the slip frequency $\hat{\phi}_r^s$ according to the block diagram of figure 3.4 or using equation 3.11, with $r_r = 0.02$, the rotor speed is found to be $\hat{\rho}^s = 0.49$.

$$\left. \begin{aligned} i_s^{\psi r1*} &= \frac{\psi_r^*}{1} = \frac{1}{3} \\ i_s^{\psi r2*} &= \frac{m_{el}^*}{\psi_r^*} = \frac{1}{2} \end{aligned} \right\} \Rightarrow i_s^* = 0.60 \quad (6.29)$$

In a normal situation, the current vector in the machine to obtain this torque and flux would have a constant amplitude of 0.60 and rotate at a constant positive angular frequency of $\hat{\epsilon}_s^s = 0.5$. If only one phase current is available, the current vector must also contain a component with equal amplitude rotating in the opposite direction, according to equation 6.28. Consider for example the current vector given by equation 6.30. The initial angle ϵ_{s01}^s can be set to zero.

$$\begin{bmatrix} i_s^{s1} \\ i_s^{s2} \end{bmatrix} = \begin{bmatrix} 0.6 \cdot \cos(0.5 \cdot t + \epsilon_{s01}^s) \\ 0.6 \cdot \sin(0.5 \cdot t + \epsilon_{s01}^s) \end{bmatrix} + \begin{bmatrix} 0.6 \cdot \cos(0.5 \cdot t + \epsilon_{s01}^s) \\ -0.6 \cdot \sin(0.5 \cdot t + \epsilon_{s01}^s) \end{bmatrix} \quad (6.30)$$

The torque corresponding to this current vector is shown in figure 6.5, for one period of i_{sa} . The average of the torque shown here is slightly lower than the desired value of 0.5, due to the torque caused by the interaction of the current component rotating in negative direction and its resulting flux. Furthermore the torque contains a component with twice the frequency $\hat{\epsilon}_s^s$ of the stator current, caused by the interaction of each of the current components with the flux resulting from the other current component.

An interesting parameter is the rms value c related to this ac component, because in an ideal (constant torque) situation it would be zero. It can be calculated using equation 6.31, in which $[m_{el}]_{av}$ is the average value of the torque. For the case of figure 6.5 the value $c = 0.4193$ is obtained.

$$c = \sqrt{\frac{\bar{\epsilon}_s^s}{2\pi} \cdot \int_0^{2\pi/\epsilon_s^s} (m_{el} - [m_{el}]_{av})^2 dt} \tag{6.31}$$

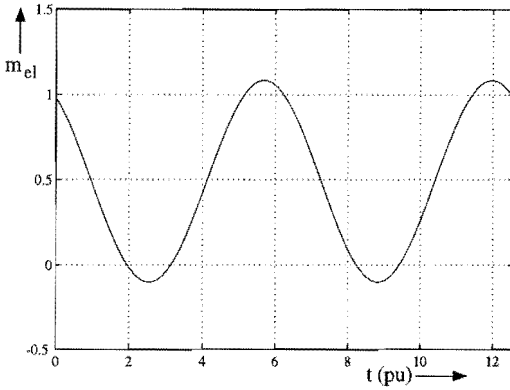


Figure 6.5. The torque in case the machine is fed with a single sinusoidal current (drawn for one period of this current).

It will now be shown that a much smaller value for the rms value of the non-constant component of the torque can be obtained by adding harmonic components to the stator current. Consider equation 6.32, which gives the stator-current vector for this case, which corresponds to the previous case given by equation 6.30 (with $i_{s1} = 1.2$ and $\epsilon_{s01}^s = 0$) plus a certain number of odd harmonics.

$$\begin{bmatrix} i_s^1 \\ i_s^2 \end{bmatrix} = \sum_{n=1,3,5,\dots}^N \left\{ \begin{bmatrix} \frac{i_{sn}}{2} \cdot \cos(n\epsilon_s^s t + \epsilon_{s0n}^s) \\ \frac{i_{sn}}{2} \cdot \sin(n\epsilon_s^s t + \epsilon_{s0n}^s) \end{bmatrix} + \begin{bmatrix} \frac{i_{sn}}{2} \cdot \cos(n\epsilon_s^s t + \epsilon_{s0n}^s) \\ -\frac{i_{sn}}{2} \cdot \sin(n\epsilon_s^s t + \epsilon_{s0n}^s) \end{bmatrix} \right\} \tag{6.32}$$

Using a numerical optimization algorithm, the value of c can be minimized as a function of the amplitude and the angle of the harmonic current components. First an optimization was performed using a third and a fifth harmonic. After a sufficient number of iterations the torque waveform of figure 6.6a was obtained. The calculation of c for this situation yields $c = 0.2425$, which is a considerable improvement compared to the previous case. The amplitudes and angles of the current components required to obtain this result are given in table 6.1.

Even better results can be obtained by adding also higher harmonics. Table 6.1 shows the effect of the optimization using also the 7th and 9th harmonics, and finally also the 11th harmonic. For this final case the torque is shown in figure 6.6b. This figure shows that the torque is nearly constant during a large part of the period, but has two dips of which only the width, not the amplitude, was reduced by adding harmonic current components.

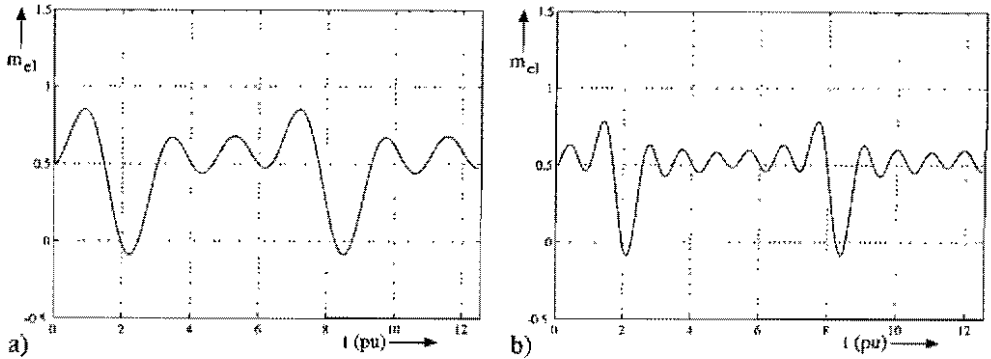


Figure 6.6. The torque in case harmonic components are added to the current in order to minimize the rms value of the ac component of the torque. a) addition of 3rd and 5th harmonic; b) addition of 3rd, 5th, 7th, 9th and 11th harmonic.

The addition of harmonic components does also cause a very slight change of the average torque. The average of the torque shown in figure 6.6a is 0.3 % higher than the torque shown in figure 6.5, while the torque in figure 6.6b is 0.7 % higher. No correction was made to ensure an exactly equal average torque for all cases given in table 6.1.

The addition of higher harmonics is of course limited by the switching capabilities of the power converter. There is however also another limitation, which is much more serious. Figure 6.7 shows the phase current for the different cases, from which it is clear that each time a harmonic component is added, the peak value of the current increases. As indicated in table 6.1, the effective use of a 7th and 9th harmonic would already require a peak value of the current of more than 3 pu, which in practical situations would require oversized converter devices and machine windings. The ability to improve the torque waveform using this method is thus very dependent on the current capability of the converter, as well as on the required average torque.

Table 6.1. Current vectors yielding an optimal torque in case only a single current can flow in the machine.

Highest harmonic	Amplitudes and angles of the current vector components			RMS value (eq. 6.31)	Peak value of current
N	n	i_{sn}	ϵ_{s0n}^s	c	$[i_{sa}]_{max}$
1	1	1.2	0	0.4193	1.2
5	1	1.2	0	0.2425	2.1083
	3	0.8132	4.324		
	5	0.4174	2.375		
9	1	1.2	0	0.1889	3.0956
	3	0.9716	4.299		
	5	0.7360	2.314		
	7	0.4840	0.322		
	9	0.2530	4.595		
11	1	1.2	0	0.1726	3.6775
	3	1.0170	4.305		
	5	0.8266	2.329		
	7	0.6198	0.358		
	9	0.4340	4.675		
	11	0.2282	2.714		

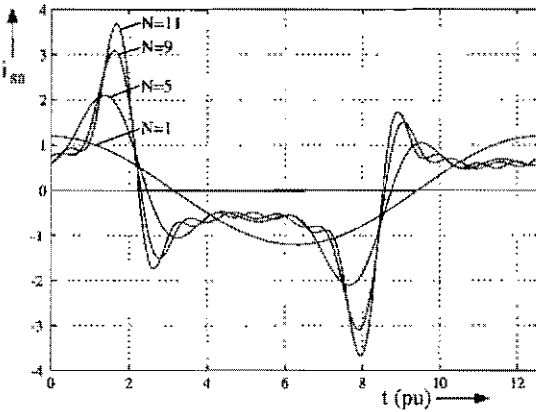


Figure 6.7. The current for the different torque-optimization cases described by table 6.1.

6.5 Addition of harmonic current components to remove low-frequency torque ripple

While in the previous section a numerical method was used to optimize the waveform of the torque, in this section an analytical, simplified expression of the torque as a function of the harmonic current components will be derived. This expression will be used to remove certain harmonic components from the torque waveform, or to minimize once again the rms value of the ac component of the torque, which should yield results very similar to those obtained in the previous section.

6.5.1 Simplification of the torque equation for high speeds

To obtain comprehensive analytical results, the torque equation 6.18 will be simplified by neglecting a number of components that are almost zero. The reasons for this can be understood from equation 6.23. This equation shows that for large values of the slip frequency $\dot{\phi}_{ri}^r$, the tangent of $\epsilon_{si}^{\psi ri}$ will be large, and $\epsilon_{si}^{\psi ri}$ will therefore be close to $\pm 90^\circ$. For example, for $\dot{\phi}_{ri}^r = 1$, $l = 3$ and $r_r = 0.02$, $\epsilon_{si}^{\psi ri}$ equals 89.6° . In fact, for most of the current components, $\dot{\phi}_{ri}^r$, which can be calculated using equation 6.24, will be so large that $\epsilon_{si}^{\psi ri}$ is even closer to 90° or -90° . An angle $\epsilon_{si}^{\psi ri}$ of $\pm 90^\circ$ means that the corresponding current component does not produce any flux: $i_{si}^{\psi ri1} = 0$, and therefore $\psi_{ri} = 0$, according to equation 6.21. An $\epsilon_{si}^{\psi ri}$ of $\pm 90^\circ$ also means that $i_{si}^{\psi ri2}$ will be equal to $\pm i_{si}$.

From equation 6.24 it can be seen that for operation with a small fundamental slip if $\dot{\rho}^s$ is small the fundamental current frequency is also small. Therefore, also the slip frequencies for the harmonic current components will be relatively small. The above mentioned simplification is therefore not valid for low rotor speeds. For the example case from the previous section, where $\dot{\rho}^s = 0.49$, $\epsilon_{si}^{\psi ri}$ can be considered equal to $\pm 90^\circ$ for all except the positive frequency fundamental current component. Using this approximation, for the current given by equation 6.32, with $\dot{\epsilon}_s^s = 0.5$, $i_{s1} = 1.2$ and $\epsilon_{s01}^s = 0$ the following equation (6.33) for the torque is obtained by using equations 6.20, 6.19 and 6.22.

$$\begin{aligned}
 m_{el} = & 0.5 - \frac{1.2}{2} \cos\left(-\dot{\epsilon}_s^s t + \frac{\pi}{2} - \left(\dot{\epsilon}_s^s t - \epsilon_{s1}^{\psi r1}\right)\right) \\
 & + \frac{i_{s3}}{2} \cos\left(\left(3\dot{\epsilon}_s^s t + \epsilon_{s03}^s\right) - \frac{\pi}{2} - \left(\dot{\epsilon}_s^s t - \epsilon_{s1}^{\psi r1}\right)\right) \\
 & - \frac{i_{s3}}{2} \cos\left(\left(-3\dot{\epsilon}_s^s t - \epsilon_{s03}^s\right) + \frac{\pi}{2} - \left(\dot{\epsilon}_s^s t - \epsilon_{s1}^{\psi r1}\right)\right) + \dots \\
 & + \frac{i_{sn}}{2} \cos\left(\left(n\dot{\epsilon}_s^s t + \epsilon_{s0n}^s\right) - \frac{\pi}{2} - \left(\dot{\epsilon}_s^s t - \epsilon_{s1}^{\psi r1}\right)\right) \\
 & - \frac{i_{sn}}{2} \cos\left(\left(-n\dot{\epsilon}_s^s t - \epsilon_{s0n}^s\right) + \frac{\pi}{2} - \left(\dot{\epsilon}_s^s t - \epsilon_{s1}^{\psi r1}\right)\right) + \dots
 \end{aligned} \tag{6.33}$$

The value for $\varepsilon_{s1}^{\psi r1}$ can be found using equation 6.23 with $\hat{\phi}_{r1}^r = 0.5 - 0.49 = 0.01$, $l = 3$ and $r_r = 0.02$, yielding $\varepsilon_{s1}^{\psi r1} = 0.982$ rad. Equation 6.33 can be simplified to obtain equation 6.34. This equation clearly shows that the fundamental current causes a constant torque plus a component at $2 \cdot \hat{\varepsilon}_s^s$, and that each harmonic component adds two different frequency components to the torque.

$$\begin{aligned}
 m_{el} = & 0.5 + 0.6 \sin\left(-2\hat{\varepsilon}_s^s t + \varepsilon_{s1}^{\psi r1}\right) \\
 & + \frac{i_{s3}}{2} \sin\left(2\hat{\varepsilon}_s^s t + \varepsilon_{s03}^s + \varepsilon_{s1}^{\psi r1}\right) \\
 & + \frac{i_{s3}}{2} \sin\left(-4\hat{\varepsilon}_s^s t - \varepsilon_{s03}^s + \varepsilon_{s1}^{\psi r1}\right) + \dots \\
 & + \frac{i_{sn}}{2} \sin\left((n-1) \cdot \hat{\varepsilon}_s^s t + \varepsilon_{s0n}^s + \varepsilon_{s1}^{\psi r1}\right) \\
 & + \frac{i_{sn}}{2} \sin\left(-(n+1) \cdot \hat{\varepsilon}_s^s t - \varepsilon_{s0n}^s + \varepsilon_{s1}^{\psi r1}\right) + \dots
 \end{aligned} \tag{6.34}$$

6.5.2 Minimization of the rms value of the torque ripple

To compare this method with the numerical torque optimization of the previous section, torque equation 6.34 will first be used to minimize the rms value c of the ac component of the torque, defined by equation 6.31, in which now $[m_{el}]_{av} = 0.5$, as can be seen from equation 6.34. To minimize c , the function f , given in equation 6.35, will be minimized as a function of the amplitudes and angles of the harmonic current components. First this will be done for the case when only a third and a fifth harmonic is added to the current, and after that for the general case in which also higher harmonics are added. Equation 6.36 shows the function that has to be minimized for the first case.

$$\int_0^{2\pi/\hat{\varepsilon}_s^s} (m_{el} - 0.5)^2 dt \tag{6.35}$$

$$\begin{aligned}
 f = & \int_0^{2\pi/\hat{\varepsilon}_s^s} \frac{1}{4} \left\{ i_{s1} \sin\left(-2\hat{\varepsilon}_s^s t + \varepsilon_{s1}^{\psi r1}\right) + i_{s3} \sin\left(2\hat{\varepsilon}_s^s t + \varepsilon_{s03}^s + \varepsilon_{s1}^{\psi r1}\right) \right. \\
 & + i_{s3} \sin\left(-4\hat{\varepsilon}_s^s t - \varepsilon_{s03}^s + \varepsilon_{s1}^{\psi r1}\right) + i_{s5} \sin\left(4\hat{\varepsilon}_s^s t + \varepsilon_{s05}^s + \varepsilon_{s1}^{\psi r1}\right) \\
 & \left. + i_{s5} \sin\left(-6\hat{\varepsilon}_s^s t - \varepsilon_{s05}^s + \varepsilon_{s1}^{\psi r1}\right) \right\}^2 dt
 \end{aligned} \tag{6.36}$$

Further evaluation of this function yields the result given in equation 6.37.

$$f = \frac{\pi}{4\epsilon_s^s} \left(i_{s1}^2 + 2i_{s3}^2 + 2i_{s5}^2 - 2i_{s1}i_{s3}\cos\left(\epsilon_{s03}^s + 2\epsilon_{s1}^{\psi r1}\right) \right. \\ \left. - 2i_{s3}i_{s5}\cos\left(\epsilon_{s05}^s - \epsilon_{s03}^s + 2\epsilon_{s1}^{\psi r1}\right) \right) \quad (6.37)$$

Because all of the amplitudes of the current components are by definition positive, minimizing this function can first be done by maximizing the cosines. This results in a relation between the initial angles of the harmonic current components, given in equation 6.38. Then the cosines have become equal to 1, and the remaining function to be minimized is given in equation 6.39.

$$\epsilon_{s03}^s = -2\epsilon_{s1}^{\psi r1} \\ \epsilon_{s05}^s = \epsilon_{s03}^s - 2\epsilon_{s1}^{\psi r1} = -4\epsilon_{s1}^{\psi r1} \quad (6.38)$$

$$f = \frac{\pi}{4\epsilon_s^s} \left(i_{s1}^2 + 2i_{s3}^2 + 2i_{s5}^2 - 2i_{s1}i_{s3} - 2i_{s3}i_{s5} \right) \quad (6.39)$$

This function f can be minimized by solving the equations $\partial f/\partial i_{s3} = 0$ and $\partial f/\partial i_{s5} = 0$ simultaneously. This is done in equation 6.40. A numerical evaluation of equations 6.40 and 6.38 yields the solution given in equation 6.41.

$$\begin{cases} 4i_{s3} - 2i_{s1} - 2i_{s5} = 0 \\ 4i_{s5} - 2i_{s3} = 0 \end{cases} \Rightarrow \begin{cases} i_{s5} = \frac{1}{3}i_{s1} \\ i_{s3} = \frac{2}{3}i_{s1} \end{cases} \quad (6.40)$$

$$\begin{cases} i_{s3} = 0.8 \\ i_{s5} = 0.4 \end{cases}, \begin{cases} \epsilon_{s03}^s = 4.317 \pmod{2\pi} \\ \epsilon_{s05}^s = 2.352 \pmod{2\pi} \end{cases} \quad (6.41)$$

A comparison of this solution with the values obtained using a numerical optimization method and without simplifying the torque equation (see table 6.1, for $N=5$) shows a very close resemblance.

In case more harmonics are added, equation 6.36 has to be extended with the corresponding extra terms, according to torque equation 6.34. Just like in the previous case, first a relation is obtained between the initial angles of the current components. For the n -th component this relation is given in equation 6.42. This equation shows that all angles are at regular intervals, and that they are independent of the number of harmonics which is added. This result can be verified with the numerical results in table 6.1, showing angles that are indeed approximately at regular intervals, and are approximately independent of N .

$$\epsilon_{s0n}^s = \epsilon_{s0(n-2)}^s - 2\epsilon_{s1}^{\psi r1} \quad (6.42)$$

Thus, after all cosines have been made equal to one, the remaining function that has to be optimized is given by equation 6.43, which is an extension of equation 6.39.

$$f = \frac{\pi}{4\epsilon_s^s} \left(i_{s1}^2 + 2i_{s3}^2 + \dots + 2i_{sN}^2 - 2i_{s1}i_{s3} - \dots - 2i_{s(N-2)}i_{sN} \right) \quad (6.43)$$

For this function f , the optimum can be found by setting again $\partial f / \partial i_{sn} = 0$ for all odd values of n from 3 to N , resulting in a solution for all current-component amplitudes. For $n = N$ equation 6.44 is valid, for $n = N - k$ equation 6.45. By induction, equation 6.46 can be proved, which gives the amplitudes of all components. Also these amplitudes can be compared with those in table 6.1, which shows approximately the same results.

$$i_{sN} = \frac{1}{2} i_{s(N-2)} \quad (6.44)$$

$$4i_{s(N-k)} - 2i_{s(N-k-2)} - 2i_{s(N-k+2)} = 0 \quad (6.45)$$

$$i_{s(N-k)} = \frac{k+2}{2} i_{sN} \quad (6.46)$$

6.5.3 Removal of low-frequency torque-ripple components

The additional harmonic current components can however not only be used to reduce the rms value of the ac component of the torque – they can also be used to eliminate certain harmonic components, at the price of introducing other components (see also [Kast-94] and [Kast-95]). This can be seen from the torque equation (6.34). For example, consider the torque equation in case only a third harmonic current is added, as given in equation 6.47.

$$\begin{aligned} m_{el} = & 0.5 + 0.6 \sin\left(-2\epsilon_s^s t + \epsilon_{s1}^{\psi r1}\right) + \frac{i_{s3}}{2} \sin\left(2\epsilon_s^s t + \epsilon_{s03}^s + \epsilon_{s1}^{\psi r1}\right) \\ & + \frac{i_{s3}}{2} \sin\left(-4\epsilon_s^s t - \epsilon_{s03}^s + \epsilon_{s1}^{\psi r1}\right) \end{aligned} \quad (6.47)$$

From this equation it becomes clear that the torque component with a frequency of $2\epsilon_s^s$ can be eliminated by taking $i_{s3} = 1.2$ and $\epsilon_{s03}^s = -2\epsilon_{s1}^{\psi r1}$. The resulting torque is given in equation 6.48. This equation shows that the component at $2\epsilon_s^s$ is eliminated completely, but that now a component with the same amplitude but with a frequency of $4\epsilon_s^s$ is present.

$$\begin{aligned} m_{el} = & 0.5 + 0.6 \sin\left(-2\epsilon_s^s t + \epsilon_{s1}^{\psi r1}\right) + 0.6 \sin\left(2\epsilon_s^s t - \epsilon_{s1}^{\psi r1}\right) \\ & + 0.6 \sin\left(-4\epsilon_s^s t + 3\epsilon_{s1}^{\psi r1}\right) \\ = & 0.5 + 0.6 \sin\left(-4\epsilon_s^s t + 3\epsilon_{s1}^{\psi r1}\right) \end{aligned} \quad (6.48)$$

In turn, the torque component at $4\dot{\epsilon}_s^s$ can be eliminated by adding a fifth harmonic to the current, with $i_{s5} = 1.2$ and $\epsilon_{s05}^s = -4\epsilon_{s1}^s$. The torque and current for this case are shown in figure 6.8a and b, respectively. The torque shown in figure 6.8a has however been calculated using the exact torque equation (6.18), without the approximation that was assumed at the beginning of section 6.5. Due to this approximation the elimination has not succeeded perfectly. As a result, the torque still contains some very small components at $2\dot{\epsilon}_s^s$ and $4\dot{\epsilon}_s^s$, which explains why the waveform in figure 6.8a is not exactly sinusoidal. Also the average torque differs slightly from its desired value of 0.5 pu.

It can be noted that the initial angles required for this method are the same as those used in the minimization explained previously (cf. equation 6.42). The required amplitudes of the current components however are even larger, as can be seen by comparing the waveform in figure 6.8b with the one for $N = 5$ in figure 6.7. The elimination of harmonic components from the torque is therefore only possible up to a certain frequency, determined mainly by the overcurrent capability of the converter.

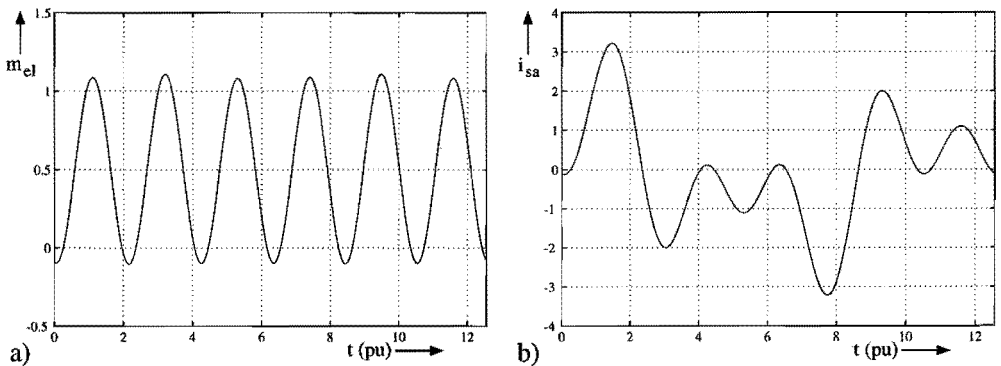


Figure 6.8. The torque and current in case the components at $2\dot{\epsilon}_s^s$ and $4\dot{\epsilon}_s^s$ are eliminated from the torque. a) the torque; b) the current.

6.6 A field-oriented approach to the torque-ripple problem

In the previous sections the main concern of the control system was to produce a torque that resembles the desired constant torque as well as possible. In field-oriented control, the torque is directly proportional to one of the current components, resulting in a very straightforward control of the torque. Therefore the field-oriented control will also be applied to this fault situation.

Whereas one current component is used to control the torque, the other component, $i_s^{\psi r1}$, is responsible for the rotor flux. As shown in equation 3.13, rapid variations of $i_s^{\psi r1}$ with respect to the rotor time constant do not noticeably affect the flux. Therefore in this section a constant rotor flux ψ_r has been assumed.

The relation between the remaining stator current i_{sa} and the field-oriented current components $i_s^{\psi r1}$ and $i_s^{\psi r2}$ is given in equation 6.49. The angle φ_r^s between the rotor-flux vector and the stator axis is supposed to be known, so that at all times the relation between the stator current and the field-oriented current components is known.

$$\begin{bmatrix} i_s^{\psi r1} \\ i_s^{\psi r2} \end{bmatrix} = R(-\varphi_r^s) \begin{bmatrix} i_{sa}^s \\ i_{sa}^s \end{bmatrix} = \begin{bmatrix} i_{sa} \cdot \cos(\varphi_r^s) \\ -i_{sa} \cdot \sin(\varphi_r^s) \end{bmatrix} \quad (6.49)$$

The first requirement of the control system is to generate a constant torque. Assuming that the rotor flux is constant, the torque is proportional to $i_s^{\psi r2}$. In equation 6.50, which can be derived from equation 6.49, the current required to obtain a constant torque is given. In this equation the desired torque producing current component $i_s^{\psi r2*}$ is equal to m_{cl}^*/ψ_r .

$$i_{sa}^* = \frac{-i_s^{\psi r2*}}{\sin(\varphi_r^s)} \quad (6.50)$$

Figure 6.9 shows the resulting current vector in flux coordinates, and the two field-oriented current components as a function of the time. A complete period of the field-oriented stator-current components is shown, corresponding to half a period of the stator current i_{sa} . As in the previous sections $i_s^{\psi r2*} = 0.5$. It has been assumed that $\dot{\varphi}_r^s = 0.5$ and $\varphi_r^s = \dot{\varphi}_r^s t$.

As can be seen from equation 6.50 and also from figure 6.9b, maintaining a constant $i_s^{\psi r2}$ requires an infinitely high current when the sine of φ_r^s equals zero. This occurs twice in every period, when the current vector is parallel with the rotor flux. Not only this infinite amplitude, but also the fact that the current would have to change instantly from plus to minus infinity makes that such a current can not be realized in practice. Therefore a second requirement for the current has to be formulated: the limitation of the current to a maximum value, $[i_{sa}]_{max}$.

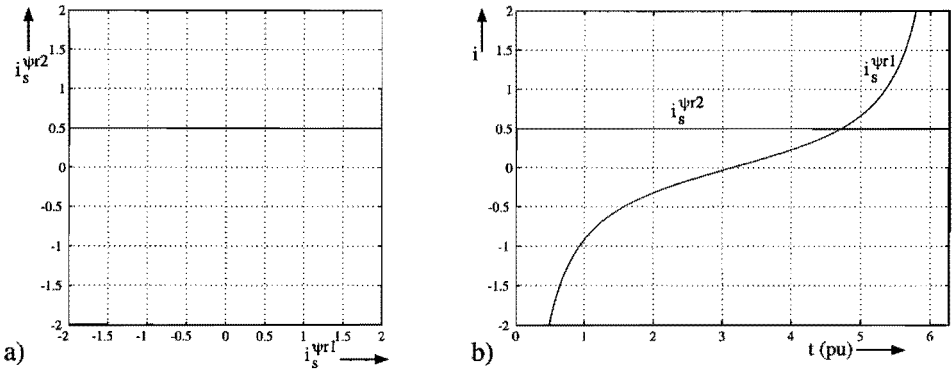


Figure 6.9. The field-oriented current in case the torque-producing current component is kept constant. a) the current vector; b) the current components as a function of the time.

In figure 6.10 the current components are shown in case the phase current is limited to $[i_{sa}]_{\max} = 1.5$. Instead of remaining constant, the torque-producing component of the stator current now contains a dip, occurring twice in every period of i_{sa} , from its constant value down to zero. If limitation of the current is applied, this current dip can not be avoided, nor can the depth of the dip be influenced: according to equation 6.49, when $\sin(\varphi_r^s)$ is zero, $i_s^{\psi r2}$ will be zero unless i_{sa} could reach an infinitely high value. To draw figure 6.10b it has again been assumed that $\hat{\phi}_r^s = 0.5$ and $\varphi_r^s = \hat{\phi}_r^s t$. In reality, $\hat{\rho}^s$ will be nearly constant if the inertia is assumed sufficiently large, but $\hat{\phi}_r^s$ will vary due to the variation of $i_s^{\psi r2}$ (cf. equation 3.11). As a result, $\hat{\phi}_r^s (= \hat{\rho}^s + \hat{\phi}_r^s)$ will in reality not be exactly constant.

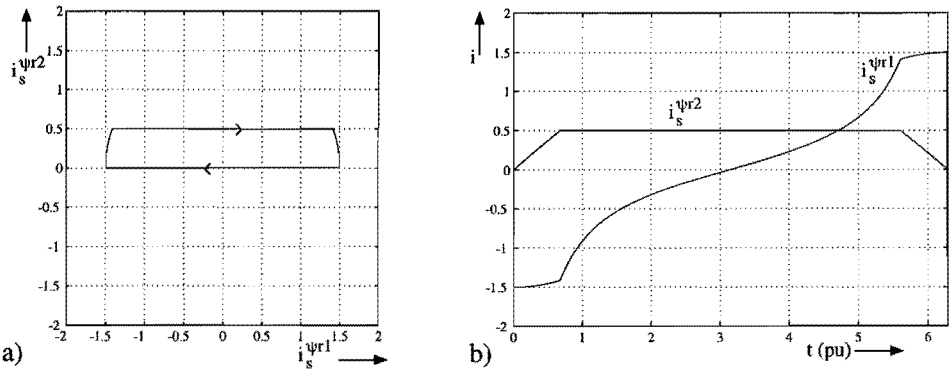


Figure 6.10. The field-oriented current in case the torque-producing current component is kept constant except during current limitation. a) the current vector; b) the current components as a function of the time.

However, figure 6.10b reveals that there is still another problem with the current shape selected in this case. The magnetizing current component, $i_s^{\psi r1}$, has an average value of zero. This would mean that in steady state the flux in the induction machine would also be

zero, which evidently does not allow operation of the machine. Thus, a third requirement has to be met: the average magnetizing current must be equal to its desired value. This is stated by equation 6.51, in which $2\pi/\dot{\phi}_r^s$ is the period of the current. Also here a constant $\dot{\phi}_r^s$ has been assumed.

$$\left[i_s^{\psi r1} \right]_{av} \equiv \frac{\dot{\phi}_r^s}{2\pi} \int_0^{2\pi/\dot{\phi}_r^s} i_s^{\psi r1} dt = i_s^{\psi r1*} \quad (6.51)$$

Using equation 6.49, and assuming that $\varphi_r^s = \dot{\phi}_r^s t + \varphi_{r0}^s$ (with constant $\dot{\phi}_r^s$ and φ_{r0}^s) it can be deduced that i_{sa} must satisfy equation 6.52, in which $\dot{\epsilon}_s^s = \dot{\phi}_r^s$, and for which equations 6.53 and 6.54 must be satisfied. One more equation is required to determine the parameters a and ϵ_{s01}^s separately.

$$i_{sa} = a \cos(\dot{\epsilon}_s^s t + \epsilon_{s01}^s) + f(t) \quad (6.52)$$

$$\frac{a}{2} \cos(\epsilon_{s01}^s - \varphi_{r0}^s) = i_s^{\psi r1*} \quad (6.53)$$

$$\frac{\dot{\phi}_r^s}{2\pi} \int_0^{2\pi/\dot{\phi}_r^s} f(t) \cdot \cos(\varphi_r^s) dt = 0 \quad (6.54)$$

The most general function $f(t)$ which will satisfy equation 6.54 is given in equation 6.55.

$$f(t) = a_0 + a_1 \sin(\dot{\epsilon}_s^s t + \varphi_{r0}^s) + \sum_{n=2}^{\infty} a_n \cos(n\dot{\epsilon}_s^s t + \varphi_{r0}^s) \quad (6.55)$$

The function given in equation 6.50, which yielded a constant torque, can be shown to satisfy the function definition given in 6.55. The resulting waveform for i_{sa} , found by replacing $f(t)$ in equation 6.52 with the function given in equation 6.50, is given in equation 6.56. However, there is still another condition that has to be met: the average torque should be equal to the desired torque ($\left[i_s^{\psi r2} \right]_{av} = i_s^{\psi r2*}$). This is calculated in equation 6.57, and results in a value for ϵ_{s01}^s . This angle should be taken equal to φ_{r0}^s in order to obtain the correct average torque.

$$i_{sa} = a \cos(\dot{\epsilon}_s^s t + \epsilon_{s10}^s) + \frac{-i_s^{\psi r2*}}{\sin(\varphi_r^s)} \quad (6.56)$$

$$\left[i_s^{\psi r2} \right]_{av} \equiv \frac{\dot{\phi}_r^s}{2\pi} \int_0^{2\pi/\dot{\phi}_r^s} -i_{sa} \cdot \sin(\varphi_r^s) dt = \frac{a}{2} \sin(\epsilon_{s01}^s - \varphi_{r0}^s) + i_s^{\psi r2*} \quad (6.57)$$

From equation 6.56, using equation 6.53 and the fact that $\epsilon_{s01}^s = \varphi_{r0}^s$, equation 6.58 is found. The waveforms of the field-oriented current components using this i_{sa} are shown in figure 6.11.

$$i_{sa} = 2i_s^{\psi r1*} \cos(\dot{\phi}_{r1}^s t + \varphi_{r0}^s) + \frac{-i_s^{\psi r2*}}{\sin(\varphi_r^s)} \tag{6.58}$$

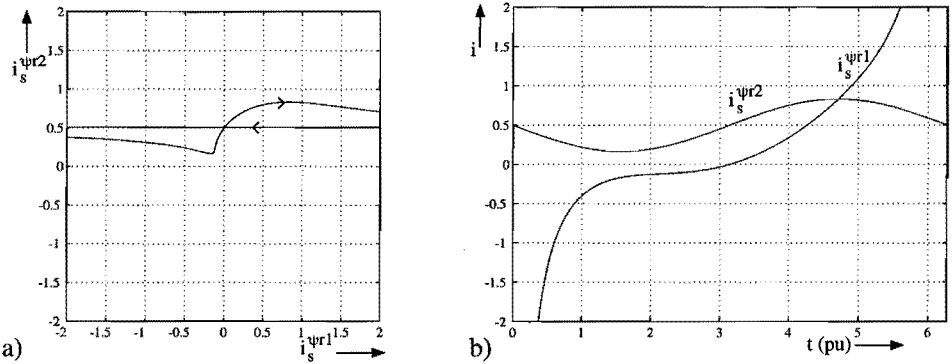


Figure 6.11. The field-oriented current in case the current waveform of equation 6.58 is used. a) the current vector; b) the current components as a function of the time.

As figure 6.11b shows, the torque-producing component which results from this current contains a component at twice the fundamental current frequency (the figure shows one half of a period of the current i_{sa}). Furthermore, limitation of the current would be needed to obtain results that can be used in practice. This limitation however would affect the average values of the two current components, and thus the above calculations would have to be performed again, now taking in account the limitation.

An option to improve on the torque waveform obtained with equation 6.58, would consist of adding harmonic components to the current. Using harmonic current components, the difference between the desired and the actual torque-producing current could be minimized, in the same way as was done for the torque in the previous section, according to equation 6.31. If the current-limitation problem is neglected, and an infinite number of harmonics is added, this method will give the same resulting current waveform as obtained in the previous section, resulting in equations 6.42 and 6.46. This calculation is not performed here, because no practically usable result is obtained due to the unlimited current.

A different approach to the problem of obtaining an average magnetizing current component $[i_s^{\psi r1}]_{av}$ different from zero, could consist of using the required current limitation to make the trajectory of the current vector different for positive and negative values of $i_s^{\psi r1}$. Consider for example figure 6.10a. Due to the fact that the current limit is set to an equal value for both positive and negative values of $i_s^{\psi r1}$, a symmetrical figure is obtained which corresponds to $[i_s^{\psi r1}]_{av} = 0$. Figure 6.12 shows the current trajectory in case different values for the current limitation are used. With the help of this figure, now the resulting $[i_s^{\psi r1}]_{av}$ will be calculated.

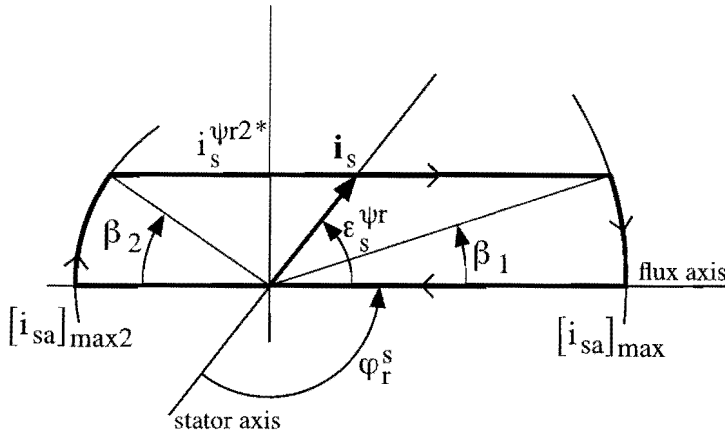


Figure 6.12. The current-vector trajectory in case different values are used for the current limitation, in order to obtain an average magnetizing current different from zero.

Equation 6.59 shows the calculation of $[i_s^{\psi r1}]_{av}$, according to the definition of equation 6.51. As the result is independent of the frequency $\dot{\phi}_r^s$, which is again assumed constant, the calculation has been simplified by taking $\dot{\phi}_r^s = 1$. Due to the periodicity of the field-oriented current components, the calculation is performed for half a period of i_{sa} . The two angles β_1 and β_2 are related to the current limitation values and the desired torque-producing current component according to equation 6.60. Substituting equation 6.60 into 6.59, finally equation 6.61 is found.

$$\begin{aligned}
 [i_s^{\psi r1}]_{av} &= \frac{1}{\pi} \left\{ \int_0^{\beta_2} -\cos t \cdot [i_{sa}]_{\max 2} dt + \int_{\beta_2}^{\pi-\beta_1} \frac{i_s^{\psi r2*}}{-\tan t} dt + \int_{\pi-\beta_1}^{\pi} -\cos t \cdot [i_{sa}]_{\max} dt \right\} \\
 &= \frac{1}{\pi} \left\{ -[i_{sa}]_{\max 2} \cdot \sin \beta_2 - i_s^{\psi r2*} \cdot \ln \left(\frac{\sin \beta_1}{\sin \beta_2} \right) + [i_{sa}]_{\max} \cdot \sin \beta_1 \right\} \quad (6.59)
 \end{aligned}$$

$$\begin{aligned}
 [i_{sa}]_{\max} \cdot \sin \beta_1 &= i_s^{\psi r2*} \\
 [i_{sa}]_{\max 2} \cdot \sin \beta_2 &= i_s^{\psi r2*} \quad (6.60)
 \end{aligned}$$

$$[i_s^{\psi r1}]_{av} = \frac{1}{\pi} i_s^{\psi r2*} \left(\ln([i_{sa}]_{\max}) - \ln([i_{sa}]_{\max 2}) \right) \quad (6.61)$$

Considering that $[i_{sa}]_{\max 2}$ can not be smaller than $i_s^{\psi r2*}$, using this equation it can be calculated that if for example $[i_{sa}]_{\max} = 2$, for an $i_s^{\psi r2*}$ of 0.5 the resulting $[i_s^{\psi r1}]_{av}$ can not be higher than 0.22. This is less than required to obtain the rated flux level for a machine with $1 = 3$. The waveforms corresponding to this case are shown in figure 6.13.

A somewhat higher value of $[i_s^{\psi r1}]_{av}$ is obtained if instead of limiting the current to $[i_{sa}]_{max2}$, it is made zero during this part of the half-period ($0 < t \pmod{\pi} < \beta_2$). The first of the three parts of equation 6.59 then becomes zero, and the resulting $[i_s^{\psi r1}]_{av}$ is given in equation 6.62. The current waveforms for this case are also shown in figure 6.13.

$$[i_s^{\psi r1}]_{av} = \frac{1}{\pi} i_s^{\psi r2*} \left(\ln([i_{sa}]_{max}) - \ln([i_{sa}]_{max2}) + 1 \right) \quad (6.62)$$

Using equation 6.62 it can be calculated that for $i_s^{\psi r2*} = 0.5$, $i_s^{\psi r1*} = 0.33$ and $[i_{sa}]_{max} = 2$, the value which has to be taken for $[i_{sa}]_{max2}$ is 0.67, which corresponds to $\beta_2 = 48^\circ$ or 0.84 rad. This means that the current – and thus also the torque – will be zero during a considerable part of each period, as can be seen in figure 6.13b. This is not a very desirable situation, but it can not be avoided. Finally, to correct for the lower average torque caused by the current limitation, a controller or correction circuit would still have to be added.

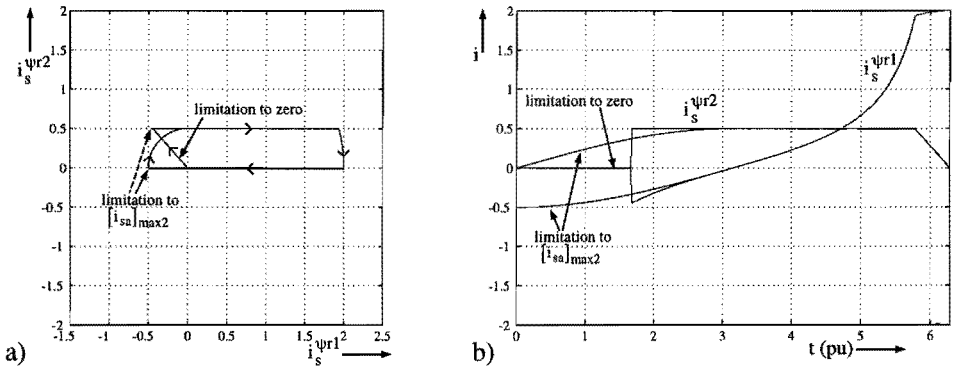


Figure 6.13. The field-oriented current in case the current is limited to two different maximal values in order to obtain a non-zero average magnetizing current. a) the current vector; b) the current components as a function of the time.

6.7 A comparison of the different fault-correction methods

For a current-fed induction machine of which the star point is connected, the correction of a single-phase current fault has been shown in section 6.2. Using the homopolar current, a compensation of the loss of a complete phase is theoretically possible. In practice only the current limitation of the other phases will limit the constant torque level that can still be obtained in this situation.

If a more serious current fault occurs, as a result of which only a single stator phase current remains available, it is no longer possible to obtain a constant torque. In sections 6.3 to 6.6 different approaches were used to optimize the torque waveform for this case,

by changing the waveform of the remaining phase current. In sections 6.4 and 6.5 an optimization was presented which consisted of adding harmonic components to the normally sinusoidal stator current. Figure 6.14 shows some of the results of this optimization. The first trace shows the current, both as a field-oriented vector and as a function of time, in case a sinusoidal current is used which yields the desired average magnetizing and torque-producing components. While, in a first approximation, the flux ψ_r will be equal to one in this and the following cases, the torque will be equal to $i_s^{\psi r 2}$. As was shown in figure 6.5 in this case the torque contains a large ripple at twice the stator-current frequency.

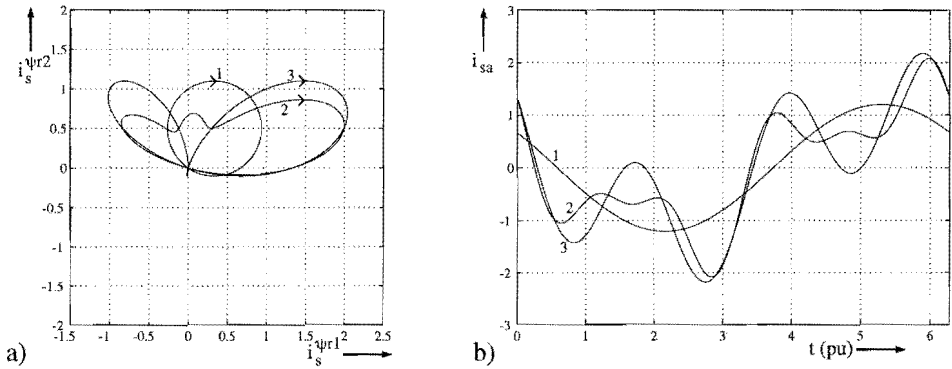


Figure 6.14. Comparison of different current waveforms. 1) sinusoidal current; 2) addition of harmonics (3rd and 5th) to minimize torque ripple; 3) addition of harmonic (3rd) to remove frequency components from the torque; a) the current vector in field-oriented coordinates; b) the stator current as a function of time.

By adding harmonic components to the current – for example a 3rd and 5th harmonic – the harmonic content of the torque ripple can be minimized. This is shown in trace 2 of figure 6.14. In this way also the amplitude of the torque ripple is reduced, but it can not be avoided that the torque temporarily crosses zero (see also figure 6.6a). Adding higher harmonics yields a further reduction of the harmonic content of the torque ripple, at the price of a higher peak value of the stator current (see figure 6.7 or table 6.1).

An even higher stator current is required if harmonic current components are used to eliminate the lowest frequency components of the torque ripple. Trace 3 of figure 6.14 shows the case when a 3rd harmonic is added to the current for this purpose. With this method the amplitude of the torque ripple is not reduced, and thus remains very large. However, this method can successfully be applied if a torque ripple at a mechanical resonance frequency has to be avoided.

The field-oriented methods presented in section 6.6 yield a torque which at least during a certain period of time is constant. As shown in trace 1 of figure 6.15, a constant torque-

producing current component can only be obtained using a current with an infinitely high peak value. Assuming that the variation of the magnetizing current is fast enough not to cause a considerable variation of the flux level, this would correspond to a constant torque.

However, limitation of the current is needed, as well as a means of controlling the average magnetizing current component. Using different current-limitation methods (trace 2 and 3 of figure 6.15), a non-zero average magnetizing current is obtained, but both the current limitation and the requirement for the magnetizing current, result in a decrease of the average torque.

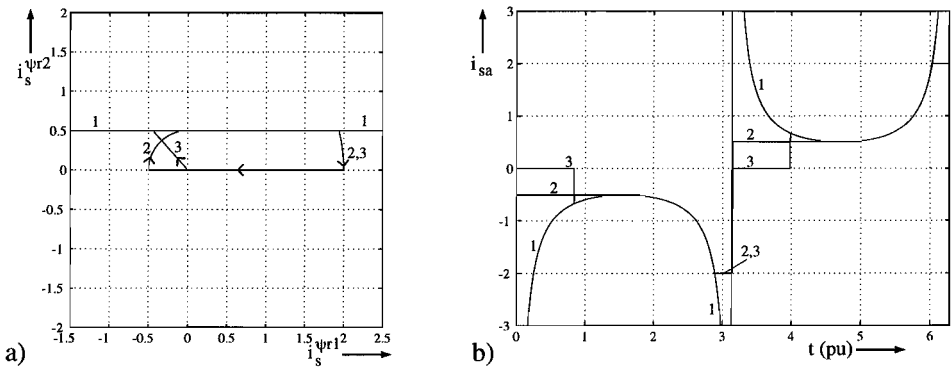


Figure 6.15. Comparison of different current waveforms. 1) current yielding a constant torque; 2) different current limitations to obtain a non-zero magnetizing current; 3) current is temporarily zero to obtain a larger magnetizing current; a) the current vector in field-oriented coordinates; b) the stator current as a function of time.

Hence the field-oriented optimization methods yield a constant torque during one part of each current period, but a decreased or zero torque during another part, due to current limitations and flux control. The harmonic-adding methods do not yield a constant torque during any part of the period, but can be used effectively to influence the harmonic content of the torque ripple. A combination of current limitation and harmonic optimization has not been considered.

Which method should be used in practice will depend on the requirements of the mechanical system and on the current capabilities of the power converter used to generate the stator current. In all cases however the mechanical system has to cope with a very high torque ripple. Unfortunately, it is not possible to reduce the amplitude of this ripple below a theoretical minimum equal to 100% of the peak value of the torque.

Chapter 7

Asymmetrical Operation of a Voltage-Fed Induction Machine with the Star Point Connected

7.1 Introduction

In Chapter 3 (section 3.5) a field-oriented control scheme was derived for the voltage-fed induction machine. In this chapter, this control will be extended with a module which allows the command of the homopolar current in case the star point of the machine is connected. This makes it possible that the machine is operated with an asymmetrical set of supply voltages and currents, as was shown for the current-fed machine in section 6.2.

One of the possible asymmetrical operation modes which can be achieved in this way is the operation with one of the phase currents equal to zero. In this case it is possible to disconnect one of the phases, and thus simulate the single-phase open-circuit fault.

The practical experiments which are shown were performed using a cycloconverter, which embodies three independent voltage sources of which the star point is easily connected to the machine's star point.

7.2 Extension of the Voltage-Vector Calculator for operation with a homopolar current

By its nature, the cycloconverter is a voltage source. Starting from three desired voltages, its control circuitry, described in detail in [Bosg-93], provides the thyristors with the required firing pulses. The result is three output voltages (and three circulating currents inside the converter, which are not important here). Using twelve thyristors for each phase – six for each half bridge – the output voltages have a maximum frequency of around one half of the grid frequency, and distortions at frequencies close to odd multiples of six times the grid frequency.

The fact that the converter requires desired voltages – not currents – as inputs, means that some circuit is needed to calculate these voltages from the desired currents. This is shown in figure 7.1. In this figure the voltage-fed (“U”) induction (“A”) machine is denoted by “UA”. The rotor flux, required to achieve field orientation, is obtained from

the u/i-model, described in section 3.6. The voltage-vector calculator (VVC) is shown in figure 3.7. For asymmetrical operation one extra control block is needed, which calculates the desired homopolar voltage u_{s0}^* required to obtain a desired homopolar current i_{s0}^* . This block is denoted by “HVC”, which stands for homopolar-voltage calculator.

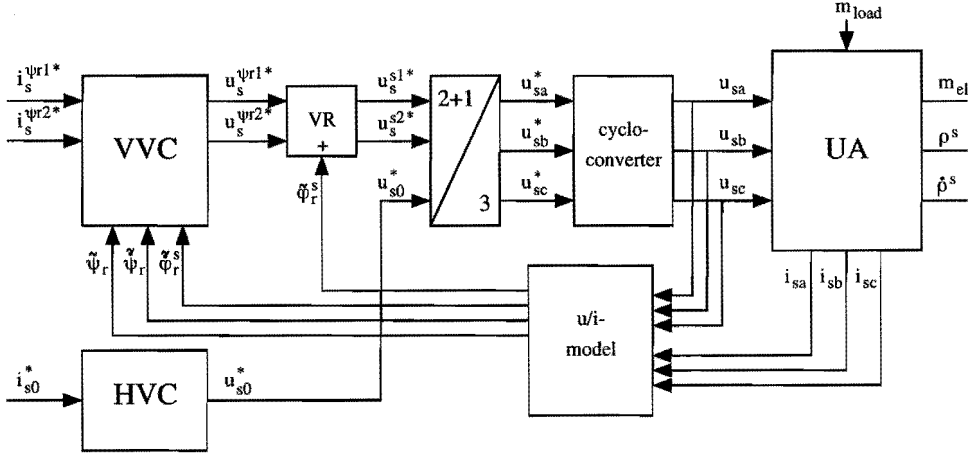


Figure 7.1. Block diagram of a cycloconverter-fed induction machine with the control circuitry required for asymmetrical position-sensorless field-oriented control.

The relation between the homopolar current and the homopolar voltage was derived in section 4.3, and resulted in equation 4.31. The desired value for the homopolar voltage can now be found from equation 7.1. This is the equation that has to be implemented in the “HVC” block.

$$u_{s0}^* = \hat{r}_{s0} \cdot i_{s0}^* + \hat{l}_0 \cdot \frac{di_{s0}^*}{dt} \quad (7.1)$$

For operation of the machine with one of the phase currents equal to zero, in section 6.2 the required value of i_{s0}^* was calculated. Equation 6.8 is repeated here in 7.2. By substitution of this equation into 7.1, equation 7.3 is obtained.

$$i_{s0}^* = k_i^{s1} \cdot i_s^{s1*} + k_i^{s2} \cdot i_s^{s2*} \quad (7.2)$$

$$u_{s0}^* = k_i^{s1} \cdot \left(\hat{r}_{s0} + \hat{l}_0 \cdot \frac{d}{dt} \right) \cdot i_s^{s1*} + k_i^{s2} \cdot \left(\hat{r}_{s0} + \hat{l}_0 \cdot \frac{d}{dt} \right) \cdot i_s^{s2*} \\ + \hat{l}_0 \cdot \left(i_s^{s1*} \cdot \frac{dk_i^{s1}}{dt} + i_s^{s2*} \cdot \frac{dk_i^{s2}}{dt} \right) \quad (7.3)$$

To implement this equation however, it is better to transform it to field-oriented coordinates first – the differentiation of i_s^{s1*} and i_s^{s2*} (which introduces an inaccuracy) is then replaced by a differentiation of $i_s^{\psi r1*}$ and $i_s^{\psi r2*}$, which yields zero in steady state.

The transformation of equation 7.3 to rotor-flux coordinates is done in very much the same way as was done in the transformation of equation 3.1 to 3.19 in section 3.5. The resulting block diagram (shown in figure 7.2) has indeed a great similarity with the block diagram of the VVC shown in figure 3.7. Equation 7.4 is the (partly) transformed equation.

$$\begin{aligned}
 \mathbf{u}_{s0}^* = & \begin{bmatrix} k_i^{s1} \\ k_i^{s2} \end{bmatrix}^T \cdot \left(\mathbf{R}(\varphi_r^s) \cdot \begin{bmatrix} \left(\hat{f}_{s0} + \hat{1}_0 \cdot \frac{d}{dt} \right) \cdot i_s^{\psi r1*} - \hat{\phi}_r^s \cdot \hat{1}_0 \cdot i_s^{\psi r2*} \\ \left(\hat{f}_{s0} + \hat{1}_0 \cdot \frac{d}{dt} \right) \cdot i_s^{\psi r2*} + \hat{\phi}_r^s \cdot \hat{1}_0 \cdot i_s^{\psi r1*} \end{bmatrix} \right) \\
 & + \hat{1}_0 \cdot \left(i_s^{s1*} \cdot \frac{dk_i^{s1}}{dt} + i_s^{s2*} \cdot \frac{dk_i^{s2}}{dt} \right)
 \end{aligned}
 \tag{7.4}$$

A block diagram of this equation, as it was implemented for simulation and control, is shown in figure 7.2. It can easily be combined with figure 7.1, replacing the ‘‘HVC’’ from this figure. It does however require the flux angle and flux frequency from the u/i-model.

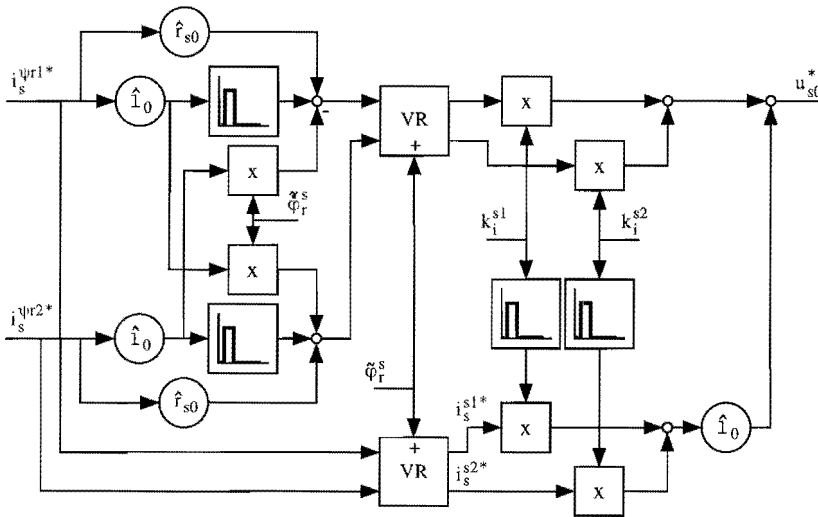


Figure 7.2. Block diagram for the calculation of the desired homopolar voltage, for operation with one of the phase currents equal to zero.

In practice, the differentiators of this block diagram evidently pose a problem. The differentiators, which have the desired stator-current components as their inputs, tend to amplify any noise to unacceptable levels, resulting in an unusable signal for u_{s0}^* . These differentiators must therefore be combined with low-pass filters.

The other two differentiators, corresponding to the second part of equation 7.4, are required during a change of k_i^{s1} or k_i^{s2} . Without these, a change in k_i^{s1} or k_i^{s2} would not

result in an immediate change of i_{s0} . However, if a step change of k_i^{s1} or k_i^{s2} occurs – as is the case when switching from symmetrical three-phase operation to operation with one of the phase currents equal to zero – these differentiators cause a delta peak in u_{s0}^* . Evidently, a step change in the homopolar current can only be achieved by a (purely theoretical) delta pulse of the homopolar voltage.

A practical converter is not able to produce such a voltage pulse, and allowing such a pulse – which will certainly be clipped off somewhere in the process – to the input of the converter is therefore not useful and might even have undesired side effects. This explains that also the differentiators of k_i^{s1} and k_i^{s2} have to be accompanied by low-pass filters. If the bandwidth of the converter is very low – as is the case with the cycloconverter – it might turn out that this part of the block diagram can be omitted completely, without a noticeable effect on the current transients. This depends on the relation between the time constant L_0/r_{s0} of the homopolar circuit and the converter bandwidth.

Finally it should be noted that the homopolar current i_{s0} will only be equal to i_{s0}^* if the parameters \hat{r}_{s0} and \hat{L}_0 are exactly equal to the machine values, and if the converter produces a homopolar voltage u_{s0} exactly equal to u_{s0}^* , without any delay, offset or amplitude error. As this is hard to achieve in practice, the circuit might be completed with a compensation for known converter imperfections – such as the considerable delay of the cycloconverter – and a current control loop to compensate for unpredictable errors. This, however, is true not only for the homopolar current control, but for any open-loop current control of a voltage-fed induction machine.

7.3 Asymmetrical operation of the healthy drive

In the previous section a control system has been described which allows operation of a voltage-fed induction machine while one of the phase currents is zero. This control can be used in case one of the machine phases is physically disconnected from the converter, but it can also be used while the converter, the machine and their interconnections are intact. In that case it should be possible to deliberately make the current in one of the phases zero by selecting the appropriate values for k_i^{s1} and k_i^{s2} . This will be verified by simulations and experiments.

7.3.1 Simulation of the asymmetrically-fed drive

The simulations in this section, but also those in the sections to follow, were performed using a multi-DSP system based on the TMS320C40 processor. A detailed description of this system, as well as of the software developed to perform the simulations, can be found in Appendix A. A shorter description is found in [Bosg-95b]. All simulations performed

in this section were real-time simulations, which made it possible to obtain a good feeling of the functioning of the control system, before it was tested on a real machine. The cycloconverter was however not modeled – in the simulations an ideal converter was assumed. For simulations and control the same DSP system was used.

The induction-machine model used in this and the following sections is basically equal to the one shown previously in figure 5.4. For clarity it has been redrawn in figure 7.3, completed with the missing phase. In this block diagram, the stator currents are calculated from the stator voltages in the three-phase system, which has the advantage that three-phase quantities are directly available, and that faults occurring in one of the three phases are easily modeled. This in contrast with the machine model of figure 4.3, which could also have been used, but does not directly give the three stator-phase currents and is not suited for the simulation of a single-phase current fault (as needed in section 7.5).

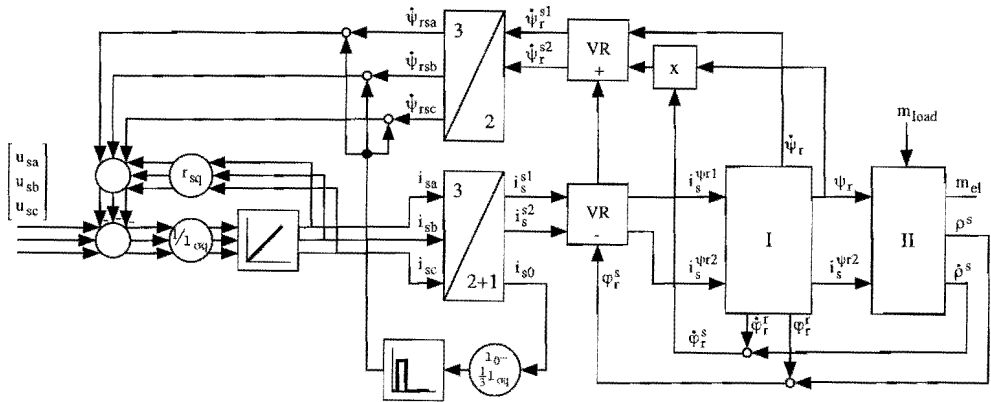


Figure 7.3. Block diagram of a voltage-fed induction machine of which the star point is connected, for simulation with asymmetrical supply and/or open circuits.

There is however one important problem with this machine model. In the simulation method that was used (see Appendix A) an integrator introduces a time delay. Therefore, an integrator followed by a differentiator does not represent a unity transfer function. Such a combination should therefore be avoided. The block diagram shown in figure 7.3 does however contain a differentiator working on i_{s0} , which is the sum of the three phase currents, each of which is the output of an integrator. This will lead to an unnecessary inaccuracy that can be avoided by eliminating the differentiator from the diagram.

The elimination of the differentiator is illustrated by figure 7.4. First, in figure 7.4a, a section of the block diagram given in figure 7.3 is redrawn to show more clearly the series connection of the integrator and the differentiator. In figure 7.4b, the differentiator has been eliminated, resulting in an algebraic loop. This loop can however easily be eliminated. Introducing the auxiliary variables x_q and z_q with $q = a, b, c$, the relation describing the loop is given by equation 7.5.

$$z_q = \frac{1}{1 - \sigma q} \left(x_q - \left(1_0 - \frac{1}{3} 1_{\sigma q} \right) \cdot (z_a + z_b + z_c) \right) \quad (q = a, b, c) \quad (7.5)$$

By eliminating the variables z_a , z_b and z_c from the right side of this equation, the loop is eliminated. The result is given in equation 7.6, as well as in the block diagram of figure 7.4c.

$$z_q = \frac{1}{1 - \sigma q} \left(x_q - \left(\frac{1}{3} - \frac{1}{9} \frac{1_{\sigma q}}{1_0} \right) \cdot (x_a + x_b + x_c) \right) \quad (q = a, b, c) \quad (7.6)$$

Using this block diagram, more accurate results are obtained than with the diagram of figure 7.3. However, using the same block diagram for the simulation of the case when one of the stator phases is disconnected, has clearly become more difficult.

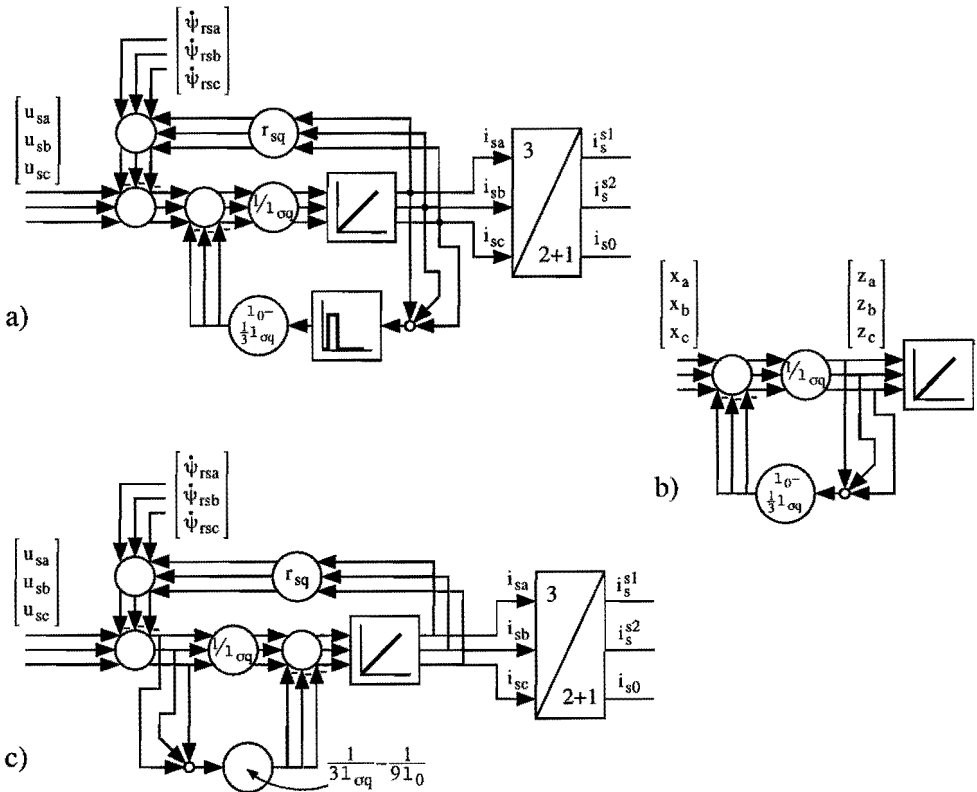


Figure 7.4. Elimination of the differentiator from the block diagram shown in figure 7.3: a) original diagram redrawn; b) intermediate step; c) final situation.

In the simulations shown in figures 7.5 to 7.8, the operation mode is changed from symmetrical three-phase mode to operation with the current in phase a equal to zero. This is done by changing (k_i^{s1}, k_i^{s2}) instantaneously from $(0, 0)$ to $(-2, 0)$, as followed from

equation 6.5. The simulations were performed at a rotor speed of 0.4 pu, while the load torque was constant and in balance with the initial torque delivered by the machine. The machine parameters used in this simulation can be found in Appendix C.2.

Figure 7.5 shows the three stator currents. Initially they have equal amplitudes and a phase difference of $2\pi/3$ rad. The amplitude and phase difference of the remaining two phase currents after i_{sa} has become zero, can be found by substituting $i_{s0} = -2 \cdot i_s \cdot \cos(\hat{\epsilon}_s^s t + \epsilon_{s0}^s)$ in equation 6.2. The result is given in equation 7.7.

$$i_{sa} = 0$$

$$i_{sb} = \frac{2}{3} i_s \cdot \left(\cos(\hat{\epsilon}_s^s t + \epsilon_{s0}^s - \frac{2\pi}{3}) - \cos(\hat{\epsilon}_s^s t + \epsilon_{s0}^s) \right) = \frac{2}{3} i_s \cdot \sqrt{3} \sin(\hat{\epsilon}_s^s t + \epsilon_{s0}^s - \frac{\pi}{3}) \quad (7.7)$$

$$i_{sc} = \frac{2}{3} i_s \cdot \left(\cos(\hat{\epsilon}_s^s t + \epsilon_{s0}^s - \frac{4\pi}{3}) - \cos(\hat{\epsilon}_s^s t + \epsilon_{s0}^s) \right) = \frac{2}{3} i_s \cdot \sqrt{3} \sin(\hat{\epsilon}_s^s t + \epsilon_{s0}^s - \frac{2\pi}{3})$$

This equation shows that the amplitude of the remaining phase currents has risen by a factor $\sqrt{3}$, while the phase difference has become $\pi/3$ rad. This can easily be verified in the simulation.

It can be noted that the current in phase a does not drop to zero immediately at the moment (k_i^{s1}, k_i^{s2}) is changed. This is due to the fact that k_i^{s1} and k_i^{s2} are filtered before being differentiated, thus avoiding a delta pulse in the voltage.

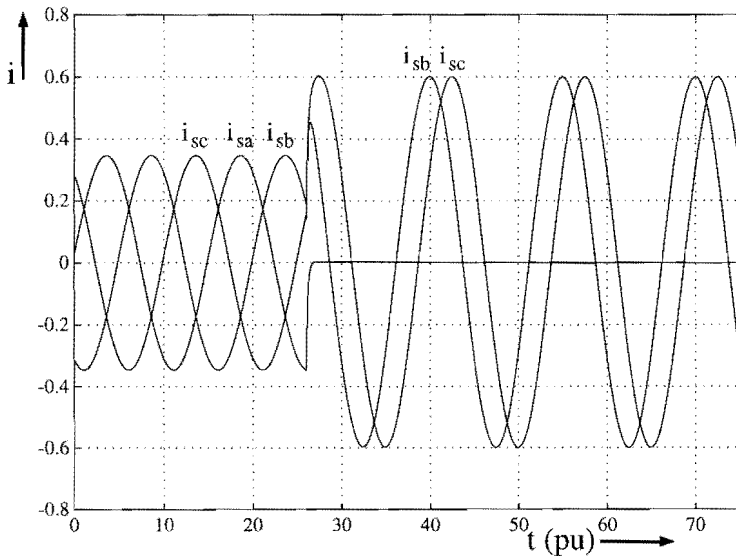


Figure 7.5. Simulation showing the stator currents of a voltage-fed induction machine at a step change of (k_i^{s1}, k_i^{s2}) from $(0,0)$ to $(-2,0)$.

To illustrate the fact that k_i^{s1} and k_i^{s2} can be changed without influencing the field-oriented control – and thus the constant torque and flux level – figure 7.6 shows some quantities that are not affected by the change. The stator-current vector in field-oriented coordinates is and remains a single point, which means that both the magnetizing current and the torque-producing current are constant.

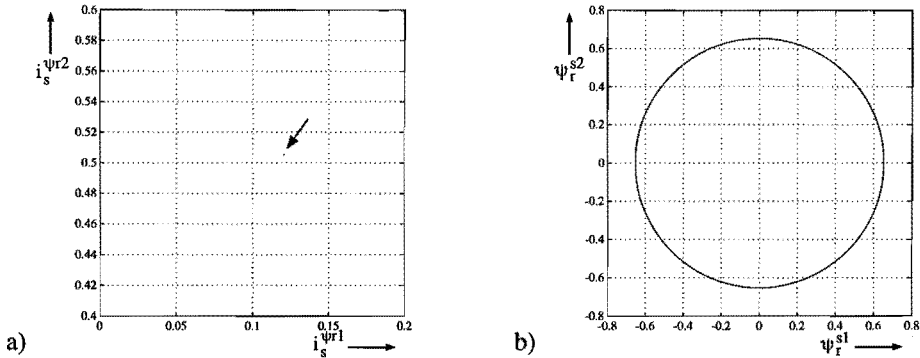


Figure 7.6. Simulations showing quantities in a voltage-fed induction machine that are not affected by a step change of (k_i^{s1}, k_i^{s2}) : a) the stator-current vector; b) the rotor-flux vector.

The stator voltages are not altered considerably by the change in (k_i^{s1}, k_i^{s2}) , as can be seen in figure 7.7. This was to be expected, because the voltages consist mainly of the voltages induced by the (unchanged) rotor flux. Yet this small change is enough to produce the very important change in the currents. The spikes on the voltages at the moment (k_i^{s1}, k_i^{s2}) is changed are due to the differentiators, and are required to achieve a rapid change of the currents.

To examine the influence of the differentiators of k_i^{s1} and k_i^{s2} , a simulation was performed in which these were omitted. In that case, at a step change of (k_i^{s1}, k_i^{s2}) , the voltages do not contain any spikes – they make a step change from one steady state to another. The resulting currents are shown in figure 7.8. Instead of changing (almost) instantaneously from one steady state to another as in figure 7.5, the currents now exhibit a transient. From figure 7.8 the time constant of this transient can be determined, which is found to correspond to the value of l_0/r_{s0} , as expected from equation 4.31.

In the experimental setup, the time constant l_0/r_{s0} is smaller, due to the fact that the internal resistance of the cycloconverter has to be added to the resistance of the machine. This particular cycloconverter has a very high internal resistance, resulting in a decay to zero of the current in little more than one half of a period (at a speed of 0.4 pu). Therefore in this setup the differentiators could have been omitted.

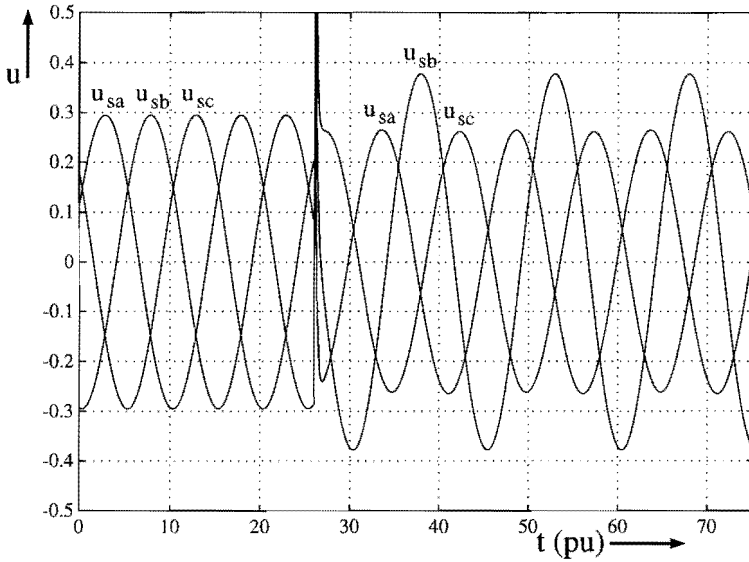


Figure 7.7. Simulation showing the stator voltages supplied to a voltage-fed induction machine at a step change of (k_i^{s1}, k_i^{s2}) from $(0,0)$ to $(-2,0)$.

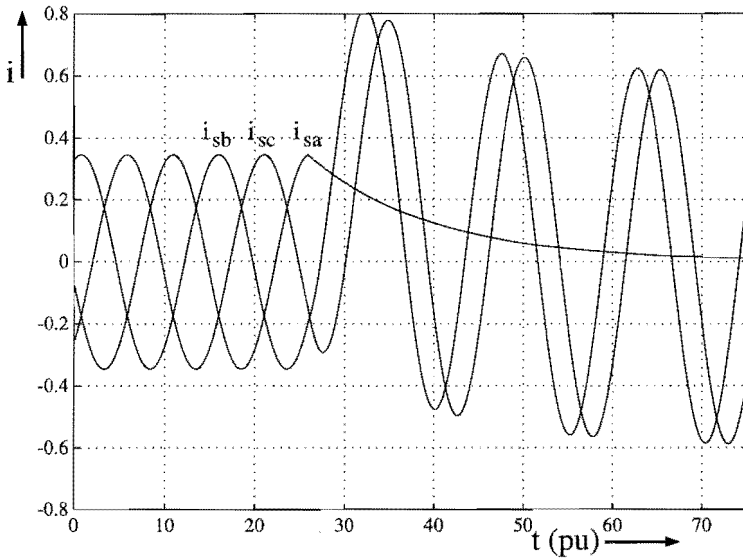


Figure 7.8. Simulation showing the stator currents in a voltage-fed induction machine at a step change of (k_i^{s1}, k_i^{s2}) from $(0,0)$ to $(-2,0)$, when differentiation of k_i^{s1} and k_i^{s2} is omitted.

7.3.2 Experimental results with the asymmetrically-fed drive

Exactly the same control system that was used with the machine model for the simulations described above, was also implemented to control a cycloconverter-fed induction machine. A major difference however between the simulations and the experimental results is related to the switching behavior of the converter, and the imperfections in its control. The switching character of the voltages causes an important near-300 Hz component in the stator currents and, as a consequence, a 300 Hz component in the torque, so that these waveforms had to be filtered before being displayed. This was performed in real time by the DSP system, on which also an FFT algorithm was implemented to study the spectrum of different signals at the same time. The imperfections in the cycloconverter control system caused small asymmetries in the voltages, as well as offset and amplitude errors. Unfortunately these imperfections are very visible in the currents, and could only partly be eliminated by careful adjustments.

To get an impression of what an unfiltered current looks like, figure 7.9 shows i_{sa} while applying a step change of (k_i^{s1}, k_i^{s2}) from (0,0) to (-2,0), as in the simulations. Clearly, this current does not become zero here. This is due to the fact that the control system was designed only to work with ideal voltage sources – evidently it can not influence the switching harmonics introduced by the converter. To examine more closely the effect of the control on the fundamental current component, the frequency spectrum of i_{sa} has to be calculated before and after the change of (k_i^{s1}, k_i^{s2}) . This is done in figure 7.10a and b, respectively. The fundamental frequency of the current was 0.4 pu, corresponding to 20 Hz.

From figure 7.10a it becomes clear that under normal conditions stator current i_{sa} contains, apart from a component at the fundamental frequency, also two components near to 300 Hz, caused by the switching behavior of the cycloconverter. More information on cycloconverter-generated harmonics can be found in [Pell-71].

After the step change of (k_i^{s1}, k_i^{s2}) , according to figure 7.10b, the fundamental component of the current is reduced to almost zero. That it is not completely zero can be explained by the imperfections of the control system, such as errors in the parameter estimation and delays, offsets and amplitude errors in the cycloconverter control. This explains also the relatively small components at other frequencies, both before and after the change of (k_i^{s1}, k_i^{s2}) . However, a remarkable difference between the symmetrical and the asymmetrical case is the apparition of a third harmonic in the current in the asymmetrical case. A third harmonic in the current, while no third harmonic is present in the voltage, is usually related to saturation effects. That this is actually the case here has been confirmed by measurements of the rotor flux, which are shown later, while the reason for this saturation will be explained in the next section.

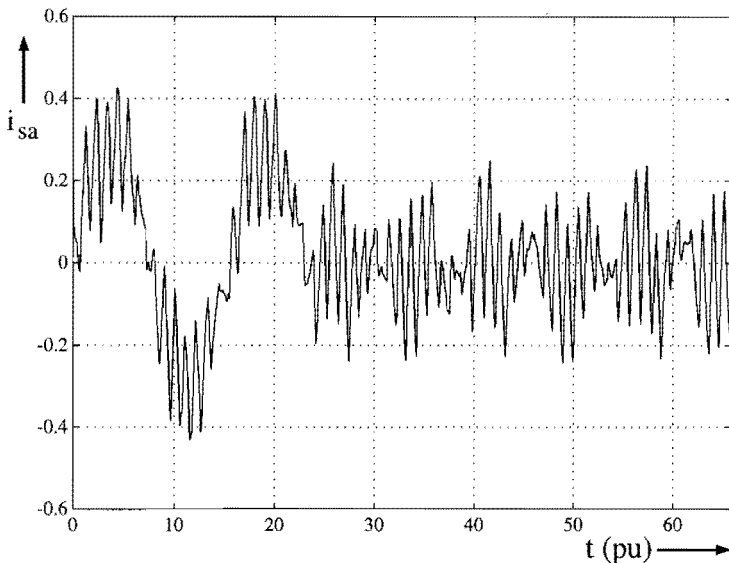


Figure 7.9. The stator current i_{sa} of the cycloconverter-fed induction machine in case of a step change of (k_i^{s1}, k_i^{s2}) from $(0,0)$ to $(-2,0)$.

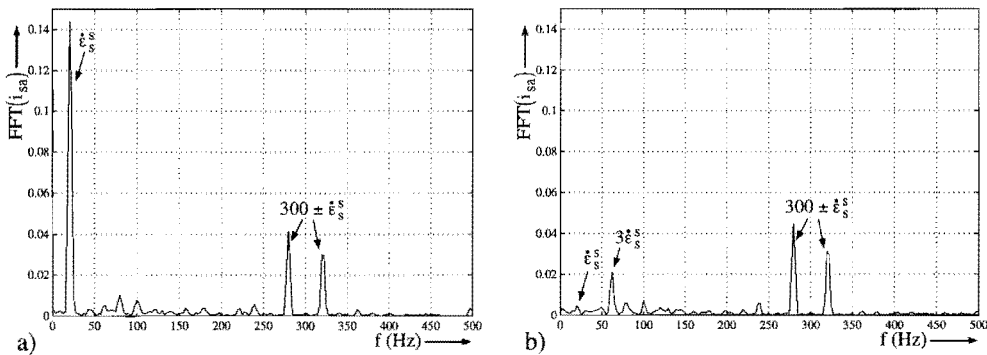


Figure 7.10. The frequency spectrum of stator current i_{sa} of the cycloconverter-fed induction machine for (k_i^{s1}, k_i^{s2}) equal to $(0,0)$ (a) and $(-2,0)$ (b).

A clear view of the current waveforms is obtained if frequencies above 250 Hz are removed using a low-pass filter. The three filtered stator phase currents $\overline{i_{sa}}$, $\overline{i_{sb}}$ and $\overline{i_{sc}}$ are shown in figure 7.11. This figure shows that, before as well as after the change of (k_i^{s1}, k_i^{s2}) , the currents do not have perfectly sinusoidal and identical waveforms, unfortunately.

The third harmonic found in the spectrum shown in figure 7.10b is now clearly visible also in this figure, in the trace of $\overline{i_{sa}}$.

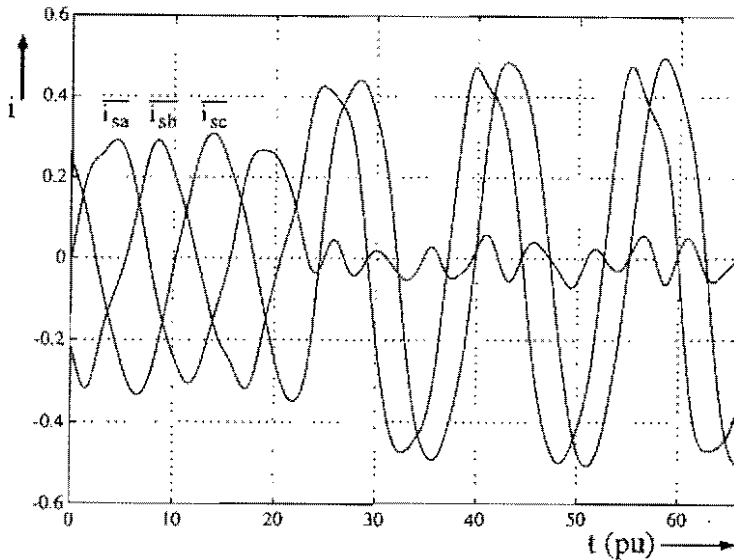


Figure 7.11. Low-pass filtered stator currents of the cycloconverter-fed induction machine in case of a step change of (k_i^{s1}, k_i^{s2}) from $(0,0)$ to $(-2,0)$.

The rotor-flux vector was expected not to change in case of a change of (k_i^{s1}, k_i^{s2}) , as shown also in the simulations in figure 7.6b. In the real machine however, as shown in figure 7.12b, the flux does change. Due to the limited measurement-time interval, this figure does not show the full transient of the flux, however. In case of asymmetrical supply, the steady-state flux is around 15 percent lower than with the symmetrical supply, although the field-oriented stator-current components did not change (shown in figure 7.12a). This indicates that in case of asymmetrical supply the main inductance is lower, which can only be due to saturation. If the flux level under symmetrical operation is chosen closer to 1 pu, instead of the relatively low value of approximately 0.6 pu, the decrease of the flux in asymmetrical operation is even larger.

This plot of the rotor-flux vector also shows an imperfection of the u/i -model that was used to determine the flux. Probably due to some measurement errors, the flux circle is not exactly centered at the origin. As explained in [Burgt-96], this could be corrected by increasing some feedback coefficients in the u/i -model. However, this would make the u/i -model less sensitive to real variations in the flux, and is therefore not applied here. No further attention is paid to this problem.

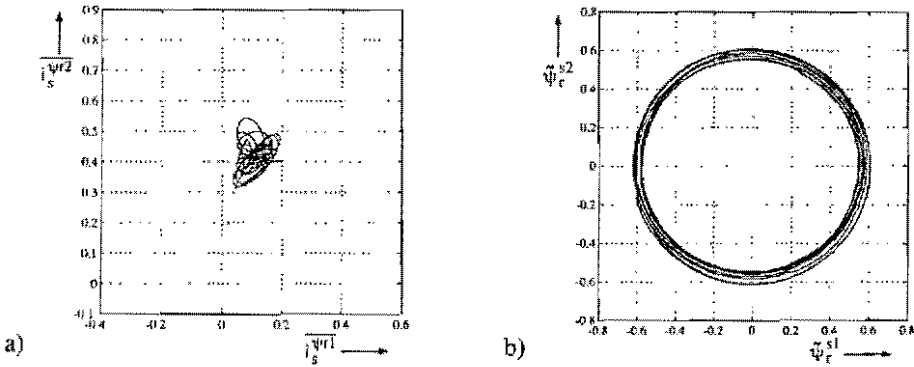


Figure 7.12. The low-pass filtered field-oriented stator-current vector of the cycloconverter-fed induction machine in case of a step change of (k_i^{s1}, k_i^{s2}) from $(0,0)$ to $(-2,0)$ (a) and the rotor-flux vector (b) (shown for a time interval twice as long as used for the other figures).

Finally, it is interesting to examine the effects of saturation and harmonic components of the stator current on the torque. Figure 7.13a shows a filtered version of the torque, which was calculated from the measured stator current and the observed rotor flux according to equation 3.6. Figure 7.13b shows the frequency spectrum of this torque during asymmetrical operation. During symmetrical operation some disturbance can already be noticed in the torque, mainly at a frequency of $2\hat{\epsilon}_s^s$ (due to an asymmetry in the converter control) and at exactly 300 Hz. After the change of (k_i^{s1}, k_i^{s2}) , torque components at $2\hat{\epsilon}_s^s$ and $4\hat{\epsilon}_s^s$ become clearly visible in both figures, while the spectrum analysis reveals that also components at $300 \text{ Hz} \pm 2\hat{\epsilon}_s^s$ and $300 \text{ Hz} \pm 4\hat{\epsilon}_s^s$ are present. All of these are a consequence of the third harmonic of the stator current.

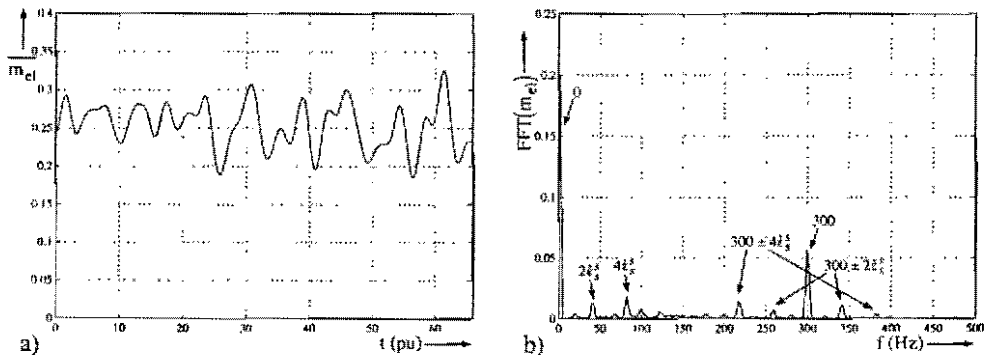


Figure 7.13. The torque of the cycloconverter-fed induction machine in case of a step change of (k_i^{s1}, k_i^{s2}) from $(0,0)$ to $(-2,0)$ (low-pass filtered) (a), and its frequency spectrum after the step change (b).

The decrease of the rotor flux causes also the torque to decrease proportionally. Due to the fact that the flux decreases only rather slowly, this is not very apparent in figure 7.13a yet, but it would be if the torque were measured over a longer period of time. If no correcting measures are taken and the load torque remains the same, the machine will therefore start slowing down. This can be corrected by a torque or speed controller, which will increase the torque-producing current component.

7.4 Why asymmetrical operation causes a high saturation level

The fact that asymmetrical operation of the induction machine can cause saturation, is not something that seems logical at first sight, if one considers sinusoidally distributed windings only. After all, during asymmetrical operation the field-oriented current components were maintained at the same level as during symmetrical operation, so the fundamental component (in space) of the air-gap induction must be the same for both cases.

One explanation might be found in the higher currents in two of the phases (see figure 7.5). Evidently these currents, which are $\sqrt{3}$ times as high as in symmetrical operation, can cause saturation of the stator-slot leakage fluxes. However, this does not yet explain the saturation of the main flux. To find an explanation, it is necessary to examine the air-gap induction under symmetrical and asymmetrical conditions.

In section 2.3.3, figure 2.7, the MMF (proportional to the air-gap induction) has been calculated for a machine with a 24-slot, double-layer stator winding under symmetrical supply while the rotor currents are zero (no-load condition). In section 4.2, figure 4.2, the MMF in the same machine was shown for supply with a homopolar current, also with the rotor currents equal to zero. Now these figures will be combined and extended for the case of asymmetrical supply (operation with one of the phase currents equal to zero) under no-load and full-load conditions.

First, the rotor current in each rotor slot will have to be calculated, to obtain the MMF caused by these rotor currents. It will be assumed that the rotor position ρ^s is zero, and that the rotor winding configuration is exactly the same as the stator's. According to figure 3.4, for steady-state operation ($\dot{\psi}_r = 0$) the field-oriented rotor-current components can be written as in equation 7.8. The rotor currents in stator coordinates are then given by equation 7.9.

$$\begin{bmatrix} i_r^{\psi r1} \\ i_r^{\psi r2} \end{bmatrix} = \begin{bmatrix} 0 \\ -i_s^{\psi r2} \end{bmatrix} \quad (7.8)$$

$$\begin{bmatrix} i_r^{s1} \\ i_r^{s2} \end{bmatrix} = R(\varphi_r^s) \cdot \begin{bmatrix} i_r^{\psi r1} \\ i_r^{\psi r2} \end{bmatrix} = \begin{bmatrix} i_s^{\psi r2} \cdot \sin(\varphi_r^s) \\ -i_s^{\psi r2} \cdot \cos(\varphi_r^s) \end{bmatrix} \quad (7.9)$$

According to figure 7.14 the angle φ_r^s can also be found from the field-oriented current components, assuming that at the moment under consideration the angle ε_s^s is equal to zero. The result is given in equation 7.10.

$$\varphi_r^s = -\varepsilon_s^{\psi r} = -\text{atan}(i_s^{\psi r2} / i_s^{\psi r1}) \quad (7.10)$$

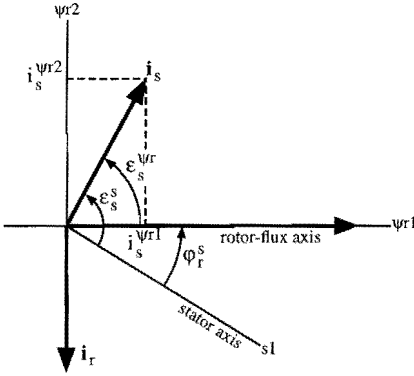


Figure 7.14. Stator- and rotor-current vectors in different reference frames.

The current in each individual rotor slot can now be found by calculating the currents in the three rotor windings and considering the winding configuration. As no homopolar rotor current will be present (see section 4.3) the current transformation of equation 7.11 will be used for this, which is equal to the transformation given in equation 4.6 without the homopolar component.

$$\begin{bmatrix} i_{ra} \\ i_{rb} \\ i_{rc} \end{bmatrix} = \begin{bmatrix} \frac{2}{3} & 0 \\ -\frac{1}{3} & \frac{1}{\sqrt{3}} \\ -\frac{1}{3} & \frac{1}{\sqrt{3}} \end{bmatrix} \cdot \begin{bmatrix} i_r^{s1} \\ i_r^{s2} \end{bmatrix} \quad (7.11)$$

The relation between the field-oriented stator-current components, the homopolar stator current and the individual stator currents, needed to calculate the current in each stator slot, is given in equation 7.12, in which again φ_r^s from equation 7.10 can be substituted.

$$\begin{bmatrix} i_{sa} \\ i_{sb} \\ i_{sc} \end{bmatrix} = \begin{bmatrix} \frac{2}{3} & 0 & \frac{1}{3} \\ -\frac{1}{3} & \frac{1}{\sqrt{3}} & \frac{1}{3} \\ -\frac{1}{3} & -\frac{1}{\sqrt{3}} & \frac{1}{3} \end{bmatrix} \cdot \begin{bmatrix} i_s^{s1} \\ i_s^{s2} \\ i_{s0} \end{bmatrix} = \begin{bmatrix} \frac{2}{3} & 0 & \frac{1}{3} \\ -\frac{1}{3} & \frac{1}{\sqrt{3}} & \frac{1}{3} \\ -\frac{1}{3} & -\frac{1}{\sqrt{3}} & \frac{1}{3} \end{bmatrix} \cdot \begin{bmatrix} i_s^{\psi r1} \cdot \cos(\varphi_r^s) - i_s^{\psi r2} \cdot \sin(\varphi_r^s) \\ i_s^{\psi r1} \cdot \sin(\varphi_r^s) + i_s^{\psi r2} \cdot \cos(\varphi_r^s) \\ i_{s0} \end{bmatrix} \quad (7.12)$$

Now that the individual stator and rotor currents are known, the MMF caused by the stator currents, the rotor currents and by all currents together can be calculated in the same way as in section 2.3.3. In figure 7.15 this is done for the case when the torque-producing current component $i_s^{\psi r^2}$ is zero. The rotor currents will then also be zero. The magnetizing current component was taken equal to $1/3$, which in case of a main inductance 1 equal to 3 corresponds to a rated rotor flux. In figure 7.15a the homopolar stator current is zero, while in 7.15b it was chosen in such a way that asymmetrical operation with $i_{sa} = 0$ resulted. These figures show that in case of asymmetrical operation, the peak value of the total MMF is a factor of 1.4 larger than in the symmetrical case.

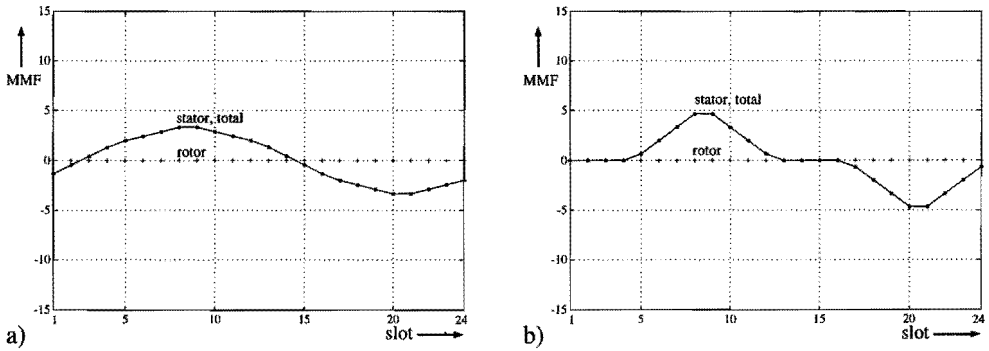


Figure 7.15. Calculated stator, rotor and total MMF in a no-load condition for symmetrical supply (a) and asymmetrical supply with one of the phase currents equal to zero (b).

In figure 7.16 the MMFs are shown for the case when $i_s^{\psi r^2} = 1$, which corresponds to a rated load. As expected, under symmetrical operation the total MMF is the same as in the no-load case – the magnetizing current component was not changed. However, under asymmetrical operation the total MMF is now far from sinusoidal and has a peak value 2.0 times higher than in the symmetrical case.

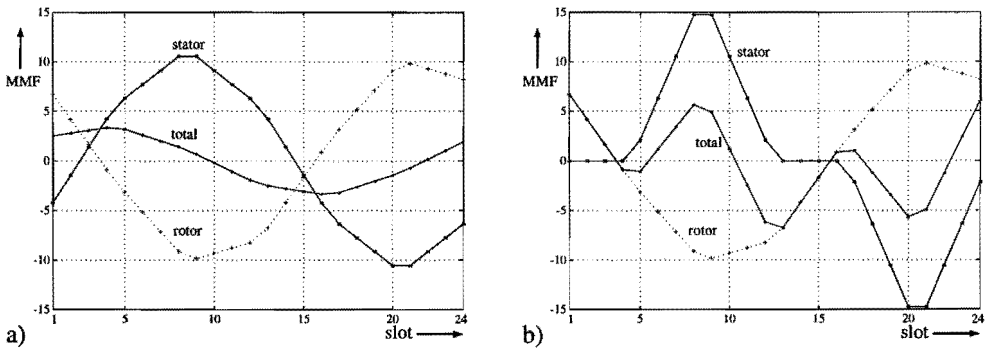


Figure 7.16. Calculated stator, rotor and total MMF in a rated-load condition for symmetrical (a) and asymmetrical supply with one of the phase currents equal to zero (b).

These very high peak values of the air-gap MMF can cause saturation at different locations in the machine. If no saturation were present, the magnetic induction in the stator and rotor teeth would be proportional to the total MMF shown in figures 7.15 and 7.16. Considering the high peak values, saturation in these teeth can be expected under asymmetrical operation. Whether or not saturation will also occur in the stator or rotor yoke, can be understood from a simplified calculation of the yoke flux. In case no saturation is present, the yoke flux is proportional to the integral of the air-gap MMF.

For the cases shown in figures 7.15 and 7.16 this integral has been calculated, as shown in figure 7.17. In a no-load condition, no saturation of the yoke is expected, because the integral of the MMF under asymmetrical operation has a peak value that is 14% lower than under symmetrical operation. Under rated load however, the peak value is 44% higher for asymmetrical than for symmetrical supply, so that saturation will almost certainly occur.

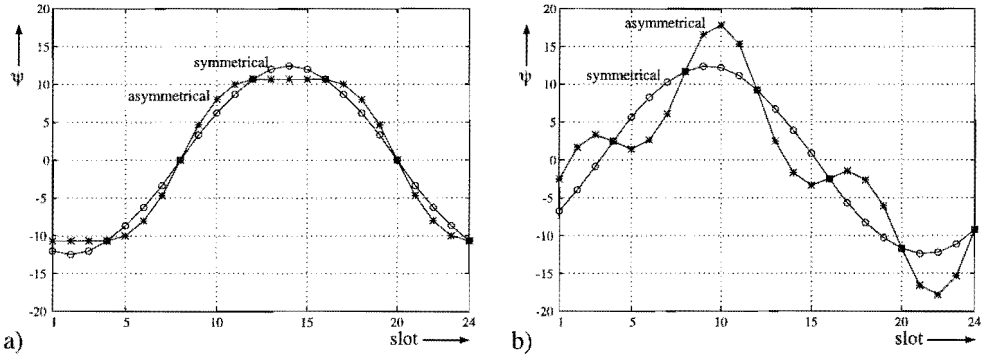


Figure 7.17. Calculation of the yoke flux for symmetrical and asymmetrical supply, under the assumption that no saturation is present, in a no-load condition (a) and under rated load (b).

For the machine used in the experiments, the situation is even worse than for the machine with the 24-slot double-layer windings used for the above calculations. Table 7.1 shows the increase factor of the MMF for both the 24-slot machine and a machine which has 36 stator slots and single-layer windings. The 36-slot configuration calculated does not yet correspond exactly to the machine used in the experiments, which has only 30 rotor slots. It is however clear that under rated load, and even at one half of the rated load, the peak value of the MMF reaches very high values.

Table 7.1. The increase factor of the peak value of the total MMF under asymmetrical operation compared to symmetrical operation for different configurations and loads.

Configuration	Zero load	Rated load	Half load
24 slots, double layer	1.4	2.0	
36 slots, single layer	1.5	3.5	2.0

To explain in detail or even compensate for the saturation observed in the experimental results of section 7.3, the machine model should be extended with saturation. In particular such a model should take in consideration the effects of the third harmonic in the total MMF, which is not the case in most studies on saturation found in literature. The elaboration of such a model however goes beyond the objective of this thesis.

For practical situations, the decrease of the rotor flux caused by the saturation can be compensated, using a controller that acts on the magnetizing current component. It should however be noted, that in this way the copper losses as well as the iron losses will increase further, and depending on the load and the dimensioning of the machine this could cause a problem if this kind of operation were maintained for a long period of time.

7.5 Asymmetrical operation in case of a single-phase current fault

In section 7.3 (the fundamental component of) one of the phase currents was made zero by imposing an appropriate homopolar voltage, resulting in asymmetrical operation during which the magnetizing and torque-producing stator-current components remain at their desired constant level. This section will examine operation of the machine in case one of the phase currents is forced to zero by an external cause, such as an open switch or a blown fuse. Using simulations and experiments, the effect on machine operation will be shown first in case no corrective measures are taken, and then while the same control method as used in section 7.3 is applied.

7.5.1 Simulations of a single-phase open circuit without fault correction

For the simulations and experiments of a single-phase open circuit in case no fault correction is applied, two different control situations will have to be considered. In the first case an open-loop voltage/frequency control is used. The amplitude, phase and frequency of the voltages applied to the remaining two healthy phases will be the same as if no fault had occurred, because no feedback of any machine quantity is present. A completely different situation occurs if a position-sensorless direct field-oriented control as shown in figure 7.1 is used. The u/i -model used in this setup represents a feedback

from the machine to the control system, and it will be interesting to notice whether this feedback improves the behavior in case of this fault.

Voltage/frequency – or u/f – control, as shown in figure 3.1, is based on the fact that the stator voltage is almost proportional to the rotor flux multiplied by the rotor-flux frequency. This can easily be understood from equation 5.13, rewritten here in equation 7.13.

$$u_{sa} = r_{sq} \cdot i_{sa} + l_{\sigma q} \cdot \frac{di_{sa}}{dt} + \frac{d\psi_{rsa}}{dt} + \left(1_0 - \frac{1}{3}1_{\sigma q}\right) \cdot \frac{di_{s0}}{dt} \quad (7.13)$$

Normally, the stator-resistance term can be neglected, the homopolar current will be zero in symmetrical operation, and hence the term containing the leakage inductance is the only difference between the stator voltage and the flux derivative. However, also this term is relatively small. Therefore it is mainly the rotor flux that determines the stator voltage, or, in case the winding is voltage-fed, it is mainly the stator voltage that determines the rotor flux.

What does this mean for a u/f -controlled machine of which one of the phases becomes disconnected? If a phase is disconnected, the corresponding phase current is zero, and except for a voltage caused by a homopolar current, the phase voltage will again be equal to the derivative of the linked rotor flux. This means that initially – before the rotor flux could have reacted to a change in the supply – this stator voltage will differ only slightly from its value under normal operation, and that this difference will be larger if the pre-fault stator current was larger. While none of the stator voltages is changed considerably, it can be expected that also in steady state the rotor flux will not be seriously affected by this fault, especially not in a zero load condition. This is indeed confirmed by the simulations (see figure 7.18).

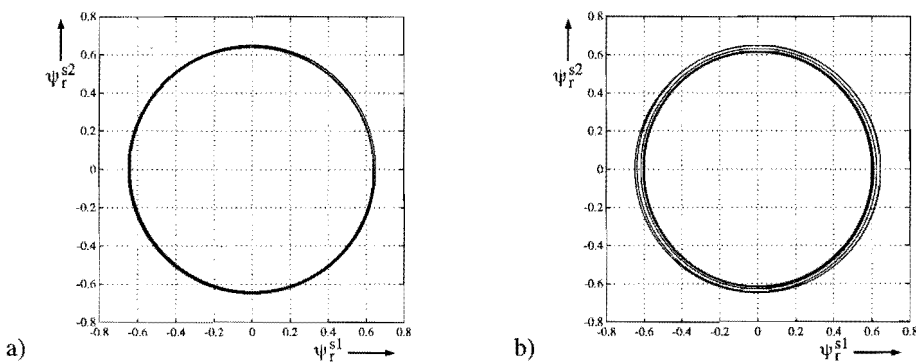


Figure 7.18. Simulation showing the rotor-flux vector of a u/f -controlled induction machine in case one phase is disconnected, under a no-load condition (a) and with a pre-fault torque-producing current of 0.5 (b).

It should be noted that for the simulations shown here not a true u/f -control was used. Instead, at the beginning of each simulation the voltage and frequency were adjusted manually to obtain the same initial flux level (0.65 pu) and rotor speed (0.40 pu) for both the no-load and load cases. During the simulation the voltage and frequency were kept constant.

While the flux level remains approximately the same, necessarily the average magnetizing current will also remain the same. The asymmetry however causes oscillations in this current component with twice the frequency of the stator current. The same oscillation is found in the torque producing current component (see also section 6.4.2 and figure 6.5). The average value of this current will also be approximately the same as before the fault, because with this type of control the machine will adjust itself in such a way that the average torque is always equal to the average load torque. The field-oriented current components are shown in figure 7.19. It should be noted that in case of a loaded machine, the ripple in the torque producing current, and therefore also in the torque, is extremely large and has a frequency equal to twice the supply frequency. Without any fault correction, this system thus shows a very degraded performance. Furthermore, the maximum torque delivered for a given supply voltage and frequency (the pull-out torque) is much lower in this case than under normal operation. This will be discussed in detail in section 7.6.1, because this effect is much more serious in case of a two-phase open circuit, where it can easily cause the machine to pull-out.

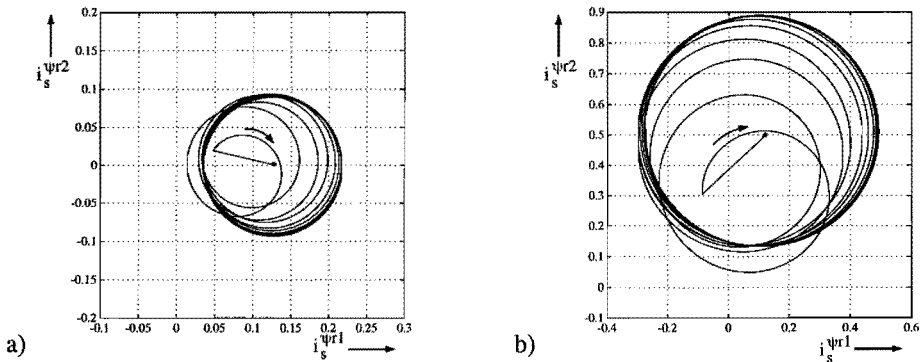


Figure 7.19. Simulation showing the stator-current vector of a u/f -controlled induction machine in case one phase is disconnected, under a no-load condition (a) and with a pre-fault torque-producing current of 0.5 (b).

While the same average values for the field-oriented current components are maintained although one of the phase currents is zero, the currents in the remaining phases must increase. That this is actually the case can be seen in figure 7.20.

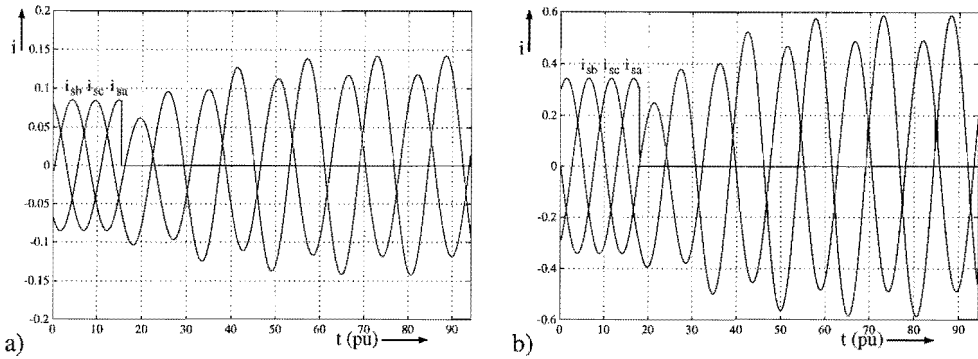


Figure 7.20. Simulation showing the stator currents of a u/f-controlled induction machine in case one phase is disconnected, under a no-load condition (a) and with a pre-fault torque-producing current of 0.5 (b).

A completely different situation occurs if the u/f-control is replaced by a position-sensorless direct field-oriented control system. In this case the applied voltages are calculated by a rotation and a two-to-three-phase transformation from the desired voltages in flux coordinates as given in equation 7.14 (cf. equation 3.19 and figure 3.7). As long as no correction is applied, the desired homopolar voltage is zero.

$$\begin{aligned} u_s^{\psi r1*} &= r_s \cdot i_s^{\psi r1*} - \perp_{\sigma} \cdot \overset{\alpha}{\Phi}_r^s \cdot i_s^{\psi r2*} + \perp_{\sigma} \cdot \dot{i}_s^{\psi r1*} + \overset{\alpha}{\Psi}_r \\ u_s^{\psi r2*} &= r_s \cdot i_s^{\psi r2*} + \perp_{\sigma} \cdot \overset{\alpha}{\Phi}_r^s \cdot i_s^{\psi r1*} + \perp_{\sigma} \cdot \dot{i}_s^{\psi r2*} + \overset{\alpha}{\Phi}_r^s \cdot \tilde{\Psi}_r \end{aligned} \quad (7.14)$$

The largest term in these equations is $\overset{\alpha}{\Phi}_r^s \cdot \tilde{\Psi}_r$, calculated by the u/i-model. If the stator resistance and the leakage inductance are neglected, this means that the desired voltages will be proportional to the actual rotor flux times the actual rotor-flux speed. If, during normal operation, this value decreases, for example due to a change of the speed, the voltages will be adapted instantaneously, resulting in a constant value of the magnetizing and torque-producing current components.

Also in a fault situation this feedback is present. If, due to a missing phase current, the flux decreases slightly (as was the case in the previous simulations), this will result in a decrease in the desired voltages, and thus in a decrease of the voltage applied to the two remaining phases. As a result, the current in the remaining two phases will remain approximately the same in amplitude and phase with respect to the flux vector as before the fault. But while one of the three phase currents is missing, this means that in a first approximation the average magnetizing current component will be reduced by one third, and so will the average torque producing component. This causes a reduction of the flux level, and a considerable reduction of the torque. Evidently, the field-oriented current components will – as with the u/f-control – contain an oscillation at twice the supply frequency.

Figure 7.21 shows the rotor-flux vector in this case. Due to the limited time interval, these figures do not show the complete transient of the flux. The final value of ψ_r was 0.36 pu for the no-load case, which is a reduction by 45%. For the case with a non-zero load it is more difficult to give a final flux value, because if the load torque is maintained at a constant level, the speed of the machine will decrease rapidly due to the reduction of the delivered torque. At a lower speed, the final flux was found to be lower than if the speed was maintained constant by reducing the load torque. In the latter case a value of 0.31 pu was found.

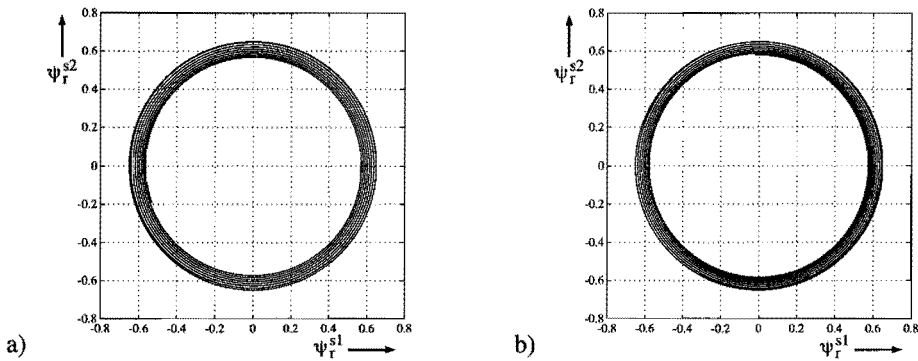


Figure 7.21. Simulation showing the rotor-flux vector of a field-oriented controlled induction machine in case one phase is disconnected, under a no-load condition (a) and with a pre-fault torque-producing current of 0.5 (b).

The field-oriented stator-current vector is shown in figure 7.22. As in the u/f-controlled case, in steady state the current describes an almost circular path. However, in that case the initial value was the middle point of this circle, due to the almost constant voltage. Here the middle point is at approximately two thirds of the initial magnetizing and torque producing current, as the field-oriented control tries to maintain the same current but is unaware of the fact that one third of the current supply is missing. Evidently this could be compensated for by adding a controller, acting on the average values of the magnetizing and torque producing currents.

The individual stator currents are shown in figure 7.23. Comparing this figure with figure 7.20 shows the main difference between the two control methods. In the u/f-controlled machine, the currents in the remaining phases increase to compensate for the loss, while in the field-oriented controlled machine the currents decrease. This decrease depends among others on the homopolar inductance: if the term $(1_0 - 1/3 l_{\sigma q})$ in equation 7.13 were zero, only a very slight decrease would occur, as was confirmed by simulations (not shown here).

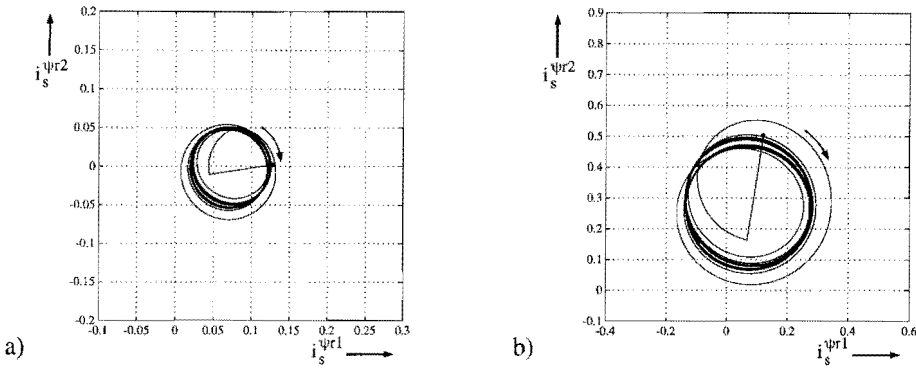


Figure 7.22. Simulation showing the stator-current vector of a field-oriented controlled induction machine in case one phase is disconnected, under a no-load condition (a) and with a pre-fault torque-producing current of 0.5 (b).

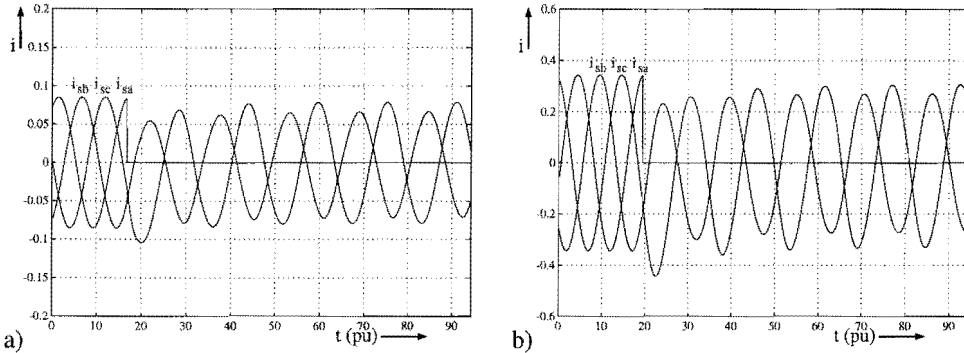


Figure 7.23. Simulation showing the stator currents of a field-oriented controlled induction machine in case one phase is disconnected, under a no-load condition (a) and with a pre-fault torque-producing current of 0.5 (b).

One remark has to be made at this point in relation to the u/i-model. In the situation studied here, the flux is no longer constant, and in fact deviates considerably from its desired value. The feedback parameters used to stabilize the u/i-model (see figure 3.8) however tend to maintain the model flux constant (parameter S2) and equal to its desired value (parameter S3). As a result, the flux calculated by the u/i-model will not always be equal to the flux in the machine.

An interesting phenomenon occurs in relation to parameter S3. A non-zero value of this parameter will try to keep the observed flux close to its desired value. As a consequence, the voltage applied to the machine during this fault situation will be higher than if S3 were zero. As a result, also the real flux in the machine will be higher, and in fact no difference between the machine flux and the observed flux was visible. This means that

parameter $S3$ has a positive influence on the behavior of the system: a higher value will result in a higher flux during the fault.

However, to study the system without having to take into account the value of $S3$, this parameter was taken zero during all simulations and experiments. To observe correctly all dynamic changes of the flux, it would be necessary to make also $S2$ equal to zero, but without any feedback the u/i-model is unusable. As a compromise, a small value was used in the simulations as well as in the experiments: $S2 = 0.05$. The influence of the u/i-model on the behavior of the system is in this way relatively small, and has not been studied in detail.

7.5.2 Experiments of a single-phase open circuit without fault correction

For these experiments one of the phases of the experimental machine was disconnected. For practical reasons, this was not done in all cases during the measurements, but beforehand. As in the simulations, first a u/f-control was implemented, in which both the voltage and the frequency could be adjusted, and then the field-oriented control of figure 7.1 was applied.

In the first experiments, the voltage and frequency during asymmetrical operation were adjusted in such a way that a flux level of 0.62 pu and a rotor speed of approximately 0.4 pu were obtained, both in a no-load condition, and in case of a load resulting in an average torque producing current of approximately 0.45 pu. The (filtered) field-oriented stator-current vectors for these cases are shown in figure 7.24. Especially in the no-load case, the shape differs from the circle found in the simulations (cf. figure 7.19). The fact that the current shape is not the same for each period is caused by the cycloconverter output voltage. This voltage is in general not the same in each period of the current, unless the period of the current is an exact multiple of 1/300 second, which is the converter's switching period. Purposely, an operation speed was chosen for which the period differed considerably from such a value. In case the machine is loaded, the current trajectory becomes more similar to that of the simulations, because at higher current levels the distortion caused by the converter becomes less important.

The individual phase currents are shown in figure 7.25. Also here the distortion of the current is very noticeable, especially at low current values. Apart from these distortions, the system behaves in the way that was expected from the simulations. The remaining currents, and especially i_{sc} , are much higher than they would be under symmetrical operation with the same average flux and torque level, but their amplitude and phase are not such that constant field-oriented current components are obtained.

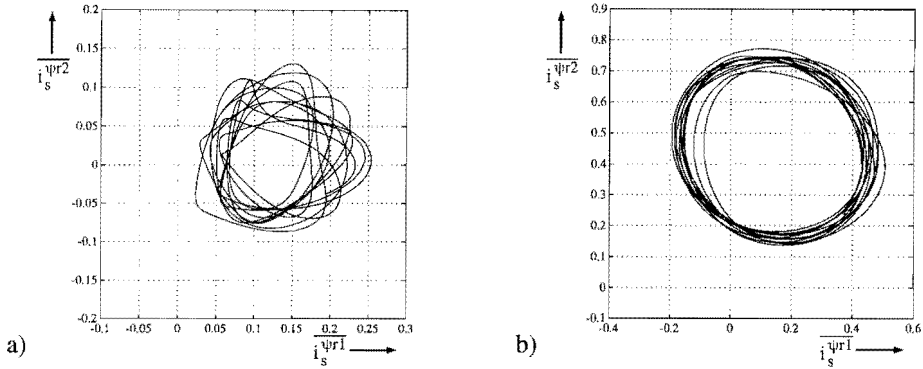


Figure 7.24. The low-pass filtered field-oriented stator-current vector of the *u/f*-controlled cycloconverter-fed induction machine of which one phase has been disconnected, under a no-load condition (a) and with an average torque-producing current component of approximately 0.45 pu (b).

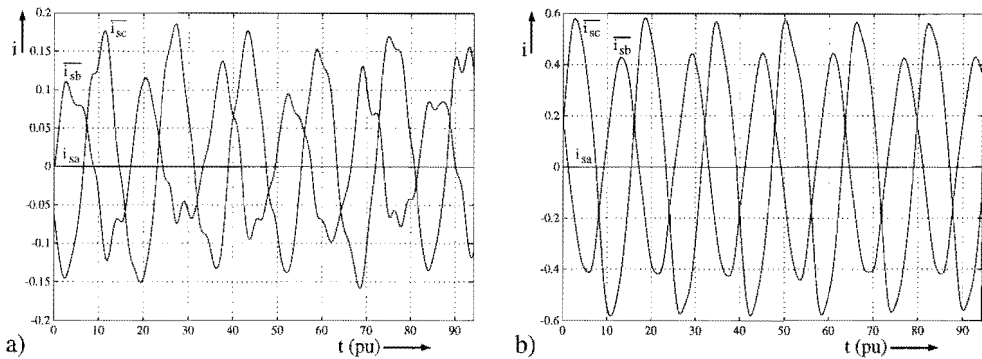


Figure 7.25. The low-pass filtered stator currents of the *u/f*-controlled cycloconverter-fed induction machine of which one phase has been disconnected, under a no-load condition (a) and with an average torque-producing current component of approx. 0.45 pu (b).

In case the machine was field-oriented, the simulations (figures 7.21 and 7.22) showed a similar behavior if the shape of the current waveforms is concerned, but at a much lower level. Characteristic for the field-oriented operation is that the field-oriented current vector has a maximal value which corresponds to the pre-fault value, while under *u/f*-control the average current corresponds to the pre-fault current. This behavior is also visible in the measurements, in particular in figure 7.26b.

As in the previous measurements, the current is very distorted for low values of the phase currents, which is especially visible now that the no-load current is even smaller than in case of *u/f*-control. The transient of the current vector is not the same as in the simulations for several reasons. First of all, in the simulations the current in one phase was switched off instantaneously, while in the experiments merely the gate signals of the

thyristors were stopped. Secondly the currents were filtered before being shown, because otherwise the 300 Hz ripple would make it impossible to observe the behavior of the lower-frequency components. Therefore fast current transients can not be observed in the same way as in the simulations.

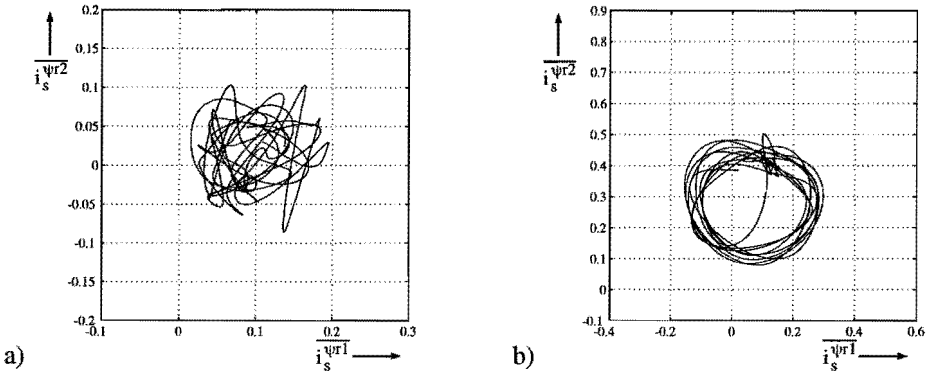


Figure 7.26. The low-pass filtered field-oriented stator-current vector of the field-oriented controlled cycloconverter-fed induction machine in case one phase is switched off, under a no-load condition (a) and with an initial torque-producing current component of approximately 0.45 pu (b).

An important difference between the simulations and the experiments can be seen by comparing figure 7.27 with figure 7.23. While the simulations showed a decrease of the remaining phase currents after the occurrence of a fault, the experiments show a slight increase. Also the final value of the rotor flux was larger than in the simulation, 0.40 pu for the no-load case resp. 0.38 pu for the loaded case under the same conditions as in the simulation. It was found that this difference can be explained by a difference of the stator resistance used for the simulations and the resistance present in the experimental setup. Due to the fact that the cycloconverter which was used, has an internal resistance which is several times the resistance of the stator windings, the apparent stator resistance is much higher in the experiments than in the simulations. If the stator resistance in the simulations is increased (results are not shown here), higher currents and a higher final rotor flux are obtained. For the no-load case with these simulations an only slightly higher final flux was found than in the experiments, while in the loaded case the experimental flux was considerably lower than in the simulations. This difference is probably caused by saturation effects, as explained in section 7.4.

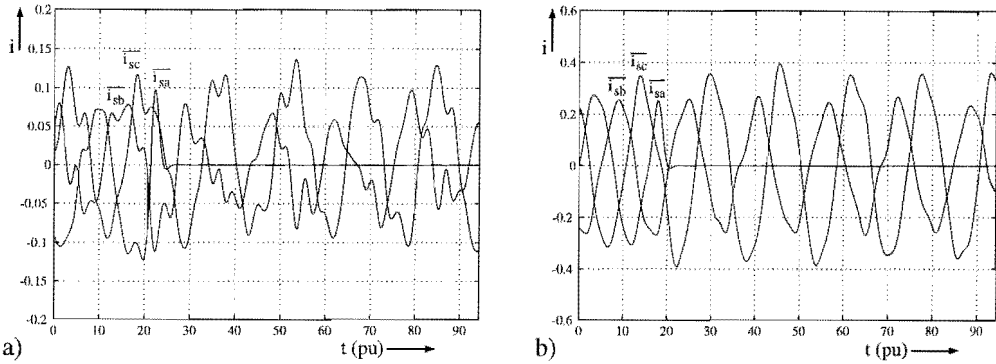


Figure 7.27. The low-pass filtered stator currents of the field-oriented controlled cyclo-converter-fed induction machine in case one phase is switched off under a no-load condition (a) and with an initial torque-producing current component of approximately 0.45 pu (b).

7.5.3 Simulations of a single-phase open circuit using fault correction

In the simulations and experiments shown above no measures were taken to improve the behavior of the system in a fault situation. However, as was shown previously, as long as the currents in two phases can still be controlled independently, it is possible to operate the machine with constant torque and flux.

In section 7.3.1, figures 7.5 and 7.6, simulations have been shown in which the machine is operated while the current in one of the phases is zero. Here the voltages applied to the other two phases had been modified in such a way that currents are obtained which result in operation with constant torque and flux. No separate simulations are performed for the case where one phase is disconnected and at the same time the correction is applied, because the results would be exactly the same as shown in these figures.

In a real situation however, the correction would only be applied shortly after one of the phase currents has become zero, due to the time needed for the functioning of a fault-detection circuit. The transient occurring during this delay will be similar to the initial part of the transients shown in section 7.5.2 (figures 7.26 and 7.27) for the field-oriented controlled machine. Whether a large variation of the torque occurs during this time interval will depend on several factors, such as the moment at which the fault occurs, the time required for the detection of the fault and the pre-fault torque. The moment at which the current in the faulty phase becomes zero is determined by the physical cause of the fault: if a fuse causes the fault, this is likely to occur while the phase current is large, while a fault in a gate driver of a thyristor would have an effect after a zero crossing of the current.

7.5.4 Experiments of a single-phase open circuit using fault correction

In this section the experimental results of the field-oriented system using the fault correction will be shown. For these experiments one of the phases was disconnected first, and then the measurements were performed while the fault-correction circuit was active. No transients are shown, because no fault detection was implemented – the correction circuit was switched on manually, by setting (k_i^{s1}, k_i^{s2}) to $(-2, 0)$ in case of a fault in phase a.

The measurements for the no-load case are not shown in this section – instead the figures show a comparison between healthy, symmetrical operation and the case when one phase is disconnected and a correction is applied, for a torque-producing current of approximately 0.45 pu. The rotor speed was equal to 0.37 pu.

Figure 7.28 shows the low-pass filtered field-oriented stator-current vector. A comparison of the two cases shows that there is a difference in the harmonic content of this current, but there is no noticeable difference in the average values. Further analysis of the data showed that there was in fact a small increase (less than 3%) in the torque-producing current component, but this can be explained from inaccuracies of the cycloconverter control. This means that the asymmetrical operation is successful: although one of the phase currents has become zero due to a fault, the machine is still operated with the same magnetizing and torque-producing currents.

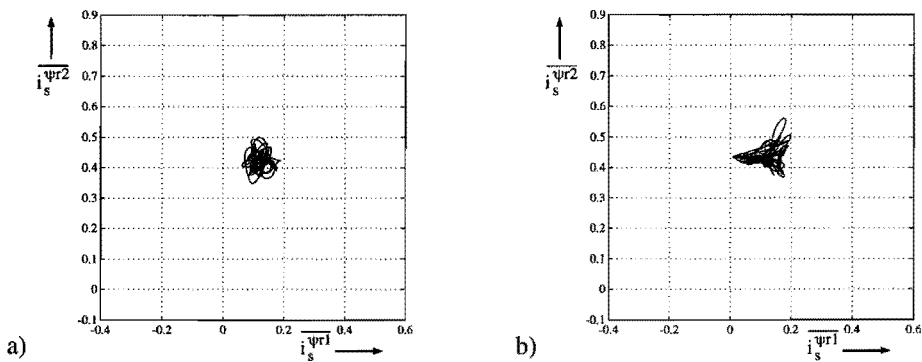


Figure 7.28. The low-pass filtered field-oriented stator-current vector of the field-oriented controlled cycloconverter-fed induction machine, under normal operation (a) and in case one phase is disconnected and correction is applied (b).

The low-pass filtered individual stator currents for the two cases are shown in figure 7.29. Due to the switching of the converter, the currents are slightly distorted, and imperfections in the control system cause a small asymmetry even in normal operation. In the no-load case (not shown) the distortion was even more visible, but also there the average field-oriented current components were the same for the symmetrical and the faulty, asymmetrical case. Figure 7.29b can be compared with figure 7.11, which showed the same asymmetrical operation mode in case all three phases were intact.

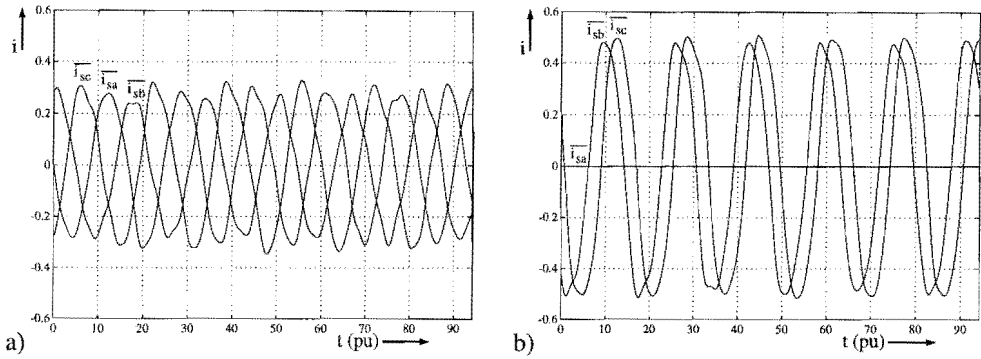


Figure 7.29. The low-pass filtered stator currents of the field-oriented controlled cycloconverter-fed induction machine, under normal operation (a) and in case one phase is disconnected and correction is applied (b).

As in the previous cases, the asymmetrical operation of the machine causes saturation, although the flux level under symmetrical operation was set to only 0.62 pu. In the no-load case, the flux under asymmetrical operation was equal to 0.59 pu, which is a decrease of 5%. For the load case shown in the figures, the flux decrease was as high as 19%, which corresponds to a flux level of 0.50 pu. Evidently such a reduction in the flux level, while the torque-producing current remains the same, causes an equal reduction of the average torque, as can be seen in figure 7.30.

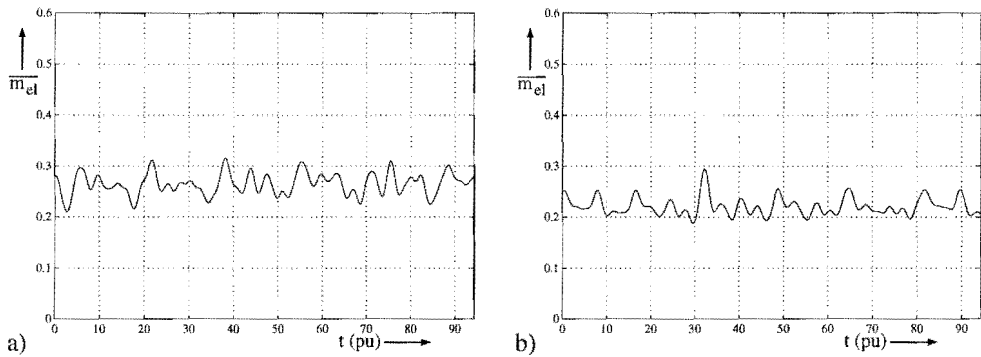


Figure 7.30. The low-pass filtered torque of the field-oriented controlled cycloconverter-fed induction machine under normal operation (a) and in case one phase is disconnected and correction is applied (b).

It is interesting to notice that the torque ripple – due to the third harmonic current caused by the saturation – is smaller in this case where one phase has been disconnected, than in the case shown in figure 7.13, where phase a still carried harmonic currents. To explain this phenomenon a more thorough study of the saturation effects would be required.

7.6 Operation of the drive in other fault situations

Operation of an induction machine of which the star point is connected while one of the phases is disconnected is a special case, for the reason that fault correction is possible in a relatively simple way. This section will deal with other kinds of faults, for which continued operation with constant torque can no longer be realized.

7.6.1 Simulations of a two-phase open circuit without fault correction

In the simulations and experiments of section 7.5, one phase of a voltage-fed induction machine was disconnected, and the resulting operating conditions were studied for different types of control, with and without fault-correcting measures. Due to the star-point connection, in that case two currents remained independently controllable, and a constant torque could be obtained. If yet another phase becomes disconnected, only a single phase current remains. As was shown in Chapter 6 for the current-fed machine, in this case it is no longer possible to obtain a constant torque. Chapter 6 further showed which current waveforms might be used for this remaining current in order to minimize the torque ripple.

For the voltage-fed machine a control circuit could be designed which applies such a voltage to the remaining phase that the current waveforms calculated in Chapter 6 are obtained. For practical reasons this was not implemented – due to the limited bandwidth and current capability of the voltage converter that was available (a cycloconverter using 12 thyristors for each phase) practical verification of this method would not have been possible. However, for the case of an induction machine fed by a current controlled voltage-source inverter this case will be discussed in detail in Chapter 8.

The case where two phases are disconnected and one phase remains voltage-fed is very similar to the case where one phase is disconnected while there is no connection of the star point. The latter case has therefore not been studied.

As for the single-phase open circuit, also in this case there is a considerable difference between a field-oriented controlled and a u/f -controlled machine. A phenomenon that can occur with u/f -control but not with field-oriented control (unless some current limitation is applied) is pulling-out of the machine. This occurs if the load torque is higher than the so-called pull-out torque, for a given voltage and frequency. If only one phase of the machine is fed instead of three, while maintaining the voltage and frequency at a constant level, the pull-out torque will decrease by more than a factor three. This will be shown using the equations given below.

In this calculation the steady-state torque will be expressed as a function of the rotor speed, the voltage applied to a remaining phase, the machine parameters and the time. The conditions for which the calculation is performed are given in equation 7.15.

$$\begin{aligned} i_{sb} &= i_{sc} = 0 \\ u_{sa} &= u_s \cdot \cos(\hat{\alpha}_s^s t) \\ u_s, \hat{\alpha}_s^s, \hat{\rho}^s &\text{ constant} \end{aligned} \quad (7.15)$$

First, the relation between the stator-current vector and the rotor flux will be derived. By combining equations 2.85 (transformed to rotor coordinates) and 2.86, equation 7.16 is obtained. Transforming this equation from rotor to stator coordinates results in equation 7.17.

$$\frac{1}{r_r} \cdot \frac{d\psi_r^r}{dt} + \frac{1}{l} \cdot \psi_r^r - i_s^r = 0 \quad (7.16)$$

$$\frac{1}{r_r} \cdot \begin{bmatrix} \frac{d\psi_r^{s1}}{dt} \\ \frac{d\psi_r^{s2}}{dt} \end{bmatrix} + \frac{\hat{\rho}^s}{r_r} \cdot \begin{bmatrix} \psi_r^{s2} \\ -\psi_r^{s1} \end{bmatrix} + \frac{1}{l} \cdot \begin{bmatrix} \psi_r^{s1} \\ \psi_r^{s2} \end{bmatrix} - \begin{bmatrix} i_s^{s1} \\ i_s^{s2} \end{bmatrix} = 0 \quad (7.17)$$

Using the three-to-two-phase current transformation (equation 4.5) it follows from equation 7.15 that $i_s^{s1} = i_{sa}$ and $i_s^{s2} = 0$. However, in a voltage-fed machine the current i_{sa} is not an input variable – it has to be derived from the applied voltage. The relation between a phase voltage and a phase current was given in equation 5.13. Substituting that $\psi_{rsa} = \psi_r^{s1}$ and that for this case $i_{s0} = i_{sa}$, equation 7.18 is obtained.

$$r_{sq} \cdot i_{sa} + l_{\sigma q} \cdot \left(1 + \frac{1}{l_{\sigma q}} \left(l_0 - \frac{1}{3} l_{\sigma q} \right) \right) \cdot \frac{di_{sa}}{dt} + \frac{d\psi_r^{s1}}{dt} = u_{sa} \quad (7.18)$$

For simplification the factor $1 + 1/l_{\sigma q} \cdot \left(l_0 - \frac{1}{3} l_{\sigma q} \right)$ will in the equations below be denoted by k . By combining equations 7.17 and 7.18, one set of differential equations is obtained, in which the rotor flux and the stator current act as state variables, and which can be written in the general form of $B\dot{\mathbf{x}} + A\mathbf{x} = \mathbf{u}$, as shown in equation 7.19.

$$\begin{bmatrix} \frac{1}{r_r} & 0 & 0 \\ 0 & \frac{1}{r_r} & 0 \\ 1 & 0 & k \cdot l_{\sigma q} \end{bmatrix} \cdot \begin{bmatrix} \frac{d\psi_r^{s1}}{dt} \\ \frac{d\psi_r^{s2}}{dt} \\ \frac{di_{sa}}{dt} \end{bmatrix} + \begin{bmatrix} \frac{1}{l} & \frac{\hat{\rho}^s}{r_r} & -1 \\ -\frac{\hat{\rho}^s}{r_r} & \frac{1}{l} & 0 \\ 0 & 0 & r_{sq} \end{bmatrix} \cdot \begin{bmatrix} \psi_r^{s1} \\ \psi_r^{s2} \\ i_{sa} \end{bmatrix} = \begin{bmatrix} 0 \\ 0 \\ u_{sa} \end{bmatrix} \quad (7.19)$$

The homogeneous solution of this equation is not of interest here, because in this calculation only the steady state will be considered. For an excitation signal, in this case the voltage u_{sa} , with a frequency ω the particular solution to this equation is of the form $x = c \cdot \cos(\omega t) + d \cdot \sin(\omega t)$. By substituting this into equation 7.19, the steady-state waveforms of ψ_r^{s1} , ψ_r^{s2} and i_{sa} can be obtained. This was done numerically, substituting the parameters and operating conditions used also in the real-time simulations: the voltage and frequency have been chosen in such a way that under symmetrical three-phase operation $\hat{\rho}^s = 0.4$, $\psi_r = 0.65$ and $i_s^{\psi r 2} = 0.5$. Finally, the torque waveform has been obtained using equation 7.20, which corresponds to equation 2.88.

$$m_{el} = \psi_r^{s1} \cdot i_s^{s2} - \psi_r^{s2} \cdot i_s^{s1} = -\psi_r^{s2} \cdot i_{sa} \tag{7.20}$$

As expected, the torque varies sinusoidally around its average value, with a frequency of twice the supply frequency, except at zero speed, where the torque is zero. Figure 7.31a shows the average torque as a function of the rotor speed, as well as the maximum and the minimum torque occurring at each speed. Also the torque vs. speed characteristic of the same machine under symmetrical three-phase supply has been drawn in the same figure. From this it becomes clear that the pull-out torque is much lower in case of a single-phase supply, and that therefore – as long as no correcting measures are taken – only a rather low load torque is possible.

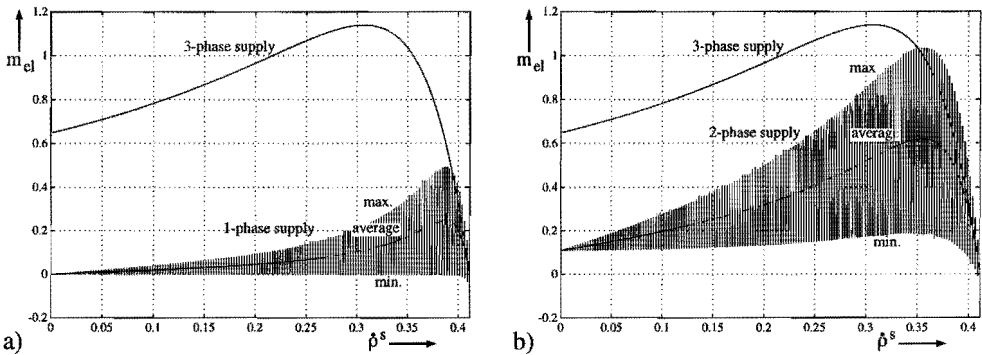


Figure 7.31. The calculated average, maximum and minimum torque vs. speed characteristics of an induction machine fed with a constant voltage and frequency, in case only one phase is fed (a) and in case two phases are fed (b).

For comparison, also the torque in case only one phase (phase c) is disconnected has been calculated, under the conditions given in equation 7.21.

$$\begin{aligned} i_{sc} &= 0 \\ u_{sa} &= u_s \cdot \cos(\hat{\alpha}_s^s t), \quad u_{sb} = u_s \cdot \cos\left(\hat{\alpha}_s^s t - \frac{2\pi}{3}\right) \\ u_s, \hat{\alpha}_s^s, \hat{\rho}^s &\text{ constant} \end{aligned} \tag{7.21}$$

In the same way as for the previous case the equations describing the system are found – the resulting matrix equation is given in equation 7.22 in which $p = 1_0 - \frac{1}{3}1_{\text{Oq}}$.

$$\begin{bmatrix} \frac{1}{r_r} & 0 & 0 & 0 \\ 0 & \frac{1}{r_r} & 0 & 0 \\ 1 & 0 & 1_{\text{Oq}}+p & p \\ -\frac{1}{2} & \frac{\sqrt{3}}{2} & p & 1_{\text{Oq}}+p \end{bmatrix} \cdot \begin{bmatrix} \frac{d\psi_r^{s1}}{dt} \\ \frac{d\psi_r^{s2}}{dt} \\ \frac{di_{sa}}{dt} \\ \frac{di_{sb}}{dt} \end{bmatrix} + \begin{bmatrix} \frac{1}{l} & \frac{\dot{\rho}^s}{r_r} & -1 & \frac{1}{2} \\ -\frac{\dot{\rho}^s}{r_r} & \frac{1}{l} & 0 & -\frac{\sqrt{3}}{2} \\ 0 & 0 & r_{sq} & 0 \\ 0 & 0 & 0 & r_{sq} \end{bmatrix} \cdot \begin{bmatrix} \psi_r^{s1} \\ \psi_r^{s2} \\ i_{sa} \\ i_{sb} \end{bmatrix} = \begin{bmatrix} 0 \\ 0 \\ u_{sa} \\ u_{sb} \end{bmatrix} \quad (7.22)$$

The resulting torque for this case is shown in figure 7.31b. This situation is much more favorable than the single phase supply. Not only is the pull-out torque much higher, but also the torque at zero speed is not equal to zero. The torque ripple however is in this case very high, except at zero speed, where the torque ripple is zero. At first sight, this is a surprising result, because at any speed the asymmetrical (single- or two-phase) supply causes the air-gap MMF to consist of two components, rotating at equal speeds but in opposite directions, which under most operating conditions causes torque ripple at twice the supply frequency.

However, it can easily be explained that at zero speed this kind of asymmetrical supply will not cause a torque ripple. For $\dot{\rho}^s = 0$ equation 7.17 can be simplified to equation 7.23, which shows that if i_s^s is a vector of a constant length rotating at a constant speed, the rotor flux ψ_r^s will be a vector rotating at the same speed, however with a different amplitude and lagging behind the current.

$$\frac{1}{r_r} \cdot \frac{d\psi_r^s}{dt} + \frac{1}{l} \cdot \psi_r^s = i_s^s \quad (7.23)$$

In section 6.4.1 it was shown how an arbitrary stator-current vector could be decomposed into components with a constant frequency and amplitude. In case of a current fault while the remaining phases are fed with a sinusoidal voltage or current of a constant frequency, the stator current will consist of the two components given in equation 7.24, in which $\dot{\epsilon}_{s2}^s = -\dot{\epsilon}_{s1}^s$. Each of these current components causes a rotor flux component, given by equation 7.25.

$$i_{s1}^s = i_{s1}^s \cdot \begin{bmatrix} \cos(\dot{\epsilon}_{s1}^s t - \epsilon_{s01}^s) \\ \sin(\dot{\epsilon}_{s1}^s t - \epsilon_{s01}^s) \end{bmatrix}, \quad i_{s2}^s = i_{s2}^s \cdot \begin{bmatrix} \cos(\dot{\epsilon}_{s2}^s t - \epsilon_{s02}^s) \\ \sin(\dot{\epsilon}_{s2}^s t - \epsilon_{s02}^s) \end{bmatrix} \quad (7.24)$$

$$\psi_{r1}^s = k_1 \cdot i_{s1}^s \cdot \begin{bmatrix} \cos(\dot{\epsilon}_{s1}^s t - \epsilon_{s01}^s - \gamma_1) \\ \sin(\dot{\epsilon}_{s1}^s t - \epsilon_{s01}^s - \gamma_1) \end{bmatrix}, \quad \psi_{r2}^s = k_2 \cdot i_{s2}^s \cdot \begin{bmatrix} \cos(\dot{\epsilon}_{s2}^s t - \epsilon_{s02}^s - \gamma_2) \\ \sin(\dot{\epsilon}_{s2}^s t - \epsilon_{s02}^s - \gamma_2) \end{bmatrix} \quad (7.25)$$

The torque generated by these currents will consist of four components. Two components are due to the interaction of i_{s1}^s with Ψ_{r1}^s and i_{s2}^s with Ψ_{r2}^s – these components are constant. The other two torque components, $\Psi_{r1}^{s1} \cdot i_{s2}^{s2} - \Psi_{r1}^{s2} \cdot i_{s2}^{s1}$ resp. $\Psi_{r2}^{s1} \cdot i_{s1}^{s2} - \Psi_{r2}^{s2} \cdot i_{s1}^{s1}$, will be pulsating with a frequency of $\dot{\epsilon}_{s1}^s - \dot{\epsilon}_{s2}^s$ and have an average value equal to zero. Calculation of these components shows however, that they will cancel each other in case $k_1 = k_2$ and $\gamma_1 = -\gamma_2$. Considering equation 7.23 it is easy to understand that for two current components with equal but opposite frequencies this condition is always met, independent of their respective amplitudes and phase angles. This explains the constant torque obtained at zero speed under asymmetrical operation caused by a disconnected phase.

It is now interesting to extend this reasoning for the general case when $\dot{\rho}^s \neq 0$ and examine which conditions the two current components must satisfy in order to obtain a constant torque. Instead of equation 7.23 then the more general equation 7.17 applies. The relation between a current and a flux vector is found from this equation more easily if a complex notation is used, assuming constant frequencies and amplitudes for the current and flux vectors. This is done in equation 7.26, and the resulting relation is given in 7.27.

$$\frac{1}{r_r} \cdot j\dot{\epsilon}_s^s \cdot \Psi_r^s - \frac{\dot{\rho}^s}{r_r} \cdot j \cdot \Psi_r^s + \frac{1}{s} \cdot \Psi_r^s = I_s^s \quad (7.26)$$

$$\Psi_r^s = \frac{I_s^s}{\frac{1}{s} + \frac{1}{r_r} j (\dot{\epsilon}_s^s - \dot{\rho}^s)} \quad (7.27)$$

Equation 7.27 shows that for two flux-current pairs to have the same amplitude factor k , the two current frequencies must satisfy equation 7.28. If this condition is met, the phase angles γ_1 and γ_2 will either be equal or opposite. If the two frequencies are equal, the angles will also be equal, and the total current vector will not consist of two frequency components, but of only one. Otherwise the angles γ_1 and γ_2 will be opposite, and as explained before, the pulsating torque components will then cancel each other.

$$(\dot{\epsilon}_{s1}^s - \dot{\rho}^s) = \pm (\dot{\epsilon}_{s2}^s - \dot{\rho}^s) \quad (7.28)$$

This implies that if a machine is fed with a frequency $\dot{\epsilon}_{s1}^s$, two frequencies $\dot{\epsilon}_{s2}^s$ can be found for which the injection of a second current component does not cause any torque ripple. This has been verified by simulations, of which some results are shown in figure 7.32. A possible application of this phenomenon might be the identification of the rotor speed and slip (or the rotor resistance): a controller could be used to adjust the second frequency until no torque ripple is present; presuming the frequency it adjusts to is not equal to the first frequency, addition and subtraction of the two frequencies can be used to obtain the rotor speed and the slip. A practical problem is however that the torque-ripple frequency will in fact be very low (depending on the slip), making the identification very difficult or impossible, especially during transients.

After this intermezzo on torque ripples and pull-out torques, now the simulations of the machine fed by only a single phase voltage will be commented. Figure 7.33 shows the simulation results for the u/f-controlled machine. The voltage, frequency and load torque have been adjusted in such a way that initially – during symmetrical three-phase operation – $\Psi_r = 0.65$, $\dot{\rho}^s = 0.4$ and $i_s^{\Psi r 2} = 0.5$. The simulation shows the effect of disconnecting phase a and phase b under these conditions.

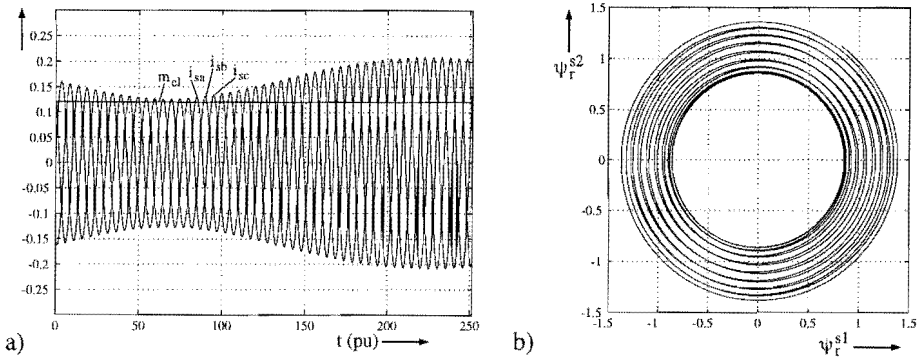


Figure 7.32. Simulation of an induction machine fed by two current sources in parallel, of which the frequencies are adjusted in such a way that a constant torque is obtained: a) the three phase currents and the torque; b) the rotor-flux vector.

Because the load torque is now higher than the pull-out torque (cf. figure 7.31a), the machine will not stabilize at a new speed. Instead, it is pulled away from its synchronous speed, and complete demagnetization and decrease of the speed result. The simulation shows a limited time interval, during which the torque has only decreased to 80 percent of its initial value. However, figure 7.33a shows that the average magnetizing current has become zero. The large oscillation of the magnetizing current does also cause an oscillation of the flux.

If a lower load torque is chosen – lower than the pull-out torque of 0.25 pu found in figure 7.31 – the machine will reach a new stable situation. However, the torque then varies between zero and twice its average value, and a very high current flows in the remaining phase. The rotor speed is evidently lower than under three- or two-phase operation, which also can be understood from figure 7.31.

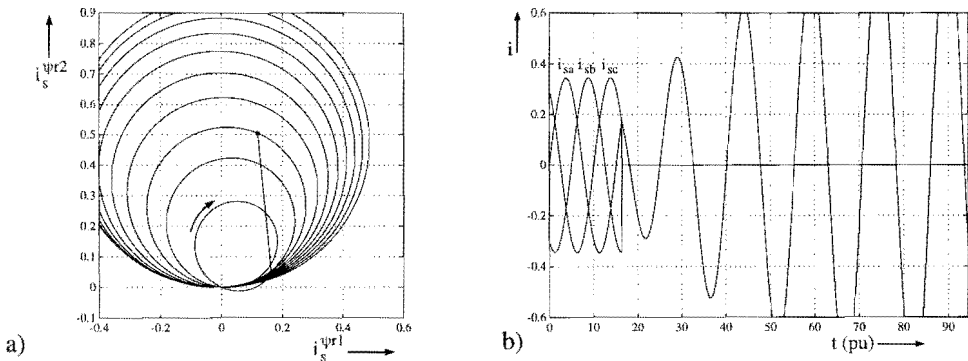


Figure 7.33. Simulation showing the stator-current vector (a) and the three stator currents (b) of a u/f-controlled induction machine in case two phases are disconnected .

Again, the field-oriented controlled machine behaves very differently from the u/f-controlled machine. In this case, the field-oriented control will adjust the frequency of the applied voltage in such a way that, although the rotor speed decreases, the slip is kept below its pull-out value. However, as was the case when only one phase was disconnected, the torque and flux in the fault situation are much lower than during normal operation, which will cause a rapid decrease of the rotor speed in case the load torque is maintained at the pre-fault level.

Figure 7.34 shows the stator currents for this situation. During the transient, an oscillation with the frequency of the supply is present in the field-oriented current components (and therefore also in the torque) due to a transient dc component in the current of the remaining phase. In the plot of the field-oriented current vector (figure 7.34a) this is visible as two circles which after some time merge into one single (which represents an oscillation at twice the supply frequency).

If the load torque is decreased in such a way that it equals m_{e1} for this situation, at a speed of $\hat{\rho}^s = 0.4$, a final value of the flux of 0.22 pu is found, or 0.29 pu if the stator resistance is increased to match the resistance of the stator and converter used in the experiments. In the experimental machine an even lower flux level is expected, due to saturation effects.

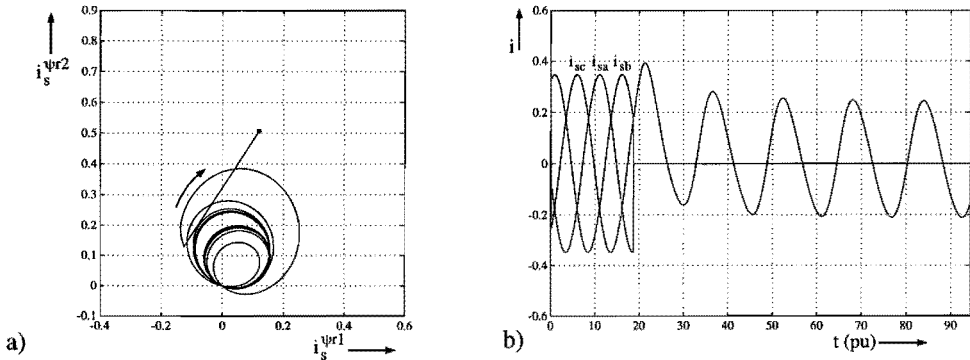


Figure 7.34. Simulation showing the stator-current vector (a) and the three stator currents (b) of a field-oriented controlled induction machine in case two phases are disconnected.

7.6.2 Experiments of a two-phase open circuit without fault correction

Also in the laboratory setup of an induction machine connected to a cycloconverter, two phases were disconnected in order to examine the behavior of the machine in case of single-phase supply. First a u/f-control was implemented, in which the voltage and frequency were adjusted in such a way that under three-phase operation $\psi_r = 0.65$,

$\hat{\rho}^s = 0.4$ and $i_s^{\psi r 2} = 0.5$ were obtained. Due to the resistance of the cycloconverter, the voltage and frequency required for this were not the same as in the simulations. The pull-out torque under single-phase operation was also lower than in the simulations, which could only partly be explained by the different parameters. Probably, saturation in the machine is again a very important cause for differences between simulations and experiments. It should be noted that under single-phase operation the air-gap MMF as a function of the position along the air gap, has again a shape which is very different from a sinus. Modeling the saturation effects in this situation would require a very thorough analysis of the complete magnetic circuit of the machine, and the results would very much depend on the winding and magnetic circuit configurations.

Figure 7.35 shows the stator currents for this situation. The load torque was adjusted in such a way that a machine torque just below pull-out was obtained. The stator-current vector has a close to circular shape, from which it differs due to the switching behavior of the converter. Necessarily, the current vector crosses the zero vector twice in every period, which occurs at the moment when all three stator currents are zero. Compared to the ripple in the magnetizing current, the flux ripple is rather small: its top-to-top value is 20% of its average value. The average flux is 26% lower than under symmetrical operation with the same voltage and frequency.

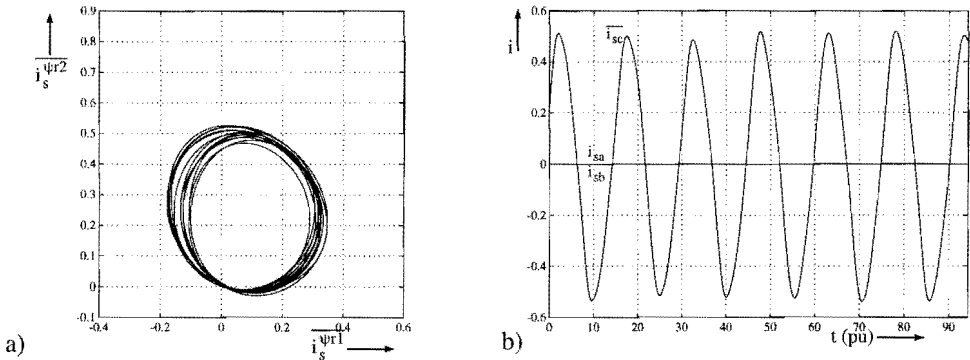


Figure 7.35. The low-pass filtered stator currents of the u/f-controlled induction machine in case two phases are disconnected: a) the field-oriented stator-current vector; b) the three stator currents.

The currents in case of a field-oriented controlled machine are shown in figure 7.36. A comparison with the simulation shown in figure 7.34 shows that there are some important differences in the current levels. These differences are caused both by the difference in stator resistance between the simulation and the real machine with the converter, and by the saturation. A new simulation was therefore performed (not shown here) in which the stator resistance was adapted to the value present in the experimental setup. The average field-oriented current components obtained with that simulation differed not more than

5% from the experimental values. Due to saturation the average flux level was however approximately 6% lower than in the simulation.

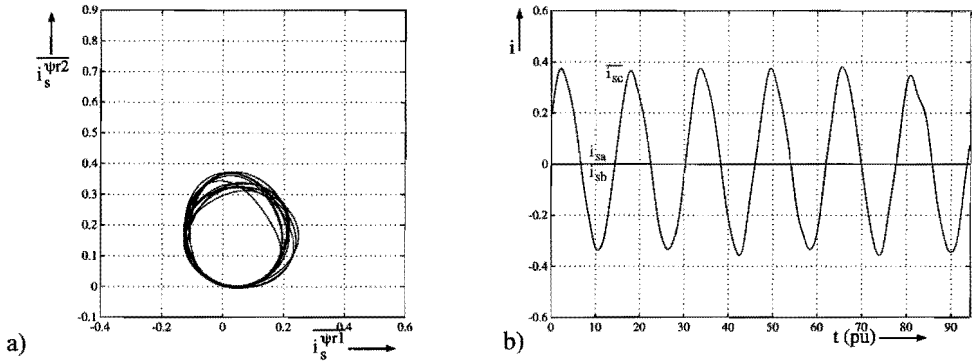


Figure 7.36. The low-pass filtered stator currents of the field-oriented controlled induction machine in case two phases are disconnected: a) the field-oriented stator-current vector; b) the three stator currents.

7.6.3 Simulations of a single-phase short circuit

In section 5.5.2 it has already been explained that the case of a short circuit of one of the machine phases (see figure 5.8b) is such a serious fault that continued operation – with or without fault correction – is not feasible. However, to identify the problems more clearly some simulations were performed, which will be presented in this section. Three cases will be examined: two cases in which no fault correction is applied (u/f-control and field-oriented control), and a case where correction is performed by applying a homopolar voltage. This homopolar voltage is a function of the non-homopolar voltage components only, and therefore correction can be applied with any type of voltage control. This is different from the correction for the current fault which required desired currents instead of voltages to calculate the desired homopolar voltage, and could therefore not be applied to a u/f-controlled machine. The correction for the voltage fault will be shown using field-oriented control.

In all simulations shown here, the initial conditions are the same as in the simulations with the current faults: $\psi_r = 0.65$, $i_s^2 = 0.5$ and $\beta^s = 0.4$. It must be noted that due to this low flux level and the relatively low speed the problems shown are much smaller than at rated speed with a rated flux level. This is due to the fact that with rated speed and flux the voltages under normal operation are more than a factor three higher than in this case, resulting in much higher currents in case of a short circuit.

In case of a simple u/f-control, the voltage over the remaining two phases will remain unchanged in case of a single-phase short circuit. As a result the rotor flux will reach a value

which is approximately two thirds of its pre-fault value (see figure 7.37a). This is closely related to the fact that the field-oriented voltage vector obtains an average value which is also approximately two thirds of the pre-fault value. The oscillation in the voltage vector (see figure 7.38) has a frequency of two times the supply frequency. It is interesting to compare this situation with figure 7.22b. That figure showed the current vector in case of a current fault while a field-oriented control – which mainly maintains the current in the remaining phases – was used. The case studied here is in some aspects dual to that case.

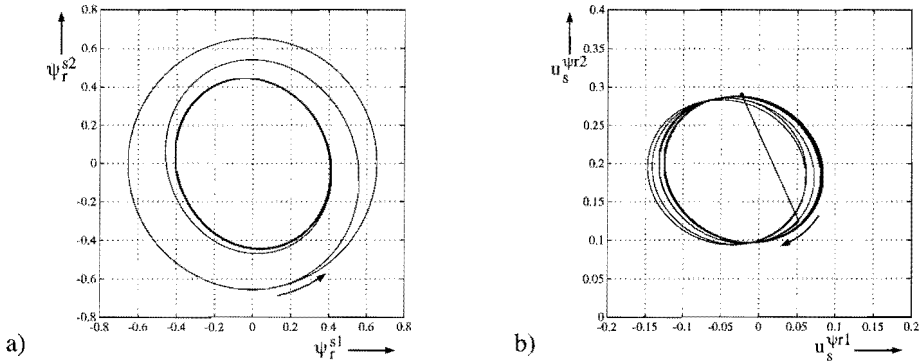


Figure 7.37. Simulation showing the rotor-flux vector (a) and the field-oriented voltage vector (b) of a u/f-controlled induction machine in case one phase is short-circuited.

Evidently, oscillations in the voltage vector cause much higher oscillations in the current. Figure 7.38a shows that the oscillation in the field-oriented current vector has a top-to-top value of 3 pu! The amplitude of the torque ripple is three times as high as the average torque, and the average torque is reduced by approximately one third due to the reduced flux. As a consequence, the machine will slow down until a new equilibrium between the average torque and the load torque has been reached.

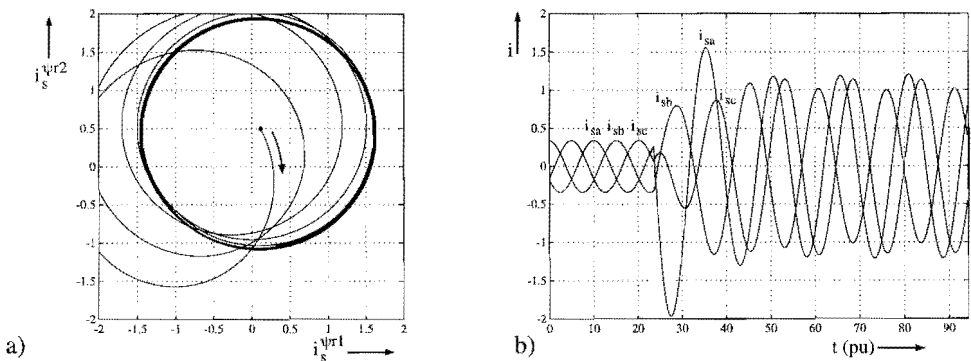


Figure 7.38. Simulation showing the field-oriented stator current vector (a) and the three stator currents (b) of a u/f-controlled induction machine in case one phase is short-circuited.

The individual currents, shown in figure 7.38b, are not extremely high, although they are much higher than in the pre-fault situation. The homopolar current has an amplitude of 1.2 pu, which means that in the real machine a considerable saturation will occur.

In case of field-oriented control, the steady-state currents have amplitudes that are similar to their pre-fault values. However, the rotor flux is reduced to only 6% (!) of its pre-fault value (see figure 7.39a). As in case of a current fault, the feedback of the flux to the VVC causes a reduction of the supply voltage (see figure 7.39b), and although this has a limiting effect on the current, the resulting torque is too low to be usable. Furthermore, the initially very high current – which occurs while the flux is still near to its initial value – causes an important breaking torque, which is characteristic for all short circuits in induction machines. The current vector and the individual currents are shown in figure 7.40. After the initial current peak, the homopolar current (not shown) has an amplitude comparable to that of the individual currents, which means that probably some saturation will be present also in steady state, but not as much as in the u/f-controlled case.

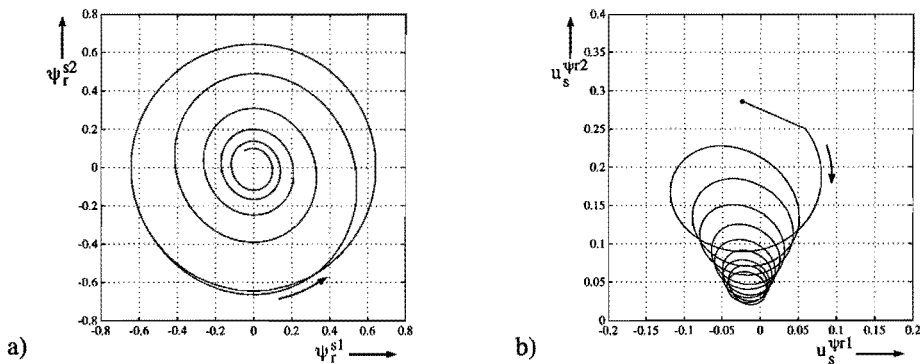


Figure 7.39. Simulation showing the rotor-flux vector (a) and the field-oriented voltage vector (b) of a field-oriented controlled induction machine in case one phase is short-circuited.

Due to the presence of the star-point connection, continued operation while one of the phase voltages is zero is theoretically possible, by applying the correct homopolar voltage. In analogy with equation 6.8 for the desired homopolar current for operation with one current equal to zero, equation 7.29 can be used to obtain a required homopolar voltage. Using the voltage transformation equation 4.28, it can easily be shown that operation with u_{sa} equal to zero is obtained by setting $(k_u^{s1}, k_u^{s2}) = (-1, 0)$.

$$u_{s0}^* = k_u^{s1} \cdot u_s^{s1*} + k_u^{s2} \cdot u_s^{s2*} \quad (7.29)$$

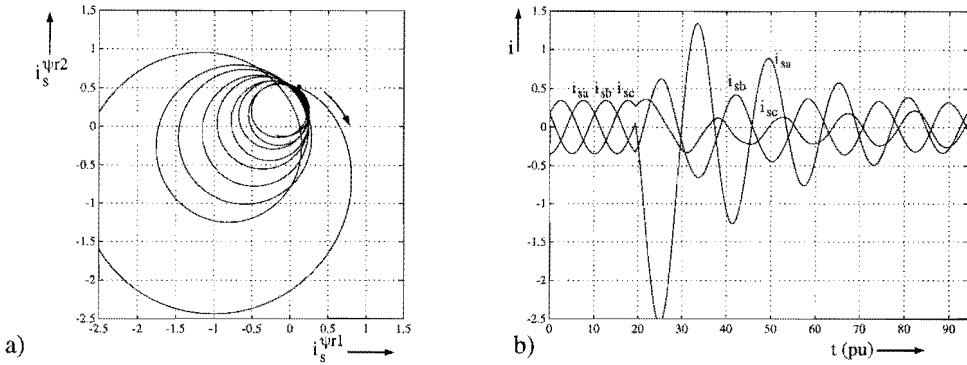


Figure 7.40. Simulation showing the field-oriented stator-current vector (a) and the three stator currents (b) of a field-oriented controlled induction machine in case one phase is short-circuited.

If this homopolar voltage is applied, asymmetrical operation with constant and unchanged field-oriented current- and voltage vectors results. The phase voltages for this situation are shown in figure 7.41a. This figure can be compared with figure 7.5, where the same method was applied to the currents. However, the homopolar voltage causes a very large homopolar current (not shown), which in this case reached an amplitude of 3.7 pu (!). This can also be understood by looking at the individual stator currents, shown in figure 7.41b. These currents are almost equal, and their sum is the homopolar current. Evidently, this very high homopolar current will cause saturation and considerable losses, which means that the machine can not be operated in this way, especially not if the flux and/or the speed are to be increased to their rated values.

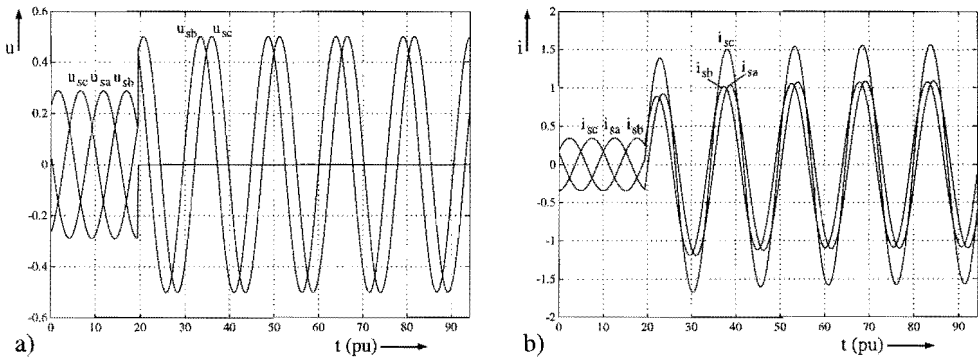


Figure 7.41. Simulation showing the stator voltages (a) and currents (b) of a voltage-fed induction machine at a step change of (k_u^{s1}, k_u^{s2}) from $(0,0)$ to $(-1,0)$.

It must therefore be concluded that in case of a single-phase short circuit, the fault should be transformed as soon as possible into an open circuit, after which the correction technique described in section 7.5 can be applied.

7.7 Conclusions

In this chapter, simulations and experiments of a voltage-fed induction machine are shown. In all cases the star point of the machine was connected, which introduced one extra degree of freedom. In the ideal induction machine – in which no saturation effects are present – the current in the star-point connection, the so-called homopolar current, can be given an arbitrary value without influencing the behavior of the machine. With an appropriate choice of the homopolar current, operation with one of the phase currents equal to zero is possible without the presence of a torque ripple.

The machine control circuit was extended with some parts that allowed to command the homopolar current. It was shown that the fundamental component of one of the stator currents could be made zero without influencing the field-oriented current components. However, due to this asymmetrical supply, the MMF along the air gap contained an important third harmonic, resulting in saturation. In turn, this saturation caused third-harmonic currents. Also due to the saturation, the flux under asymmetrical operation is lower than under symmetrical operation if the same magnetizing current is applied.

For the cases when one or two stator phases are disconnected due to some fault, first the behavior when no fault correction was applied has been examined. An important difference exists between voltage/frequency-control and (position-sensorless) field-oriented control, because the former maintains a constant voltage at the remaining phase or phases, while the other tends to maintain first of all the current. Therefore, the current in the remaining phase or phases is much higher for a fault in a u/f -controlled system, and the same is true for the resulting torque. However, both controls have in common that, in case of a current fault, the torque will contain a ripple at twice the supply frequency. In case only one phase is disconnected, for high torques the amplitude of this ripple will be smaller than the average torque – if two phases are disconnected, the amplitude will be equal to the average torque. For the u/f -controlled machine it must be noted that the pull-out torque will decrease considerably if one or more phases are disconnected.

If only one phase is disconnected, the field-oriented control can be extended with a homopolar-current command circuit, which compensates for the missing phase. The experiments showed that indeed the field-oriented current components are in that case approximately the same as in the no-fault situation. However, due to saturation the flux is lower than under symmetrical operation, and as a result the same is true for the torque. This effect could be compensated for by using a flux or torque controller. It must however be noted that this asymmetrical operation not only requires a much higher current from the remaining two phases of the power converter, but also causes much higher losses in the machine, both copper losses caused by the increased phase currents and iron losses related to the increased saturation.

If two phases are disconnected, there is no possible fault correction technique to continue operation without a torque ripple. As shown in Chapter 6, some improvements can be made, but these require high currents and high converter bandwidth. As these two conditions could not be met with the cycloconverter used in the experiments, no investigations were made in this area.

If a voltage fault occurs which short circuits one of the phases of the machine, no continued operation is possible. With a u/f -control, this fault causes an extremely high ripple in the torque, and much increased stator currents, while the rotor flux is reduced to two thirds of its pre-fault value. If the machine is field-oriented, the steady-state currents are not higher than before the fault, but the rotor flux is reduced to almost zero. Instantaneously a very high current in the shortened phase occurs, causing a very large braking torque pulse. Fault correction is theoretically possible by applying an easily calculated homopolar voltage, but this results in high phase currents and in an extremely high homopolar current. It will therefore result in considerable losses and saturation, and is of no practical use.

Chapter 8

Asymmetrical Operation of a Voltage-Inverter-Fed Induction Machine

8.1 Introduction

In the previous chapters, the power converters in which a fault occurred were modeled as if they were ideal converters, composed of three current or voltage sources. These sources could either be connected to the machine directly, without fault, or would be disabled completely due to a short or open circuit. The star point of the machine could be connected or not, as a free choice of the system designer.

However, in practical applications converter failures are not always caused by a short or open circuit of a complete phase, but more often by the failure of a single device. If this device is for example a GTO, the most common failure will be a short circuit. On the other hand, if it is an IGBT, an open circuit is most common. Also a failure of the gate driver of a power device will result in a single-device open circuit. To study this kind of faults it is no longer possible to represent the converter by three sinusoidal sources – instead it becomes necessary to study the behavior of the individual devices.

There is a very large number of different topologies for power converters, and on each of them the failure of one device will have a different effect. In general it can be expected that if more devices are present, the failure of a single device will have a smaller impact on the capabilities of the converter. Yet the converter that nowadays finds widespread use in industrial drives – the voltage-source inverter – consists of only six switching devices, making it quite vulnerable to failures.

A possible solution to this problem is the addition of extra devices. For example, the star point of the machine could be connected to a fourth inverter branch, which allows continued operation even in case of complete failure of one of the other branches. This was proposed among others by T. Elch-Heb in [Elch-94]. It is also possible to connect the star point to the dc midpoint (if present), as proposed by Liu Tian-Hua in [Liu-91]. Or, as proposed by Fu Jen-Ren in [Fu-93], the phase in which the failure occurred could be connected to the dc midpoint. However, all these methods have in common that extra devices have to be added, and that some devices have to be dimensioned differently, such as the dc capacitors in case a connection to the dc midpoint has to be made. Finally, if

reliability of the drive is a very important issue, it might even be considered to increase the number of phases of the machine and of the converter, as proposed by Fu Jen-Ren in [Fu-93b]. Each phase which is added to the standard three-phase configuration will add another degree of freedom, and reduces the overcapacity needed in the other phases to compensate for the loss of a phase.

An interesting question is whether any remedial operation is possible in case of a device failure in the voltage-source inverter of a three-phase induction machine *without* any modifications to the power circuit. This means that also the star point of the machine will not be connected. This will be studied in this chapter. First, the different switching states of the converter and their effect on the machine quantities will be examined. Then, to perform real-time simulations of different fault situations and controls, a model of the inverter-machine combination will be developed.

A control technique will then be designed that guarantees an optimal torque control during different fault situations. This sophisticated control will be compared with the most elementary control method, three-phase hysteresis current control. Simulations using a DSP system as well as practical experiments will be used for this purpose. Finally, the results which are found will be compared with the results obtained for the ideal converters with phase faults, examined in chapters 6 and 7.

8.2 Overview of the switching states of an inverter

The basic circuit under consideration is shown in figure 8.1. The voltage-source inverter shown here is fed from an ideal dc voltage source, and supplies voltages to a three-phase induction machine. The switching devices can either be IGBTs (drawn here), GTOs or other devices that have turn-on and turn-off capability. They will be assumed to have only two possible states: conducting and non-conducting. The same will be assumed for the diodes that are connected antiparallel to the switches. Both the diodes and the switches can carry a current only in one direction.

Each of the switches can either receive gate signals, or not. If the switch is not faulty, it will start conducting as soon as it receives gate signals while a positive voltage is present across its terminals. If this voltage is negative, the antiparallel diode will conduct. In normal operation either the top switch of a branch (eg. s_1) or the bottom switch (eg. s_2) will receive gate signals, possibly with a short dead-time in-between. If no fault is present, due to the behavior of the diodes and the switches, whenever switch s_1 receives gate signals either switch s_1 or diode d_1 will conduct. The same is true for each of the other diode-switch pairs.

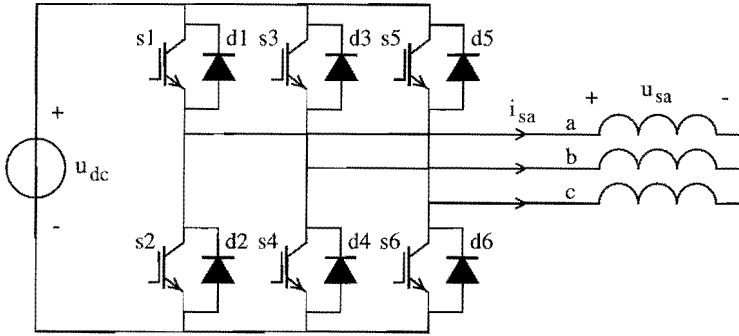


Figure 8.1. Basic circuit of an IGBT voltage-source inverter used to supply a three-phase induction machine.

The functioning of one branch of the inverter has been resumed in table 8.1. In this table, the presence of gate signals at a switch is denoted by ‘1’, the absence by ‘0’. For example, the notation ‘10’ means that switch s1 receives gate signals, and s2 does not. Depending on the phase current, either the switch or the diode will conduct (or none, if the current is exactly zero). The state of a complete branch is also denoted by a binary number. For example, ‘10’ means that either s1 or d1 conducts, and s2 and d2 do not. The voltage at point ‘a’ with respect to the negative pole of the dc voltage source will then be equal to u_{dc} . A special situation occurs if none of the switches and diodes in a branch are conducting (state ‘00’). The voltage at point ‘a’ will then depend on the machine voltages and on the states of the other branches. A command state of ‘11’ is not allowed, because it would cause a short circuit of the dc voltage source, resulting at least in a failure of one of the switches.

Table 8.1. Relation between the inverter branch command, the related phase current, the devices that are conducting and the resulting branch output voltage.

command	current	conducting	branch state	voltage at ‘a’
01	$i_{sa} > 0$	d2	01	0
	$i_{sa} < 0$	s2	01	0
10	$i_{sa} > 0$	s1	10	u_{dc}
	$i_{sa} < 0$	d1	10	u_{dc}
00	$i_{sa} > 0$	d2	01	0
	$i_{sa} < 0$	d1	10	u_{dc}
	$i_{sa} = 0$	-	00	see text
11	NOT ALLOWED			

From the table it can be seen that if a normal command state is applied to a branch of the inverter, i.e., '01' or '10', the branch state will be equal to the command state, and for the user it is not important whether a diode or a switch is conducting (which depends on the sign of the corresponding phase current). However, in case of a '00' command, the branch state will be determined completely by the sign of the current. Therefore, the voltage applied to the concerning phase of the machine is then dependent on the corresponding actual phase current.

When studying the control and behavior of a complete inverter, it is practical to describe the actual state of the inverter in the same way as was done for a single branch. The state of the three-phase inverter is thus represented by a six-bit binary number, in which the first two bits correspond to the phase-a branch state, the middle two bits to the phase-b branch state, etc. An example is shown in figure 8.2.

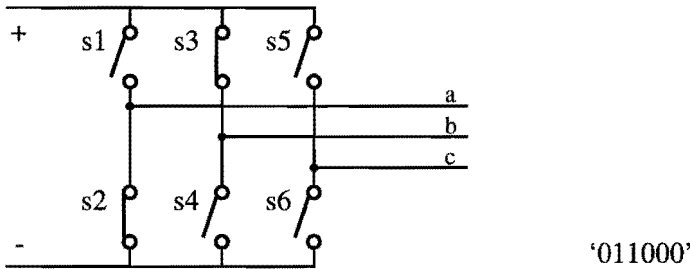


Figure 8.2. Example of the relation between the inverter state number and the conducting paths that are present in the inverter.

The fact that the inverter state can be represented by a six-bit binary number means that there are theoretically $2^6 = 64$ possible states. However, most of these states do not represent a useful operating state. It can be shown that there are 37 different states that represent a short circuit of the dc source. The 27 states that do not cause a dc-source short circuit are given in table 8.2.

Table 8.2. Inverter states that do not correspond to a dc-source short circuit.

000000	000001	000010	000100	000101
000110	001000	001001	001010	010000
010001	010010	010100	010101	010110
011000	011001	011010	100000	100001
100010	100100	100101	100110	101000
101001	101010			

Most of these 27 states leave one or two machine phases unconnected, which is not a desired situation during normal, symmetrical operation. In fact there are only eight different states for which each of the machine phases is connected to one of the terminals of the dc source. These eight states, which all are used during normal operation, are given in table 8.3.

Table 8.3. Inverter states that are used during normal operation.

010101	010110	011001	011010	100101
100110	101001	101010		

In normal operation there is no reason to use any other than one of these eight states. However, if a fault is present, no longer all of these eight states may be available, and it can then be necessary to use also some of the other states. For example, consider the situation in which switch s_1 is short-circuited, or constantly receives gate pulses due to a fault in the driver circuit. The first branch of the inverter will then constantly remain in the '10' state (short-circuiting of the dc source should always be avoided). The states that remain possible are given below. Four of them correspond to normal inverter states (indicated with '*'), the other five represent operation with one or three phase currents equal to zero.

Table 8.4. Inverter states that do not correspond to a dc-source short circuit in case switch s_1 is short-circuited.

100000	100001	100010	100100	100101*
100110*	101000	101001*	101010*	

Another example of a fault is an open-circuit of one of the switch-diode pairs (e.g. s_1 - d_1). The other pair in the concerning branch can either be conducting or non-conducting. The other branches are not affected, and table 8.5 shows that in this case there are 18 possible inverter states. However, six of these 18 states (indicated with '*') do not allow any current to be present in the machine because only one or not a single diode-switch pair is conducting. This means that there are only twelve states that might represent a useful operation state of the converter.

Table 8.5. Inverter states that do not correspond to a dc-source short circuit in case switch s_1 and diode d_1 are open circuited.

000000*	000001*	000010*	000100*	000101
000110	001000*	001001	001010	010000*
010001	010010	010100	010101	010110
011000	011001	011010		

If a failure occurs in a gate driver, causing an IGBT to remain open, or if the physical construction of the circuit is such that an IGBT might fail without a simultaneous failure of the antiparallel diode, a different situation occurs. Then, the switching device can be thought to be removed, while the conduction state of the diode will determine the branch state. Consider for example the case in which switch s_1 remains open. This can be represented by making the first bit zero in all of the normal eight command states (which correspond to the inverter states given in table 8.3). The resulting inverter states will depend on the current in phase a , as shown in table 8.6.

Table 8.6. Relation between the command state and the inverter state, in case switch s_1 receives no gate signals. A number (eg. 2) means that either the corresponding switch (s_2) or diode (d_2) is conducting.

command	current	conducting	inverter state
010101	don't care	2, 4, 6	010101
010110	don't care	2, 4, 5	010110
011001	don't care	2, 3, 6	011001
011010	don't care	2, 3, 5	011010
000101 (was 100101)	$i_{sa} > 0$	d2, 4, 6	010101
	$i_{sa} < 0$	d1, 4, 6	100101
	$i_{sa} = 0$	4, 6	000101
000110 (was 100110)	$i_{sa} > 0$	d2, 4, 5	010110
	$i_{sa} < 0$	d1, 4, 5	100110
	$i_{sa} = 0$	4, 5	000110
001001 (was 101001)	$i_{sa} > 0$	d2, 3, 6	011001
	$i_{sa} < 0$	d1, 3, 6	101001
	$i_{sa} = 0$	3, 6	001001
001010 (was 101010)	$i_{sa} > 0$	d2, 3, 5	011010
	$i_{sa} < 0$	d1, 3, 5	101010
	$i_{sa} = 0$	3, 5	001010

This table shows that if s_2 receives no gate signals and $i_{sa} < 0$, the diode which is antiparallel to the faulty IGBT will conduct. As a result, the inverter state will be the same as if no fault were present. Actually, if $i_{sa} < 0$ and switch s_2 is not conducting, the current will flow in diode d_1 whether or not switch s_1 is commanded, and a failure of s_1 is not a problem. However, if $i_{sa} > 0$, diode d_2 will conduct, and the resulting inverter states will be the same as if switch s_2 was commanded. Only in case $i_{sa} = 0$ neither d_1 nor d_2 will conduct and point 'a' will be non-connected.

Table 8.6 further shows that from only eight command states, twelve different inverter states can result – these are exactly the twelve states mentioned previously in the text related to table 8.5. An effective control of the inverter in this fault situation must take into account the sign of the stator current i_{sa} , to determine which inverter state will be obtained when applying a certain command state, and then select the optimal command state.

8.3 Modeling the machine and the inverter for normal and fault situations

To determine the effect of an inverter state on the machine, it is necessary to calculate for each state the resulting voltages or currents applied to the machine. Basically, the voltage-source inverter imposes the stator voltages of the machine, but in case of an open circuit in the converter it will under circumstances impose a phase current equal to zero.

8.3.1 The model used for simulation of the machine and the inverter

When modeling the inverter itself, it is practical to express all voltages for example with respect to the negative pole of the dc source. The output voltage of a branch under normal operation is then either equal to zero or to the voltage of the dc source. The dc-source voltage is assumed to have a given and constant value. The converter output voltages are denoted by u_{va} , u_{vb} and u_{vc} . Their relation to the stator voltages can be seen from figure 8.3, in which the voltage u_{v0} between the star point of the machine and the converter voltage reference point seems an unknown quantity. It can however be calculated, using equation 8.1, deduced from figure 8.3 and equation 4.27.

$$\begin{aligned} u_{va} &= u_{sa} + u_{v0} \\ u_{vb} &= u_{sb} + u_{v0} \\ u_{vc} &= u_{sc} + u_{v0} \quad + \\ \hline u_{va} + u_{vb} + u_{vc} &= 3 u_{s0} + 3 u_{v0} \end{aligned} \quad (8.1)$$

Considering that u_{s0} must be zero, according to equation 4.31 (no homopolar current i_{s0} can be present in this circuit), it follows that u_{v0} can be calculated from equation 8.2.

$$u_{v0} = \frac{1}{3}(u_{va} + u_{vb} + u_{vc}) \quad (8.2)$$

The individual stator voltages can now be found by subtracting u_{v0} from the converter output voltages. This corresponds to saying that the individual stator voltages are equal to the converter voltages minus their homopolar part. In this circuit, the converter can therefore not impose a homopolar stator voltage.

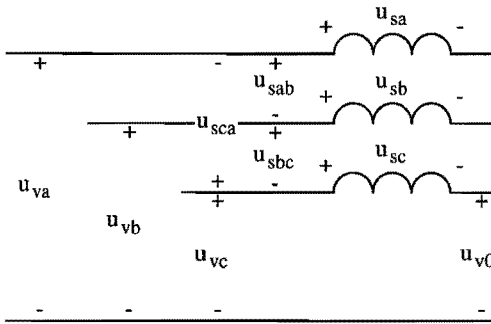


Figure 8.3. Relation between the inverter output voltages and the stator voltages.

When modeling the machine with a converter in which one of the switches remains open, it is not necessary to know the stator voltages with respect to the star point. Instead, the voltages between the stator phases, the line voltages, become important quantities. This can be understood from figure 8.4. This figure shows a part of the circuit in case both switches of the phase-a branch do not conduct, one due to a fault and one which at this particular moment does not receive any gate signals. Phase b of the machine is connected to the positive pole of the dc voltage through s3 or d3. At a certain moment the current i_{sa} will be zero, and none of the diodes d1, d2 will conduct. This situation will change if the voltage across one of the diodes becomes positive – this diode will then start conducting and i_{sa} will become unequal to zero, after which conduction of this diode will last until i_{sa} becomes zero again. As can be seen from figure 8.4, the voltage over e.g. diode d1 is equal to the voltage between the two stator phases a and b.

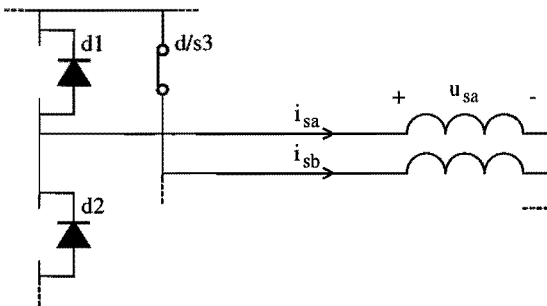


Figure 8.4. Diagram showing that if both switches in a branch are open, the voltage over a diode equals the voltage between two stator phases.

The line voltages thus play an important role in the operation of the inverter in case of device faults. Furthermore, the voltages with respect to the star point are not of so much practical interest because the star point is not connected – it might even be unavailable if the stator windings have a delta connection. Therefore it was chosen to use a model in which the stator windings are represented by equivalent delta-connected windings, using

the line voltages as inputs. These voltages are defined by equation 8.3. The definitions of both the voltages and the currents in the delta-connected circuit are shown in figure 8.5.

$$\begin{aligned} u_{sab} &= u_{sa} - u_{sb} \\ u_{sbc} &= u_{sb} - u_{sc} \\ u_{sca} &= u_{sc} - u_{sa} \end{aligned} \quad (8.3)$$

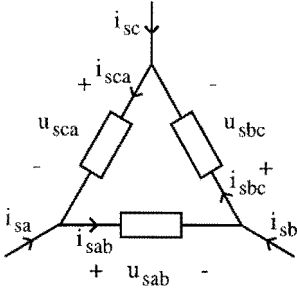


Figure 8.5. Voltage and current definitions for a delta-connected stator.

Using equations 4.27 and 4.28, the relation between the equivalent two-phase voltages and the line voltages can be calculated, as given in equations 8.4 and 8.5. The homopolar voltage u_{s0} is zero, as mentioned previously.

$$\begin{bmatrix} u_{sab} \\ u_{sbc} \\ u_{sca} \end{bmatrix} = \begin{bmatrix} \frac{3}{2} & -\frac{\sqrt{3}}{2} \\ 0 & \sqrt{3} \\ -\frac{3}{2} & -\frac{\sqrt{3}}{2} \end{bmatrix} \cdot \begin{bmatrix} u_s^{s1} \\ u_s^{s2} \end{bmatrix} \quad (8.4)$$

$$\begin{bmatrix} u_s^{s1} \\ u_s^{s2} \end{bmatrix} = \begin{bmatrix} \frac{1}{3} & 0 & -\frac{1}{3} \\ 0 & \frac{1}{\sqrt{3}} & 0 \end{bmatrix} \cdot \begin{bmatrix} u_{sab} \\ u_{sbc} \\ u_{sca} \end{bmatrix} \quad (8.5)$$

For the fluxes, which determine the induced voltages in the windings of the delta-connected stator, the same transformations are valid as for the voltages. However, for the currents a different transformation is used. The relation between the currents in the star-connected stator and the currents in the equivalent delta-connected stator is given in equation 8.6. It has been assumed that there is no circulating current in the delta-connected stator, because only an axial flux could cause such a current, and this case is not taken into consideration. The factor $1/3$ in this equation may seem illogical in comparison with equation 8.3, but is simply the result of the star-delta transformation starting from the fact that $i_{sa} = i_{sab} - i_{sca}$ etc.

$$\begin{aligned}
 i_{sab} &= \frac{1}{3}(i_{sa} - i_{sb}) \\
 i_{sbc} &= \frac{1}{3}(i_{sb} - i_{sc}) \\
 i_{sca} &= \frac{1}{3}(i_{sc} - i_{sa})
 \end{aligned} \tag{8.6}$$

Using equations 4.5 and 4.6, the relation between the equivalent two-phase currents and the currents in the delta-connected stator windings can be calculated, as given in equations 8.7 and 8.8.

$$\begin{bmatrix} i_{sab} \\ i_{sbc} \\ i_{sca} \end{bmatrix} = \begin{bmatrix} \frac{1}{3} & -\frac{1}{3\sqrt{3}} \\ 0 & \frac{2}{3\sqrt{3}} \\ -\frac{1}{3} & -\frac{1}{3\sqrt{3}} \end{bmatrix} \cdot \begin{bmatrix} i_s^1 \\ i_s^2 \end{bmatrix} \tag{8.7}$$

$$\begin{bmatrix} i_s^1 \\ i_s^2 \end{bmatrix} = \begin{bmatrix} \frac{3}{2} & 0 & -\frac{3}{2} \\ -\frac{\sqrt{3}}{2} & \sqrt{3} & -\frac{\sqrt{3}}{2} \end{bmatrix} \cdot \begin{bmatrix} i_{sab} \\ i_{sbc} \\ i_{sca} \end{bmatrix} \tag{8.8}$$

Using these equations, the relation between the voltages and the currents in the equivalent delta circuit can be calculated. Starting from equation 5.13 and its equivalent for the other two phases, setting $i_{s0} = 0$, equation 8.9 is obtained.

$$\begin{aligned}
 u_{sab} &= 3r_{sq} \cdot i_{sab} + 3l_{\sigma q} \cdot \frac{di_{sab}}{dt} + \frac{d\psi_{rsab}}{dt} \\
 u_{sbc} &= 3r_{sq} \cdot i_{sbc} + 3l_{\sigma q} \cdot \frac{di_{sbc}}{dt} + \frac{d\psi_{rsbc}}{dt} \\
 u_{sca} &= 3r_{sq} \cdot i_{sca} + 3l_{\sigma q} \cdot \frac{di_{sca}}{dt} + \frac{d\psi_{rsca}}{dt}
 \end{aligned} \tag{8.9}$$

This equation can be simplified using the relation between the parameters r_{sq} and $l_{\sigma q}$ of the windings of the star-connected stator and $r_{s\Delta}$ and $l_{\sigma\Delta}$ of the equivalent delta-connected stator windings, given in equation 8.10. The result is given in equation 8.11. The corresponding block diagram used in the simulations is shown in figure 8.6.

$$\begin{aligned}
 r_{s\Delta} &= 3r_{sq} \\
 l_{\sigma\Delta} &= 3l_{\sigma q}
 \end{aligned} \tag{8.10}$$

$$\begin{aligned}
 u_{sab} &= r_{s\Delta} \cdot i_{sab} + l_{\sigma\Delta} \cdot \frac{di_{sab}}{dt} + \frac{d\psi_{rsab}}{dt} \\
 u_{sbc} &= r_{s\Delta} \cdot i_{sbc} + l_{\sigma\Delta} \cdot \frac{di_{sbc}}{dt} + \frac{d\psi_{rsbc}}{dt} \\
 u_{sca} &= r_{s\Delta} \cdot i_{sca} + l_{\sigma\Delta} \cdot \frac{di_{sca}}{dt} + \frac{d\psi_{rsca}}{dt}
 \end{aligned} \tag{8.11}$$

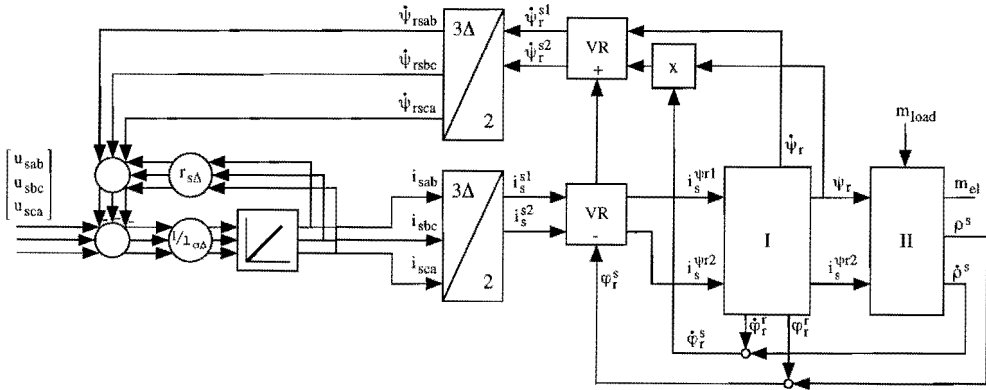


Figure 8.6. Block diagram of a voltage-fed induction machine of which the star-connected stator windings are represented by an equivalent delta connection.

It is relatively easy to modify this circuit for operation with one phase current of the star-connected stator of the machine, e.g. i_{sa} , equal to zero. From figure 8.5 it can be seen that in this case $i_{sab} = i_{sca}$, and that the voltage at terminal a with respect to the negative pole of the dc-link voltage has become an unknown quantity, say x . From equation 8.11 and the fact that $u_{sab} + u_{sca} = -u_{sbc}$ equation 8.12 is deduced. This equation can be used to calculate the current $i_{sab} = i_{sca}$.

$$i_{sab} = i_{sca} = \frac{1}{2l_{\sigma\Delta}} \int \left(-u_{sbc} - \dot{\psi}_{rsab} - \dot{\psi}_{rsca} - 2r_{s\Delta} \cdot i_{sab} \right) dt \tag{8.12}$$

It is possible to split this equation into two parts that are equal to those used for the healthy machine, by reintroducing the unknown voltage at terminal a. This is shown in equation 8.13 and in figure 8.7. For the unknown voltage an arbitrary value can be taken, because in the sum of the two integrals this value is no longer present. The advantage of this method is that the part of the block diagram containing the integrators is the same for normal and fault situations. In figure 8.7 the block diagram has been completed with the relation between the converter voltages and the line voltages, derived from figure 8.3, except that u_{va} has been replaced by the unknown voltage x .

$$i_{sab} = i_{sca} = \frac{1}{2l_{\sigma\Delta}} \left(\int \left(u_{sab} - \dot{\psi}_{rsab} - r_{s\Delta} \cdot i_{sab} \right) dt + \int \left(u_{sca} - \dot{\psi}_{rsca} - r_{s\Delta} \cdot i_{sca} \right) dt \right) \tag{8.13}$$

The simulation of a machine fed from an inverter of which one of the switches remains open, now consists of two parts: the simulation for the time interval where the current in the concerning phase is not zero (using the diagram of figure 8.6) and the time interval during which it is zero (figure 8.7). Switching between these topologies is triggered by the current in the faulty phase becoming zero or by a diode voltage becoming positive.

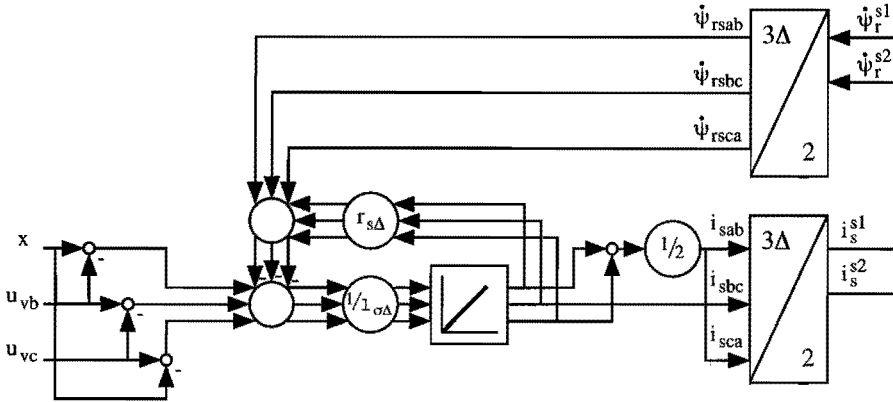


Figure 8.7. Part of the block diagram for the simulation of an inverter-fed induction machine of which one of the phase currents of the star-connected stator is zero.

However, this simulation method has one important drawback. The abrupt changing from one topology to another as soon as a variable crosses zero, causes an unstable behavior: in certain situations, the system switches between the two topologies every two or three simulation time steps. Therefore, an alternative simulation method has been implemented. Instead of using the diagram of figure 8.7 in case of an open circuit, it was assumed that a non-conducting diode can be represented by a high resistance. The voltage at terminal a in case both diodes (and switches) of branch a are non-conducting is then given by equation 8.14.

$$u_{va} = \frac{u_{dc} - r_{off} \cdot i_{sa}}{2} \quad (8.14)$$

Unfortunately, the value that can be used for r_{off} is limited by the simulation time step. If r_{off} is taken too large, instability will result. It can be shown that the value for which this occurs is proportional to the leakage inductance and inversely proportional to the time step. If a time step of $10 \mu s$ is used (which is so small that real-time simulation is not possible on the available DSP system) r_{off} has to be smaller than 117 pu. This is not a very large value, which means that the current in the simulated open phase will not be exactly equal to zero. This will be visible in the simulations.

The state of a diode (conducting or non-conducting) was determined by observing the diode current: if it surpassed a certain minimal value (i_{lim}), the diode was assumed to conduct (resistance zero), otherwise it was modeled by r_{off} . Figure 8.8 resumes the model used for each branch of the inverter.

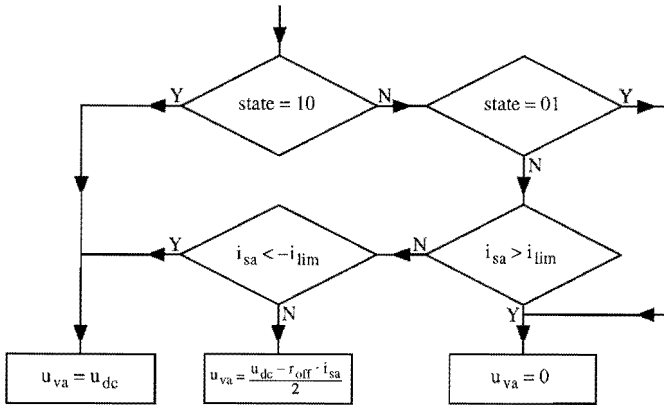


Figure 8.8. Flowchart representing the model used for each phase of the inverter.

8.3.2 The choice of a reference coordinate system for inverter control

When studying the effect of different inverter states in normal and fault operation on the behavior of the machine, it is important to choose which quantities will be considered. Many authors (see e.g. [Depe-85], [Taka-86]) base their studies either on the current or the flux vector in stator coordinates, or on the current vector in stator-flux coordinates. It is even possible to consider the stator-flux vector (or actually the integral of the voltage vector) in stator-flux reference coordinates ([Velt-94]). All of these methods have in common that they use a coordinate system that is closely related to the behavior of the inverter. In fact, under normal operation the inverter (with zero internal impedance) produces seven different voltage vectors (in stator coordinates), and the effect of these voltages on quantities such as the stator-flux vector or the current in stator (flux) coordinates is relatively easy to calculate. The effect of such a voltage vector on air-gap or rotor-flux oriented quantities is much more difficult to understand.

Yet there is an important advantage to rotor-flux orientation that makes it a good choice for studying and optimizing inverter control in case of device faults. This becomes clear when the influence of voltage harmonics on the stator, air-gap and rotor fluxes is compared.

To derive the relation between harmonic voltage components and the different flux vectors, first the relation between the voltage- and the rotor-flux vector will be derived, in complex notation. In this notation the real part of each quantity corresponds to the $s1$ component of the original vector, and the imaginary part to the $s2$ component. The derivation has been based on figure 2.14, redrawn in figure 8.9 using the complex notation. Differentiation and integration have been replaced by a multiplication by s or $1/s$, respectively. Here s is equal to $j\hat{\alpha}_s^s$, where $\hat{\alpha}_s^s$ is the frequency of the stator voltage. This derivation is only valid for a constant $\hat{\alpha}_s^s$, and can therefore not be used to calculate

transients. Furthermore, the two vector rotators have been eliminated – the term $-j\dot{\rho}^s$ is the result of this elimination, assuming a constant rotor speed $\dot{\rho}^s$.

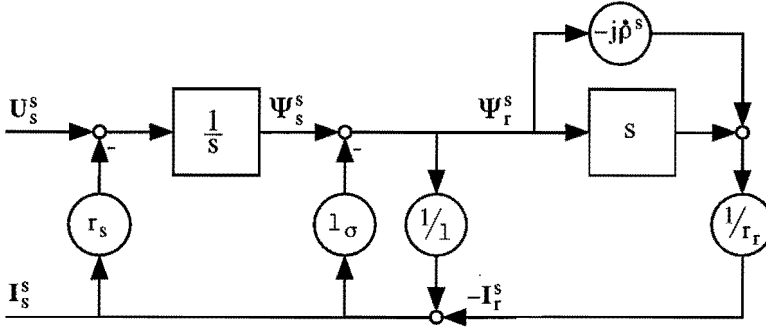


Figure 8.9. Block diagram of the machine using complex notation.

From the block diagram, equation 8.15 can be derived, in which q_1 and q_2 are given by equation 8.16. The relation between the complex voltage and the rotor-flux vector derived from this equation is given in equation 8.17.

$$\Psi_r^s = \frac{1}{s} U_s^s - \left(\frac{r_s}{s} + 1_{\sigma} \right) (q_1 s + q_2) \Psi_r^s \quad (8.15)$$

$$q_1 = \frac{1}{r_r} \quad (8.16)$$

$$q_2 = \frac{1}{1} - j\dot{\rho}^s \frac{1}{r_r}$$

$$\frac{\Psi_r^s}{U_s^s} = \frac{1}{q_1 1_{\sigma} s^2 + (1 + q_1 r_s + q_2 1_{\sigma}) s + q_2 r_s} \quad (8.17)$$

The relation between the current and the rotor flux, and between the current and the voltage is given in equation 8.18.

$$I_s^s = (q_1 s + q_2) \Psi_r^s = \frac{(q_1 s + q_2) U_s^s}{q_1 1_{\sigma} s^2 + (1 + q_1 r_s + q_2 1_{\sigma}) s + q_2 r_s} \quad (8.18)$$

Now that the relation between the voltage, the current and the rotor flux is known, the relation between the voltage and other fluxes can be derived. The general relation between the stator voltage and current and an arbitrary flux is given in equation 8.19. If in this equation \tilde{r}_s is taken equal to r_s and $\tilde{1}_{\sigma}$ equal to 1_{σ} , the flux obtained is equal to the rotor flux. Taking $\tilde{1}_{\sigma}$ equal to zero results in the stator flux, while a certain intermediate value of $\tilde{1}_{\sigma}$ corresponds to the air-gap flux. Values of $\tilde{1}_{\sigma}$ larger than 1_{σ} do not result in a flux with a physical meaning.

$$\tilde{\Psi}^s = \frac{1}{s} U_s^s - \left(\frac{\tilde{r}_s}{s} + \tilde{l}_\sigma \right) I_s^s \tag{8.19}$$

Substitution of equation 8.18 into 8.19 gives the relation between the arbitrary flux $\tilde{\Psi}^s$ and the stator voltage U_s^s . This relation is given in equation 8.20.

$$\frac{\tilde{\Psi}^s}{U_s^s} = \frac{q_1(1_\sigma - \tilde{l}_\sigma) s^2 + (1 + q_1(r_s - \tilde{r}_s) + q_2(1_\sigma - \tilde{l}_\sigma)) s + q_2(r_s - \tilde{r}_s)}{q_1 1_\sigma s^3 + (1 + q_1 r_s + q_2 1_\sigma) s^2 + q_2 r_s s} \tag{8.20}$$

Substitution in this equation of $\tilde{l}_\sigma = 1_\sigma$ and $\tilde{r}_s = r_s$ yields equation 8.17, as expected. The relation between the voltage and the rotor flux as given in equation 8.17 corresponds for high frequencies to a second order low-pass filter, which means that high frequency components in the stator voltage will have little or no effect on the rotor flux. The relation given in equation 8.20 is for $\tilde{l}_\sigma \neq 1_\sigma$ at high frequencies only a first order low-pass filter. This means that on fluxes such as the air-gap and stator flux, high frequency voltage components will have much more influence than on the rotor flux. This is illustrated by figure 8.10, which shows the transfer function from the voltage to different fluxes, with $\tilde{l}_\sigma / 1_\sigma$ as a parameter, for a rotor speed of $\hat{\rho}^s = 1$ pu.

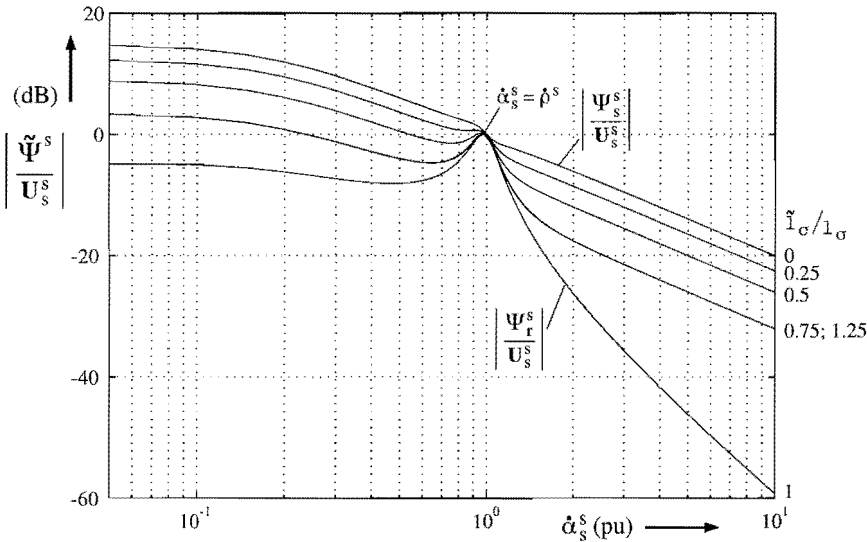


Figure 8.10. Transfer function from the stator voltage to different fluxes.

After this consideration the advantage of rotor-flux orientation can easily be explained. In case of a fault, the stator current and voltage no longer have their desired values, but will contain important oscillations at a frequency higher than the rotor speed (see the simulations and experiments in Chapter 7). These oscillations will find their way to the torque produced by the machine for two different reasons. First of all, the oscillation of the current will have a direct influence on the torque, as the torque depends directly on the

current. Secondly, the current oscillations will also cause an oscillation in the flux, and the oscillation of the flux has also a direct effect on the torque. The rotor flux is the flux that is most insensitive to current or voltage oscillations. Therefore, if rotor-flux orientation is used, it is possible to neglect in a first approximation the oscillations of the flux, and assume that torque variations depend only on the current component perpendicular to this flux.

Rotor-flux orientation can therefore be seen as a means of decomposing the stator current into two components that influence the torque in a very different way. The “torque producing component” $i_s^{\psi r2}$ has a direct influence on the torque: even the fastest transients in this current component are exactly reproduced by the torque. The other current component, the magnetizing current $i_s^{\psi r1}$, also influences the torque, but any fast transients in this component are maximally damped because of the low-pass characteristic of the transfer function between the current and the rotor flux.

This means that for converter control most attention has to be paid to $i_s^{\psi r2}$, while $i_s^{\psi r1}$ can be allowed to contain some oscillations. Orientation on any other flux does not have this interesting property, and seems therefore less appropriate for converter control in case of faults.

It may be noted that equation 8.19 is actually the equation of a u/i -model, a model to calculate the rotor flux from given stator-voltage and -current vectors (cf. section 3.6). The calculation results shown in figure 8.10 indicate a possibility to estimate the parameter l_σ of the machine. To find l_σ , it is sufficient to supply the machine from a non-sinusoidal source (such as a switching power converter), and then tune the parameter \check{l}_σ until the ripple in the model flux is minimized. This was also shown in [Casa-93]. It can be calculated that also in case \check{r}_s is not equal to r_s the ripple will be minimal for $\check{l}_\sigma = l_\sigma$. This method was used in the experimental setup to determine the leakage inductance of the machine. The resulting \check{l}_σ will however only be correct if l_σ is not frequency dependent.

8.3.3 Relation between the inverter state and the machine currents

In this section the effect of each inverter state on the machine will be studied, to be able to select the optimal inverter states during normal and fault operation. For this purpose the rate of change of the field-oriented current components will be calculated for different inverter states. The basic equation used for this has been derived from equation 3.19, and is given below in equation 8.21.

$$\begin{bmatrix} \dot{i}_s^{\psi r1} \\ \dot{i}_s^{\psi r2} \end{bmatrix} = \frac{1}{l_\sigma} \begin{bmatrix} u_s^{\psi r1} \\ u_s^{\psi r2} \end{bmatrix} - \frac{1}{l_\sigma} \begin{bmatrix} \dot{\psi}_r \\ \dot{\phi}_r^s \cdot \psi_r \end{bmatrix} + \begin{bmatrix} \dot{\phi}_r^s \cdot i_s^{\psi r2} \\ -\dot{\phi}_r^s \cdot i_s^{\psi r1} \end{bmatrix} - \frac{r_s}{l_\sigma} \begin{bmatrix} i_s^{\psi r1} \\ i_s^{\psi r2} \end{bmatrix} \quad (8.21)$$

According to this equation, the rate of change of the field-oriented current vector can be split into two parts: one which depends only on the applied voltage, and another which depends on the rotor flux and the actual current, given in equation 8.22.

$$\left. \begin{bmatrix} \dot{i}_s^{\psi r1} \\ \dot{i}_s^{\psi r2} \end{bmatrix} \right|_{\mathbf{u}=0} = -\frac{1}{L_\sigma} \begin{bmatrix} \dot{\psi}_r \\ \dot{\phi}_r^s \cdot \psi_r \end{bmatrix} + \begin{bmatrix} \dot{\phi}_r^s \cdot i_s^{\psi r2} \\ -\dot{\phi}_r^s \cdot i_s^{\psi r1} \end{bmatrix} - \frac{r_s}{L_\sigma} \begin{bmatrix} i_s^{\psi r1} \\ i_s^{\psi r2} \end{bmatrix} \quad (8.22)$$

If the applied voltage is zero and the machine is operating in normal conditions at a sufficiently high speed, the rate of change is approximately equal to the value given in equation 8.23. This means that if zero voltage is applied, the torque-producing current will change in such a direction that it slows down the machine.

$$\left. \begin{bmatrix} \dot{i}_s^{\psi r1} \\ \dot{i}_s^{\psi r2} \end{bmatrix} \right|_{\mathbf{u}=0} \approx -\frac{1}{L_\sigma} \begin{bmatrix} 0 \\ \dot{\phi}_r^s \cdot \psi_r \end{bmatrix} \quad (8.23)$$

For non-zero voltage vectors, first the voltage vector in rotor-flux oriented coordinates has to be calculated according to equation 8.24.

$$\begin{bmatrix} u_s^{\psi r1} \\ u_s^{\psi r2} \end{bmatrix} = \mathbf{R}(-\varphi_r^s) \cdot \begin{bmatrix} u_s^{s1} \\ u_s^{s2} \end{bmatrix} \quad (8.24)$$

The stator-voltage vector in stator coordinates can easily be calculated in case no open circuits are present in the converter. For example, if the inverter state is '010110', the converter voltages will be $u_{va} = 0$, $u_{vb} = 0$ and $u_{vc} = u_{dc}$. The stator voltages will then be $u_{sab} = 0$, $u_{sbc} = -u_{dc}$ and $u_{sca} = u_{dc}$, from which (according to equation 8.5) $u_s^{s1} = -1/3 u_{dc}$ and $u_s^{s2} = -1/\sqrt{3} u_{dc}$. The results for the other states in which no open circuit is present are given in the first eight rows of table 8.7.

If one of the phases of the star-connected stator is opened, the calculation of the stator-voltage vector is slightly more difficult. For example, if phase a is not connected, the voltage u_{sbc} is still determined by the inverter state, but u_{sab} and u_{sca} have to be calculated using equation 8.11. However, due to the fact that now i_{sab} equals i_{sca} , the stator voltages can be described using equation 8.25, in which u_x is still an unknown voltage.

$$\begin{aligned} u_{sab} &= u_x + \dot{\psi}_{rsab} \\ u_{sbc} &= u_{vb} - u_{vc} \\ u_{sca} &= u_x + \dot{\psi}_{rsca} \end{aligned} \quad (8.25)$$

It is possible to calculate u_x by substituting equation 8.25 into 8.26. Using equation 8.27, equation 8.28 is obtained.

$$u_{sab} + u_{sbc} + u_{sca} = 0 \quad (8.26)$$

$$\dot{\psi}_{rsab} + \dot{\psi}_{rsbc} + \dot{\psi}_{rsca} = 0 \quad (8.27)$$

$$2u_x - \dot{\psi}_{rsbc} + u_{sbc} = 0 \Rightarrow u_x = \frac{1}{2} \dot{\psi}_{rsbc} - \frac{1}{2} u_{sbc} \quad (8.28)$$

By combining equations 8.28 and 8.25 and using equation 8.5, the value of the stator-voltage vector is found, as shown in equation 8.29.

$$\begin{aligned} u_s^{s1} &= \frac{1}{3} (u_x + \dot{\psi}_{rsab}) - \frac{1}{3} (u_x + \dot{\psi}_{rsca}) = \frac{1}{3} (\dot{\psi}_{rsab} - \dot{\psi}_{rsca}) \\ u_s^{s2} &= \frac{1}{\sqrt{3}} (u_{vb} - u_{vc}) \end{aligned} \quad (8.29)$$

In the same way the stator-voltage vector can be found for the cases where phase b or phase c are opened. The results are given in equation 8.30 and 8.31, respectively. Using these equations, the stator-voltage vector has been calculated for all possible inverter states in which one phase is opened. A part of the results is listed in table 8.7.

$$\begin{aligned} u_s^{s1} &= \frac{1}{3} \dot{\psi}_{rsab} + \frac{1}{6} \dot{\psi}_{rsca} - \frac{1}{2} u_{sca} \\ u_s^{s2} &= -\frac{1}{\sqrt{3}} \dot{\psi}_{rsab} - \frac{1}{2\sqrt{3}} \dot{\psi}_{rsca} - \frac{1}{2\sqrt{3}} u_{sca} \end{aligned} \quad (8.30)$$

$$\begin{aligned} u_s^{s1} &= -\frac{1}{6} \dot{\psi}_{rsab} - \frac{1}{3} \dot{\psi}_{rsca} + \frac{1}{2} u_{sab} \\ u_s^{s2} &= -\frac{1}{2\sqrt{3}} \dot{\psi}_{rsab} - \frac{1}{\sqrt{3}} \dot{\psi}_{rsca} - \frac{1}{2\sqrt{3}} u_{sab} \end{aligned} \quad (8.31)$$

Table 8.7. Relation between the inverter state and the stator-voltage vector.

inverter state	u_s^{s1}	u_s^{s2}
010101	0	0
100101	$2/3 u_{dc}$	0
101001	$1/3 u_{dc}$	$1/\sqrt{3} u_{dc}$
011001	$-1/3 u_{dc}$	$1/\sqrt{3} u_{dc}$
011010	$-2/3 u_{dc}$	0
010110	$-1/3 u_{dc}$	$-1/\sqrt{3} u_{dc}$
100110	$1/3 u_{dc}$	$-1/\sqrt{3} u_{dc}$
101010	0	0
000101	$1/3 \dot{\psi}_{rsab} - 1/3 \dot{\psi}_{rsca}$	0
001001	$1/3 \dot{\psi}_{rsab} - 1/3 \dot{\psi}_{rsca}$	$1/\sqrt{3} u_{dc}$
001010	$1/3 \dot{\psi}_{rsab} - 1/3 \dot{\psi}_{rsca}$	0
000110	$1/3 \dot{\psi}_{rsab} - 1/3 \dot{\psi}_{rsca}$	$-1/\sqrt{3} u_{dc}$
010001	$1/3 \dot{\psi}_{rsab} + 1/6 \dot{\psi}_{rsca}$	$-1/\sqrt{3} \dot{\psi}_{rsab} - 1/2\sqrt{3} \dot{\psi}_{rsca}$
100001	$1/3 \dot{\psi}_{rsab} + 1/6 \dot{\psi}_{rsca} + 1/2 u_{dc}$	$1/\sqrt{3} \dot{\psi}_{rsab} - 1/2\sqrt{3} \dot{\psi}_{rsca} + 1/2\sqrt{3} u_{dc}$
etc.		

For each of the inverter states, the voltages indicated in table 8.7 can be used to calculate the effect of that state on the field-oriented current components. Equations 8.21 and 8.24 show that the result will depend heavily on the actual flux angle, speed and amplitude, but also the actual current plays a role. To visualize the influence of the different quantities, figure 8.11 has been drawn. This figure shows a rotor-flux plane, in which for different values of $(\psi_r^{s1}, \psi_r^{s2})$ equation 8.21 has been evaluated. The inverter state examined was '100101'. The dc-link voltage u_{dc} was equal to 2 pu, and the magnetizing current $i_s^{\psi r1}$ was set to $\psi_r/1$ in all of the calculation points. The direction of the arrows indicates the direction in which the field-oriented stator current vector $i_s^{\psi r}$ would change if this inverter state were applied: an arrow to the right indicates an increase of $i_s^{\psi r1}$, to the left a decrease of $i_s^{\psi r1}$, up an increase of $i_s^{\psi r2}$, down a decrease. The length of the arrows indicates the speed at which this change would occur. The circle represents normal operation with a rotor flux of 1 pu. No values were calculated for the point where the rotor flux is zero, because no field-oriented current can be defined in this case.

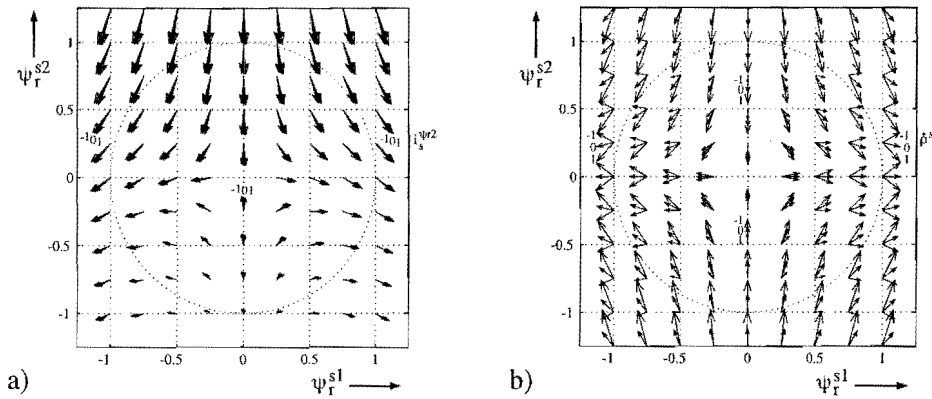


Figure 8.11. Rate of change of the rotor-flux-oriented stator-current vector as a function of the rotor-flux vector, for different values of the torque producing current (a) and of the rotor speed (b), for inverter state '100101'.

In figure 8.11a the rotor speed is set to a constant positive value of 1 pu, while different values are used for the torque-producing current component. For positive values of ψ_r^{s2} the arrows become very large, indicating a very large rate of change of the current. This can be explained from the fact that the flux-induced voltage and the applied voltage are in this case approximately opposite to each other (see table 8.7 for the voltage). For $(\psi_r^{s1}, \psi_r^{s2}) = (0, -1)$, the rate of change is almost zero because the induced and applied voltages are nearly equal. For high flux values all arrows point downwards. This indicates that operation with a flux level higher than 1 pu is not possible at this speed with this dc-link voltage.

Inverter state '100101' is normally used only in those operating points where it causes a small rate of change of the current, i.e., around $(\psi_r^{s1}, \psi_r^{s2}) = (0, -1)$ (for positive rotor speeds). This can also be understood by considering the effect of this state on the (stator) flux. The rate of change of the stator-flux vector is approximately equal to the applied stator-voltage vector, and for this state this means a change in the positive $s1$ direction. Such a flux movement is normally required (at positive speed) when $(\psi_r^{s1}, \psi_r^{s2})$ is around $(0, -1)$.

Figure 8.11b shows the influence of the rotor speed on the rate of change of the current. Whereas for positive speed inverter state '100101' causes a small rate of change around $(\psi_r^{s1}, \psi_r^{s2}) = (0, -1)$, for negative speed a small rate of change is obtained at completely the opposite site of the flux circle.

Together, these figures show that there is no simple approximation of the rate of change of the rotor-flux-oriented current which is valid for all speeds and all currents. This is a clear disadvantage of any control method based on this rate of change compared to a control method based for example on the easy-to-calculate rate of change of the stator-flux vector.

An overview of the effect of all inverter states for operation with $s1$ constantly opened is shown in figure 8.12. In figure 8.12a the rate of change of the current has been drawn for the eight inverter states under normal operation, for a rotor speed of 1 pu and a torque-producing current equal to zero. There are six so-called active states – those are the states for which the applied voltage vector is not zero. These states (numbers 1 to 6) result in six different current directions. If at one position in the flux plane a certain state is found to result in one current change, 60 degrees from that position the next inverter state will result in the same current change. States 0 and 7 correspond to a zero voltage vector. They both have the same effect on the current: in all cases (for positive speed) they have the effect of decreasing the torque-producing current component. This corresponds to the well-known phenomenon that a machine which is short-circuited will act as a brake.

In figure 8.12b, the states in which either switch $s1$ or diode $d1$ was active have been replaced by states in which the complete phase-a branch of the inverter is non-conducting. As a result, this figure shows all possible current-change directions for the case where both $s1$ and $d1$ are non-conducting. In this figure, states 1 and 7 coincide, because both represent the situation where i_{sa} and u_{sbc} are zero. Examination of this figure shows that the most difficult operation point occurs when the rotor-flux vector points in the $(0, -1)$ direction. In that direction there is no vector available to increase the torque-producing current component. The vectors that maintain $i_s^{\psi r2}$ at a constant level do either cause an important increase or an important decrease of the magnetizing current. This means that at this operating point it will be very difficult or impossible to select switching states that maintain a desired average value of $i_s^{\psi r2}$ and $i_s^{\psi r1}$.

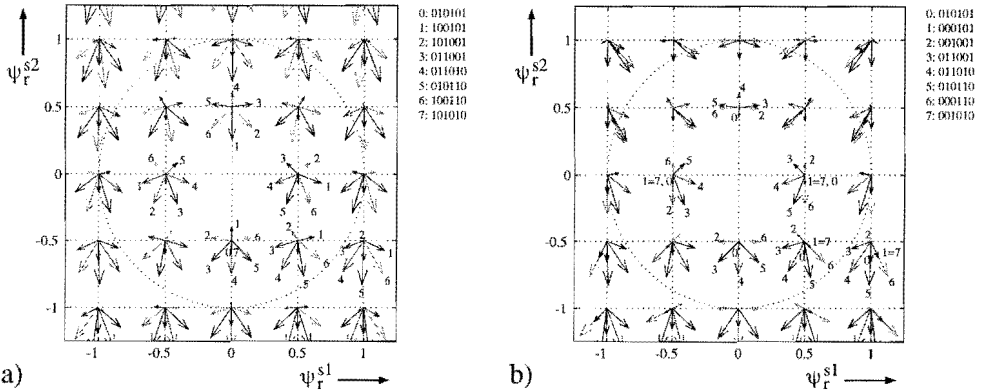


Figure 8.12. Rate of change of the rotor-flux oriented stator-current vector as a function of the rotor-flux vector, for all inverter states used for normal operation (a) and for those inverter states that are available in case $s1$ and $d1$ are non-conducting (b).

The challenge for the inverter control will be to choose both under normal operation and under fault operation those inverter states that yield as closely as possible the desired average field-oriented current vector. Whereas under normal operation (see figure 8.12a) there is often more than one inverter state that causes a change of one of the current components in a given direction, during a fault (figure 8.12b) it may occur that there is not even one state available to generate a current change in a required direction.

8.3.4 The limit between normal and fault operation

In case switch $s1$ is constantly open, if diode $d1$ is present and functioning, figure 8.12b alone does not represent the correct current-change directions for all command states. For certain values of the flux, diode $d1$ will conduct, so that the inverter states of figure 8.12a are available, while for other values not, resulting in the states of figure 8.12b. In this section it will be shown for which values of the flux and under which other conditions, normal operation according to figure 8.12a can be expected, and when not.

First of all it must be noted that out of the eight normal inverter states, four states are not affected by an open circuit of $s1$ and $d1$ (numbers 0, 3, 4 and 5). These are the states for which $s2$ receives gate signals, so that either $s2$ or $d2$ is conducting. To determine the operating conditions where these states are normally used and where they will be used also in case of this fault, it is practical to consider the rate of change of the flux. For simplicity it will be assumed that the stator resistance and the leakage inductance can be neglected, so that the time derivative of the rotor-flux vector in stator coordinates is equal to the applied stator voltage vector. Figure 8.13 shows the flux directions for the six normal active inverter states, and the sectors in the flux plane where they are normally applied. In

each 60-degree sector, two active states are used, while the two zero-voltage states can be used in all sectors, causing the flux vector in stator coordinates to remain constant.

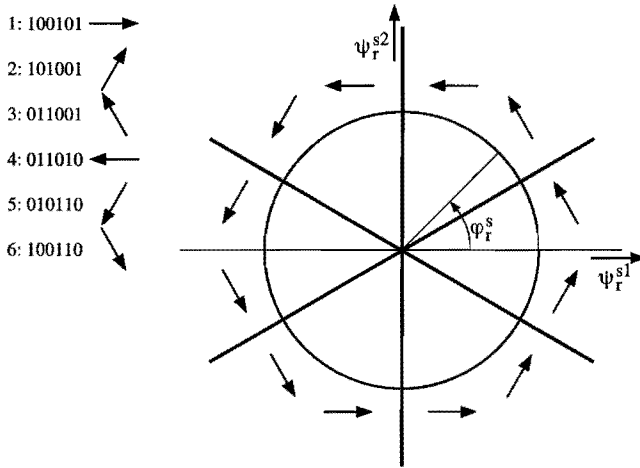


Figure 8.13. Rate of change of the flux vector for different active inverter states and the sectors in which these states are normally used (for a positive flux speed).

From this figure it becomes clear that in the two sectors for which the flux angle φ_r^s lies between 30° and 150° , only states are used that are not affected by the $s1$ fault (states ‘011001’, ‘011010’ and ‘010110’). In all other sectors of the flux plane at least one of the affected states is required (states ‘100101’, ‘101001’ and ‘100110’). The zero-voltage states (‘010101’ and ‘101010’) are both used in all sectors, but in case one of them is not available the other might be used instead. Normally, a zero-voltage state is chosen in such a way that the number of switching operations is minimized, but if there is only one zero-voltage state available, this is no longer an option.

In that part of the rotor flux plane where $i_{sa} < 0$, operation is also not affected by an open circuit of $s1$. In this case, as soon as switch $s2$ stops conducting, the current commutates to diode $d1$, not $s1$. This operation is limited by the points where $i_{sa} = 0$. From equation 4.6 it follows that this corresponds to $i_s^{s1} = 0$, while $i_{s0} = 0$. Using equation 8.32, equation 8.33 is derived, from which equation 8.34 is found by taking $i_s^{s1} = 0$.

$$\begin{bmatrix} i_s^{s1} \\ i_s^{s2} \\ i_s^s \end{bmatrix} = R(\varphi_r^s) \cdot \begin{bmatrix} i_s^{\psi r1} \\ i_s^{\psi r2} \end{bmatrix} = \begin{bmatrix} \cos \varphi_r^s & -\sin \varphi_r^s \\ \sin \varphi_r^s & \cos \varphi_r^s \end{bmatrix} \cdot \begin{bmatrix} i_s^{\psi r1} \\ i_s^{\psi r2} \end{bmatrix} \tag{8.32}$$

$$i_s^{s1} = i_s^{\psi r1} \cdot \cos \varphi_r^s - i_s^{\psi r2} \cdot \sin \varphi_r^s \tag{8.33}$$

$$\varphi_r^s = \arctan \left(\frac{i_s^{\psi r1}}{i_s^{\psi r2}} \right) \pmod{\pi} \tag{8.34}$$

After substituting $i_s^{\psi r1} = 1/1$ to obtain a rated rotor flux, this equation can be used to calculate the angles φ_r^s for which $i_{sa} = 0$, as a function of $i_s^{\psi r2}$. From this it can be shown that for example for $i_s^{\psi r2} = -1$, the area with $i_{sa} > 0$ corresponds to the area where $-11^\circ < \varphi_r^s < 169^\circ$, while for $i_s^{\psi r2} = 1$ this area is defined by $-169^\circ < \varphi_r^s < 11^\circ$.

Figure 8.14 shows those areas where states using s1-d1 are used while at the same time $i_{sa} > 0$. These are the areas where normal operation of the inverter is no longer possible, so that a special control technique will have to be designed for them. This will be most difficult for motor operation with a large, positive $i_s^{\psi r2}$, because then the problem area is very large.

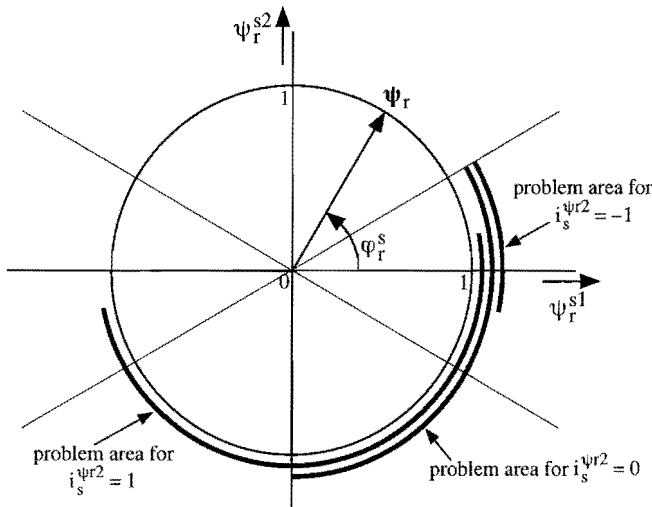


Figure 8.14. Problem areas for operation when switch s1 refuses to conduct under different load situations for positive speed, in case the stator resistance and the leakage inductance are neglected.

8.4 Control methods for the voltage-source inverter

The objective of a control system for an inverter-fed induction machine is to command the inverter switches in such a way that the machine operates with the required torque, flux, speed, etc. In the most simple situation, the control system consists of a separate inverter control and machine control. The inverter control is in that case only responsible for either the machine voltages or the machine currents, while the machine control calculates the voltages or currents required to obtain a desired flux and torque, speed or rotor position. The machine control can then be designed without knowledge of the switching characteristics of the inverter, assuming the inverter to be ideal, as was done in Chapter 3.

The most elementary and simple inverter control is the three-phase hysteresis current control, which will be discussed in section 8.4.1. Its switching behavior is far from ideal and leaves much room for improvement. In this thesis it is only used as a reference, to compare a simple current control with a more sophisticated control.

Better performance of the system (regarding for example switching losses) can be obtained by integrating the inverter and machine controls. In such a control system, switching actions of the inverter are triggered by comparing machine quantities such as the stator flux, the torque or field-oriented currents with their command values. This type of control allows to prioritize the control of certain quantities compared to others. For example, it is possible to guarantee that the torque remains within certain limits while at the same time minimizing the number of switching operations, by putting less severe restrictions on the control of other quantities.

For inverter control during fault situations this is the preferred method, because in fault situations priorities will be different from those under normal operation, and the control must be adapted to this. In section 8.4.2 priorities during fault operation will be defined, and an optimal control will be developed. Section 8.4.3 will show how this control was implemented on the multi-DSP system.

8.4.1 Three-phase hysteresis control

Three-phase hysteresis control is the most elementary current control that exists for the voltage-source inverter. It is extremely easy to realize using analog electronics, resulting in a cheap and fast control circuit. The switching rules of the inverter are described for each inverter branch separately and independently, and are given in equation 8.35. In this equation, Δ_i is equal to one half of the hysteresis band width.

$$\begin{aligned} i_{sq} > i_{sq}^* + \Delta_i &\Rightarrow \text{switch to } 01 \\ i_{sq} < i_{sq}^* - \Delta_i &\Rightarrow \text{switch to } 10 \end{aligned} \quad (8.35)$$

In practice however, the three phase currents cannot be controlled fully independently, as the sum of the currents is zero. Switching one branch will affect also the currents in the other two phases. This can be seen from figure 8.15, which shows one of the phase currents, its hysteresis band and the command state of the corresponding inverter branch. Whenever any of the three branches is switched, the gradient of the shown current changes.

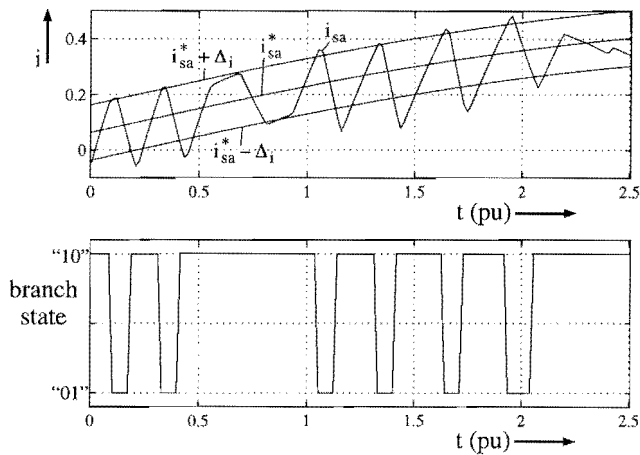


Figure 8.15. One of the phase currents and its hysteresis band together with the branch command state of the three-phase hysteresis-controlled inverter-fed induction machine.

The three-phase hysteresis control is implemented completely using quantities given in the fixed stator-coordinate frame. Control of field-oriented quantities or the torque is done at a higher level. As a result, the average values of the field oriented currents and the torque correspond to their desired values, but the ripple in these quantities varies and can not be controlled directly. This is illustrated by figure 8.16. Figure 8.16a shows the field-oriented stator-current components, while figure 8.16b shows the torque.

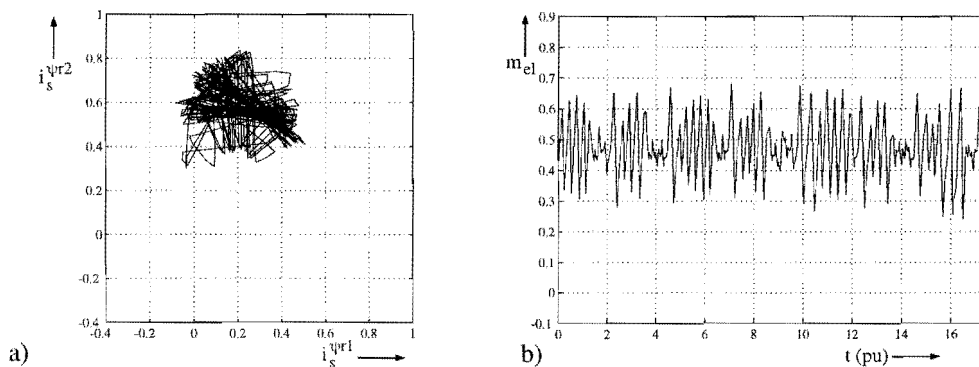


Figure 8.16. The rotor-flux oriented stator-current vector (a) and the torque (b) of the three-phase hysteresis-controlled inverter-fed induction machine.

The hysteresis control shown in these figures was implemented on the same DSP system as used for the control described in the next section. The calculation time step was chosen equal for both controls. Due to the number of calculations required for the more complicated control, the time step could not be made smaller than $55 \mu\text{s}$. As a result, the hysteresis band had to have a relatively large width of $2\Delta_i = 0.2 \text{ pu}$. Normally this parameter would be determined by the maximum allowed switching frequency of the

inverter, resulting for this inverter in a much smaller hysteresis band. A clear disadvantage of the DSP implementation of this control is also the delay between the current measurement and the resulting switching action, causing considerable current overshoot. This delay of approximately $25 \mu\text{s}$ makes the behavior of this control even worse than it would have been in an analog implementation. However, as will be shown in the simulations in the following sections, it does not considerably change the behavior of the inverter in case of a fault situation.

In the measurements shown here the average torque was set to almost 0.5 pu. The rotor flux was 0.8 pu, for which in this machine already saturation is noticeable. The rotor speed was 0.4 pu or 1200 rpm, which is the same speed as used for the experiments and simulations of the previous chapter. At no-load, this corresponds to a stator-current period of 15.7 pu. The dc-link voltage was chosen equal to 1 pu, allowing a maximum speed (without flux weakening) of approximately 0.5 pu. This corresponds to the maximum speed that could be obtained with the cycloconverter and dc-load machine that were used on the same setup previously.

8.4.2 Optimized control for operation during faults

In case of a failure of one of the inverter devices or of one of the gate drivers, it will no longer be possible to maintain under all circumstances the desired torque or field-oriented current components, due to the lack of complete redundancy. In this situation it is necessary to know, the control of which quantities is most important for the functioning of the drive. For example, a control in which the torque is kept as constant as possible will show a very different behavior from a control in which the instantaneous power flowing into the converter is maintained at a constant level. The priorities that will be used to develop an optimal control of the machine during faults are given below, in order of descending priority. This means that the second priority will only be taken into consideration if the first priority has already been met, and so forth.

1. Current limitation. The most important condition that the control must satisfy is current limitation, because a current which becomes too high could damage the converter or disable more devices due to the tripping of fuses. Normally, currents are already limited by limitation of the desired values. In case of a fault however, when currents will necessarily deviate from their desired values, instantaneous current limitation must be implemented in the inverter control itself.
2. Desired torque. The torque should be kept within a hysteresis band around its desired value. If this condition can not be met, measures must be taken to limit as much as possible the deviation from the hysteresis band, and the torque must be made to return to the band as soon as possible. This condition does not yet guarantee that the average

torque will be equal to the desired torque – a possible difference under fault conditions could be compensated by a controller at a higher level.

3. Desired rotor flux. To maintain the rotor flux at its desired value, the magnetizing current component should be kept within a hysteresis band around its desired value. If this condition can not be met, measures must be taken to limit the deviation from the hysteresis band, and the magnetizing current should be made to return to the band as soon as possible. At sufficiently high speeds, this condition is less important than maintaining the torque within its hysteresis band, due to the time constant of the rotor circuit. Again, this condition does not guarantee that the average flux will be equal to the desired flux – a possible difference under fault conditions could be compensated by a controller at a higher level.
4. Minimal switching frequency. Limitation of the number of switching operations is required to limit the converter losses and in order not to exceed the maximum switching frequency of the inverter. Practically, this condition means that if the torque or the magnetizing current is within its hysteresis band, preferably that switching state should be chosen which causes the slowest change of this quantity. If a state causing a rapid change were chosen, soon a new switching operation would be required. In case the deviation of the torque or of the magnetizing current from their respective hysteresis bands is very large, it is no longer useful to choose the state that causes the slowest change of the torque and magnetizing current. Instead, a state will be chosen which returns them to their hysteresis bands as soon as possible, first the torque and then the magnetizing current. Evidently the width of the hysteresis bands must also be chosen in function of the allowable or desired switching frequency.

Now that these priorities have been defined, an inverter control can be developed which acts according to these priorities under all circumstances. There are two possible approaches to this problem. A first possibility is to define a separate set of inverter switching rules for each normal operating condition and each fault condition. The other possibility is to define switching rules in such a way that they are valid under all circumstances. In the first case an existing inverter control can be extended with special rules for operating conditions that occur during a fault, using standard switching rules for normal operation, while in the second case a completely new set of rules must be developed.

If the first option is chosen, the system must recognize the operating and fault condition it is in, and act accordingly. For each of these conditions, the switching rules are very simple, such as “if, in this condition, the torque is increasing, switch back to the inverter command state used previously, otherwise don’t do anything”. Defining the conditions is however more complicated. An example of such a condition is “switch s_1 constantly open, current in phase a is zero, current in other phases close to current limit, torque within its hysteresis band, magnetizing current high above its hysteresis band, rotor flux

in the fourth quadrant, rotor speed positive". From this description it will be clear that there is a very large number of possible conditions, and that one of the difficulties is to reduce this number to a minimum while at the same time keeping the switching rules for each of them as simple as possible.

Using this method, if more different types of converter faults have to be taken into consideration, the control will rapidly become very complicated, due to the increasingly large number of possible conditions. Here the second method has a clear advantage. If general rules can be designed to choose under all circumstances between the different possible inverter command states, these rules will function independently of device faults, rotor speed, etc.. These switching rules must be based on the effect that each of the inverter command states has on the system, as determined in section 8.3.3.

The priorities defined above can now be translated into a number of generally valid rules to select an optimal inverter command state. If none of the priorities had to be met, it would be possible to choose at random one of the possible command states. Each of the priorities limits this number of allowable states, until one optimal choice remains. For example, the first priority prohibits the choice of command states that cause the current to exceed the current limit, and only currents that do not cause this to happen are then available to satisfy the second priority. If none of the command states can satisfy a priority, the command state that comes closest to satisfying it has to be chosen, and lower priorities cannot be considered.

A complete overview of the switching rules is shown in figure 8.17. Starting at the top, where all possible inverter command states are eligible, each of the priorities eliminates a number of possibilities, until finally only one state remains. For the current limitation, the criterion is given in equation 8.36. In this equation h is a small positive number, and the derivatives of the current-vector components are calculated for each command state according to the method described in section 8.3.3. The value $[i_s]_{\max}$ is the maximum allowed value of the length of the current vector. Under symmetrical operation, this corresponds to 1.5 times the maximum amplitude of each of the phase currents, while under operation with one phase current equal to zero it is equal to $\sqrt{3}$ times this value (cf. equation 5.19).

$$\left(i_s^{\psi r1} + h \cdot \frac{di_s^{\psi r1}}{dt} \right)^2 + \left(i_s^{\psi r2} + h \cdot \frac{di_s^{\psi r2}}{dt} \right)^2 \leq [i_s]_{\max}^2 \quad (8.36)$$

By how much the torque and the magnetizing current are out of their hysteresis bands, is calculated using two auxiliary quantities Δm_{el}^* and $\Delta i_s^{\psi r1*}$, defined in equations 8.37 and 8.38. In these equations, Δm and Δi_j are equal to one half of the hysteresis band width of the torque and of the magnetizing current, respectively.

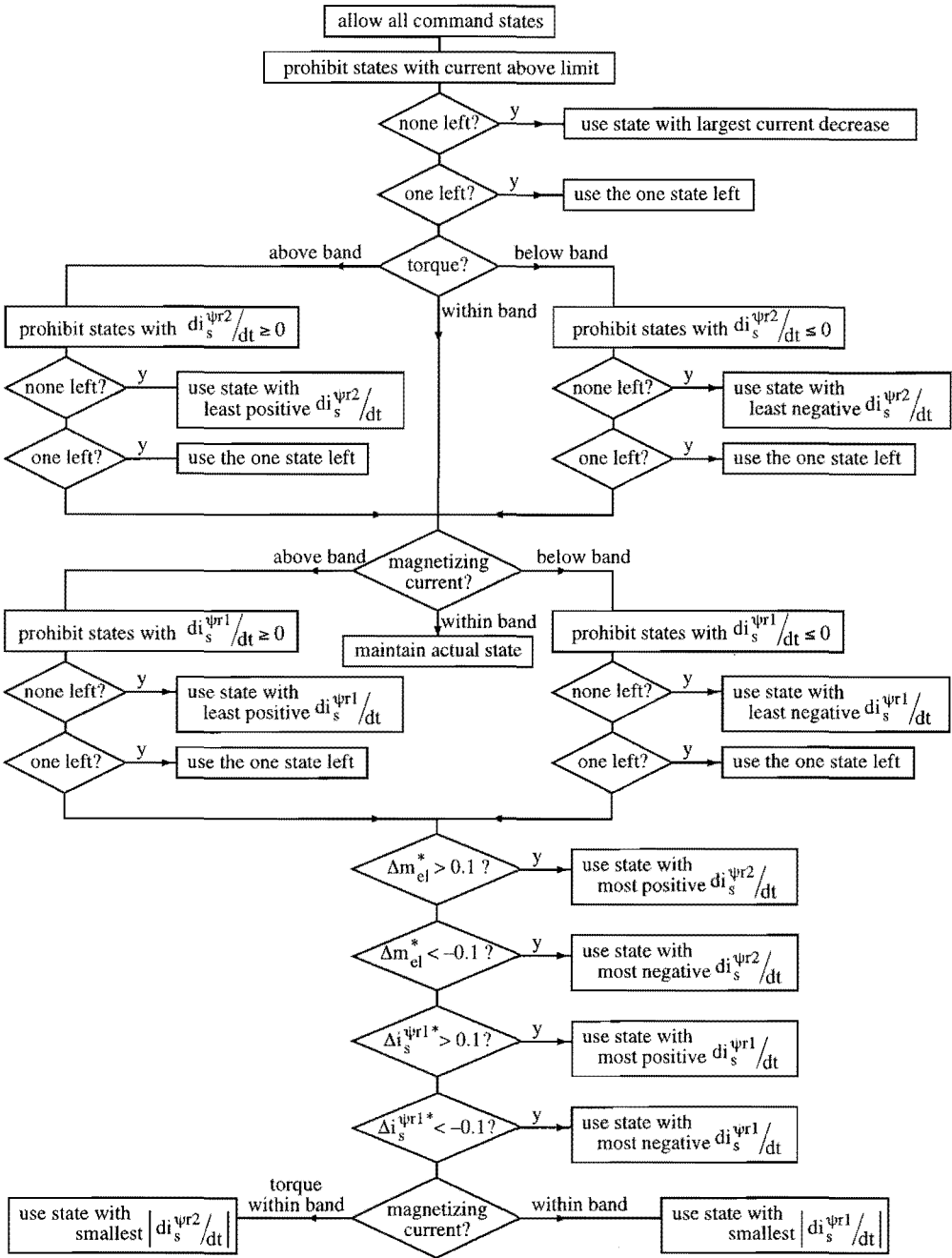


Figure 8.17. Flowchart of the selection procedure for inverter command states.

$$\Delta m_{el}^* = \begin{cases} (m_{el}^* + \Delta m) - m_{el} & (m_{el} \geq m_{el}^* + \Delta m) \\ (m_{el}^* - \Delta m) - m_{el} & (m_{el} \leq m_{el}^* - \Delta m) \\ 0 & (m_{el}^* - \Delta m < m_{el} < m_{el}^* + \Delta m) \end{cases} \quad (8.37)$$

$$\Delta i_s^{\psi r1*} = \begin{cases} (i_s^{\psi r1*} + \Delta i) - i_s^{\psi r1} & (i_s^{\psi r1} \geq i_s^{\psi r1*} + \Delta i) \\ (i_s^{\psi r1*} - \Delta i) - i_s^{\psi r1} & (i_s^{\psi r1} \leq i_s^{\psi r1*} - \Delta i) \\ 0 & (i_s^{\psi r1*} - \Delta i < i_s^{\psi r1} < i_s^{\psi r1*} + \Delta i) \end{cases} \quad (8.38)$$

Figure 8.18 shows into which areas this control method divides the $i_s^{\psi r1} - m_{el}$ plane. In area number 0, no control action takes place, because both the torque and the magnetizing current are within their hysteresis bands. Area 9 is the current limitation area. In figure 8.18 this area has been drawn for the case where $\psi_r = 1$, which means that $m_{el} = i_s^{\psi r2}$. Under no circumstances the current vector will enter this area.

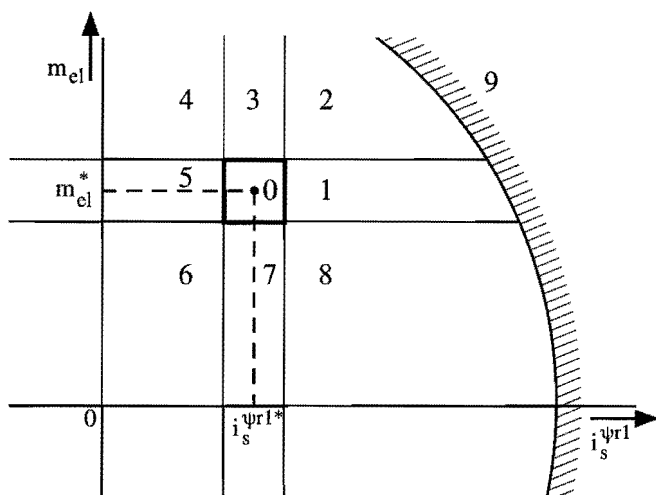


Figure 8.18. Areas in the $i_s^{\psi r1} - m_{el}$ plane for which a different control strategy results.

To give a further example, the areas 2, 3 and 4 are the areas in which a new command state will be chosen that reduces the torque, requiring a state with $di_s^{\psi r2}/dt < 0$. Only in fault situations the system might be in one of these areas for a longer period of time. If the torque reaches a value very much outside the hysteresis band, for example more than 0.1 pu, an extra effort must be made to return it to normal operation (see figure 8.17, at the bottom).

A special strategy has been implemented for the areas 1 and 5. This is not shown in figure 8.17. In case a zero-voltage state is selected, the current vector will move almost vertically, according to equations 8.22 and 8.23. If in such a situation the system leaves area 0 to enter area 1 or 5, it is not necessary to take any action, because the limits for i_s^{pr1} are not so strict as those for m_{e1} . By not switching in this case, the number of switching operations (priority 4) is reduced considerably.

8.4.3 Implementation of the control on a multi-DSP system

Development and implementation of the different inverter-control methods has been performed in three distinct steps. First, a “single-step” simulation program was developed. This program had two different operation modes. In the first mode, the machine model was fed from an ideal current source, and simulation was run in real time. This allowed to bring the machine model into the desired operating condition (speed, flux, load). In the other operation mode, the machine model was fed from the inverter model. The command state of the inverter was selected manually by the user of the program – after selection of a new inverter command state, the simulation was allowed to run during a predefined small number of time steps, after which another state could be chosen. This method allowed a detailed observation of the effect of each inverter command state on the machine quantities. If the selected command state had not the desired effect, the built-in undo feature allowed to go back in time and select another state.

After this, the different control methods described in section 8.4.1 and 8.4.2 were implemented in the simulation. Due to the large number of calculations required, combined with a required small calculation time step of 10 or 55 μs , it was not possible to simulate in real time using only a single DSP. The simulations were therefore performed at a speed below real time – the time in the simulations was running a factor two to six slower than the real time, depending on the simulation time step. The simulation program was set up in such a way that an inverter fault could be switched on and off during the simulation, which allowed to test the control method under development both in a healthy situation and under fault conditions.

As a final step, after the control had been thoroughly tested in the simulations, the program had to be adapted for control of the experimental setup. The machine model was eliminated from the program, and tasks were divided over two processors in such a way that both processors needed the same amount of calculation time for each control time step. Using two processors was absolutely necessary to satisfy the real-time constraint. At the same time, a large effort was put into optimizing the different macro routines on the DSP. Without this optimization it would not have been possible to realize a control that was fast enough. This means that for the current generation of signal processors the use of a high level programming language was not an option (see Appendix A).

Figure 8.20 shows the block diagram of the control system corresponding to the control described in section 8.4.2. The control functions as follows. First, processor B obtains measured voltages and currents from the machine. After a transformation, these values are transmitted to processor A. Processor A contains the rotor-flux observer. From the given stator voltages and currents it estimates first the stator-flux, then the rotor-flux vector. From this vector also the (filtered) rotor-flux angle and speed are calculated. Using these data, equation 8.21 is implemented for eight possible command states. First equation 8.22 is evaluated, which is a common part of equation 8.21 for all states, and then for each state the part containing the voltage is added. The rate of change of the field-oriented stator-current components for each of the possible command states is then transferred to processor B, where they will be used one time step later. Processor B performs the selection of the optimal command state, and outputs this state to the inverter.

The current and torque obtained using this control in a no-fault situation are shown in figure 8.19. Figure 8.19a shows the field-oriented current components. The control should keep both components within a hysteresis band, resulting in a rectangular area for the current vector. Due to delays introduced by the digital system, as well as non-ideal switching at points near to the corners of the area, some current overshoot is present. In the torque, shown in figure 8.19b, this overshoot can be seen as short dips to levels outside the normal torque hysteresis band. Furthermore, it can be seen that although the torque hysteresis band was set to $2\Delta_m = 0.2$ pu, the actual band is larger, due to the delay of approximately $50 \mu\text{s}$ introduced by the control. It will thus be clear that this is by no means an “ideal” inverter control – its main purpose is to obtain a truly optimal behavior in case of converter faults.

As in figure 8.16, the rotor speed was 0.4 pu, the rotor flux 0.8 pu, the average torque nearly 0.5 pu and the dc-link voltage 1 pu. These values will also be used in all simulations and measurements in case of converter faults throughout the rest of this chapter, unless stated otherwise.

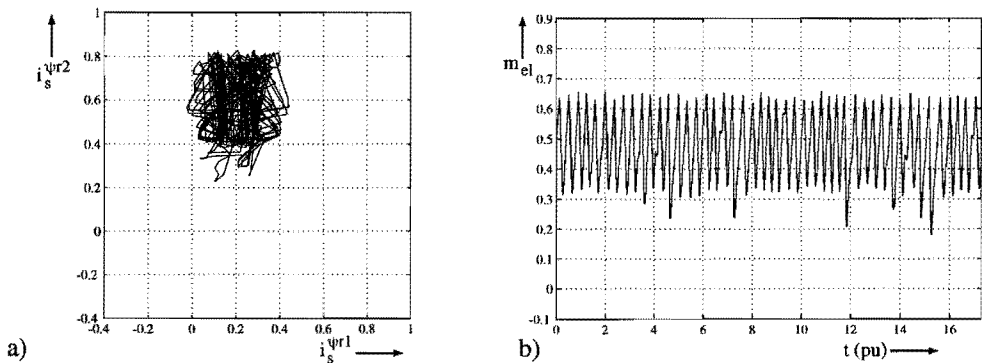


Figure 8.19. The rotor-flux oriented stator-current vector (a) and the torque (b) of the optimally controlled inverter-fed induction machine.

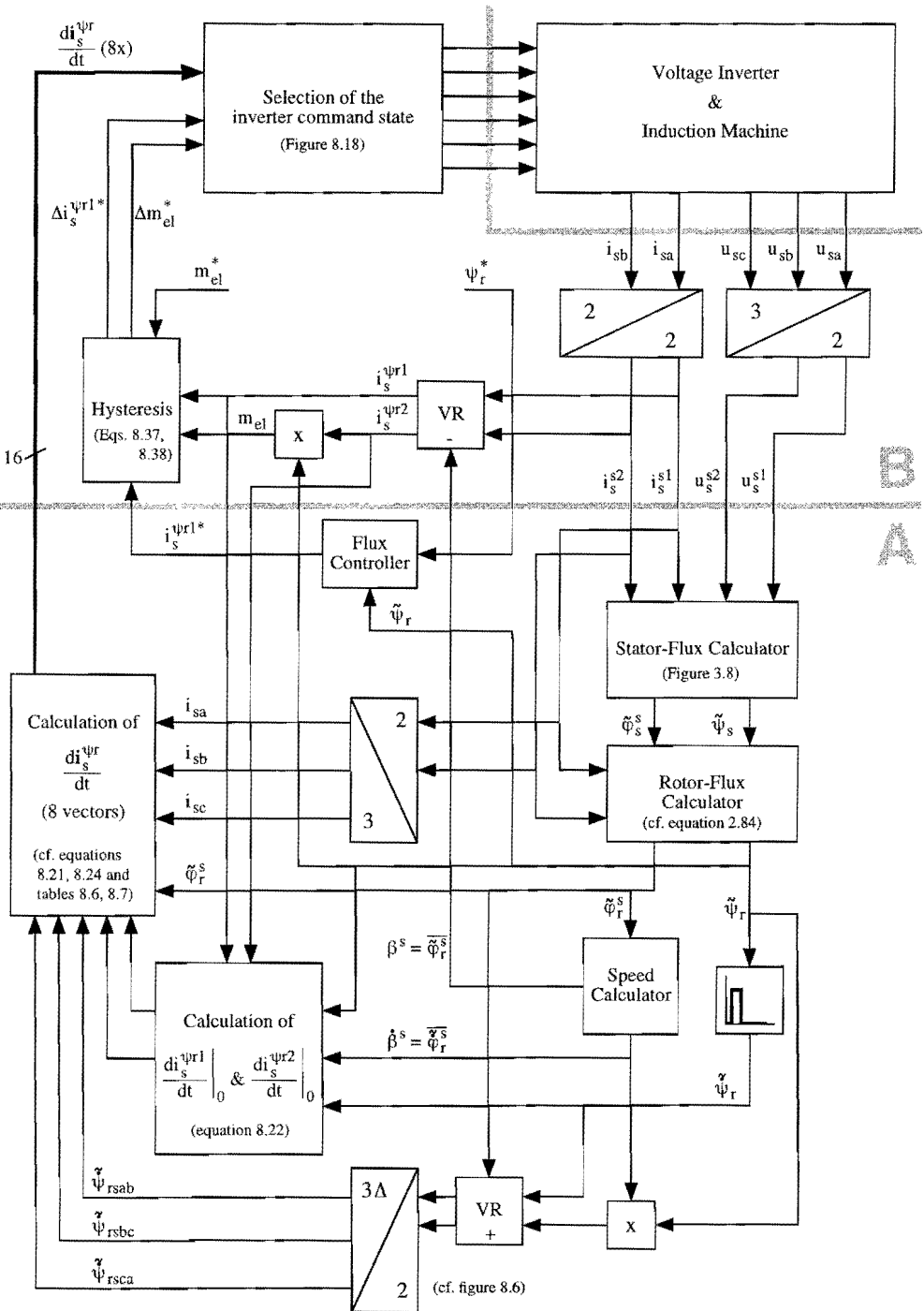


Figure 8.20. Block diagram of the inverter and machine control according to section 8.4.2, showing the distribution of tasks over two digital signal processors A and B.

8.5 Asymmetrical operation in case of a single-device fault

In this section both types of inverter control will be tested in case one IGBT refuses to conduct. In a simulation also the effect of a short circuit of one of the switching devices will be shown. The two controls will then be compared.

8.5.1 Simulation of the three-phase hysteresis control during an IGBT fault

First, the three-phase hysteresis control was tested in case of a single-IGBT fault. The initial conditions were the same as in the experiments shown in the previous section, only the load torque was reduced to match the reduced average torque produced by the machine during this fault. As operation was expected to be different for motor and generator modes, simulations were performed for both a desired torque of 0.5 and -0.5 pu. First the results for motor operation will be discussed.

Figure 8.21 shows the field-oriented stator-current vector and the torque, in case of a fault of IGBT s_1 . In the problem area (see figure 8.14), the phase currents will not respond to the controller in the desired way, and as a result a long and deep torque dip occurs. During the rest of the period, the system behaves almost as normally (cf. figure 8.16).

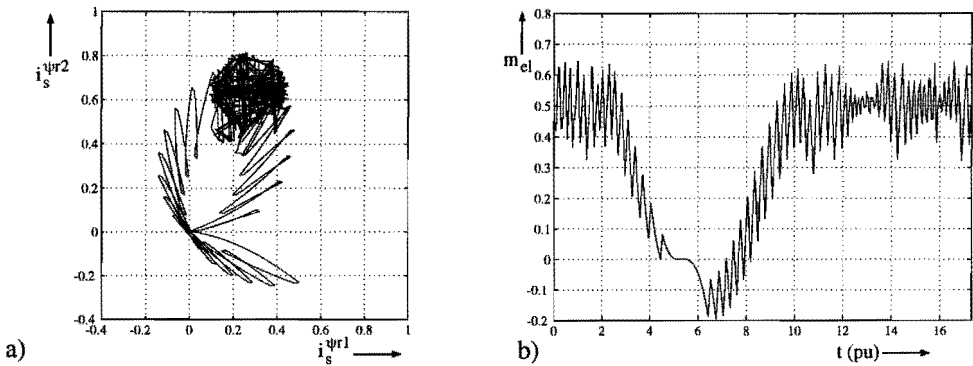


Figure 8.21. Simulation showing the field-oriented stator-current vector (a) and the torque (b) of a three-phase hysteresis-controlled inverter-fed induction machine under motor operation, in case of a single-IGBT fault.

It is interesting to observe also the behavior of the individual stator currents, shown in figure 8.22. Due to the fact that in motor operation a positive i_{sa} almost exclusively depends on IGBT s_1 and only slightly on diode d_2 , in this case i_{sa} hardly ever becomes positive. Instead, i_{sa} is zero during half a period, and so is i_s^{s1} . It can be noted that in this simulation these currents are not exactly zero, due to the fact that non-conducting switches and diodes have been modeled using an off-resistance of 110 pu. Using a higher

resistance was not possible without further decrease of the simulation time step, which already was set to the relatively small value of $10 \mu\text{s}$. While $i_{sa} = 0$, evidently $i_{sb} = -i_{sc}$, and as a result the current controllers for these two phases are not capable of maintaining the desired sinusoidal current in these two phases.

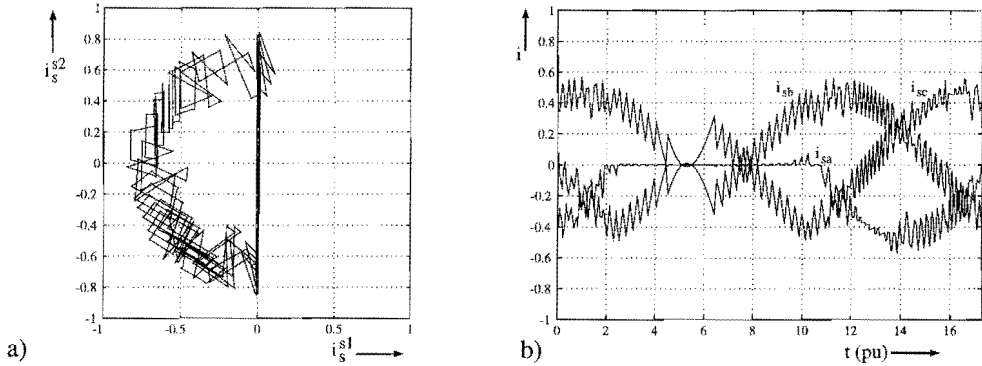


Figure 8.22. Simulation showing the stator-current vector (a) and the three stator currents (b) of a three-phase hysteresis-controlled inverter-fed induction machine under motor operation, in case of a single-IGBT fault.

Finally, figure 8.23 shows the rotor- and stator-flux vectors. In figure 8.23a, for motor operation, it can be seen that the stator flux is affected by the fault during a large time interval, as expected from figure 8.14. The rotor flux is however hardly affected at all.

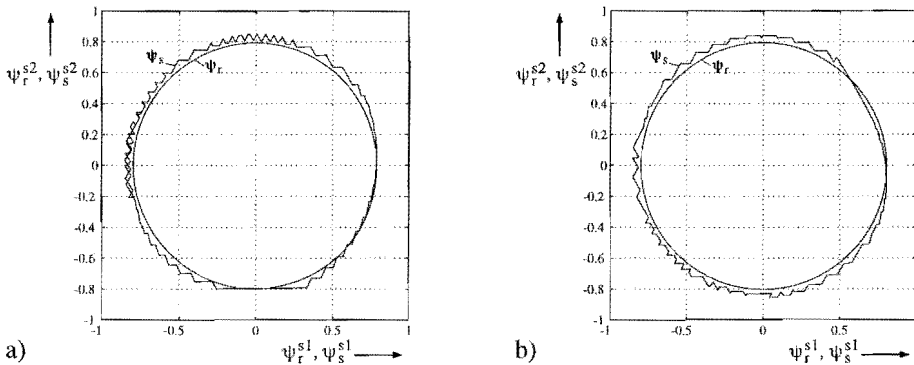


Figure 8.23. Simulation showing the rotor-flux and stator-flux vectors of a three-phase hysteresis-controlled inverter-fed induction machine, under motor operation (a) and generator operation (b), in case of a single-IGBT fault.

A different situation occurs in generator mode. The time interval during which quantities are affected by the fault is much smaller, as can be seen in figure 8.23b for the fluxes. The field-oriented stator current, shown in figure 8.24a, mainly shows some demagnetization,

which is compensated by the flux controller. The torque, shown in figure 8.24b, only shows a rather small – yet noticeable – dip.

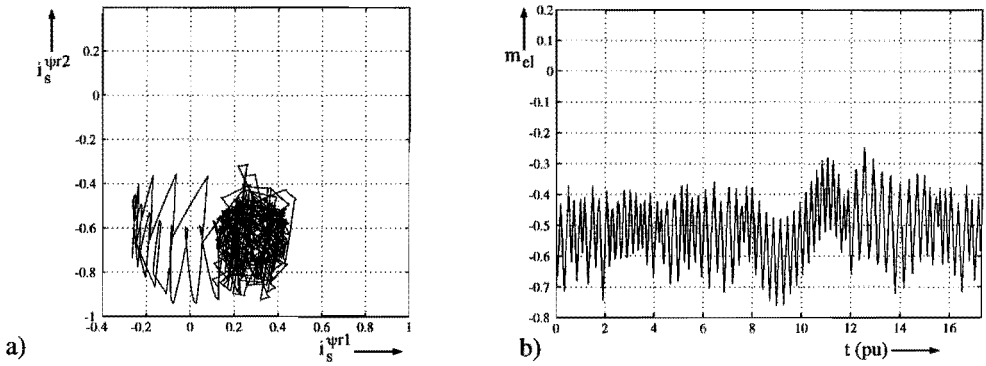


Figure 8.24. Simulation showing the field-oriented stator-current vector (a) and the torque (b) of a three-phase hysteresis-controlled inverter-fed induction machine under generator operation, in case of a single-IGBT fault.

The explanation for this more favorable situation can be understood from figure 8.25. Although the current i_{sa} is zero during a short interval of time, diode d2 now allows i_{sa} to become positive. For the stator-current vector, shown in figure 8.25a, this means that although it seems to stop moving at the bottom of the figure, as was the case in figure 8.22a, it succeeds to “catch up” with its desired value shortly afterwards. However, as in the previous case, the stator currents do deviate from their desired values, and the torque shows an uncontrolled dip. The fact that this dip is relatively small is however already an indication that with a proper control technique this dip might be avoided.

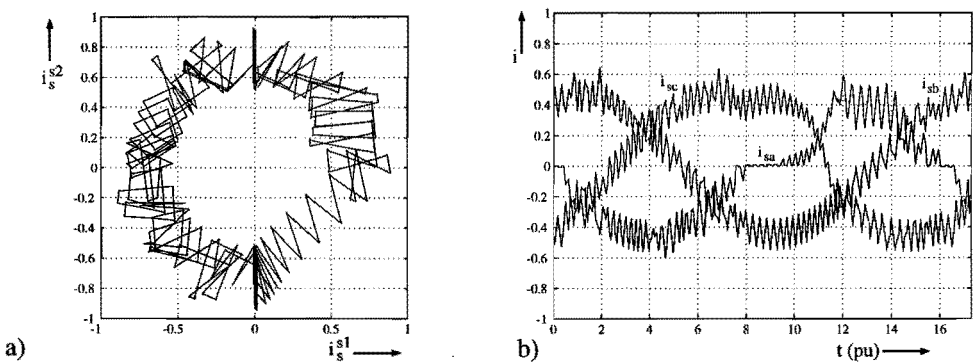


Figure 8.25. Simulation showing the stator-current vector (a) and the three stator currents (b) of a three-phase hysteresis-controlled inverter-fed induction machine under generator operation, in case of a single-IGBT fault.

8.5.2 Experiments with the three-phase hysteresis control during an IGBT fault

Using the same control program as in the simulations, the hysteresis control was also tested on a real machine for the case of a fault of IGBT s_1 . There are however some important differences between the simulations and the experiments. First of all the calculation time step in the experiments could not be made smaller than $55 \mu\text{s}$. As a result, the currents are outside their hysteresis bands by a larger amount before a correcting action is taken.

A second difference is the delay between the current measurement and the change of the inverter command signals. In the experiments, this delay is approximately $25 \mu\text{s}$, while in the simulations no delay is present. On the other hand, the integration method used in the simulations introduces also a small delay, which is visible if the current waveforms of the simulation (flattened peaks) are compared with the measurements (sharp peaks).

Finally, the problem occurring in the simulation regarding the limited off-resistance of switching devices is not present in the experiments. As a result, when no IGBTs or diodes in a branch are conducting, the corresponding phase current will really be zero.

Figure 8.26 shows the stator-current vector and the torque for motor operation, with all parameters equal to those in the simulations shown in figure 8.21. Comparison of the figures reveals that there is a good correspondence between simulations and experiments, while the differences can be explained with the considerations given above. The most noticeable difference is that in the experiments the hysteresis control performs less well due to the delays which this control introduces.

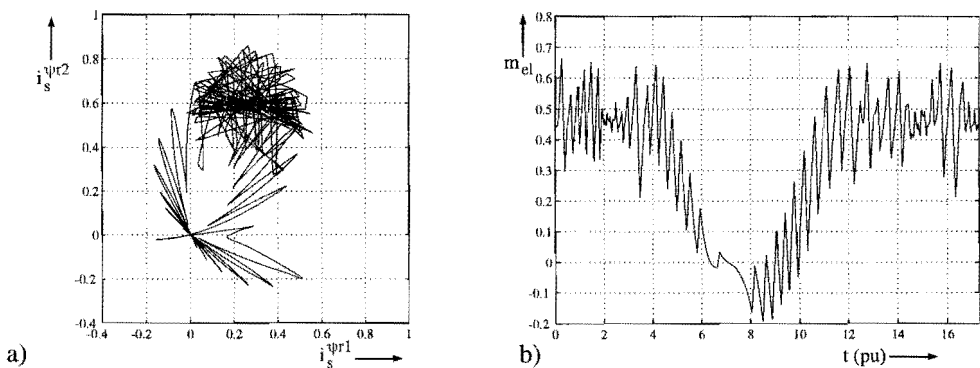


Figure 8.26. The field-oriented stator-current vector (a) and the torque (b) of a three-phase hysteresis-controlled inverter-fed induction machine under motor operation, in case of a single-IGBT fault.

The stator currents for this case are shown in figure 8.27, to be compared with the simulated currents from figure 8.22.

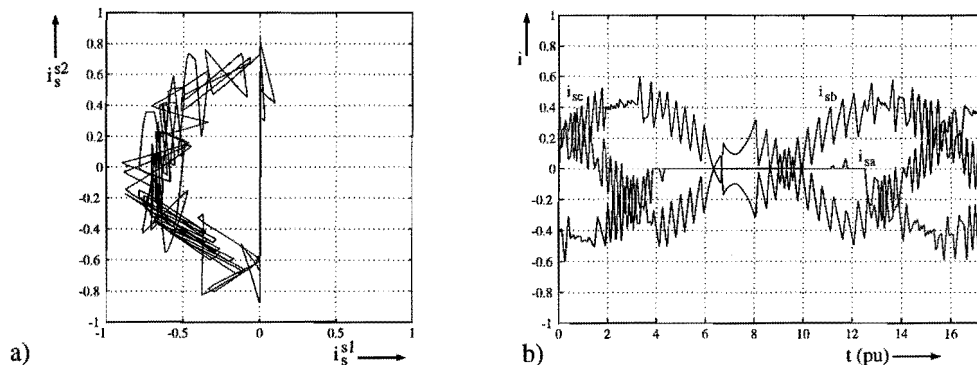


Figure 8.27. The stator-current vector (a) and the three stator currents (b) of a three-phase hysteresis-controlled inverter-fed induction machine under motor operation, in case of a single-IGBT fault.

For generator mode, only the stator-current vector and the torque are shown, in figure 8.28. Parameters for the measurements presented in this figure correspond to those of the simulation shown in figure 8.24. Also here the experimental hysteresis control performs less well than the much faster simulated control, but essentially the experimental system behaves as was expected.

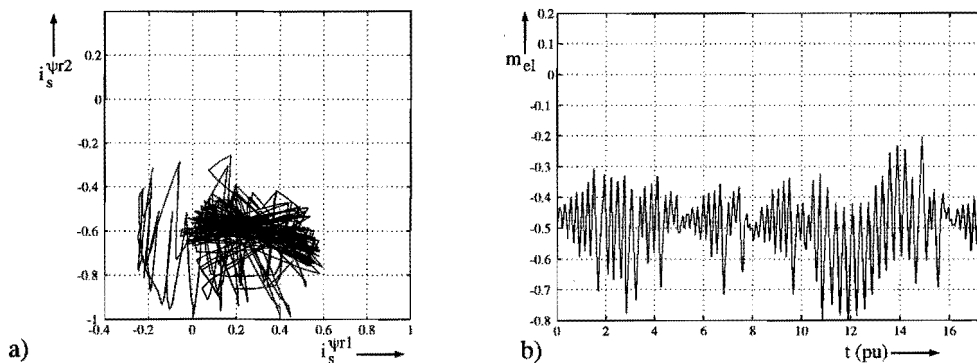


Figure 8.28. The field-oriented stator-current vector (a) and the torque (b) of a three-phase hysteresis-controlled inverter-fed induction machine under generator operation, in case of a single-IGBT fault.

8.5.3 Simulation of the optimized control during an IGBT fault

The three-phase hysteresis control used in the previous section showed under fault situations a behavior that was far from ideal. Under motor operation, during almost one half of the period the torque was below the desired level, remaining close to, or even below zero during one quarter of the period. If the machine was used as a generator, a shorter and less severe dip occurred. In this section, it will be examined what the torque would look like in these situations if all the attention of the control system were focused on maintaining a constant torque level, giving a higher priority only to current limitation.

For this purpose, simulations were performed using the control method developed in section 8.4.2. To facilitate a comparison of the results, all conditions were taken equal to those in the simulations with the hysteresis control. This includes also the simulation time step of $10 \mu\text{s}$. The current limitation for i_s (cf. equation 8.36) was set to 1.4 pu, which under operation with one phase current equal to zero results in a limitation for the phase currents of 0.82 pu. First, motor operation was simulated.

Figure 8.29 shows the field-oriented stator-current vector and the corresponding torque. By comparing the torque with the one shown in figure 8.21b it is clear that the optimized control method results in a torque that is much less affected by the fault. The reason for this is found by comparing figure 8.29a with figure 8.21a. In case of a three-phase hysteresis current control, the torque-producing current component will start decreasing as soon as the current in phase a becomes zero. This causes a torque dip that lasts for half a period. With the optimized control, as soon as i_{sa} becomes zero, the current in the other phases will be adapted in such a way that the torque-producing current remains constant. At the same time however, the magnetizing-current component will increase, and at a certain moment, current limitation will become necessary. As soon as current limitation occurs, decrease of the torque to zero becomes unavoidable. However, as soon as the torque reaches zero, the current in the remaining phases can be reversed (see figure 8.30b), and the torque will increase again.

Evidently, the current reversal takes a certain amount of time, depending among others on the dc-link voltage. After the reversal, current limitation will occur again, which ends as soon as the torque reaches the top of its hysteresis band. From that moment on, the torque will remain within its hysteresis band, and also the magnetizing current will return to its band.

Due to the variation in the magnetizing current, the rotor flux will not be perfectly constant. At the time of the current reversal, the flux will be above its average value, and as a result a slightly smaller torque-producing current is required to obtain the same torque. This explains why the hysteresis band of the torque-producing current is centered around a lower value at the left side of figure 8.29a than at the right side.

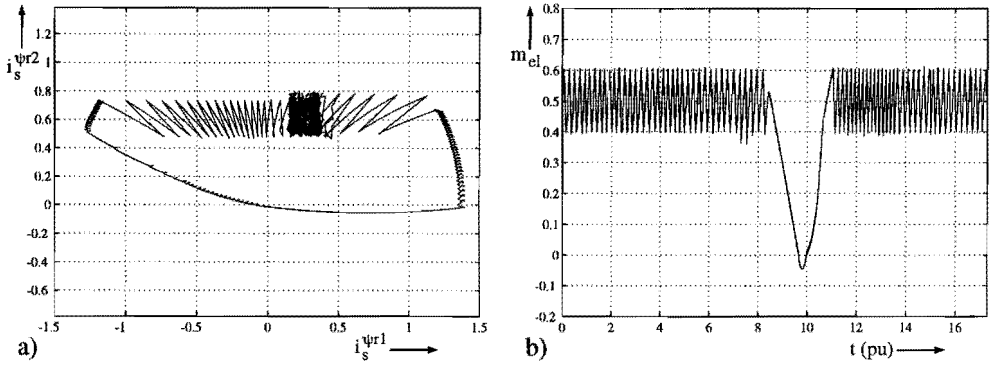


Figure 8.29. Simulation showing the field-oriented stator-current vector (a) and the torque (b) of an inverter-fed induction machine using the optimized control under motor operation, in case of a single-IGBT fault.

At current limitation, rapid switching of the inverter occurs, maintaining the current at a level just below the limit. In a real system, the switching frequency occurring in this case has to be limited more than in this simulation, to avoid very high switching losses.

Figure 8.30a shows the stator-current vector for this case. At first sight it is not very different from the stator current shown in figure 8.22a. However, as soon as i_{sa} becomes zero, instead of decreasing, the length of the stator-current vector now increases until its limit. Depending on the dimensioning of the IGBTs and the diodes, this limit might even be increased to a higher value. However, at the same time also the time required for the current reversal will increase, thus increasing the time during which the torque is below zero.

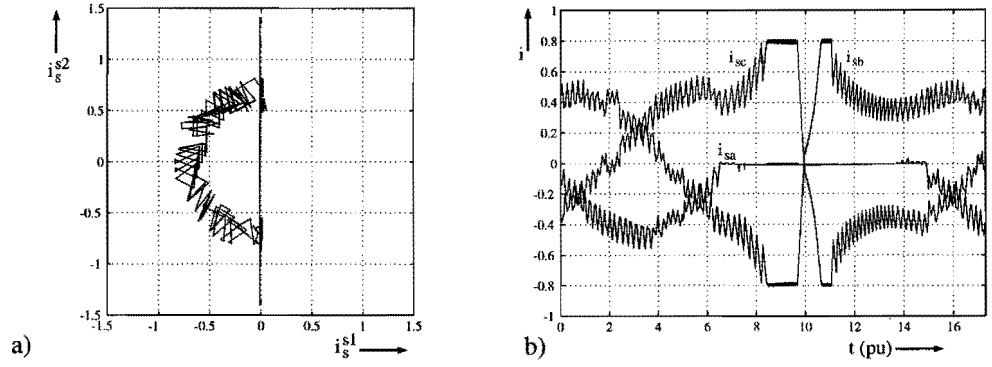


Figure 8.30. Simulation showing the stator-current vector (a) and the three stator currents (b) of an inverter-fed induction machine using the optimized control under motor operation, in case of a single-IGBT fault.

The average torque obtained with this method was 0.46 pu, which is 9 percent lower than the desired torque. In case of a three-phase hysteresis control, an average (simulated) torque of only 0.32 pu was obtained, which is 30 percent less. An increase of the current limit can only slightly improve the result obtained with the optimized control.

The stator-flux and rotor-flux vectors are shown in figure 8.31. While i_{sa} is zero, the stator flux will increase considerably, until the moment of current reversal. At current reversal, the stator flux decreases to a value below the rotor flux, and then increases again, until its normal value. The rotor flux is also affected by the fault, but evidently much less than the stator flux. The influence of saturation on the fluxes has not been examined.

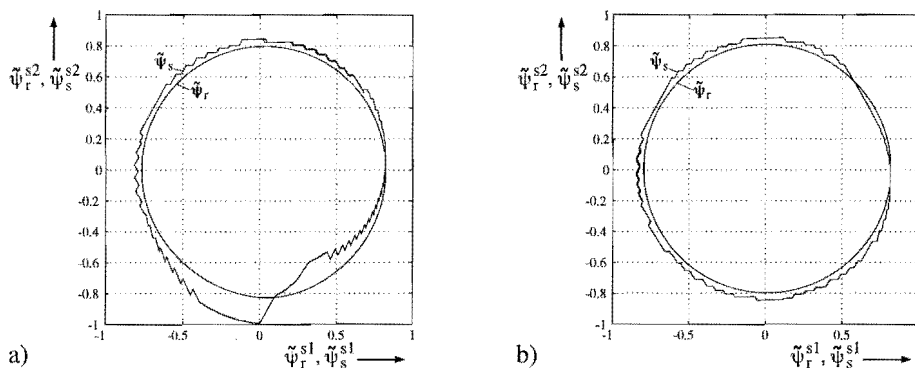


Figure 8.31. Simulation showing the rotor-flux and stator-flux vectors of an inverter-fed induction machine using the optimized control, under motor operation (a) and generator operation (b), in case of a single-IGBT fault.

The u/i-model used in the simulations and experiments was unfortunately not optimally fit for this situation. The feedback parameters S2 and S3, explained in section 3.6, were meant for operation with a constant stator flux, which is clearly not the case here. As a result, a considerable difference between the estimated and the real rotor flux may occur, causing a difference between the estimated and the real torque. This can be avoided by reducing these parameters to very small values. A better solution would however be to implement this feedback not on the stator flux, but on the rotor flux, which by its nature varies much less. This has not been tested.

For generator operation the results obtained with the optimized control are even more promising. Whereas the torque, when using three-phase hysteresis control, showed a dip of approximately 20 percent (see figure 8.24b), the optimized control yields a perfectly constant torque, as shown in figure 8.32b. As can be seen from figure 8.32a, the torque is maintained at a constant level at the expense of temporarily reducing the magnetizing-current component. To avoid a decrease of the rotor flux, the magnetizing current had to

be chosen slightly higher during the rest of the period. The rotor flux, shown in figure 8.31b, is not noticeably affected by the fault.

Comparison of figure 8.33, showing the stator currents, with the equivalent figure for hysteresis control, figure 8.25, reveals that only a small change in the shape of the currents was required to obtain this constant torque.

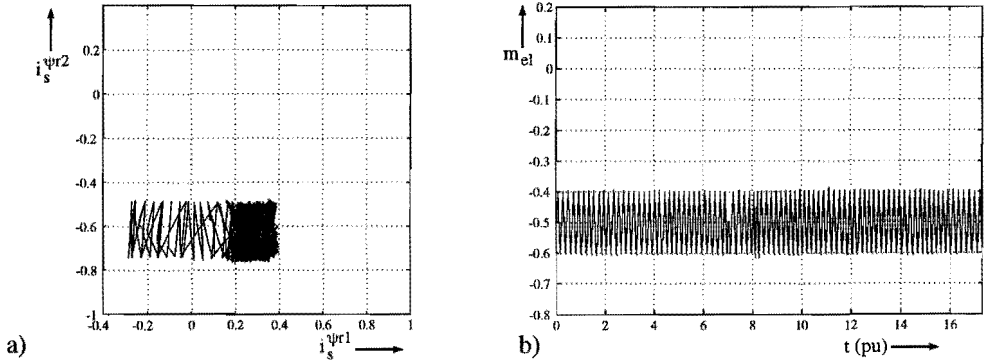


Figure 8.32. Simulation showing the field-oriented stator-current vector (a) and the torque (b) of an inverter-fed induction machine using the optimized control under generator operation, in case of a single-IGBT fault.

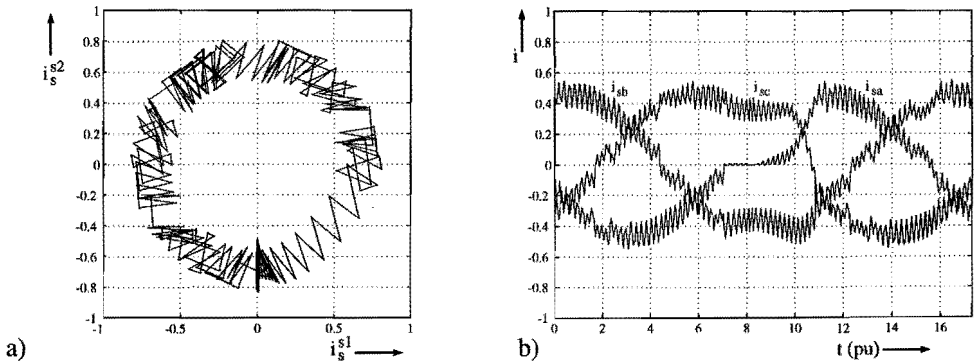


Figure 8.33. Simulation showing the stator-current vector (a) and the three stator currents (b) of an inverter-fed induction machine using the optimized control under generator operation, in case of a single-IGBT fault.

8.5.4 Experiments with the optimized control during an IGBT fault

Between the experimental results and the simulations the same differences were expected as mentioned for the case of the three-phase hysteresis control in section 8.5.2. This corresponds mainly to slower and therefore less accurate switching in the experiments than in the simulations. Experimental results are shown in the figures below. Figure 8.34 and 8.35 show the currents and torque for motor operation, and correspond to the simulations in figures 8.29 and 8.30. For generator operation the results are shown in figures 8.36 and 8.37, which in turn correspond to 8.32 and 8.33. As for the case of the hysteresis control, a good correspondence between simulated and experimental results exists.

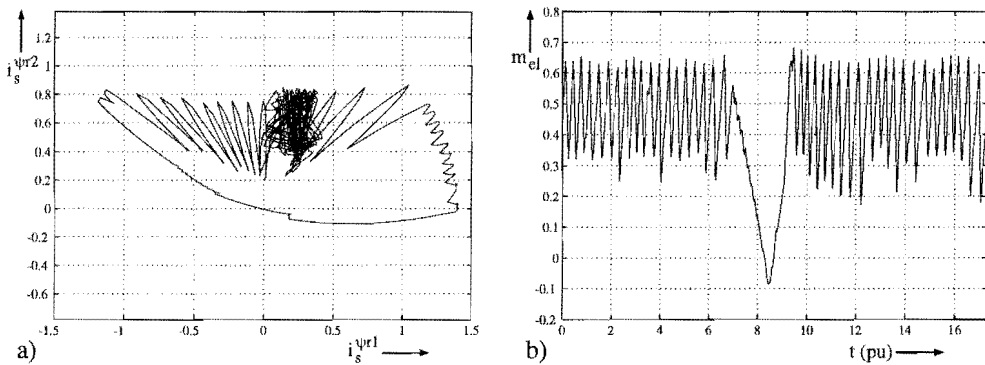


Figure 8.34. The field-oriented stator-current vector (a) and the torque (b) of an inverter-fed induction machine using the optimized control under motor operation, in case of a single-IGBT fault.

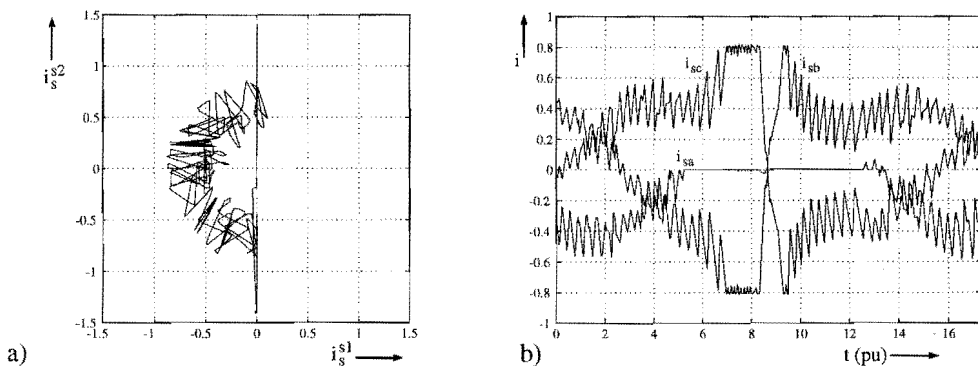


Figure 8.35. The stator-current vector (a) and the three stator currents (b) of an inverter-fed induction machine using the optimized control under motor operation, in case of a single-IGBT fault.

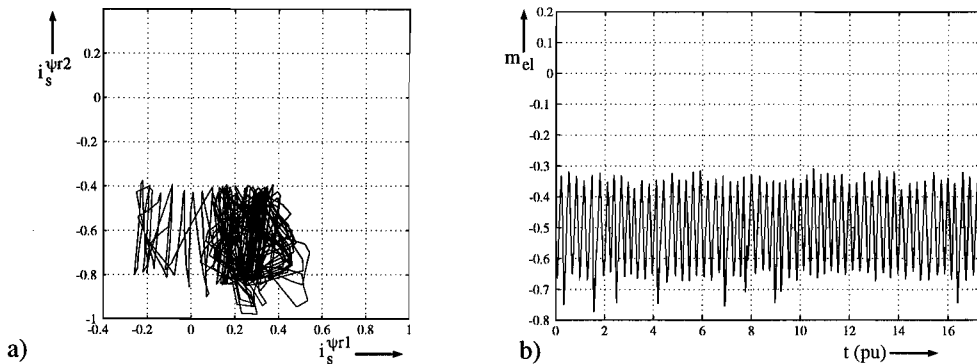


Figure 8.36. The field-oriented stator-current vector (a) and the torque (b) of an inverter-fed induction machine using the optimized control under generator operation, in case of a single-IGBT fault.

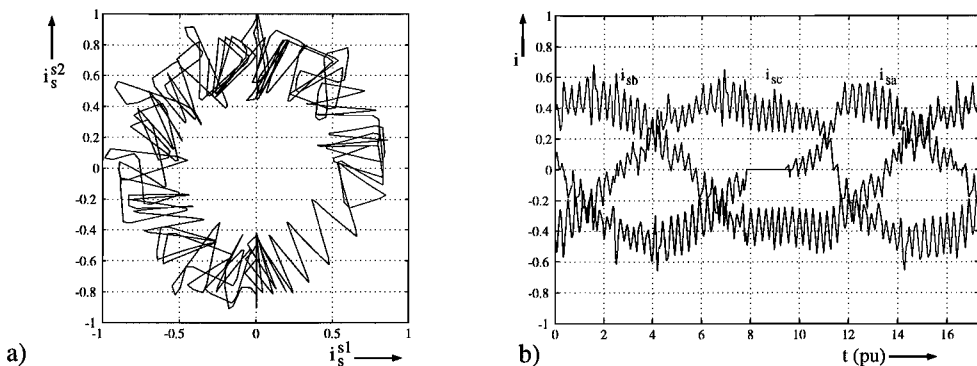


Figure 8.37. The stator-current vector (a) and the three stator currents (b) of an inverter-fed induction machine using the optimized control under generator operation, in case of a single-IGBT fault.

For motor operation, where the currents in the remaining phases differ considerably from their values under no-fault operation, it is interesting to examine the extra stress on the remaining healthy devices. There are two possible reasons for extra stress: higher currents causing higher conduction losses, and a higher number of switching operations causing higher switching losses. Furthermore, these effects are not fully unrelated to each other, as a higher current in a device will also increase its switching losses.

To examine the first reason for extra losses, the average value of the current in each of the switches and each of the diodes has been calculated, during one period of the currents shown in figure 8.35, in comparison with those under no-fault operation. It must be noted that although the desired torque was equal for both cases, the average torque was

9 percent lower in the fault case. When using a torque controller, the currents during fault operation would be slightly higher than those measured here.

To get a first impression of the extra switching losses, the number of times each IGBT and each diode starts or stops conducting was counted during one period. This number is not exactly proportional to the switching losses in a device, because these depend also on the current and voltage before and after the switching, but it does give an indication.

The results are shown in figures 8.38 and 8.39. Figure 8.38 shows the average values of the currents in all twelve devices. In figure 8.38a, the currents are normalized with respect to the IGBT current under no-fault operation (0.10 pu), averaged over one period and over all six IGBTs. In figure 8.38b the average diode current under no-fault operation (0.033 pu) was used for normalization. Figure 8.39 shows the number of times an IGBT or a diode starts or stops conducting, normalized with respect to the average numbers under no-fault operation (38 for the IGBTs and 39 for the diodes). The results will be discussed separately for each of the three inverter branches (see figure 8.1 for device numbering).

As the fault occurred in IGBT s_1 , the current in s_1 is evidently zero, and so is the number of times s_1 is switched. The current during the negative half period of i_{sa} is however hardly affected by the fault, resulting in an unchanged current in both s_2 and d_1 . As i_{sa} hardly ever becomes positive (see figure 8.35b), the current in d_2 is almost zero. A remarkable increase is visible in the number of times d_1 switches. However, this is due to the fact that while $i_{sa} = 0$ this diode balances at the limit of conduction. This does not cause considerable extra losses. If the current for which diode d_1 is said to conduct is increased from 0 to 0.005 pu this number decreases by almost 40 percent.

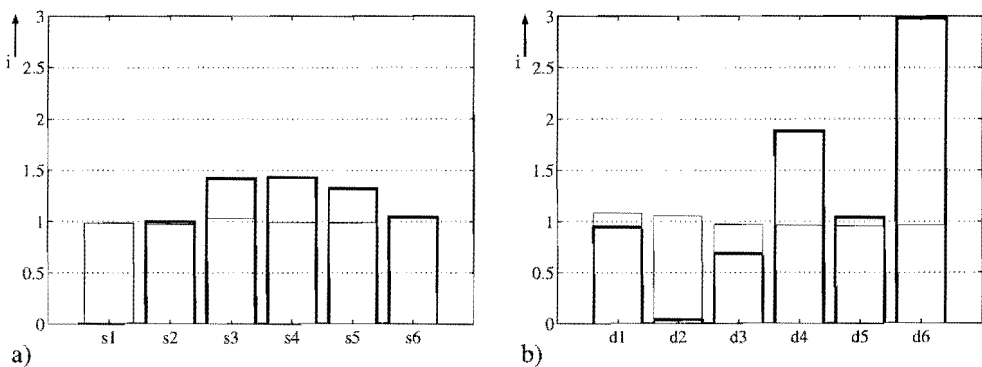


Figure 8.38. The average value of the current in each of the IGBTs (a) and diodes (b) for no-fault operation (thin line) and in case of a single-IGBT fault (fat line), normalized with respect to the current under no-fault operation, averaged over one period and over all six devices, while using the optimized control, under motor operation.

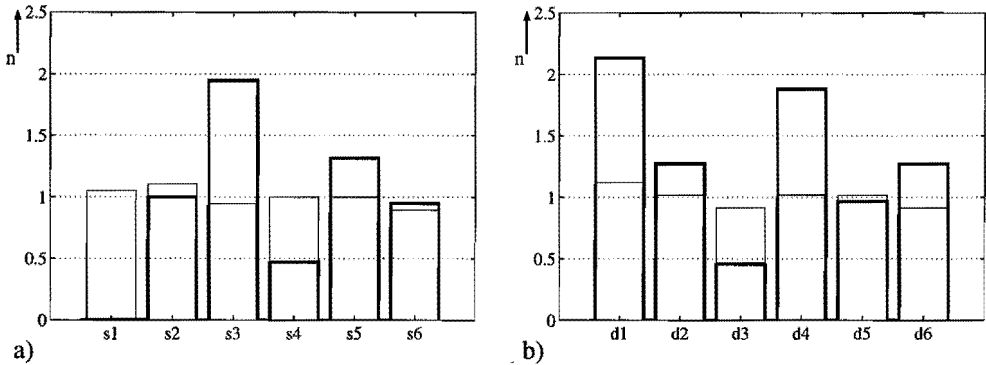


Figure 8.39. The number of switching actions of the IGBTs (a) and diodes (b) for no-fault operation (thin line) and in case of a single-IGBT fault (fat line), normalized with respect to the average number under no-fault operation, while using the optimized control, under motor operation.

In the second inverter branch, IGBTs s3 and s4 show a considerable current increase. For s3, this is due to the fact that during positive current limitation of i_{sb} , the current flows alternately in d4 and s3. This also causes the very high average current in d4. The current increase in s4 can be explained by the fact that s4 carries the current during negative current limitation of i_{sb} . The high switching numbers for d4 and s3 are due to switching during the second half of the current reversal. This switching is actually an unsuccessful attempt of the controller to increase the torque more rapidly, and could be avoided by improving the control. The switching numbers of d3 and s4 are lower than normal because no switching occurs in this branch during negative current limitation of i_{sb} and during the first half of the current reversal.

The highest current increase occurs in diode d6 which, alternated by IGBT s5, carries the current during positive limitation of i_{sc} (cf. figure 8.35b). This limitation is realized by switching between d6 and s5, which explains the increased switching numbers for these devices.

In general it can be said that the highest switching numbers are either not causing high extra losses or could be reduced by improving the control. The high currents however are inherent to the control method, whose main purpose was to replace the current missing in one device by an extra current in other devices. The most effective way to limit this current is to reduce the set point for current limitation – this will however increase the duration of the torque dip.

8.5.5 Limitations and problems related to the optimized control

The optimized control described in the previous sections performs very well for fault situations at a normal flux level and for a speed which is neither too high nor too low. Yet does this control perform well enough to be implemented for operation under all circumstances? In practice there are still some problems remaining to be solved.

First off all, when defining the priorities in section 8.4.2, it has silently been assumed that even while prioritizing torque control over flux control, there is always a sufficiently high flux level in the machine to operate. This means for example that when starting the machine, the user should first provide a non-zero command value for the flux, and only request torque when the flux is present. During an IGBT fault however, at very low speeds and especially at standstill, the variation of the magnetizing current will cause a much higher variation of the rotor flux than at the speed used in the experiments shown. The flux could then even become zero. As a result, it is not possible with all types of loads to start the machine from standstill while one of the switches refuses to conduct.

Also at very high speeds a problem can occur. At very high speeds the inverter will no longer be able to provide the voltage required to maintain a certain flux level. Normally, field weakening and speed limitation are used to avoid this problem. This has however not yet been implemented in the control presented here. As a result, the machine might become demagnetized if operation at very high speed is attempted without applying sufficient field-weakening.

An other point to consider is that, under normal operation, other requirements might be more important than maintaining constant torque and a constant torque ripple. Examples of this are certain requirements on the harmonic content of the dc-link current or of the torque, or further limitation of the switching losses. As a result, there are many different control methods that under specific conditions could easily outperform the control presented here. The main purpose of this control however, was to provide optimal performance for a converter in which a fault might occur.

A practical problem is also that the torque during a fault under motor operation, contains a component at the stator-current frequency (one torque dip occurs in every period). This component may excite a mechanical resonance of the system. One way to avoid a torque component at this frequency is to introduce another torque dip having the same shape at exactly 180° from the first. This will double the frequency of the lowest frequency component contained in the torque.

Finally, there is still another practical problem that limits the industrial usefulness of this control nowadays. The control as it was implemented here requires a large amount of calculation power, and even using two state-of-the-art digital signal processors in parallel it performs not as well as desired. It can however be expected that as the development of

signal processors progresses, controls of this complexity will eventually make their way into those applications where high cost is outweighed by high performance, which includes high reliability.

8.5.6 Simulation of the optimized control during a single-device short circuit

In Chapter 5, section 5.5, it has already been shown that a short circuit of one or even more stator windings represents a very serious fault, during which continued operation can not be realized. The case that will be examined here is not directly a short circuit of a stator winding, but a short circuit of a single device of the voltage-source inverter. In practice, this situation occurs if a GTO fails. As a result, the voltage at one of the machine terminals will be fixed to one of the dc-link terminal voltages. For example, if s_2 (see figure 8.1) is shortened, the voltage at terminal a will equal that of the negative pole of the dc-link. The voltage at the other two machine terminals can now no longer be made negative with respect to the voltage at terminal a.

For this analysis it has been assumed that if a device is short circuited, the other switching device belonging to the same inverter branch will not start conducting, so that short-circuiting of the dc-link is avoided. This does not correspond to the practice in industrial installations, where such a short circuit is purposely provoked. This short circuit is used there to rapidly blow one or more fuses, disconnecting the inverter from its power source.

The control method described in section 8.4.2 provides the most constant torque under all circumstances, thus also in case of a short circuit. By means of a simulation, its performance has been tested for the case of a short circuit of s_1 . Problems are expected during that part of the period in which normally the voltage at either terminal b or terminal c would be higher than that at terminal a.

Figure 8.40 shows the stator-current vector and the torque during the time interval in which the short circuit occurs. At first, the control succeeds to maintain a constant torque, but as soon as the current limitation is reached, the torque starts decreasing rapidly. Shortly after this, none of the available switching states can still limit the current – even if none of the other switching devices receives gate signals, a very high current will flow in the short-circuited device s_1 and diode d_3 . The currents i_{sa} and i_{sb} reach a peak value of more than 3 pu, while a breaking torque of 3.8 pu occurs. One half of a period later however, the inverter becomes controllable again – but not for long, as a new torque dip occurs another half period after this. Meanwhile the rotor flux decreases rapidly.

It is clear that in a practical system this situation should never be allowed to occur. Even the control presented here cannot avoid the high currents and torque. The best option seems to attempt to transform the short circuit into an open circuit as soon as possible,

while at the same time keeping as many as possible of the other devices connected, to enable continued operation.

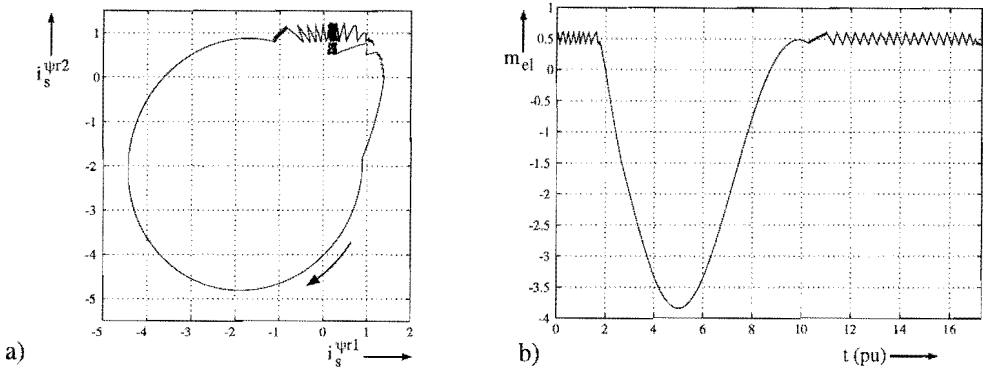


Figure 8.40. Simulation showing the field-oriented stator-current vector (a) and the torque (b) of an inverter-fed induction machine using the optimized control under motor operation, in case of a single-device short circuit.

8.6 Comparison with operation with one phase current equal to zero

In this chapter, faults have been examined that were related to a single device of a voltage-source inverter. This is in contrast with the previous chapters, where one or more complete phases of the machine or the converter were either short-circuited or open-circuited. For example, in Chapter 6, in a theoretical way optimal current waveforms were designed for the case where one stator phase was completely disconnected. The approach used in this chapter, Chapter 8, was much more practical, and allowed to cope with the presence of nonlinear devices such as diodes and non-sinusoidal sources. To conclude this chapter, it will be shown that the approach of Chapter 6 can also be used in the inverter device-fault case.

Observation of the experimental results shown for example in figure 8.35b reveals that the single-IGBT fault under motor operation corresponds to a temporary open circuit of one phase. While $i_{sa} < 0$, the inverter and machine operate normally, but as soon as i_{sa} should become positive, the phase becomes disconnected. At the point where i_{sa} would normally become negative again, the connection is “repaired”, and normal operation is resumed. During the interval in which one phase is disconnected, the control attempts to maintain a constant torque, until current limitation forces the torque down to zero.

This is exactly the same situation that was discussed in section 6.6, except that in that section both i_{sb} and i_{sc} were zero, while here $i_{sa} = 0$ and $i_{sb} = -i_{sc}$. Furthermore, in

section 6.6 the star point was connected, while here it is not. The method of section 6.6 will now be used to derive the stator current required to maintain a constant torque. Using equation 4.5 it can be shown that equation 8.39 is valid for the stator currents in this case. Rotation over the rotor-flux angle φ_r^s yields the relation between the field-oriented stator-current components and the remaining stator current $i_{sb} = -i_{sc}$, given in equation 8.40.

$$\begin{aligned} i_s^{s1} &= 0 \\ i_s^{s2} &= \sqrt{3} \cdot i_{sb} \end{aligned} \tag{8.39}$$

$$\begin{aligned} i_s^{\psi r1} &= \cos(\varphi_r^s) \cdot i_s^{s1} + \sin(\varphi_r^s) \cdot i_s^{s2} = \sqrt{3} \cdot i_{sb} \cdot \sin(\varphi_r^s) \\ i_s^{\psi r2} &= -\sin(\varphi_r^s) \cdot i_s^{s1} + \cos(\varphi_r^s) \cdot i_s^{s2} = \sqrt{3} \cdot i_{sb} \cdot \cos(\varphi_r^s) \end{aligned} \tag{8.40}$$

From equation 8.40, using the fact that $m_{el} = i_s^{\psi r2} \cdot \psi_r$, it follows that a desired constant torque is obtained if i_{sb} satisfies equation 8.41, which is very similar to equation 6.50.

$$i_{sb} = \frac{m_{el} / \psi_r}{\sqrt{3} \cdot \cos(\varphi_r^s)} (= -i_{sc}) \tag{8.41}$$

To compare the current realized using the optimized control, with this theoretical value, figure 8.35b has been redrawn in figure 8.41a, now including the theoretical value and omitting i_{sc} . The result of equation 8.41 has however been limited to 0.82 pu, corresponding to the current limit used in the experiment. From figure 8.41a it is clear that during the time interval in which $i_{sa} = 0$, the current in phase b corresponds more or less to the limited theoretical value of equation 8.41. At current reversal however, the current i_{sb} can not change as rapidly as desired, making the slopes of the current dip less steep.

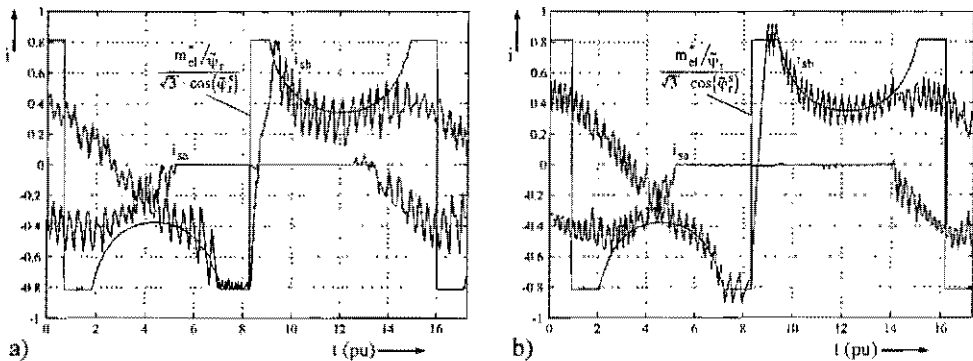


Figure 8.41. a) The stator currents i_{sa} and i_{sb} , and the ideal value for i_{sb} during a fault, of an inverter-fed induction machine using the optimized control under motor operation, in case of a single-IGBT fault. b) Simulation showing the same quantities using a modified three-phase hysteresis current control.

Given the fact that the optimized control in case of a single-IGBT fault realizes almost the current derived in equation 8.41, a logical step is to use this current as a command value for the much simpler three-phase hysteresis control, and to compare the results. This was done by means of a simulation, the results of which are shown in figures 8.41b and 8.42. Figure 8.41b shows how the current i_{sb} is made to follow the current derived in equation 8.41 during the interval in which $i_{sa} = 0$. A difference with the optimized control is the way in which the current limitation is realized: in the optimized control it is an absolute limitation, while in the three-phase hysteresis control the current exceeds the limit by one half of the hysteresis band width.

Figure 8.42 shows the simulated field-oriented stator-current vector and the torque. By comparing this figure with figure 8.29 it can be noted that under these circumstances the seemingly complex behavior of the optimized control can be imitated successfully by a slightly modified three-phase hysteresis control.

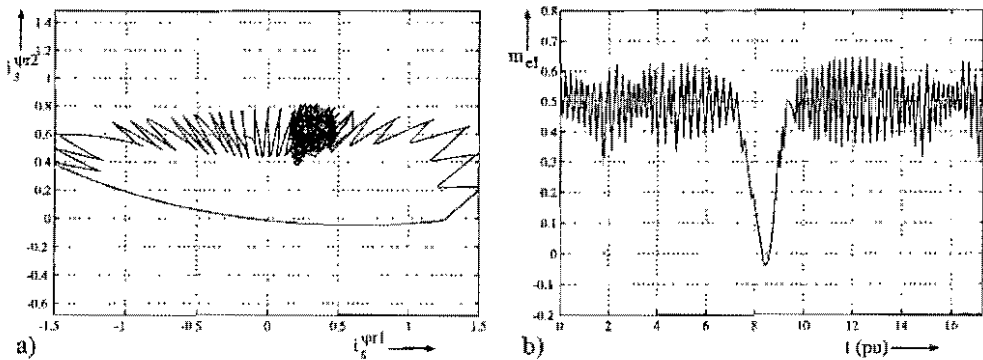


Figure 8.42. Simulation showing the field-oriented stator-current vector (a) and the torque (b) of an inverter-fed induction machine using a modified three-phase hysteresis control, under motor operation, in case of a single-IGBT fault.

However, the modified three-phase hysteresis control does not perform well under all circumstances. Under generator operation, adaptation of this control to imitate the optimized control is not as simple as under motor operation. Considering for example figure 8.37b, it can be seen that just like in motor operation there is a time interval during which $i_{sa} = 0$. During this time interval the command value for i_{sb} can be taken from equation 8.41. If the command value for i_{sc} is taken exactly opposite to this value, branches b and c of the inverter will switch simultaneously. Simulations showed however that in this case the current in phase a never becomes positive (in contrast with figure 8.33b), and as a result the torque in generator mode shows the same dip as in motor mode. This can be avoided by giving i_{sc}^* a small offset with respect to i_{sb}^* . However, between operation with $i_{sa} = 0$ and normal operation there is a transition period during which the phase currents are not within their hysteresis bands. Whereas the optimized control succeeds to control

the currents in such a way that a constant torque is obtained, it is not yet clear how the command values for the three-phase hysteresis control should be chosen to obtain a similar result. Setting the command values back to their normal values as soon as $i_{sa} \neq 0$ results in a small torque dip.

8.7 Conclusions

In this chapter remedial operation in case of a single-device fault in a voltage-source inverter has been studied. It has been assumed that all other devices still were fully functional. In current industrial installations, as a result of the integration of several devices into a single package, this is unfortunately almost only the case if a failure occurs in one of the gate drivers, and not in a device itself. In contrast with the faults studied in previous chapters, a highly nonlinear situation occurs, caused by the diodes that are present in the inverter. Due to these diodes, the machine either operates normally, or with one phase disconnected, or with a short circuit between phases, depending on the actual phase currents and the induced voltages.

To cope with these nonlinearities, a control method has been developed which at any moment considers the actual currents and voltages to determine the effect on the machine of each of the many possible command states of the inverter. This control was based on the rotor-flux oriented stator-current vector. As compared with controls working in other coordinate systems, this offers the advantage that flux and torque control are at most decoupled. In practice this means that large variations of one current component can be allowed without a serious effect on the torque, while the other current component is under all circumstances directly proportional to the torque.

The main task of this control – except from limiting the currents to acceptable values – is to maintain a constant torque, equal to the desired torque. By means of simulations and experiments its performance was tested in different situations, and compared with a very simple three-phase hysteresis current control.

In case of motor operation while one switching device is constantly open, a constant torque can not be realized. The optimized control performs however much better than the three-phase hysteresis control. By maintaining a constant torque until current limitation becomes necessary, the resulting torque dip has a much shorter duration. Evidently, most of the remaining devices must carry a higher current, and for some devices a considerable increase in the number of commutations occurs. This causes extra losses that have to be taken into consideration in the inverter design and in the choice of the current limitation.

For generator operation much better results are obtained: the torque could be maintained within its desired hysteresis band. This is due to the diodes in the inverter, which in

generator operation conduct during a large amount of time. The three-phase hysteresis control showed in this case a small torque dip.

In case of a short circuit of one of the inverter devices, not even the optimized control is capable of avoiding extremely high currents and an exceptionally high braking torque. If such a short circuit occurs, it must be transformed into an open circuit as soon as possible to prevent further damage. If a sufficient number of other devices can be kept operational, remedial operation might then be possible.

Although the optimized control performs well under fault situations, it is not yet very well suited for industrial application. Not only does it require considerable calculation power due to its complexity, but also it does not yet perform well under all normal operating conditions. The results obtained with the optimized control can however be used as a reference to compare the performance of other types of control with.

Finally it was noted that operation with a single-device fault can partly be treated in the same way as operation with a failure of a complete phase. The single-device fault results in operation in which during one part of each period the system acts as if no fault were present, while during another part a complete-phase fault occurs. In the first time interval the machine can be controlled normally, while in the second interval the techniques described in Chapter 6 can be used. Whereas the optimized control masters also the transient between these two time intervals, there is not yet for all circumstances a way to make a simple control – such as the three-phase hysteresis control – perform as well during this transient. The simulations for motor operation showed however that for this case a simple control, such as the three-phase hysteresis current control, can easily be adapted to obtain optimal results, which is a promising sign for industrial application of these techniques.

Chapter 9

Conclusions and Recommendations

9.1 Asymmetrical supply of induction machines

In this thesis, the operation of a converter-fed induction machine was investigated for the case when the power converter can no longer provide the usual set of phase currents. Under steady-state operation this set of currents would be a symmetrical set of three sinusoidal currents. After giving a definition of such a set, it was shown that a symmetrical set of sinusoidal currents is a requirement for operation with constant torque and flux at a minimum of copper losses.

First a model of an induction machine was derived without assuming symmetrical or sinusoidal supply. A number of other assumptions were however made. One assumption was the linearity of the magnetic circuit, resulting in the neglect of saturation. Another important assumption was that the induction in the air gap does not contain space harmonics with an order higher than three. First the model was derived for the case no homopolar current is present in the machine. This is often the case in practice, because the star point of the machine is hardly ever connected. Then the model was extended for the case a homopolar current is present. It was shown that only a small extension to the machine models found in literature was required for this purpose. Practical experiments showed however that when a homopolar current is present, saturation effects can already occur at relatively low levels of the main flux. This was explained considering the resulting air-gap induction, but no attempt was made to model this effect.

Evidently, the behavior of the converter-fed induction machine largely depends on the control system. Some basic control methods were presented, with a special interest for rotor-flux oriented control. It was shown that rotor-flux oriented control has an important advantage over controls in other flux-oriented coordinate systems. In all flux oriented-control systems, the torque is the result of a multiplication of one field-oriented stator-current component with the flux. In this multiplication, the rotor flux depends only on very low frequency components of the other field-oriented stator-current component. Other fluxes, such as the stator or the air-gap flux, also depend on current components with a higher frequency. Therefore, whenever a converter fault causes rapid current variations, the rotor flux can be assumed constant, while other fluxes can not.

Of all possible reasons why a converter would not supply a desired current or voltage, only those were considered that are caused by a failure in the converter. Two main categories of faults were investigated: current faults and voltage faults. With the objective

of continued operation during the fault in mind, most attention was given to those faults that still allow the control over at least one of the machine's phase currents.

9.1.1 Current faults

Current faults are those faults that impose a direct limitation on one or more phase currents of the machine. These faults are due to an open-circuit of, for example, a converter switching device, caused by a failure of the device or its driver. For the machine such an open circuit means that one or more phase currents will be zero constantly or at least during a part of each period.

A model of the machine was derived for the case of mixed supply, i.e., supply of one or two phases with a voltage, while the remaining phases or phase is supplied with a current, *in casu* a current equal to zero.

It was shown that the presence of a star-point connection has considerable influence on the seriousness of a current fault. For example, if one phase current is zero due to a fault, while a homopolar current can flow in the star-point connection, the remaining two independent currents can be used to obtain constant-torque operation. If no homopolar current can flow, the loss of one phase current results in operation with an oscillating torque. Whenever two phase currents are zero, operation is only possible if a current can flow in the remaining phase and the star-point connection. Also in that case, constant torque cannot be obtained.

Simulations and experiments demonstrated operation of a voltage-fed induction machine of which one or two phase currents were made zero. The star point of the machine was connected to the star point of the applied cycloconverter. If one phase current is zero and the voltages across the remaining phases are unchanged, the flux level does not change considerably. In that case the field-oriented current vector oscillates around its pre-fault value at twice the stator-current frequency, causing a considerable torque ripple. If field-oriented control is used, in which the voltages applied to the machine depend on the estimated flux level, this fault causes a reduction of the rotor flux by more than 30%. Also here, similar current oscillations occur, but at a lower current level. In case two currents are zero, the oscillating stator-current vector will be equal to zero twice in every period, and so will the torque. If the voltage across the remaining phase is unchanged, this fault reduces the pull-out torque by approximately a factor of four.

A different configuration for which a current fault was investigated, included a current-controlled voltage-source inverter. In this configuration the star-point of the machine was not connected. It was shown that open-circuiting one of the inverter switching devices resulted during each period in a temporary open circuit of one phase of the machine. If a simple three-phase hysteresis current control is used, the torque under motor operation

temporarily drops below zero during each period. The duration of this torque dip equals half a period of the stator current, corresponding to the interval during which one of the phase currents is zero. Under generator operation also a torque dip occurs, but this dip is much less serious. This is due to the fact that the diode connected antiparallel to the open-circuited device conducts during an important time interval.

9.1.2 Voltage faults

Voltage faults are those faults that are due to a short circuit of a converter switching device. This includes also the case in which a device constantly remains in a conducting state due to a fault in its driver. These faults impose a direct limitation on one or more phase or line voltages of the machine.

It was shown that if a short circuit in the converter causes a short-circuit of one or more machine phases or a short circuit between two machines phases, very high currents result. Unless the other inverter switching devices are considerably oversized, those currents will cause damage to these other devices. Already for that reason, measures must be taken to prevent operation with such a fault.

For a voltage-fed induction machine of which the star point is connected, simulations were performed to demonstrate the effect of a single-phase short circuit. The remaining two phases were either supplied with an unaltered voltage, or with a voltage determined by a field-oriented controller. In both cases a very high braking torque pulse was noted, as well as very high instantaneous currents. In case of field-oriented control, the flux in the machine decreases rapidly as the voltages across the remaining phases are reduced in such a way that the individual phase currents decrease to approximately their pre-fault values. If the voltage across the remaining phases is not changed during the fault, the currents remain high, causing an unacceptably high torque ripple of several times the rated torque value.

Simulations including a voltage-source inverter showed that a short circuit of a single switching device results in a short circuit between two or three machine phases. This cannot be avoided by using an appropriate control for the remaining devices, because the short-circuit path will be formed by the faulty device and diodes belonging to other inverter branches. Also in this case a braking torque pulse occurs, accompanied with extreme current levels.

9.2 Remedial operating strategies

In the previous section it was shown that without special measures, converter faults often cause unacceptably high torque and/or current ripple. By adapting the control to the asymmetry of the converter, this situation can be improved. For different faults it was investigated whether and how an acceptable remedial operation – operation of the machine during a fault using asymmetrical supply – can be realized. Investigations were limited to modifying the control system only, leaving the power circuit unchanged.

9.2.1 Current faults

The most important category of faults for which remedial operation was investigated consisted of different current faults. The purpose was to find control methods that result as much as possible in a non-oscillating torque equal to its desired value. At the same time the remaining healthy devices had to be protected against possible overcurrents.

The most favorable condition for remedial operation was shown to exist in case the star point of the machine is connected. In a current-fed machine the homopolar current can then easily be controlled in such a way that operation with one phase current equal to zero is possible. In this case an increased current must be supplied to the other phases, which puts a limit on the maximum allowable torque. The same kind of remedial operation can be realized using a voltage-fed machine. The homopolar current is then controlled using the homopolar voltage. This control was realized in a similar way as the control of the two field-oriented current components, using an estimation of the homopolar inductance and the stator resistance.

Experiments with a cycloconverter-fed induction machine showed the feasibility of this remedial operation. Differences between simulations and experiments were mainly caused by the idealized representation of the converter in the simulations. Another important difference was however the presence of saturation in the real machine. It was shown that a homopolar current can cause saturation of the main flux path, resulting in a reduced torque. For higher levels of the torque-producing current component a higher saturation level was observed than in a no-load condition. This effect can be compensated by adding a flux or torque controller, which will increase the current in the remaining phases to obtain the desired torque.

If the star point is not connected, a remedial operating strategy that resulted in constant-torque operation could not be found for all current faults. In case one phase current is constantly zero, operation with constant torque was even shown to be theoretically impossible. However, there are several methods to optimize the torque waveform in this case.

A first approach considered the frequency spectrum of the resulting torque ripple. If the single remaining independent current is sinusoidal, the torque ripple will consist of a single frequency component at twice the stator-current frequency, with an amplitude slightly higher than the average torque. Two methods to improve the torque-ripple spectrum were investigated. In the first method all frequency components were equally valued, and an attempt was made to reduce the total harmonic content of the torque ripple. It was shown that a considerable reduction is possible by adding harmonic components to the current. However, the resulting current has a very high peak value, and requires a considerable converter bandwidth. This method reduces also the amplitude of the torque ripple, but it cannot avoid torque dips of more than 100% of the average torque.

The second method consisted also of adding harmonic components to the current, but now with the objective of completely removing low-frequency components of the torque ripple. However, if a low-frequency component is removed, a component with an equal amplitude but a higher frequency arises. Also this method requires very high peak currents and converter bandwidth. It does not reduce the amplitude of the torque ripple.

Another approach was based on field-oriented control. Instead of considering the frequency spectrum of the torque ripple, in this approach it was attempted to maintain a constant torque at every moment of time. Theoretically this requires an infinitely high current. Due to current limitation, the torque contained a dip down to zero, twice in every period. A difficulty in this approach was the control of the flux. The flux was assumed constant despite variation of the magnetizing current, but this requires that at least the average magnetizing current is controlled. This can be realized by introducing different current limitations, depending on whether the magnetizing current is positive or negative. Unfortunately the control of the average magnetizing current introduces an increase in the duration of the torque dips.

A second current fault that was investigated for the case the star point was not connected, was the open circuit of a single switching device in a voltage-source inverter. This fault causes, during each current period, a time interval during which one machine phase is open-circuited. The duration of this interval was shown to depend on the torque delivered by the machine. For a large positive torque – which corresponds to motor operation – the interval has the length of half a period, while for a large negative torque it is only approximately one tenth of a period. This difference is due to the presence of a diode antiparallel to the open-circuited device, which conducts during a larger time interval under generator operation.

During this interval, the torque-producing and magnetizing current components cannot both be maintained constant. A control method was designed which prioritizes the control of the torque, allowing variations of the magnetizing current if necessary. It was shown

that with this method under generator operation the torque can be maintained constant, and that only a small variation of the magnetizing current occurs. Under motor operation this control at first also succeeds to maintain a constant torque, but then the need for current limitation forces the torque down to zero. Hence under motor operation a torque dip cannot be avoided. Compared with the torque using a standard three-phase hysteresis current control, the torque dip was however considerably reduced in time, depending on the overcurrent capability of the remaining switching devices and diodes. Simulations and experiments showed a good resemblance.

While one phase current is zero, the inverter control specially designed for operation with an open-circuit of a device, is very similar to the field-oriented control mentioned previously for the current-fed induction machine of which one phase is open-circuited. Simulations showed that for motor operation, the special control can be replaced by a standard control when all phase currents are different from zero, and with a somewhat modified control when one phase current is zero. During generator operation however, the behavior of the special control could not be reproduced by a less complicated control.

9.2.2 Voltage faults

The possibility for remedial operation while a voltage fault is present was investigated for two cases. In the first case, one phase of an induction machine of which the star point was connected was short circuited. Simulations showed that remedial operation with constant torque and flux is theoretically possible. However, the currents required for this operation are so high that it is not realistic to assume that a normally sized converter can supply them.

In the second case, one device of a voltage-source inverter was short-circuited. The control mentioned previously, which targeted to maintain as much as possible a constant torque during faults, was also applied to this case. It was shown that not even this control can avoid extreme overcurrents and an extreme braking torque pulse.

Voltage faults are thus much more serious than current faults, and should be avoided under all circumstances. If a voltage fault cannot be avoided, measures should be taken to disconnect the short-circuited part of the converter as soon as possible. This disconnection will transform the voltage fault into a current fault, which offers better perspectives for remedial operation.

9.3 Recommendations

Finally a number of recommendations will be given to improve the possibilities for remedial operation of standard induction machine drives, as well as options to replace the standard drive with more reliable configurations. Also a number of topics requiring further investigation will be mentioned.

It was shown that short circuits in the converter should be avoided under all circumstances. To allow remedial operation without having to disconnect part of the circuit, devices should be chosen that open-circuit in case of a failure. Hence IGBTs are preferable to GTOs. Also the design of the device drivers should be such that a failure can only cause an open circuit, or protective measures should be taken to ensure opening of a device if the driver fails. If remedial operation over a longer period of time is required, devices must be sized to withstand an increased current.

If a device fails, preferably all other devices should remain intact. The tendency to combine all devices of an inverter branch into a single package is not very favorable in this perspective. Preferably an IGBT and its antiparallel diode should be physically separated. However, packaging an IGBT together with a series diode (in opposite direction) seems an interesting option, which also finds an application in converters for switched reluctance machines.

It was shown that rotor-flux orientation has important advantages when used in a control for remedial operation. If a voltage/current model is used, it can best be used for rotor-flux estimation, because feedback loops in this model are designed for constant-flux operation. Other fluxes (the stator and the air-gap flux) are much less constant than the rotor flux during certain types of remedial operation, resulting in larger estimation errors.

A considerable increase of reliability is obtained if the star point of the machine is connected. This is realized most easily if a converter is used that has a star point itself. If a three-phase inverter is used, a connection of the star point can be realized by adding an extra branch or by implementing a connection to a midpoint of the dc link. Control of the homopolar current must then also be added. One step further is the implementation of separate converters for each phase of the machine.

Increased reliability can also be obtained using other types of machines. For example, a machine with more than three phases could be used. Another option is using a permanent-magnet machine designed in such a way that mutual coupling of phases is avoided as much as possible. This option should be combined with separate supplies for each phase.

For practical applications of remedial operation, the interaction between fault detection, remedial operation and protection circuits has to be investigated. It should also be

investigated whether the mechanical system of the drive can withstand the torque ripples that might occur during remedial operation. If a possible torque ripple is not allowed while remedial operation is a requirement, redundancy (the number of phases or the number of converter devices) has to be increased.

A topic remaining to be investigated is saturation due to a homopolar current, or generally speaking, saturation due to harmonic current distributions along the air gap.

Finally, it would be interesting to investigate the possibilities for remedial operation using different configurations of multi-level and matrix converters. With their increased number of switching devices it can be expected that these converters are less sensitive to the loss of a single device than the six-switch inverter investigated in this thesis.

References

- [Akpi-96] K. Akpinar, P. Pillay, G.G. Richards, "Induction motor drive behavior during unbalanced faults", *Electr. Power Syst. Res.*, vol. 36, p. 131-138, 1996.
- [Alwa-95] J.H.H. Alwash, S.H. Ikhwan, "Generalised approach to the analysis of asymmetrical three-phase induction motors", *IEE Proc., Electr. Power Appl.*, vol. 142, no. 2, p. 87-96, Mar. 1995.
- [Arka-94] A.A. Arkadan, B.W. Kielgas, "Switched reluctance motor drive systems dynamic performance prediction under internal and external fault conditions", *IEEE Trans. Energy Convers.*, vol. 9, no. 1, p. 45-52, Mar. 1994.
- [Bier-96] J. Bier, C. Kellerhof, "Qual der Wahl – der 'richtige' DSP", *Elektronik*, 1996, no. 10, p. 94-107.
- [Blas-71] F. Blaschke, "Das Prinzip der Feldorientierung, die Grundlage für die Transvektor-Regelung von Drehfeldmaschinen", *Siemens-Zeitschrift*, vol. 45, no. 10, p. 757-760, 1971.
- [Blas-73] F. Blaschke, *Das Verfahren der Feldorientierung zur Regelung der Drehfeldmaschine*, Ph.D. thesis, Technische Universität Braunschweig, 1973.
- [Blas-96] F. Blaschke, A.J.A. Vandenput, *Regeltechnieken voor draaiveldmachines*, Eindhoven University of Technology, EUT Report 96-E-296, ISBN 90-6144-296-6, 1996.
- [Blas-96b] F. Blaschke, A.J.A. Vandenput, J. v.d. Burgt, "Feldorientierung der gerberlosen Drehfeldmaschine", *ETZ*, 1995, no. 21, p. 14-23.
- [Bosg-93] S.G. Bosga, J.L. Duarte, L.J. Offringa, A.J.A. Vandenput, "Natural circulating current control of a cycloconverter", in *Conf. Rec. IEEE Industry Applications Society Annual Meeting*, Toronto, 1993, p. 1160-1165.
- [Bosg-93b] S.G. Bosga, *Regeling van een cycloconverter met kringstroom*, M.Sc. thesis, Eindhoven University of Technology, EMV 93-05, 1993.
- [Bosg-95] S.G. Bosga, J.J.A. v.d. Burgt, J.L. Duarte, A.J.A. Vandenput, "Unsymmetrical operation of a voltage-controlled field-oriented electrical drive system", in *Proc. of the Aegean Conf. on Electrical Machines and Power Electronics (ACEMP)*, Kuşadası, 1995, p. 549-554.

- [Bosg-95b] S.G. Bosga, J.J.A. v.d. Burgt, J.L. Duarte, A.J.A. Vandenput, "A multi-DSP system for real-time simulation and control of electric drive systems", in *Proc. of the Eur. Conf. on Power Electron. and Appl. (EPE)*, Sevilla, 1995, p. 3971-3975.
- [Bosg-97] S.G. Bosga, A.J.A. Vandenput, "Asymmetrical supply during fault situations in an induction machine drive system", to be published in *Proc. of the Eur. Conf. on Power Electron. and Appl. (EPE)*, Trondheim, 1997.
- [Bosg-97b] S.G. Bosga, J.J.A. v.d. Burgt, A.J.A. Vandenput, "Asymmetrical operation of a voltage-inverter-fed induction machine", to be published in *Proc. of the Eur. Conf. on Power Electron. and Appl. (EPE)*, Trondheim, 1997.
- [Burg-95] J.J.A. v.d. Burgt, S.G. Bosga, F. Blaschke, A.J.A. Vandenput, "Stability analysis of a new voltage/current model in open loop operation in direct field-oriented control", in *Proc. of the Int. Conf. on Power Electron. (ICPE)*, Seoul, 1995, p. 398-402.
- [Burg-95b] J.J.A. v.d. Burgt, S.G. Bosga, F. Blaschke, A.J.A. Vandenput, "Improved voltage/current model in closed loop operation in direct field-oriented control at very low speeds", in *Proc. of the Int. Conf. on Power Electron. (ICPE)*, Seoul, 1995, p. 769-774.
- [Burg-96] J.J.A. van der Burgt, *The Voltage/Current Model in Field-Oriented AC Drives at Very Low Flux Frequencies*, Ph.D. thesis, Eindhoven University of Technology, ISBN 90-386-0120-4, 1996.
- [Burg-96b] J.J.A. v.d. Burgt, S.G. Bosga, F. Blaschke, A.J.A. Vandenput, "Improved voltage/current model in direct field-oriented control at very low speeds", in *Proc. of the 32nd Int. Intelligent Motion Conf. (PCIM)*, Nürnberg, 1996, p. 79-93.
- [Casa-93] D. Casadei, G. Grandi, G. Serra, "Rotor flux oriented torque-control of induction machines based on stator flux vector control", in *Proc. of the Eur. Conf. on Power Electron. and Appl. (EPE)*, Brighton, 1993, vol. 5, p. 67.
- [Crai-93] E. Craig, B.B. Mecrow, D.J. Atkinson, A.G. Jack, "A fault detection procedure for single phase bridge converters", in *Proc. of the Eur. Conf. on Power Electron. and Appl. (EPE)*, Brighton, 1993, vol. 4, p. 466-471.
- [Depe-85] M. Depenbrock, "Direkte Selbstregelung (DSR) für hochdynamische Drehfeldantriebe mit Stromrichterspeisung", *ETZ Arch.*, vol. 7, no. 7, p. 211-218, 1985.

- [Donc-95] R.W. De Doncker, F. Profumo, M. Pastorelli, P. Ferraris, "Comparison of universal field oriented (UFO) controllers in different reference frames", *IEEE Trans. Power Electron.*, vol. 10, no. 2, p. 205-213, Mar. 1995.
- [Elch-91] T. Elch-Heb, J.P. Hautier, "Remedial strategies for inverter - a.c. motor system at the occurrence of a transistor drive fault", in *Proc. of the Eur. Conf. on Power Electron. and Appl. (EPE)*, Firenze, 1991, vol.4, p. 286-291.
- [Elch-94] T. Elch-Heb, Y. Fan, J.P. Hauter, "Reliability improvement of field-oriented controlled three-phase ac drives by means of two-phase remedial operation", in *Proc. Int. Conf. on Electric Machines (ICEM)*, Paris, 1994, vol. 2, p. 194-198.
- [Fu-93] Fu Jen-Ren, T.A. Lipo, "A strategy to isolate the switching device fault of a current regulated motor drive", in *Conf. Rec. IEEE Industry Applications Society Annual Meeting*, Toronto, 1993, p. 1015-1020.
- [Fu-93b] Fu Jen-Ren, T.A. Lipo, "Disturbance free operation of a multiphase current regulated motor drive with an opened phase", in *Conf. Rec. IEEE Industry Applications Society Annual Meeting*, Toronto, 1993, p. 637-644.
- [Gent-92] G. Gentile, N. Rotondale, M. Tursini, "Investigation of inverter-fed induction motors under fault conditions", in *Conf. Record of the 23rd Annual IEEE Power Electron. Specialists Conf. (PESC)*, Toledo, 1992, vol. 1, p. 126-132.
- [Hann-93] R.A. Hanna, J. Luscombe, "Survey of users' experience with adjustable speed drives rated 500 hp and above", in *Conf. Record of the IEEE-IAS Petroleum and Chemical Industry Conf. (PCIC)*, St. Louis, 1993, p. 271-277.
- [Hoek-93] M.H.H. Hoeks, *A DSP-based system for experiments with systolic arrays*, M.Sc. thesis, Eindhoven University of Technology, ESP-16-93, 1993.
- [IEEE-93] *The New IEEE Standard Dictionary of Electrical and Electronics Terms*, 5th ed., New York: IEEE, ISBN 1-55937-240-0, 1993.
- [Jack-96] A.G. Jack, B.C. Mecrow, J.A. Haylock, "A comparative study of permanent magnet and switched reluctance motors for high-performance fault-tolerant applications", *IEEE Trans. Ind. Appl.*, vol. 32, no. 4, p. 889-895, July/Aug. 1996.

- [Jaeck-93] A.A. Jaecklin, "Future devices and modules for power electronic applications", in *Proc. of the Eur. Conf. on Power Electron. and Appl. (EPE)*, Brighton, 1993, vol. 1, p. 1-8.
- [Jahn-80] T.M. Jahns, "Improved reliability in solid-state ac drives by means of multiple independent phase-drive units", *IEEE Trans. Ind. Appl.*, vol. 16, no. 3, p. 321-331, May/June 1980.
- [Jong-93] R. de Jong, *Realisering van real-time digitale simulaties van veldgeoriënteerde vermogenselektronisch gestuurde draaistroom-aandrijvingen met behulp van een multi-DSP-systeem*, M.Sc. thesis, Eindhoven University of Technology, EMV 93-06, 1993.
- [Jord-54] H. Jordan, F. Lax, "Vorausberechnung des Nullsystems unsymmetrischer Schaltungen von Drehstrom-Asynchronmaschinen", *Elektrotech. Z. ETZ A*, 1954, no. 20, p. 696-699, Oct. 1954.
- [Jord-75] H. Jordan, V. Klíma, K.P. Kovács, *Asynchronmaschinen*, Braunschweig: Vieweg and Budapest: Akadémiai Kiadó, ISBN 3-528-04600-7, 1975.
- [Kast-94] D. Kastha, B.K. Bose, "Fault mode single-phase operation of a variable frequency induction motor drive and improvement of pulsating torque characteristics", *IEEE Trans. Ind. Electron.*, vol. 41, no. 4, p. 426-433, Aug. 1994.
- [Kast-95] D. Kastha, B.K. Bose, "On-line search based pulsating torque compensation of a fault mode single-phase variable frequency induction motor drive", *IEEE Trans. Ind. Appl.*, vol. 31, no. 4, p. 802-811, July/Aug. 1995.
- [Krau-86] P.C. Krause, *Analysis of Electric Machinery*, New York: McGraw-Hill, 1st ed., ISBN 0-07-035436-7, 1986.
- [Lax-42] F. Lax, "Über die Wirkung von Nullsystemen in unsymmetrischen Ständerschaltungen von Drehstromasynchronmotoren", *Jahrbuch der AEG-Forschung*, vol. 9, p. 113-148, 1942.
- [Leon-85] W. Leonhard, *Control of Electrical Drives*, Berlin: Springer Verlag, ISBN 3-540-13650-9, 1985.
- [Leon-91] W. Leonhard, "30 years space vectors, 20 years field orientation, 10 years digital signal processing with controlled ac-drives, a review", *EPE Journal*, vol. 1, no. 1, p. 13-20, July 1991 (Part 1) and vol. 1, no. 2, p. 89-102, Oct. 1991 (Part 2).

- [Liu-91] Liu Tian-Hua, Fu Jen-Ren, T.A. Lipo, "A strategy for improving reliability of field oriented controlled induction motor drives", in *Conf. Rec. IEEE Industry Applications Society Annual Meeting*, Dearborn, MI, 1991, p. 449-455.
- [Liu-93] Liu Tian-Hua, Fu Jen-Ren, T.A. Lipo, "A strategy to isolate the switching device fault of a current regulated motor drive", in *Conf. Rec. IEEE Industry Applications Society Annual Meeting*, Toronto, 1993, p. 1015-1020.
- [Luk-96] P.C.-K. Luk, K.D. El Khamlichi, "An innovative DSP-based teaching module for electrical machine drives", *IEEE Trans. Educ.*, vol. 39, no. 2, p. 158-164, May 1996.
- [Mecr-96] B.C. Mecrow, A.G. Jack, J.A. Haylock, J. Coles, "Fault-tolerant permanent magnet machine drives", *IEE Proc., Electr. Power Appl.*, vol. 143, no. 6, p. 437-442, Nov. 1996.
- [Novo-96] D.W. Novotny, T.A. Lipo, *Vector Control and Dynamics of AC Drives*, Oxford: Clarendon Press, ISBN 0-19-856439-2, 1996.
- [Pell-71] B.R. Pelly, *Thyristor Phase Controlled Converters and Cycloconverters: Operation, Control and Performance*, New York: Wiley, ISBN 0-471-67790-6, 1971.
- [Ring-92] E.A.P. Ringoot, *Modellering en simulatie van een veldgeoriënteerde draaistroomaandrijving op een multi-DSP systeem*, M.Sc. thesis, Eindhoven University of Technology, EMV 92-15, 1992.
- [Schr-93] M. Schroedl, D. Hennerbichler, T.M. Wolbank, "Induction motor drive for electric vehicles without speed- and position sensors", in *Proc. of the Eur. Conf. on Power Electron. and Appl. (EPE)*, Brighton, 1993, vol. 5, p. 271-275.
- [Serr-93] L. Serrano-Iribarnegaray, "The modern space-phasor theory, Part I: Its coherent formulation and its advantages for transient analysis of converter-fed ac machines" and "Part II: Comparison with the generalized machine theory and the space-vector theory", *Eur. Trans. Electr. Power Eng.*, vol. 3, no. 2, p. 171-180, Mar./Apr. 1993 and no. 3, p. 213-219, May/June 1993.
- [Smol-92] H.A. Smolleck, "A new look at the effects of unbalanced voltages upon synchronous and induction machines", *Electr. Power Syst. Res.*, vol. 25, no. 3, p. 199-206, 1992.

- [Spée-90] R. Spée, A.K. Wallace, "Remedial strategies for brushless dc drive failures", *IEEE Trans. Ind. Appl.*, vol. 26, no. 2, p. 259-266, 1990.
- [Štěp-67] J. Štěpina, "Raumzeiger als Grundlage der Theorie der elektrischen Maschinen", *Elektrótech. Z. ETZ A*, vol. 88, no. 23, p. 584-588, 1967.
- [Swam-93] M. Swamy, S. Rossiter, "Typical problems encountered with variable frequency drives in the industry", in *Conf. Rec. IEEE Industry Applications Society Annual Meeting*, Toronto, 1993, p. 503-510.
- [Taka-86] I. Takahashi, T. Noguchi, "A new quick-response and high-efficiency control strategy of an induction motor", *IEEE Trans. Ind. Appl.*, vol. 22, no. 5, p. 820-827, Sept./Oct. 1986.
- [Tiit-95] P. Tiitinen, P. Pohjalainen, J. Lalu, "The next generation motor control method: direct torque control (DTC)", *EPE Journal*, vol. 5, no. 1, p. 14-18, Mar. 1995.
- [Thor-95] O.V. Thorsen, M. Dalva, "A survey of the reliability with an analysis of faults on variable frequency drives in industry", in *Proc. of the Eur. Conf. on Power Electron. and Appl. (EPE)*, Sevilla, 1995, vol. 1, p. 33-38.
- [Velt-94] A. Veltman, *The fish method – Interaction between ac-machines and switching power converters*, Ph.D. thesis, Delft University of Technology, ISBN 90-9006763-9, 1994.
- [Veth-94] J. de Veth, *Een 30 kVA converter met IGBT's als vermogensschakelaars*, Project Report, Eindhoven University of Technology, 1994.
- [Wyk-95] J.D. van Wyk, "Present and future trends in power electronic converters", in *Proc. of the Eur. Conf. on Power Electron. and Appl. (EPE)*, Sevilla, 1995, vol. 0, p. 1-16.
- [Zhao-96] Y. Zhao, T.A. Lipo, "Modeling and control of a multi-phase induction machine with structural unbalance (Parts I and II)", *IEEE Trans. Energy Convers.*, vol. 11, no. 3, p. 570-584, Sept. 1996.

Appendix A

Real-Time Simulation of AC Drive Systems

A.1 Introduction

For all simulations presented in this thesis a Digital Signal Processor (DSP) system was used. Although using such a system seems more difficult than using a standard simulation package on a personal computer or mainframe, this method offers many important advantages. In this appendix the advantages and drawbacks will be discussed, and it will be shown how a simulation environment for ac drives was set up. It will also be shown how the same DSP system, running largely the same software, was also used for controlling real ac drives.

In the past, analog simulators were often used to gain insight in the functioning of electrical drive systems. Both the machine and the control system were modeled using analog integrators, amplifiers, adders and analog or hybrid multipliers. By adjusting different potentiometers, the effects of for example parameter detuning could be studied in real time, which facilitated getting a “feeling” for the system. Furthermore, because the control system built for the simulator was basically identical to the one built for a real machine, the transition from simulation to experiment was easy to make.

However, analog simulators had many drawbacks. To change a single parameter, often more than one potentiometer had to be adjusted, and component tolerances made it difficult to reproduce exactly the same results on different occasions. Another drawback was the lack of flexibility of these systems. For example, experimenting with another type of controller or changing from a voltage-fed to a current-fed machine, required important hardware changes in the simulator circuitry. To return from this new setup to the old one, required changing the hardware again.

With the appearance of personal computers, the analog simulators were almost completely abandoned in favor of simulation programs. Important advantages were the relatively limited hardware requirements, the flexibility and the reproducibility. At the same time however, the distance between simulation and experiment was enlarged considerably. Not only the hardware used for the control of a real machine was different from the hardware used for the simulation of this control, but also the computer simulations were very much slower than real time. Often, while testing the influence of a parameter on the system, this parameter had to be changed before starting a simulation run, while the effect could only

be studied after it was finished. Although nowadays more and more simulation programs also allow to change parameters during a simulation, this is still very different from adjusting a parameter in a system running in real time.

Only several years ago the developments in digital computers had come to a level where the properties of analog drive simulators could be equaled by programmable digital systems. Using Digital Signal Processors it became possible to build a digital simulator capable of real-time simulations with sufficient accuracy and considerable flexibility. For such a system to be preferable to the use of a simulation package on standard computer hardware, it must fulfill a number of requirements. These requirements will be given in the next section, while in the sections after this one it will be shown how these requirements were met in the DSP system used for this thesis.

A.2 Requirements for a real-time digital drive simulator

To make a special hardware system a serious alternative to simulation using a standard digital computer, one very important requirement is speed. Whereas simulations on a standard computer are often a factor 10 to 100 slower than real time, the digital drive simulator must be capable of simulating in real time. This is not only very useful to obtain a "feeling" for the dynamics of the drive, but also allows to synchronize or adapt in real time the simulation model to a real drive. Furthermore, if a control system can be tested in real time during a simulation, the same control can easily be implemented on the real drive, in particular if the same digital system is used for simulation as well as for control.

The speed requirement is an important factor in the selection of an appropriate processor, see for example [Bier-96] or [Hoek-93]. However, requirements differ depending on the kind of simulation. For the simulation of an induction machine fed by an ideal sinusoidal source, a much larger simulation time step can be used than for a simulation including a fast-switching power converter. Also the simulation of advanced converter control algorithms requires more computing power than that of a simple voltage/frequency control. Although the progress in the development of DSPs allows to implement ever more complicated algorithms in a single processor, it can furthermore be an important advantage to have the possibility to extend the capabilities of a system by adding several processors in parallel.

An important aspect in the design of a digital simulator is its interfacing. To display the calculated quantities in real time, a computer screen is not fast enough, because the refresh frequency of computer screens lies within the same range as the fundamental frequency of signals in most drives running at rated speed. Only parts of the signals could be shown, reducing the speed advantage of the system. Analog oscilloscopes seem to be the only alternative, and offer an extra advantage over current digital displays: variations

in the brightness of displayed signals reveal whether a signal only instantaneously had a certain value or remained at that value for a longer period of time. Connecting analog oscilloscopes to a digital system requires a number of digital to analog converters, and a method for the user to find out what signals are displayed and using which scaling factor.

For real-time comparison of calculated data with measured data, and to control a real drive using the same system, analog to digital converters are required in a sufficient number and with sufficient speed and accuracy. Digital to analog converters are required as an interface to external analog circuits, while digital outputs are needed to control power converters. Digital inputs are useful for acquiring data from for example a rotor-position sensor.

To change set points in a real-time simulation or control, a computer keyboard or mouse is not very well suited. Especially if rapid action by the operator is required, separate switches and knobs are much more practical. Even programs that simulate rotating knobs on a computer screen can not compete with the ease of use of real knobs. Extra analog or digital inputs to the digital system are therefore required to connect external switches and knobs.

One disadvantage (!) of real-time simulations is that they are very fast. In some cases it is necessary to observe a sample of a signal in more tranquility. The system must therefore be able to store data, to display stored data, and to make this data available for post-processing on an ordinary computer system.

For the control of a real drive, some protection mechanism must be present to prevent damage to the drive in case of a program fault. For example, if the user decides to stop the program while the drive is running, it must be avoided that converter command values retain their last values, which would correspond to suddenly connecting a dc voltage to a running ac machine.

Finally there is also a number of requirements for the software of the digital simulator. First of all, speed is very important. For the time being, to fulfill the real-time requirement, algorithms have to be coded in a very efficient way. This means that a very efficient compiler or code optimizer is required, or that the user himself must provide very efficient code for at least the most time-critical parts of the simulation program. On the other hand, the programs should be easy to develop and easy to modify, which calls for the use of a high-level programming language. While simulation and control systems are often designed using block diagrams, even the use of a graphical programming language might be considered. However, even if a graphical programming language is used, functions such as converter switching control are often expressed more efficiently using a textual programming language. A combination of both might be ideal. On the other hand, also in a structured high-level textual language it is possible to write a program reflecting clearly the structure of a block diagram or a set of equations. Evidently, there must be easy means

of debugging the program, and once a program is functioning correctly, parts of it must be usable in the design of other programs.

A.3 Hardware description of the multi-DSP system

This section will describe the hardware of a DSP-based system meeting as much as possible the requirements mentioned in the previous section. An overview of the system is shown in figure A.1.

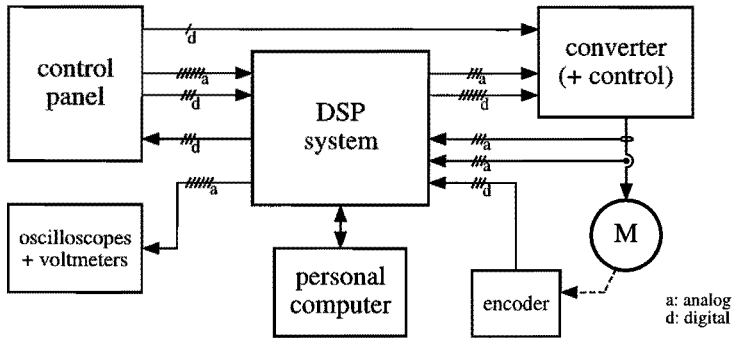


Figure A.1. An overview of the hardware of the DSP-based simulation and control system for electrical drives.

The core of the system consists of a (multi-)DSP system, initially equipped with two Texas Instruments TMS320C40 processors. Whereas for many simulations and controls a single processor provides sufficient calculation power, through communication channels and shared memory the power of the second processor can be used when needed. Extra or more recent processors can easily be added. The DSP system was developed within the Electrical Machines and Power Electronics research group (see [Hoek-93]). This facilitated troubleshooting as well as extending the system with different interfaces.

The DSP system was equipped with 16 A/D converters as well as 16 D/A converters, numbers that could easily be increased or decreased by adding or removing interface cards. The converters were equipped with analog filters, which had to be changed for different sample frequencies. During simulations, the analog outputs were used only to monitor signals on oscilloscopes and voltmeters, while during control they could also be used to transmit command values to an analog converter controller. Analog inputs were used for command values for quantities such as the torque and the flux as well as different parameters. A control panel provided a number of single-turn and multi-turn knobs for fast or accurate adjustments. During control, a number of analog inputs was used to acquire the values of machine currents and voltages.

Digital inputs were connected to several switches on the control panel, and served for example to start and stop data storage or to choose between different display modes. Also the signals of a rotor-position encoder were connected to the digital inputs. Between the physical digital inputs and the DSP was an Erasable Programmable Logic Device (EPLD). This device could be programmed (using a separate programmer) to preprocess the digital signals. In a similar way an EPLD was present between the processor and the digital outputs. When the digital outputs were used to command the gate drivers of a voltage inverter, the EPLD was programmed to switch off the inverter if the DSP for some reason provided no valid signals. Another protection mechanism using a digital output was built into the control panel: by means of this signal the control panel could detect whether the program had been stopped, and switch off the converter accordingly.

A connection, the so-called JTAG interface, between the DSP system and a personal computer allowed to download, start and debug programs on the DSPs. The same connection was also used to transfer data from each DSP to the personal computer for further processing. This connection required a special interface card in the PC. For all functions except for debugging also another interface was developed. This other interface linked a communication port of a TMS320C40 with a serial (RS232) interface, which is a standard interface present on any PC. This interface allowed to transfer data to and from the DSP while it was running. The JTAG interface allowed data transfers only while the processor was halted.

A.4 Simulation of an ac drive

In this section the software for the DSP system will be presented. First the simulation method will be discussed. Then it will be shown how the block diagrams and equations used in this thesis were translated into DSP programs. Finally some additional DSP programs will be mentioned, that were not a part of the actual simulation or control itself.

A.4.1 Integration method and calculation order

A fundamental characteristic of real-time simulations is that the speed at which calculations are performed must be synchronized to the real time. Simulation techniques that require more calculations during rapid signal transitions and fewer calculations in time intervals when signals are nearly constant, can therefore hardly be applied in real-time systems. Instead, a simulation method using a fixed time step has been chosen.

In the simulations, integrators play a crucial role. The simulations have been set up (see [Ring-92]) in such a way that first the inputs for all integrators are calculated. During this calculation the outputs of all integrators are maintained constant. The order of

calculation has to be chosen in such a way that operations relying on the result of others are performed later than those others. Algebraic loops must be avoided. After all integrator inputs have been calculated, new output values of the integrators can be calculated, to be used in the following time step.

In this simulation method two closely related choices have to be made: the simulation time step and the integration method. According to the sampling theorem, the time step determines the maximum bandwidth of the simulated or controlled signal. In practice, the sample frequency must be chosen sufficiently higher than the highest signal frequency of interest. Whereas for field-oriented control using a cycloconverter with a switching frequency of 300 Hz a sample frequency of 10 kHz is sufficient, simulation of a voltage-source inverter with a switching frequency of several kilohertz requires a much higher frequency. High sample frequencies correspond to short sample periods, and therefore short calculation times. An important criterion in the selection of an integration method was therefore the calculation time required for each integration. Another criterion was the accuracy. Whereas a higher-order integration method provides a better accuracy for a given time step, it does so at the expense of an increased calculation time. A compromise (see [Ring-92]) was found in the use of the second order Adams-Bashfort integration method, described by equation A.1. In this equation, $y(n)$ denotes the integrator output during calculation time step n , while $x(n)$ is the integrator input calculated for that time step. The duration of the time step equals Δt .

$$y(n+1) = y(n) + \frac{\Delta t}{2} (3 \cdot x(n) - x(n-1)) \quad (\text{A.1})$$

For most simulations a time step Δt of 100 μs was shown to be sufficiently small to obtain stable and accurate results.

A.4.2 From block diagram to simulation software

At first, the simulation algorithms to be implemented in the real-time digital simulator were tested on a personal computer. For this purpose a program called FORCEPS (Field Orientation in C for Educational PurposeS) was developed, as described in [Jong-93]. This program, written in C, allowed low-speed testing of algorithms in an environment where results were easily displayed graphically and numerically on a computer screen.

For programming the DSP system itself, two different choices were available: assembly language (using a macro assembler) and C. The use of C would have the following characteristics:

- C is a high level language, therefore the individual instructions are powerful. Through the use of procedures and functions, a block – as used in the block diagrams – can be represented by a single instruction. This can result in very readable programs.

- C is a well known language, so that new users of the simulation programs easily get accustomed to the programs.
- C is not closely related to the DSP code. This is an advantage if a program has to be translated from one system to another, but inevitably results in suboptimal code. Whenever speed is important, this is a strong argument against the use of a high-level language.
- As any high level language, C is not very well suited to make optimal use of hardware related features of a DSP system, such as interrupts, timers, interfaces, inter-processor communication, shared memory, etc. Therefore a DSP program written in C would have to be interfaced with some assembly code.

In comparison to this the characteristics of assembly language are quite different:

- Individual instructions are directly linked with DSP operations. Therefore, programs are executed extremely fast: for example a 32-bit floating-point multiplication takes only a single clock cycle.
- The instruction set is, compared to C, relatively limited. However, there are several means to bypass this limitation, as indicated below.
- All functions available in C can also be used by assembly-language programs, although using these functions is evidently more complicated than directly from C.
- In case a macro assembler is used, the user can practically define his own, more powerful instructions. In this way, an integrator or the calculation of a sine is described by a single line of code. From the user's point of view, this corresponds to the use of procedures and functions in C. However, macros are much faster because they require no extra overhead. Individual macros can be optimized for speed. For example, for the calculation of a sine and a cosine of an angle, a speed gain of a factor of five (!) was obtained by replacing the routines from a C-function library with a newly written macro.
- Learning to use the DSP assembly language efficiently, requires a greater effort than learning to program the simulations in a well-known language such as C. However, starting from an existing program, students have been able to write their own simulation programs in less than two weeks.
- Assembly-language programs tend to be less readable than high-level language programs. However, both in C and in assembly language, programs can always be written in a structured and well-documented way.

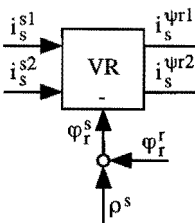
- Assembly-language programs are usually suited only for a single type of processor, and can therefore not easily be used on a different system. Only for similar processors from a single manufacturer largely the same language can be used.

Based on these considerations assembly language was chosen for all simulation programs. Through the extensive use of macros, the ease of use of a high-level language was approached. The following categories of macros were designed (see also [Bosg-95b]):

- Low-level mathematical macros for functions such as sine, cosine, vector rotator, universal filter, integrator, differentiator. For multiplication and addition no macros were required, as they exist already as DSP instructions.
- High-level macros combining several instructions and low-level macros, cf. the blocks used in a block diagram such as the one shown in figure 7.3.
- Input/output macros facilitating the use of analog and digital inputs and outputs. These included for example routines to display different signals (individually or alternating between different signals) depending on the position of output selection switches on the control panel. Also some macros were written allowing to display the name of the signals along with the signals on an analog oscilloscope.

An example of how these macros are used in DSP programs is shown in figure A.2. This figure shows the relation between a block diagram of an adder and a vector rotator and the program code in assembly language. For comparison, also the corresponding C code is shown. Theoretically, both the program in C and the assembly program could have been simplified by including the cosine and sine calculation in the vector-rotator procedure or macro. However, often several vector rotators require the same cosine and sine, and for that reason it is more efficient to calculate them only once, separate from the actual rotator code. In the assembly-language program, the simple addition requires three lines and includes the use of an extra variable, a register. The code could be made more readable by replacing these three lines by a single macro, or faster by eliminating the variable “phi_r_s”, using a register instead. In the actual programs a compromise had to be found between speed and readability.

Block diagram:



Program in C:

```
phi_r_s = phi_r_r + rho_s;
cosphi_r_s = cos(phi_r_s);
sinphi_r_s = sin(phi_r_s);
VECROTN(i_s_s1,i_s_s2,cosphi_r_s,sinphi_r_s,&i_s_ps1,&i_s_ps2);
```

Program in C40 macro-assembly language:

```
LDF    @phi_r_r, R1
ADDF   @rho_s, R1
STF    R1, @phi_r_s
cossin @phi_r_s, @cosphi_r_s, @sinphi_r_s
vecrotn @i_s_s1, @i_s_s2, @cosphi_r_s, @sinphi_r_s, @i_s_ps1, @i_s_ps2
```

Figure A.2. Example of the relation between a block diagram and program code.

More difficult programs in which less standard macros could be used, had to be written for simulation and control of a voltage-source inverter. As mentioned in section 8.3.1, accurate simulations of an inverter with a power-device open circuit could only be performed using a simulation time step of $10\ \mu\text{s}$. With such a small time step, real-time simulation was not possible – simulations were performed at a speed which was a factor of six below the real speed.

A.4.3 Additional DSP software

To complement the actual simulation programs for the DSP system, a number of additional programs and routines has been written. Two of these are mentioned in this section.

One of the strengths of the TMS320C40 processor is its ability to perform Fast Fourier Transforms (FFTs) in a very efficient and rapid way. The FFT is used to calculate the frequency spectrum of a signal. For the DSP system, a program was written that implemented a complex FFT. The advantage of using a complex FFT is that instead of a scalar, a vector, such as a field-oriented or stator-oriented current vector, can be used as an input. A vector rotating clockwise appears in the spectrum as a negative frequency, and vice versa. While one processor was used for simulation or control, the other processor could be used for this FFT calculation. This allowed to observe frequency spectra of any signal in the DSP system. This feature was very useful while adjusting parameters or correcting for offsets present in certain measurements.

An important addition to the simulation programs was also a set of routines that allowed the creation of MATLAB data files directly by the DSP system. MATLAB is a popular signal-processing software package available for many different computer platforms, and was used to post-process and present simulated and measured data. The MATLAB-file created on the DSP system included important information on the sampled data, such as the time step used for sampling and the names of all included variables.

A.5 Conclusions

The DSP-based digital control system developed for this and other research project was an invaluable tool for the simulations and the controls required for this thesis. Its speed and the obtained close relation between the simulations and the actual experiments were the main reasons to prefer the use of this system for both simulations and control.

In almost all situations the calculation power of the DSP system has been sufficient to simulate in real time and to implement advanced control methods on an experimental setup. In those occasions where the speed of the control was limited by the DSP speed,

using more processors in parallel would not result in a higher speed. In future, faster processors are expected to allow faster controls or less efficient programs. Then, the usage of a high-level programming language or a graphical programming language would have to be reconsidered. However, even then some knowledge of the hardware and of assembly language would remain necessary to use features such as interrupts and timers.

Display of data using analog oscilloscopes was shown to be an effective way to observe rapidly changing signals, if combined with the possibility to switch easily between different signals. Mainly for educational purposes the display of variable names along with the signals on the analog scopes was an interesting feature. Data storage in standard MATLAB format, including variable names, provided a practical means to post-process and present data. Stored data could be previewed on an analog oscilloscope.

A control panel has been designed to adjust command values and parameters, as well as to switch between display modes. The use of real buttons and knobs was preferable to the use of a computer keyboard or a pointing device such as a mouse. A more advanced future version might include a method to display on screen the values set by the control panel.

The protection mechanisms added externally to the DSP system, turned out to be very effective. Users of another DSP system without processor-halt detection experienced the loss of several IGBTs due to overcurrents arising after suddenly halting the processor. Also software failures (such as a program being too long for a chosen time step) were successfully detected. Not a single device or component failure occurred (!).

To obtain sufficient speed also using advanced inverter control methods, manual optimization of assembly code was required. However, through the use of standardized macros, all current and future users will benefit from these optimizations. The use of macros also transformed the assembly language into a less low-level language and helped in creating well readable programs. Students and other users could easily start using the system basing their simulations on existing macro libraries. Translation from a block diagram to a program is relatively easy when using these macros.

The transition from simulations to experiments was by far more practical than it would have been with other simulation systems. Here, the programs developed for the control of a simulated machine could be used directly for a real machine. The translation of a control method from a different simulation package to the DSP system might have required more time than the development of the control directly on the DSP system.

Appendix B

Symbols and Notations

B.1 Notation

In this thesis, the difference between scalar and vector quantities is shown using bold print for vectors. Scalars can either be constant parameters or time dependent quantities, a difference that will not be shown in the notation. Also to denote the length of a vector, or the peak value of a time-dependent quantity, the simple scalar notation will be used. Matrices are denoted by capitals in normal print, while capitals in bold print are used for complex vectors. The real and imaginary axes correspond in this case with the axes of the coordinate system. A bar under a symbol is used to indicate a complex representation of a time-dependent scalar. A summary of these and other notations is given in table B.1.

Table B.1. Notation.

x	scalar
\mathbf{x}	vector
X	matrix
\mathbf{X}	complex representation of a vector quantity: $\mathbf{X} = x + jy$
\underline{x}	complex representation of a scalar: $x = \text{Re}(\underline{x})$

Several marks are used to distinguish between for example real quantities and estimates, as well as command values for these real quantities. These are shown in table B.2.

Table B.2. Marks.

\tilde{x}	quantity estimated for/by a flux observer
\hat{x}	quantity estimated for/by the control system
x^*	command value, also called desired value
\dot{x}	time derivative of a quantity, dx/dt
x'	scaled quantity, see section 2.7
\bar{x}	low-pass filtered quantity

B.2 Symbols

The symbols used throughout this thesis are summarized in table B.3. Auxiliary variables that are used only locally in the derivation of certain equations are not included in this list. The symbol 'Θ' is not in conformity with the notation introduced in table B.1, but as it will not be used in combination with any mark, super- or subscript, it was maintained in this form for compatibility with eg. [Blas-96].

Table B.3. Symbols.

t	time	ρ	rotor position
i	current*	ε	current angle
ψ	flux (linkage)*	φ	flux angle
u	voltage	α	voltage angle
a	current distribution	β	filtered flux angle
b	magnetic induction	ζ	conductor position angle
h	magnetic field strength	θ, η, τ	other position angles
r	resistance*	ω	angular frequency
l_{σ}	leakage inductance	ℓ	length of the rotor iron
l	inductance*	r	radius of the rotor iron
m_{el}	electromagnetical torque	d	width of the air gap
m_{load}	load torque	n	number of turns
$R(\alpha)$	rotation matrix over angle α	k	number of coils
Θ	moment of inertia	k_i	current multiplication factor
μ_0	permeability in vacuum	v	winding distribution factor
f	force		

* In section 2.7 scale factors have been introduced for the rotor current, the rotor flux, the rotor resistance, and the main inductance. Whereas in section 2.7 real values and scaled values were distinguished by accentuating the scaled values, this has been omitted throughout all later sections. This means that before section 2.7, the symbols for rotor current, rotor flux, rotor resistance and main inductance denote actual values, while after this section scaled values are meant.

B.3 Reference frames and vector components

Vectors as well as complex numbers represent quantities with respect to different reference frames, such as the stator reference frame, which is fixed to the stationary part of the machine. Another reference frame that is often used in this thesis is the rotor-flux

reference frame. This frame is fixed to the rotor-flux vector, which represents the flux linking the windings of an equivalent two-phase (semi-four-phase) rotor. The reference frame to which a vector or complex number is related, is denoted by a superscript, as shown in table B.4. Whenever this vector or complex number is decomposed into two scalar components, the first component – often called the direct component – is denoted by an additional superscript ‘1’, the second – the quadrature component – by ‘2’. These components can be thought of as referring to appropriately and orthogonally placed windings of an equivalent two-phase (semi-four-phase) machine. A vector decomposed into its components is written in a column form using square brackets.

For angles, the primary superscript is used to indicate the reference axis. If an angle x^y is zero, the vector to which it refers points into the ‘y1’ direction, the “direct” or parallel direction of the ‘y’ reference frame. The ‘y2’ axis is located at 90° in positive (counter-clockwise) direction from the ‘y1’ axis.

Table B.4. Superscripts: Reference frames and vector components.

x^s	quantity oriented to the fixed stator reference frame
x^r	quantity oriented to the rotor reference frame
$x^{\psi s}$	quantity oriented to the stator-flux reference frame
$x^{\psi 1}$	quantity oriented to the air-gap-flux reference frame
$x^{\psi r}$	quantity oriented to the rotor-flux reference frame
x^{y1}	vector component parallel to the reference axis of the y reference frame
x^{y2}	vector component perpendicular to the reference axis of the y reference frame

B.4 Circuits, windings and coils

Primary subscripts are used to distinguish between quantities related to physically distinct circuits, such as the stator, the rotor, the power converter and the dc-link (if present). A separate subscript is also introduced for quantities related to an imaginary set of windings that is located in the air gap of the machine. Subscripts referring to a circuit are given in table B.5.

Table B.5. Primary subscripts: Circuits.

x_s	quantity related to the stator circuit
x_\perp	quantity related to the (imaginary) air-gap circuit
x_r	quantity related to the rotor circuit
x_{dc}	quantity related to the dc-link circuit
x_v	quantity related to the power-converter circuit

Whenever no primary subscript is used, the concerning quantity is related to the machine as a whole. This is the case for e.g. the main inductance and the rotor position (the stator position is zero by agreement, so that the rotor position is the only position of interest).

To distinguish between the different windings, phases or branches of which a circuit is composed a secondary subscript is added, as listed in table B.6. Whenever an equation is valid for any of the windings, a subscript 'q' is used. This subscript is also used to distinguish between parameters related to the orthogonal two-phase machine model (no subscript) and the parameters of the real (three-phase) windings of the machine (subscript 'q'). For the homopolar circuit, needed to complete the two-phase model, the subscript '0' is used.

For parameters used in the delta-connected equivalent machine model the subscript ' Δ ' is used. The windings are then denoted by a double secondary subscript.

If a circuit or winding is considered as a number of separate coils, the subscript 'k' refers to one of these coils.

Table B.6. Secondary subscripts: Windings and coils.

x_{ya}	quantity related to phase a of the y circuit
x_{yb}	quantity related to phase b of the y circuit
x_{yc}	quantity related to phase c of the y circuit
x_{yq}	quantity related to phase q of the y circuit, where $q = a, b, c$
x_{yqk}	quantity related to coil k belonging to the phase-q winding of the y circuit
x_{yk}	quantity related to coil k belonging to the y circuit
x_y	(no secondary subscript) quantity related to the y circuit of the orthogonal two-phase machine model
x_{y0}	quantity related to the homopolar part of the y-circuit model
$x_{y\Delta}$	quantity related to one winding of the equivalent delta-connected y circuit
x_{yab}	quantity related to the phase-ab winding of the equiv. delta-conn. y circuit
x_{ybc}	quantity related to the phase-bc winding of the equiv. delta-conn. y circuit
x_{yca}	quantity related to the phase-ca winding of the equiv. delta-conn. y circuit
$x_{yq,q}$	(only used with $x=1$) self-inductance of the phase-q winding of the y circuit
$x_{ya,b}$	(only used with $x=1$) mutual inductance between the phase-a and phase-b windings of the y circuit
$x_{ya,c}$	(only used with $x=1$) mutual inductance between the phase-a and phase-c windings of the y circuit

B.5 Harmonic components and other special notations

In some cases, quantities are decomposed into fundamental and non-fundamental (frequency) components. If the quantity is decomposed into components that represent the fundamental and each harmonic frequency (second harmonic, third harmonic, etc.), a subscript 'n' is used to denote these components. If only a limited number of harmonics is considered (third, fifth, seventh) these are indexed by the subscript 'i'. The individual components are in both cases indicated by replacing the 'n' or 'i' with a number (1, 2, 3, ...), as shown in table B.7. The harmonic subscript is always placed after all other subscripts.

The value of an angle at $t=0$ is denoted by using a '0' as a secondary subscript. No confusion with homopolar quantities occurs, because no separate angles are introduced for a homopolar system.

In some cases a double primary subscript is used. This is done to indicate a quantity that is physically related to one circuit, but is considered in an other circuit. Consider for example the flux linking one winding of the stator circuit. This flux consists of a part which is also linking an imaginary identical winding at the same position located in the rotor, plus a stator and a rotor leakage flux (see for example equation 5.13). The first part receives the primary subscript 'rs', followed by a secondary subscript to indicate the concerning stator winding.

Table B.7. Subscripts for harmonic components and other special notations.

x_n	frequency component with a frequency n times that of the fundamental of x
x_i	frequency component number i of x
$x_{1,2,\dots}$	numbered component, either a frequency component or a quantity related to a specific coil
α_{y0}^z	value of α_y^z at $t=0$ (only for angles)
x_{yzq}	quantity related to the y circuit considered in winding q of the z circuit
$[x]_{av}$	average value of a quantity
$[x]_{max}$	maximum allowed value of a quantity

Some additional symbols are given in table B.8.

Table B.8. Additional symbols.

$s1..s6$	numbers of the switching devices in an inverter
$d1..d6$	numbers of the diodes in an inverter
r_{off}	resistance of a non-conducting diode, used in simulations
i_{lim}	current limit above which a diode is assumed to conduct, in simulations
Δi	one half of the hysteresis bandwidth used for current control
Δm	one half of the hysteresis bandwidth used for torque control
$\Delta i_s^{\psi r1*}$	amount by which $i_s^{\psi r1}$ is outside of its hysteresis control band
Δm_{el}^*	amount by which m_{el} is outside of its hysteresis control band
$S2, S3$	feedback parameters used in the u/i-model

B.6 Examples

Some examples illustrating the usage of the numerous super- and subscripts are given in table B.9.

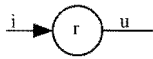
Table B.9. Examples of symbols.

$i_s^{\psi r1}$	magnetizing component of the stator current
$i_s^{\psi r2}$	torque-producing component of the stator current
ϕ_r^r	frequency of the rotor flux with respect to the rotor
$\tilde{\psi}_r^s$	observed rotor-flux vector in stator coordinates
\tilde{r}_s	stator resistance used in the flux observer
ε_{s1}^s	fundamental frequency of the stator current
$u_s^{\psi r1*}$	desired (command) value for the component of the stator voltage that is parallel to the rotor flux vector
l_σ	total leakage inductance
$l_{\sigma sq}$	leakage inductance of one of the three stator windings
\hat{l}_0	estimated value of the homopolar inductance

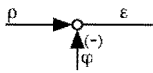
B.7 Elements used in block diagrams

The most commonly used blocks for the block diagrams throughout this thesis are listed in table B.10. Blocks not listed here are combinations of these elementary blocks.

Table B.10. Elements used in block diagrams.



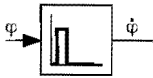
amplification ($u = i \cdot r$)



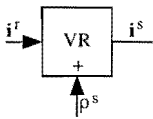
addition/subtraction ($\epsilon = \rho \pm \varphi$)



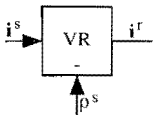
integration ($\varphi = \int \dot{\varphi} dt$)



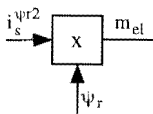
differentiation ($\dot{\varphi} = \frac{d\varphi}{dt}$)



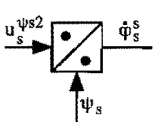
positive vector rotation ($\mathbf{i}^s = \mathbf{R}(\rho^s) \cdot \mathbf{i}^r$)



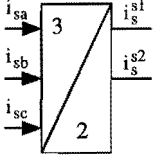
negative vector rotation ($\mathbf{i}^r = \mathbf{R}(-\rho^s) \cdot \mathbf{i}^s$)



multiplication ($m_{el} = i_s^{\psi_r2} \cdot \psi_r$)



division ($\dot{\varphi}_s^s = \frac{u_s^{\psi s 2}}{\psi_s}$)



transformation (different equations for different transformations)

Appendix C

Description and Parameters of the Experimental Setup

C.1 Per-unit reference values

The four independent reference values for the per-unit system have been based on the rated machine parameters according to equations 2.72 to 2.75, using the machine data given in section C.2. The results are given in equation C.1 to C.4. Other reference values can be derived using equations 2.76 to 2.81.

$$[u]_{\text{ref}} = \sqrt{2} \cdot 220 = 311.1 \text{ V} \quad (\text{C.1})$$

$$[i]_{\text{ref}} = \frac{3}{2}\sqrt{2} \cdot 55 = 116.7 \text{ A} \quad (\text{C.2})$$

$$[\omega]_{\text{ref}} = 2\pi \cdot 50 = 314.2 \text{ rad/s} \quad (\text{C.3})$$

$$[\theta]_{\text{ref}} = 1 \text{ rad} \quad (\text{C.4})$$

C.2 The cycloconverter-fed induction-motor drive

The cycloconverter-fed induction-motor drive consisted of a slip-ring induction machine fed by a cycloconverter, a dc machine used as a positive or negative load, and a DSP-based control system (see Appendix A). The name-plate data of the induction machine are:

ASEA MAC 20; 30 kW; 3-phase 50 Hz motor; $\cos \varphi = 0.93$; 2930 rpm;

Pr. Y: 380 V, 55 A; Pr. Δ : 220 V, 95 A; Sec. 295 V, 63 A.

The stator of this machine has a single-layer winding, distributed symmetrically over 36 slots. The rotor has 30 slots. The parameters of this machine, as used in the two-phase-plus-homopolar machine model, from which the three-phase parameters can be derived, given in per unit, are:

$$r_s = 0.027; \quad l_{\sigma} = 0.15; \quad r_r = 0.015; \quad l_0 = 0.19$$

$$l |_{\psi_r=0.65} = 5.1; \quad l |_{\psi_r=0.8} = 4.4$$

The moment of inertia of the coupled rotors of the induction machine and the dc machine equals $\Theta = 2.79 \cdot 10^3$ pu.

The name-plate data of the dc machine are:

SMIT Slikkerveer DC Generator Type G 34/26; 27 kW; Max. 1500 rpm;

Armature max. 440 V; Field: 220 V, 3.2 A;

The three-phase cycloconverter was of the circulating-current type, which means that the thyristor bridges for positive and negative phase current were both conducting continuously. The circulating-current control as well as the output-voltage control was implemented in a hybrid analog/digital circuit, and has been described in detail in [Bosg-93] and [Bosg-93b]. The twelve thyristors for each phase were from Semikron, type SKKT 91/12 D.

C.3 The voltage-source inverter-fed induction-motor drive

For the experiments with a voltage-source inverter, the same machines were used as in the experiments with the cycloconverter. The inverter was built using IGBTs from Eupec, type FZ 75A 12KL. A description of the inverter is found in [Veth-94]. The digital, optical inputs of the gate drivers were connected to digital outputs of the DSP system. The dc voltage for the inverter was generated using a dc generator coupled with a synchronous machine.

Samenvatting

Asymmetrische voeding van inductiemachines Strategieën voor overbruggingsbedrijf in geval van convertorfouten

De driefasige inductiemachine is een robuuste en betrouwbare machine die industrieel wordt toegepast in een grote verscheidenheid van elektrische aandrijvingen. Het toenemende gebruik van vermogenselektronica om deze machine te voeden breidt bovendien deze verscheidenheid nog verder uit naar het gebied van de – soms hoog-dynamisch – regelbare aandrijvingen. Tegelijkertijd echter, garandeert de toevoeging van vermogenselektronica niet noodzakelijkerwijs dat de betrouwbaarheid van de complete aandrijving gelijk of beter is dan de betrouwbaarheid van een inductiemachine die direct, zonder convertor, op het net is aangesloten.

In de praktijk leidt het falen van een enkele vermogensschakelaar of diens stuurcircuit er vaak toe dat de complete aandrijving wordt uitgeschakeld. Echter, onder bepaalde omstandigheden is zo'n uitschakeling niet strikt noodzakelijk. Het voorkomen van dergelijke onnodige uitschakelingen zou leiden tot een verbetering van de betrouwbaarheid van de aandrijving. Daarvoor is het nodig om te weten wat voor bedrijf van de aandrijving nog mogelijk is terwijl er een defect in de convertor aanwezig is.

In dit proefschrift wordt een classificatie van dergelijke defecten gepresenteerd, gebaseerd op hun effect op de aandrijving. Hierbij zijn stroomdefecten die defecten die gerelateerd zijn aan een open circuit in de convertor, en zijn spanningsdefecten gerelateerd aan een kortsluiting. Een belangrijk onderscheid is ook of het sterpunt van de statorwikkelingen van de machine zó is aangesloten dat een sterpunt- ofwel homopolaire stroom kan vloeien. In dat geval is er namelijk meer redundantie in de configuratie aanwezig, en kan overbruggingsbedrijf in geval van een defect eenvoudiger worden toegepast.

In het geval dat een complete statorfase door een defect wordt geopend, maakt een geschikte regeling van de sterpuntstroom overbruggingsbedrijf mogelijk met een constant koppel, dat echter wordt beperkt door de verhoogde stroombehoefte van de twee resterende fasen. Om dit soort bedrijf te onderzoeken, moest het standaard machinemodel worden uitgebreid met een homopolaire impedantie. Op basis van dit uitgebreide model werd een sturing van de sterpuntstroom gerealiseerd voor een spanningsgevoede machine. Experimenten lieten een geslaagd overbruggingsbedrijf zien, maar toonden ook aan dat een sterpuntstroom leidt tot verzadiging in het circuit van de hoofdflux.

Zonder sterpuntaansluiting is het verlies van één statorfase een zeer ernstig defect dat overbruggingsbedrijf in de meeste gevallen niet toelaat. Een snelle regeling van de stroom in de overgebleven fasen kan in dat geval de harmonische inhoud van de onvermijdelijke koppelpulsaties verminderen, of kan worden gebruikt om laagfrequente componenten uit de koppelpulsatie te verwijderen. Helaas is het niet mogelijk om de amplitude van de rimpel te reduceren tot minder dan 100% van het gemiddelde koppel, en vereist een noemens-

waardige verbetering van het koppel een hoge piekstroom in de resterende fasen. Overbruggingsbedrijf is derhalve alleen mogelijk als het mechanische deel van de aandrijving een aanzienlijke koppelrimpel kan verdragen en als de convertor in staat is hoge piekstromen te leveren.

Een open circuit van één enkele schakelende component is een defect waarbij overbruggingsbedrijf met meer succes kan worden toegepast. Onderzocht werd het geval van een open circuit van een enkele component van een spanningsinverter met zes schakelaars. Dit defect veroorzaakt een open circuit van een enkele statorfase gedurende een beperkt tijdsinterval in iedere periode van de statorstroom. Wordt de machine gebruikt als generator, dan kunnen de resterende componenten worden gebruikt voor overbruggingsbedrijf met constant koppel. Dit werd gerealiseerd met behulp van een nieuwe rotorfluxgeoriënteerde regelmethode, die tot doel had het koppel constant te houden door – indien nodig – variaties van de magnetiseringsstroom toe te staan. Tijdens motorbedrijf duurt het open circuit van een fase veel langer. In dat geval is het helaas niet mogelijk om een constant koppel te behouden, noch is het mogelijk om de amplitude van de koppelrimpel te reduceren tot beneden een theoretisch minimum van 100% van het gemiddelde koppel. De nieuwe regelmethode beperkt echter de duur van de optredende koppeldip aanzienlijk. Deze beperking vereist een verhoogde stroom in de meeste overige componenten. Ook in dit geval hangt de realiseerbaarheid van overbruggingsbedrijf af van het mechanische systeem en van de overstroomcapaciteit van de convertor.

Spanningsdefecten – kortsluitingen van een gehele fase of van een enkele component – staan in de praktijk geen overbruggingsbedrijf toe. Indien het sterpunt is aangesloten, is overbruggingsbedrijf theoretisch mogelijk, zelfs al is een gehele statorfase constant kortgesloten. Dit zou echter extreem hoge stromen vereisen, die geen enkele normaal gedimensioneerde convertor in staat is te leveren. In geval van een spanningsinverter resulteert de kortsluiting van een enkele component eveneens in extreem hoge stromen. Het is theoretisch onmogelijk om de overgebleven componenten zó aan te sturen dat overbruggingsbedrijf zonder extreme koppelpulsaties en overstromen wordt verkregen.

Om enige vorm van overbruggingsbedrijf mogelijk te maken, moeten kortsluitingen zoveel mogelijk worden vermeden. Treden zij toch op, dan moeten ze zo snel mogelijk worden omgezet in open circuits. Het aansluiten van het sterpunt van de statorwikkelingen vergroot de mogelijkheden voor overbruggingsbedrijf aanzienlijk. Tenslotte is het belangrijk om defecten zoveel mogelijk te beperken tot één enkele component, zodat een maximaal aantal componenten operationeel blijft.

Overbruggingsbedrijf vereist een toename in de complexiteit van het regelsysteem. In het kader van dit proefschrift werden regelingen en ook real-time simulaties geïmplementeerd op een krachtig digitaal-signaalprocessor-systeem. Terwijl verdere ontwikkeling van dergelijke systemen industriële toepassing ervan in elektrische aandrijvingen mogelijk zal maken, is aangetoond dat ook met minder geavanceerde hardware, strategieën voor overbruggingsbedrijf kunnen worden gerealiseerd.

Resumo

Nesimetria nutrado de nesinkronaj maŝinoj Strategioj por daŭrigata funkciado kaze de konvertordifektoj

Trifaza nesinkronmotoro estas tre fortika kaj fidinda maŝino uzata en industrio en larĝa gamo de elektraj motorsistemoj. Kreskanta uzo de povumelektroniko por nutri la nesinkronmaŝinon pli kaj pli larĝigas tiun gamon en la kampon de – foje tre dinamike – rapidecvarieblaj motorsistemoj. Samtempe tamen la aldono de povumelektroniko ne nepre garantias ke la fidindeco de la kompleta motorsistemo egalas aŭ superas tiun de nesinkronmaŝino ligata rekte al la reto, sen povumkonvertoro.

Praktike, la ekdifekton de unuopa ŝaltkapabla komponanto aŭ ĝia ŝaltgicirkvito en povumkonvertoro sekvas kutime la elŝalto de la kompleta motorsistemo. Tamen, en certaj cirkonstancoj tia elŝalto ne estas necesa. Se eblas estonte eviti tiajn elŝaltojn, la fidindeco de motorsistemoj plialtiĝos. Pro tio, necesas scii kia funkciado de la motorsistemo realigeblas okaze de difekto en la povumkonvertoro.

En tiu ĉi tezo prezentiĝas klasifiko de tiaj difektoj, bazita sur ilia efiko je la motorsistemo. Kurentdifektoj estas difektoj kiuj rilatas malferman cirkviton en la konvertoro, dum tensidifektoj rilatas kurtan cirkviton. Grava distingo estas ankaŭ ĉu aŭ ĉu ne la stelpunkto de la statorvolvaĵoj de la maŝino ligiĝis tiel ke stelpunkta (t.n. homopolara) kurento povas flui. Se jes, pli da malmanko enestas la cirkviton kaj pro tio daŭrigata funkciado okaze de difekto pli facile realiĝas.

Se kompleta statorfazo malligiĝas, taŭga regado de la stelpunktkurento ebligas daŭrigata funkciado kun konstanta tordmomanto, kiu tamen estas limigita pro altigita kurentbezono de la ceteraj du fazoj. Por pristudi tian ĉi funkciadon, necesis aldoni homopolaran impedancon al la kutima modelo de la nesinkronmaŝino. Surbaze de tiu ĉi etendita modelo, regulilo por stelpunktkurento realiĝis por tensi-nutrata maŝino. Eksperimentoj montris sukcesan daŭrigatan funkciadon, sed ankaŭ indikis ke stelpunktkurento kaŭzas saturiĝon de la ĉeffluks-cirkvito.

Sen ligo de la stelpunkto, la perdo de kompleta statorfazo estas tre grava difekto, post kiu daŭrigata funkciado en plej multaj okazoj ne eblas. Rapida regulado de la kurento en la restantaj fazoj povas malpliigi la harmonan enhavon de la neevitebla pulsado de la tordmomanto, aŭ povas esti uzata por forigi malaltfrekvencajn komponantojn de tiu ĉi pulsado. Malgraŭ tio, ne eblas malpliigi la amplitudon de la pulsado ĝis sub 100% de la averaĝa tordmomanto, kaj konsiderinda plibonigo de la tordmomanto postulas altajn kurentmaksimumojn en la restantaj fazoj. Tial, daŭrigata funkciado eblas nur se la mekanika sistemo kuplita kun la maŝino kapablas pretervivi konsiderindan pulsadon de la tordmomanto, kaj se la povumkonvertoro kapablas disponigi altajn kurentmaksimumojn.

Malferma cirkvito de unuopa ŝaltkapabla komponanto estas difekto dum kiu daŭrigata funkciado pli sukcese aplikeblas. Esploriĝis la kazo de malferma cirkvito de unuopa komponanto en ses-ŝaltita tensi-alternilo. Tiu ĉi difekto kaŭzas malferman cirkviton de unu fazo de la maŝino dum limigita parto de ĉiu periodo de la storkurento. Se la nesinkronmaŝino uziĝas kiel generatoro, la restantaj komponantoj de la konvertoro povas esti uzataj por daŭrigata funkciado kun konstanta tordmomanto. Tia ĉi funkciado realiĝis pere de nova rotorfluks-orientita regulmetodo, celanta konstantan tordmomanton dume permesante laŭnecese variadon de la magnetiganta kurentkomponanto. Dum motora funkciado, la malferma cirkvito de unu fazo daŭras multe pli longe. Tiam bedaŭrinde ne eblas teni konstanta la tordmomanton, nek eblas malpliigi la amplitudon de la pulsado de la tordmomanto sub teoria minimumo je 100% de la averaĝa tordmomanto. Tamen la nova regulmetodo konsiderinde reduktas la daŭron de la neevitebla malpliigo de la tordmomanto. Tiu ĉi redukto postulas altigitan kurenton en plejmulto de la restantaj komponantoj. Konklude, ankaŭ en tiu ĉi kazo la realigebleco de daŭrigata funkciado dependas de la mekanika sistemo kaj de la kapablo je trokurento de la konvertoro.

Tensidifektoj – kurtaj cirkvitoj de kompleta maŝinfazo aŭ de unuopa komponanto – en praktiko ne permesas ajnan daŭrigatan funkciadon de la nesinkronmaŝino. Se ĉeestas stelpunktligo, daŭrigata funkciado kun konstanta tordmomanto teorie eblas, eĉ se unu maŝinfazo konstante suferas je kurta cirkvito. Tamen, por tio ekstreme altaj kurentoj estus necesaj, kiujn neniu povumkonvertoro normale kapablas disponigi. Ankaŭ en la kazo de tensialternilo, daŭrigata funkciado dum kurta cirkvito de unuopa komponanto kaŭzas ekstreme altajn kurentojn. Teorie ne eblas reguli la restantajn ŝaltkapablajn komponantojn tiel, ke rezultigu daŭrigata funkciado sen ekstremaj tordmomant-impulsoj kaj sen trokurentoj.

Tial, por ebligi la realiĝon de iu daŭrigata funkciado, oni laŭeble evitu kurtajn cirkvitojn. Se kurta cirkvito tamen okazas, plej eble rapide ĝi estu transformata en malferman cirkviton. Ebligi la fluon de stelpunktkurento konsiderinde pligrandigas la eblecojn realigi daŭrigatan funkciadon. Fine, difektoj laŭeble estu limigataj al unuopa komponanto, lasante maksimuman nombron de aliaj komponantoj sendifekta.

Daŭrigata funkciado postulas plikomplikigon de la regelsistemo. Kadre de tiu ĉi tezo, regelsistemoj kaj ankaŭ realtempaj simuloj realiĝis pere de forta cifera signal-procezila sistemo. Plia evoluo de tiaj sistemoj permesos estontece ilian uzadon en industriaj motorsistemoj. Montriĝis tamen, ke ankaŭ uzante malpli ellaboritan regelsistemon oni povas realigi strategiojn por daŭrigata funkciado.

Curriculum Vitae

Sjoerd Bosga was born on December 1, 1969 in 's-Hertogenbosch. From 1982 to 1987 he went to the primary school "Mgr. Bekkersschool" in 's-Hertogenbosch, followed by six years at the "Stedelijk Gymnasium", also in 's-Hertogenbosch. In 1987 he started studying Electrical Engineering at Eindhoven University of Technology. As a part of these studies he spent one year (1989-1990) at the National Polytechnical Institute of Grenoble (INPG-ENSIEG) in France. In 1991 he performed a three-month traineeship at the Royal Institute of Technology in Stockholm, Sweden, on the control of an HVDC power converter. One year later he worked as a trainee for Philips Singapore on Quality Assurance in a tv-tuner factory. In February 1993 he received his Master of Science degree in Electrical Engineering from Prof.dr.ir. A.J.A. Vandenput for a project on the control of a cycloconverter. For this project he was awarded the HOLEC-prize. In March 1993 he started the Ph.D. research project that led to this thesis. Under the supervision of Prof.dr.ir. A.J.A. Vandenput the research was performed in the Electromechanics and Power Electronics group (EMV).

Stellingen

behorende bij het proefschrift

Asymmetrical Supply of Induction Machines

Remedial Operating Strategies in case of Converter Faults

door

Sjoerd G. Bosga

Eindhoven, 23 mei 1997

1. Wetenschappelijk onderzoek wordt extra interessant als men de tijd neemt om regelmatig te controleren waarheen de zijwegen zouden kunnen leiden die men *en passant* ontdekt. Niet alleen leert men op die manier de hoofdweg beter kennen, maar ook kan het gebeuren dat men zijwegen ontdekt die veel interessanter en nuttiger zijn dan de hoofdweg. Werken onder grote tijdsdruk is slechts dan nuttig wanneer men op zijn hoofdweg een bepaald doel op een gegeven tijdstip wil bereiken.
2. Hoewel het mogelijk is om met beperkte middelen de betrouwbaarheid van een standaard elektrische aandrijving te verbeteren, kan een veel grotere betrouwbaarheid bereikt worden door af te wijken van dit standaardconcept, bijvoorbeeld door toepassing van een ander type motor of andere topologieën, of door toepassing van meerdere onafhankelijke systemen in parallel.
3. Wie zich serieus bezighoudt met de regeling van elektrische machines, zal zich vroeger of later moeten verdiepen in ontwikkelingsconfiguraties en andere constructietechnische of fysische aspecten van die machines.

Ref.: H. Jordan, V. Klíma, K.P. Kovács, *Asynchronmaschinen*, Braunschweig: Vieweg and Budapest: Akadémiai Kiadó, ISBN 3-528-04600-7, 1975.

4. Terwijl enkelen wanhopig proberen een fasor te ontdekken in iedere vectorgrootheid die betrekking heeft op grootheden binnenin een elektrische machine, getuigen ze niet van veel fysisch inzicht als ze vervolgens hun redeneringen baseren op een spanning welke geïnduceerd zou worden in één geleider in de machine, dus in een niet gesloten kring.
5. Een van de grootste uitdagingen voor de wetenschap vandaag is het vinden van langetermijn oplossingen voor problemen die tijdens de afgelopen 100 jaar zijn ontstaan. Helaas is – om financiële redenen – veel onderzoek gericht op het vinden van oplossingen op korte termijn, wat meer als symptoombestrijding dan probleemoplossing gezien kan worden.
6. Weinig is zo boeiend als het lezen van een goed woordenboek. Nog interessanter wordt het echter als men fouten of op zijn minst eigenaardigheden in woordenboeken (zowel technische als “gewone”) gaat vinden.

7. Indien voor een bepaald probleem wereldwijd in meer dan 80% van de gevallen voor een bepaalde oplossing wordt gekozen, dient men als wetenschapper deze oplossing te kennen en toe te passen. Echter, juist een wetenschapper mag niet nalaten om ook andere oplossingen te beschouwen, en waar deze betere resultaten opleveren, ze toe te passen en een breder gebruik ervan aan te moedigen.

Ref.: *Why do people prefer Macintosh?*, Apple Computer, Inc., April 1996.

Pierre Janton, *Het Esperanto*, Culemborg: Meulenhoff/Edinfo, 1987.

8. Het is een illusie om te denken dat de kwaliteit van een student, een onderzoeker, een vakgroep, een faculteit of een hele universiteit kan worden uitgedrukt in een verzameling cijfers of punten. Wie dit toch probeert, verwacht de begrippen “kwaliteit” en “kwantiteit”. Het zou bestreden moeten worden dat nu zelfs ook studenten met financiële middelen ertoe worden gedwongen zich meer te richten op het halen van – volgens een willekeurige norm – voldoende cijfers dan op het studeren om kwalitatief goede ingenieurs te worden.

Aanbevolen literatuur: R.M. Pirsig, *Zen and the art of motorcycle maintenance – an inquiry into values*, 1974.

9. Hoewel het bij de Europese eenwording, overigens net zoals bij een huwelijk, lijkt te gaan om een belangrijke intensivering van samenwerking, brengt dit proces vanzelf ook een verslechtering van relaties met derden met zich mee. Nu dit besef, en tevens de ontdekking dat niet iedere – vaak met compromissen bezaaide – samenwerking voordelen oplevert, bij hen begint door te dringen, zijn de vroegere voorstanders van de Europese Gemeenschap, en met name zij die haar beschouwden als een tussenstap in de richting van meer wereldwijde samenwerking, langzaam aan het veranderen in tegenstanders. Als voorstanders blijven slechts zij die hier zelf op korte termijn profijt van hebben.
10. In een dichtbevolkte regio – die overigens niet beperkt wordt door nationale grenzen – is veelgebruikt openbaar vervoer onmisbaar om een aangenaam leefmilieu te behouden. Aangezien een groot deel van de reizenden zich prettiger voelt alleen in zijn of haar eigen auto, is het de taak van de overheid om het openbaar vervoer tot een aantrekkelijk alternatief te maken door het creëren en onderhouden van snelle en frequente verbindingen binnen, tussen maar ook buiten de dichtstbevolkte gebieden, en door het garanderen van lage prijzen. Het uitbreiden van een luchthaven of het verhogen van de prijs van benzine draagt niet bij aan een verbetering van het openbaar vervoer.